Dissertation

submitted to the

Combined Faculty of Natural Sciences and Mathematics

of the Ruperto Carola University Heidelberg, Germany

for the degree of

Doctor of Natural Sciences

Presented by

M.Sc. Carolin Schmelas

Born in Ellwangen (Jagst), Germany

Oral examination: June 19th, 2020

One for all, all for one:

Combining and improving AAV, RNAi and CRISPR technologies to combat HBV infection and HBV/HDV co-infections

Referees: Prof. Dr. Ralf Bartenschlager

Prof. Dr. Dirk Grimm

ABSTRACT

In recent years, the field of gene and cell therapy has experienced major breakthroughs in the development of novel gene-based therapies and has been increasingly appreciated as versatile and innovative platform to cure hitherto untreatable diseases. Gene therapy resorts to biotechnological tools and approaches, such as recombinant (r)AAV vectors, RNAi and CRISPR/Cas9, that are employed to replace, silence or edit malfunctioning genes. The accomplishments of these technologies are highlighted in numerous clinical trials and culminated in the authorization of three rAAV-based therapies (Glybera, Luxturna and Zolgensma) and in one RNAi-based therapeutic (Onpattro). The presented doctoral thesis combines and further improves these technologies by drawing on several principles of synthetic biology and bioengineering and demonstrates their potential to tackle HBV infections and/or HBV/HDV co-infections as clinically relevant targets.

The first part of this study was intended to validate an innovative generation of rAAV vectors previously established in our lab (by Florian Schmidt) and named TRISPR that enables the combination of the CRISPR/Cas9 and RNAi technologies. TRISPR facilitates the juxtaposition of three small RNA triggers (short-hairpin (sh)RNAs and single guide (sg)RNAs as required by the RNAi and CRISPR machineries, respectively) on a single rAAV vector and was experimentally reassessed in the presented study as superior strategy to knock-out HBV antigens via CRISPR. We further engineered TRISPR to co-express sgRNAs and shRNAs against HBV infections and HBV/HDV co-infections and showed that the combination of RNAi and CRISPR/Cas9 yielded a synergistic benefit in the elimination of both pathogens in cell culture experiments. Thus, this thesis paves the way for subsequent *in vivo* studies in HBV and HBV/HDV mouse models to test the effect of a combinatorial knock-down and knock-out strategy on the host immune response, which is typically blunted during HBV infection.

Next, we evaluated the addition of 2.5% DMSO to the media as a new method to enhance rAAV transduction in cell culture experiments. A comprehensive screen via an automated microscopy assay with a fluorescence reporter revealed that the DMSO-mediated enhancement is dependent on selected rAAV variants and cell lines. Transduction rates increased up to 5-fold and 10-fold in Hepa16 and HepG2 cells, respectively, and culminated in N2A cells, in which transduction and expression rates of several rAAV variants that otherwise barely transduced these cells were boosted towards upper detection limits. Furthermore, the addition of DMSO also resulted in

strongly enhanced rAAV uptake and improved expression of CRISPR components in N2A cells that yielded up to 20-fold increased targeted mutagenesis rates. Although the mechanism remains to be elucidated, DMSO represents an alternative method to improve rAAV transduction with less cytotoxic side effects compared to currently applied enhancers.

We further harnessed the inherent power of double-stranded (ds)AAV vectors to express the CRISPR components more rapidly and more efficiently than conventional single-stranded (ss)AAV counterparts. Yet, expression from the superior dsAAV vector comes at the cost of a further reduction of the rAAV packaging capacity, from about 5 kb for ssAAVs, to only 2.4 kb for dsAAVs. Previously, others have circumvented the inherent size limit of ssAAV vectors by splitting the *Streptococcus pyogenes* (*Sp*)Cas9 endonuclease into two parts, which are reconstituted in the cell to the holo-enzyme by intein *trans*-splicing. We previously worked towards an intein-mediated splitCas9 system (MSc thesis, C. Schmelas) to split the smaller Cas9 ortholog from *Staphylococcus aureus* (*Sa*Cas9) in two halves, each of which was sufficiently small to allow packaging in dsAAV vectors. Here, we experimentally confirmed that the dsAAV/split*Sa*Cas9 system can induce up to 5-fold higher knock-out efficiencies compared to the conventional ssAAV/full-length*Sa*Cas9, depending on cell type and incubation time. In addition, dsAAV/split*Sa*Cas9 induced about 2-fold increased mutagenesis rates in a luciferase reporter in the liver of mice. In order to restrict the strong dsAAV/split*Sa*Cas9 expression after successful gene editing, we further implemented a self-inactivating (SIN) approach developed by Julia Fakhiri from our lab that contributed to safeguard the rAAV/CRISPR technology.

Lastly, we increased the safety profile of the CRISPR/Cas9 system from *Staphylococcus aureus* by collaborating with the Niopek and Correia labs that have engineered its first designer anti-CRISPR protein. To this end, they made use of AcrIIC1, a broad-spectrum inhibitor targeting various other Cas9 orthologs and re-designed its binding surface towards the *Sa*Cas9 HNH domain. Together, we then demonstrated on various genomic loci that the novel AcrX inhibitor efficiently prevents *Sa*Cas9 cleavage activity and also implemented a microRNA-based switch to restrict *Sa*Cas9 activity towards hepatocytes.

In summary, this doctoral thesis demonstrated the compatibility and great potential of major tools in the field of gene therapy and presented several technological improvements that could be harnessed in future work either alone or in combination to enable a more efficient and safer approach to tackle HBV infections and HBV/HDV co-infections.

ZUSAMMENFASSUNG

Das Fachgebiet der Gen- und Zelltherapie hat in den letzten Jahren bedeutende Erfolge in der Entwicklung neuer, genbasierter Therapien erzielt und wird zunehmend als vielseitige und innovative Möglichkeit gewürdigt, um bislang unbehandelbare Krankheiten zu heilen. Die Gentherapie verwendet biotechnologische Werkzeuge und Ansätze, wie rekombinanter (r)AAV Vektoren, RNAi und CRISPR/Cas9, um fehlerhafte Gene zu ersetzen, auszuschalten oder zu editieren. Der Erfolg dieser Technologien wird durch zahlreiche klinische Studien deutlich und kulminiert in der Genehmigung dreier rAAV-basierter Therapien (Glybera, Luxturna and Zolgensma) und einer RNAi-basierten Therapie (Onpattro). Die vorliegende Doktorarbeit kombiniert und verbessert diese Technologien, indem sie auf mehrere Prinzipien der Synthetischen Biologie und Biotechnologie zurückgreift und demonstriert deren große Potentiale, um klinisch relevante Erkrankungen als Folge von HBV Infektionen und HBV/HDV Koinfektionen zu heilen.

Der erste Teil dieser Studie zielte darauf ab eine innovative Generation von rAAV Vektoren zu validieren, welche zuvor in unserem Labor (Florian Schmidt, Bachelorarbeit) entwickelt und als TRISPR bezeichnet wurden und die Kombination von CRISPR/Cas9 und RNAi ermöglichen. TRISPR vereinfacht die Nebeneinanderreihung von drei „kleinen RNA-Triggern“ (short-hairpin (sh)RNAs und single guide (sg)RNAs, die für die RNAi and CRISPR Maschinerien benötigt werden) auf einem einzelnen rAAV Vektor und wurde in der vorliegenden Arbeit erneut experimentell validiert als überlegene Strategie um mittels CRISPR HBV Antigene auszuschalten. Zudem verwendeten wir TRISPR, um sgRNAs und shRNAs gegen HBV Infektionen und HBV/HDV Koinfektionen zu ko-exprimieren und zeigen, dass die Kombination von RNAi und CRISPR/Cas9 einen synergistischen Vorteil bei der Eliminierung beider Pathogene in Zellkulturexperimenten bietet. Daher ebnet diese Studie den Weg für folgende *in vivo* Arbeiten in HBV und HBV/HDV Mausmodellen, um den Effekt eines kombinatorischen knock-down und knock-out Verfahrens am Immunsystem des Wirtes zu prüfen, welches typischerweise bei HBV Infektionen in der Funktion beeinträchtigt ist.

Als nächstes evaluierten wir die Zugabe von 2.5% DMSO zum Medium als neue Methode die rAAV Transduktion in Zellkulturexperimenten zu steigern. Eine umfangreiche Untersuchung mittels eines automatisierten Mikroskopieverfahrens mit Fluoreszenzreporter zeigte, dass eine DMSO-vermittelte Steigerung abhängig von der rAAV Variante und Zelllinie ist. Transduktionsraten steigerten sich bis zu 5- und 10-fach in Hepa16 und HepG2 Zellen und kulminierten in N2A Zellen, in denen sich

Transduktions- und Expressionsraten mehrerer rAAV Varianten zum Detektionsmaximum verstärken ließen, die ansonsten diese Zelllinien kaum transduzierten. Außerdem resultierte die Zugabe von DMSO in einer stark erhöhten rAAV Aufnahme und verbesserter Expression von CRISPR Komponenten in N2A Zellen, was eine 20-fache Steigerung von zielgerichteten Mutageneseraten bewerkstelligt. Obwohl der Mechanismus noch aufgeklärt werden sollte, repräsentiert DMSO eine alternative und weniger toxische Methode um rAAV Transduktionen zu verbessern, als derzeit verwendete Verstärker.

Des Weiteren nutzten wir das intrinsische Leistungsvermögen von doppelsträngigen (ds)AAV Vektoren, um die CRISPR Komponenten schneller und effizienter zu exprimieren im Vergleich zu den üblichen einzelsträngig (ss)AAV Gegenstücken. Jedoch kommt die Expression von den überlegenen dsAAV Vektoren teuer zu stehen, da die bereits begrenzte Verpackungsgröße von ssAAV Vektoren von 5 kb auf 2.4 kb für dsAAV Vektoren reduziert ist. Andere Arbeitsgruppen konnten zuvor die Größenlimitation von ssAAV Vektoren umgehen, indem sie die *Streptococcus pyogenes* (*Sp*)Cas9 Endonuclease in zwei Hälften teilten und in der Zelle das Holoenzym durch die trans-Spleißaktivität von Inteinen wieder rekonstituierten. Wir haben zuvor ebenfalls eine splitCas9 system entwickelt (Masterarbeit, C. Schmelas), um die kleinere Cas9 Orthologe von *Staphylococcus aureus* (*Sa*Cas9) in zwei Hälften zu teilen, wobei jede Hälfte klein genug ist um sie als dsAAV Vektoren zu verpacken. Hier zeigen wir experimentell, dass das dsAAV/split*Sa*Cas9 System abhängig von Zelltyp und Inkubationszeit bis zu 5-fach höhere Knock-out Effizienzen erzielt. Zusätzlich induziert dsAAV/split*Sa*Cas9 eine 2-fach erhöhte Mutageneserate einer Luziferasereporters in der Leber von Mäusen. Um die starke Expression des dsAAV/split*Sa*Cas9 Systems nach erfolgreicher Geneditierung zu begrenzen, erweiterten wir das System mit einem Selbst-Inaktivierungsansatz (SIN), welcher zuvor von Julia Fakhiri aus unserem Labor entwickelt wurde und die rAAV/CRISPR Technologie absichert.

Zuletzt konnten wir in einer Kooperation mit dem Niopek and Correia Labor zur Verbesserung des Sicherheitsprofil der CRISPR/Cas9 Orthologen von *Staphylococcus aureus* beitragen, die dazu den ersten Designer-Inhibitor entwickelten. Dazu nutzen sie den Breitband-Inhibitor AcrIIC1, der viele Cas9 Orthologe hemmt und modulierten dessen Bindungsoberfläche, um sie der *Sa*Cas9 HNH Domäne anzupassen. Wir demonstrierten in dieser Arbeit, dass der neue AcrX Inhibitor *Sa*Cas9 Aktivität an vielen genomischen Loci effizient hemmt und etablierten außerdem ein microRNA-basierten Schalter, um die *Sa*Cas9 Aktivität ausschließlich auf Hepatozyten zu begrenzen.

Zusammengefasst demonstriert diese Doktorarbeit die Kompatibilität und das große Potential bedeutender Gentherapie-Werkzeuge und präsentiert technologische Verbesserungen, welche in zukünftigen Arbeiten allein oder in Kombination genutzt werden können, um HBV Infektionen und HBV/HDV Koinfektionen effizienter und sicherer zu behandeln.

TABLE OF CONTENTS

LIST OF TABLES

LIST OF FIGURES

LIST OF ABBREVIATIONS

µg	Microgram
µl	Microliter
µM	Micromolar
AAP	Assembly-activating protein
AAV	Adeno-associated virus
AAVR	AAV receptor
Acr	Anti-CRISPR
Ad	Adenovirus
Adh	Adenoviral-helper plasmid
Ago	Argonaute
Bp	Base pairs
C	Celsius
Cas9	CRISPR associated protein 9
cccDNA	Covalently closed circular DNA
cDNA	Complementary DNA
CMV	Cytomegalovirus
CRISPR	Clustered regularly interspaced short palindromic repeats
crRNA	CRISPR RNA
dCas9	Dead Cas9
ddPCR	Droplet digital PCR
DMEM	Dulbecco's Modified Eagle Medium
DMSO	Dimethyl sulfoxide
DNA	Deoxyribonucleic acid
dNTP	Deoxynucleoside triphosphate
DR	Direct repeat
dsAAV	Double-stranded AAV
DSB	Double-strand break
dslDNA	Double-stranded linear DNA
E. coli	Escherichia coli
ELISA	Enzyme-linked immunosorbent assay
ER	Endoplasmic reticulum
FCS	Fetal calf serum
g	Gram
gDNA	Genomic DNA

GFP	Green fluorescent protein
gp41-1 intein	Split intein from DNA helicase, gp41 subunit
h	Hour
HBcAg	Hepatitis B core antigen
HBsAg (S-, M-, L-)	Hepatitis B surface antigen (small, medium, large)
HBxAg	Hepatitis B X antigen
HBV	Hepatitis B Virus
HCC	Hepatocellular carcinoma
HDAg (S-, L-)	Hepatitis D antigen (small, large)
HDV	Hepatitis D Virus
HEK	Human embryonic kidney cells
Hep	Hepatocyte
HIV	Human immunodeficiency virus
hNTCP	Human sodium taurocholate co-transporting peptide
HSPG	Heparan sulfate proteoglycan
Huh7	Human hepatoma cells
IFN	Interferon
indel	Insertions and deletions
ITR	Inverted Terminal Repeat
kb	Kilobases
kDA	Kilodalton
mA	Milliampere
min	Minute
miRNA	MicroRNA
ml	Milliliter
mM	Millimolar
mRNA	Messenger RNA
nCas9	Nickase Cas9
NES	Nuclear export signal
ng	Nanogram
NLS	Nuclear localization signal
nM	Nanomolar
NPC	Nuclear pore complex
Npu DnaE intein	Split intein from *Nostoc punctiforme* DNA Polymerase III DnaE subunit
NTCP	Sodium taurocholate co-transporting peptide

NUC	Nucleos(t)ide analogue
NUC lobe	Nuclease lobe
ORF	Open reading frame
PBS	Phosphate-buffered saline
PCR	Polymerase chain reaction
PD-1	Programmed cell death protein 1
PEI	Polyethylenimine
pgRNA	Pregenomic RNA
PI domain	PAM-interacting domain
qRT-PCR	Quantitative reverse transcription PCR
rAAV	Recombinant AAV
rcDNA	Relaxed circular DNA
REC lobe	Recognition lobe
RISC	RNA-induced silencing complex
RNA	Ribonucleic acid
RNAi	RNA interference
RNP	Ribonuleoprotein
rpm	Revolutions per minute
*Sa*Cas9	Cas9 from *Staphylococcus aureus*
scAAV	Self-complementary AAV
sgRNA	Single guide RNA
shRNA	Short hairpin RNA
SIN	Self-inactivating
siRNA	Small interfering RNA
*Sp*Cas9	Cas9 from *Streptococcus pyogenes*
ssAAV	Single-stranded AAV
SVP	Subviral particles
TGN	Trans-Golgi network
tracrRNA	Trans-activating CRISPR RNA
TRS	Terminal resolution site
UTR	Untranslated region
Vg	Vector genomes
VP	Viral proteins
WHO	World Health Organization
WT	Wild-type
YFP	Yellow fluorescent protein

1. INTRODUCTION

Viral hepatitis represents a leading cause of death and disability worldwide (section 1.1) and so far no curative treatments are available for hepatitis B (section 1.2) and, in particular, for hepatitis D (section 1.3). As cessation of conventional antiviral therapy is often associated with viral relapse and rebound of the disease, new curative therapy approaches are urgently needed. In this study, we combine the powerful RNAi (section 1.4) and CRISPR/Cas9 (section 1.5) technologies to tackle HBV infection and HBV/HDV co-infections. Recombinant Adeno-associated viral (rAAV) vectors are lead candidates for the delivery of the CRISPR/Cas9 and RNAi components in cell culture and *in vivo* (section 1.6). In non-dividing cells, rAAV vectors persist as stable episomes and mediate persistent transgene expression. While this is beneficial for applications that require long-lasting expression such as RNAi, safety concerns could arise from the continuous expression of Cas9 endonuclease. Several strategies that control Cas9 activity have been reported, including splitCas9 systems (section 1.6.3) and anti-CRISPR proteins (section 1.5.3). In this thesis, we build upon these approaches in order to contribute to efficient and safe applications of the CRISPR/Cas9 technology.

1.1. Viral Hepatitis represents a global health challenge

Hepatitis, an inflammatory state of the liver, is most commonly caused by infection with hepatitis virus A (HAV), B (HBV), C (HCV), D (HDV) or E (HEV). Acute hepatitis can resolve spontaneously within 6 months or progress to chronic hepatitis, occasionally leading to liver cirrhosis and/or hepatocellular carcinoma (HCC). With a growing world population, the mortality and morbidity rates for viral hepatitis increased substantially between 1990 and 2013, leading to the death of an estimated 1.45 million people each year [1]. This exceeds the numbers of deaths associated with any other infectious disease including tuberculosis, malaria and AIDS caused by the human immunodeficiency virus (HIV). In 2013, viral hepatitis was the 7th leading cause of death worldwide and therefore represents a major public health threat. To this end, the World Health Organization (WHO) urges countries to invest in eliminating hepatitis, aiming for a global reduction of 65% in hepatitis-related mortality and a reduction of 90% in new infections by 2030 [2].

While all viral hepatitis infections affect the liver, they differ in transmission route, epidemiology, clinical manifestation and treatment. HAV and HEV are transmitted via the

fecal-oral route and are epidemic in many low-income countries due to poor hygienic conditions. In most cases, HAV and HEV are self-limiting and only cause acute illness. An effective vaccination is available for HAV [3] and also for HEV in China [4].

By contrast, HBV, HCV and HDV are transmitted parenterally when blood or mucosa comes in contact with contaminated blood or body fluids. HBV and HCV infections account for the majority of hepatitis-related deaths with 47% and 48%, respectively, and vary between geographical regions (Figure 1). The highest prevalence of HCV-infected patients is found in developing regions of South America, Africa and Asia, where about 10% of the population are chronic carriers. The WHO estimates that more than 71 million people are chronically infected with HCV, representing about 1% of the world population [5; 6]. Infection with HCV leads to chronicity in about 70% of all cases frequently leading to cirrhosis and HCC [7]. While there is no vaccine available for HCV infection, recent advances in interferon-free treatment options via direct acting antiviral drugs (DAAs) are able to cure chronic hepatitis C with a sustained viral response of over 90% [8].

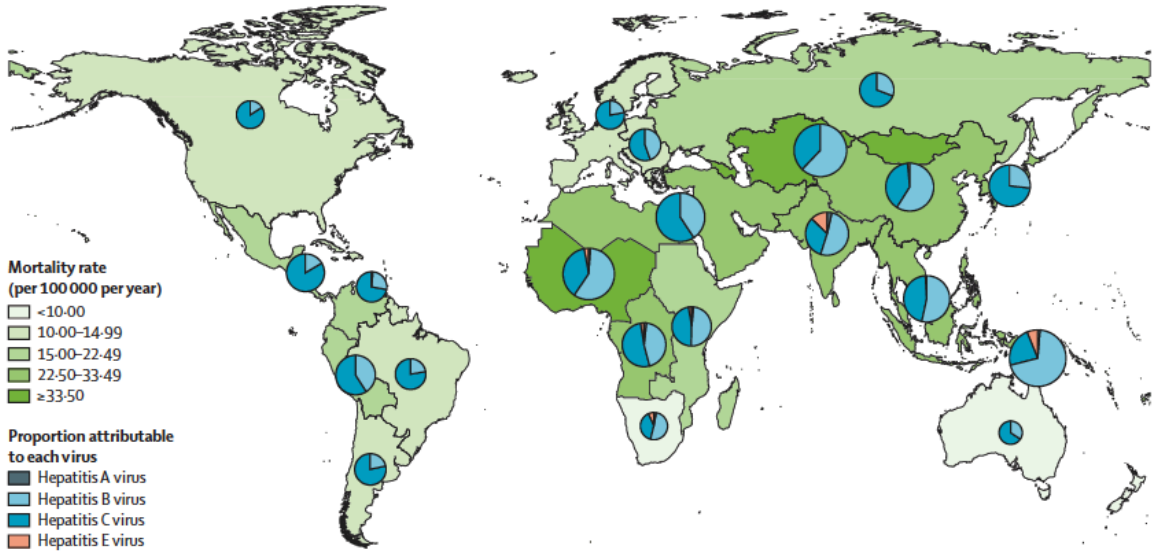

Figure 1. Map of hepatitis-related mortality rate.

Intensity of green color indicates the extent of mortality per 100 000 people per year. Pie charts indicate the contribution of each hepatitis virus to the total hepatitis-related mortality. HDV is not included in this representation. Figure from Stanaway *et al*. (2016) [1].

On the other hand, chronic hepatitis B affects up to 10% of the sub-Saharan African and East Asian population. Worldwide, more than 257 million people, representing 3.5% of the world population, are chronically infected with HBV [5; 6]. HBV is mostly self-limiting

and leads to chronic states in only 5% of infected patients. However, children commonly develop a more severe and chronic hepatitis B. Indeed, about half of the chronically infected patients were infected perinatally or during early childhood with HBV [9]. Furthermore, HDV is a satellite virus of HBV and requires its co- or superinfection, as it is dependent on the HBV surface (HBs) antigen. Chronic HBV/HDV co-infection leads to the most severe progression of virally induced liver disease [10]. Although a vaccine against HBV is available that is also effective against HDV, some individuals are non-responders and unable to develop anti-HBs antibodies. Moreover, HBV could mutate in vaccinated patients and escape the immunization acquired by vaccination [11]. In contrast to hepatitis C, there is no curative treatment available for hepatitis B or D. Current treatment options, based on interferon (IFN) and nucleos(t)ide analogues (NUCs), control viral replication and delay disease progression [12; 13]. However, cessation of antiviral therapy is often associated with virological relapse and rebound of the disease [14]. Given the global burden of viral hepatitis and the lack of curative treatments, new curative therapy approaches are urgently needed for hepatitis B and D in particular.

1.2. Hepatitis B Virus

HBV is classified as the type species of the genus *Orthohepadnavirus* that in turn is part of the *Hepadnaviridae* family. Natural hosts are humans and other great apes, such as orangutans, gibbons, gorillas and chimpanzees. The high species-specificity of HBV hampers research on its life cycle, as common laboratory animals, such as mice, rats or macaques, are not susceptible for HBV infections. Also, for a long time, primary human hepatocytes have been the only suitable *in vitro* model, since cultured human cell lines are inherently not susceptible for HBV infections. In 2012, the research field flourished with the identification of the HBV entry receptor, the sodium taurocholate co-transporting peptide (NTCP) [15; 16] and experiments in otherwise unreceptive human cell lines became possible with the overexpression of human NTCP. Nonetheless, HBV infections require the addition of dimethyl sulfoxide (DMSO) and polyethylene glycol 8000 (PEG) to the media to enhance infectivity in cell culture systems [17-20].

Furthermore, the use of surrogate models, such as duck hepatitis B virus (DHBV) or woodchuck hepatitis virus (WHV) enabled research in lower species, and the development of HBV-transgenic mice [21-23] or the delivery and expression of HBV via hydrodynamic injection of plasmid DNA [24], Adenoviral (Ad) [25] or rAAV vectors [26; 27], enable the reconstruction of the viral life cycle at least partly. However, animal models

with authentic antiviral immune reactions that mirror the disease in human patients are still lacking and hamper the development of novel treatments.

1.2.1. Structure and genome organization

The infectious hepatitis B virion, also called Dane particle, is 42 nm in diameter and consists of a viral DNA genome, an icosahedral nucleocapsid and an outer lipid envelope (Figure 2A). The membrane envelope derives from the host cell´s endoplasmic reticulum (ER) and harbors the HBV surface antigen (HBsAg) that comprises the small (S-HBsAg), medium (M-HBsAg) and large (L-HBsAg) variants. The lipid envelope encloses the nucleocapsid that consists of the core protein, the main structural protein of HBV [28]. The capsid encompasses the partly double-stranded DNA genome that maintains a relaxed circular conformation (rcDNA) within the virion (Figure 2B). The genome spans 3.2 kb for the full-length minus strand and about two thirds of the size for the short plus strand [29].

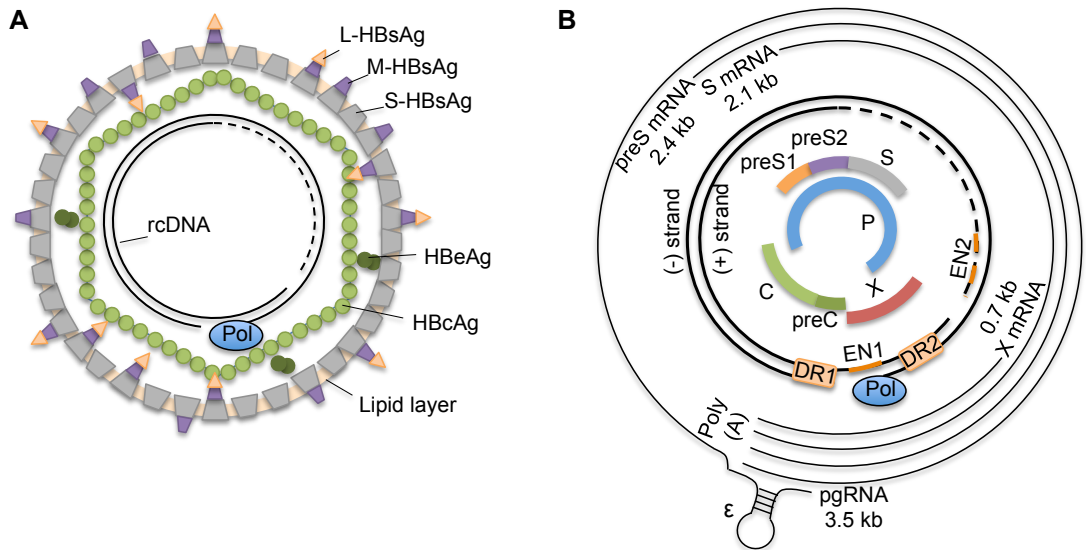

Figure 2. Structure and genome organization of HBV.

A) Schematic view of infectious HBV virion (Dane particle). The HBV rcDNA is covalently linked to the viral DNA polymerase via a tyrosyl-DNA phosphodiester bond [30]. The nucleocapsid consists of HBcAg and the envelope harbors the three surface antigen variants. **B)** Overview of HBV genome. The rcDNA consists of the complete minus-strand and incomplete plus-strand (dashed lines) and encodes four overlapping ORFs (C, S, P and X). Further regulatory elements such as the four promoters (C, preS1, S and X), two enhancers (Enh1, Enh2), encapsidation signal (ε) and replication signals (DR1, DR2) are also encoded within the ORFs. The rcDNA gives rise to three subgenomic RNAs (preS, S and X mRNA) and the pregenomic RNA that serves as mRNA for translation of the precore, core protein and polymerase. All viral transcripts share the same polyadenylation site and are 5´ capped and 3´ polyadenylated. Illustration in B was adapted from Tong & Revill (2016) [31].

The HBV genome encodes four partially, sometimes even completely overlapping ORFs. The largest ORF encodes the 90 kDa, 838 aa viral polymerase that consists of i) a terminal protein (TP) that binds the 5´ end of the rcDNA, ii) the reverse-transcriptase/polymerase domain that generates the minus strand of the DNA genome from an RNA intermediate and subsequently uses the minus strand as template for plus strand synthesis, and iii) an RNase H domain that degrades the RNA intermediate during synthesis of the minus DNA strand [32].

Another ORF encodes the precore (HBeAg) and core protein (HBcAg). The core protein is 21 kDa in size and forms homodimers that built up the nucleocapsid [33]. The precursor HBeAg consists of the entire core protein and a further N-terminal extension that harbors a signal for ER translocation. As a consequence, it is further cleaved proteolytically at the N- and C-termini to give rise to the 16 kDa HBeAg and secreted into the serum. Although its function is not clearly understood, it serves as an indicator of active viral replication [34]. It has been suggested that HBeAg is involved in a complex modulation of the host immune response upon HBV infection [35; 36]. HBcAg, HBeAg and polymerase are expressed from the core promoter. Thereby, the ribosome occasionally omits the initial start codon for the core protein and commences elongation on the downstream start codon of the polymerase. The core protein is expressed at much higher rates compared to the polymerase, which reflects the demand of the viral particle for 120 core-dimers relative to a single molecule of polymerase.

The S-, M- and L-HBsAg variants are encoded by the preS/S ORF. The S-HBsAg is 24 kDa in size and its C-terminal region is shared among all HBsAg variants [37]. The M-HBsAg consists of the S-HBsAg sequence and is further extended on the N-terminus, which is called the preS2 region. Whereas S- and M-HBsAg share the same promoter, translation is initiated at a downstream or upstream start codon, respectively. The L-HBsAg is expressed via its own mRNA transcript from the preS1 promoter. It contains the S-HBsAg, the preS2 sequence and a further N-terminal extension, which is called the preS1 sequence. The shared C-terminal region of the small antigen comprises four trans membrane (TM) domains that anchor all HBsAg variants to the ER membrane upon synthesis. Once the nucleocapsid gets enveloped on the ER membrane, it incorporates all HBsAg variants. Only the L-HBsAg is able to translocate between the inside and outside of the ER membrane [38]. When the N-terminal preS1 region faces the cytosol, the L-antigen binds to the nucleocapsid and mediates envelopment. Outward-facing preS1 of the L-antigen is essential for viral entry of hepatocytes as it contains the receptor binding region of HBV entry receptor, NTCP [15].

Besides the infectious Dane particles, also non-infectious subviral particles (SVPs) are released into the serum of infected patients that miss the nucleocapsid and consist mainly of the S-HBsAg, as well as M- and L-HBsAg in minor amounts [39]. The SVPs are released in great abundance and reach up to a 10.000-fold higher concentration compared to the Dane particle in the serum of infected patients. The biological function of SVPs is still a matter of debate, but they seem to impair the humoral and cellular immune response to HBV [40].

The last ORF encodes the X antigen (HBxAg), which is the only regulatory protein encoded by HBV. The HBxAg is 17 kDa in size and transcribed from the X promoter. Studies in primary human hepatocytes and mice with humanized livers showed that HBxAg-deficient HBV mutants were not able to replicate the viral genome [41; 42]. Only restoration of HBxAg expression reconstituted viral replication. Additionally, HBxAg is generally associated with the development of HCC [43].

1.2.2. HBV life cycle

The HBV life cycle (Figure 3) commences with its entry into hepatocytes via a two-step mechanism that involves an initial loose and reversible binding to heparin sulfate proteoglycans (HSPG) [44] and a subsequent highly specific attachment of the L-HBsAg preS1 region to the NTCP receptor [15]. HBV enters the cells via clathrin-dependent endocytosis in primary human hepatocytes [45] or caveolin-1-dependent endocytosis in HepaRG cells [46], but the precise mechanism remains unclear. The nucleocapsid is transported to the nucleus via microtubules and translocated via a nuclear localization signal (NLS) that is located on the C-termini of the core protein [47]. The nucleocapsid disintegrates at the nuclear pore complex (NPC) and releases the HBV genome as rcDNA into the nucleoplasm [23; 48].

The covalently closed circular DNA (cccDNA) represents the transcriptionally active conformation of the viral genome, which is only established after nuclear entry by host cell factors [49] and further epigenetically modified by host histone methylases, acetylases and kinases [50-52]. The cccDNA gives rise to subgenomic and pregenomic (pg)RNA transcripts by using the host cell RNA polymerase II and hepatocyte-specific factors, such as the hepatocyte nuclear factors (HNF) 1, 3 and 4 that contribute to the cell-type specific infection of HBV [53; 54]. Subsequently, the viral transcripts are exported and translated in the cytoplasm in order to produce the HBV proteins.

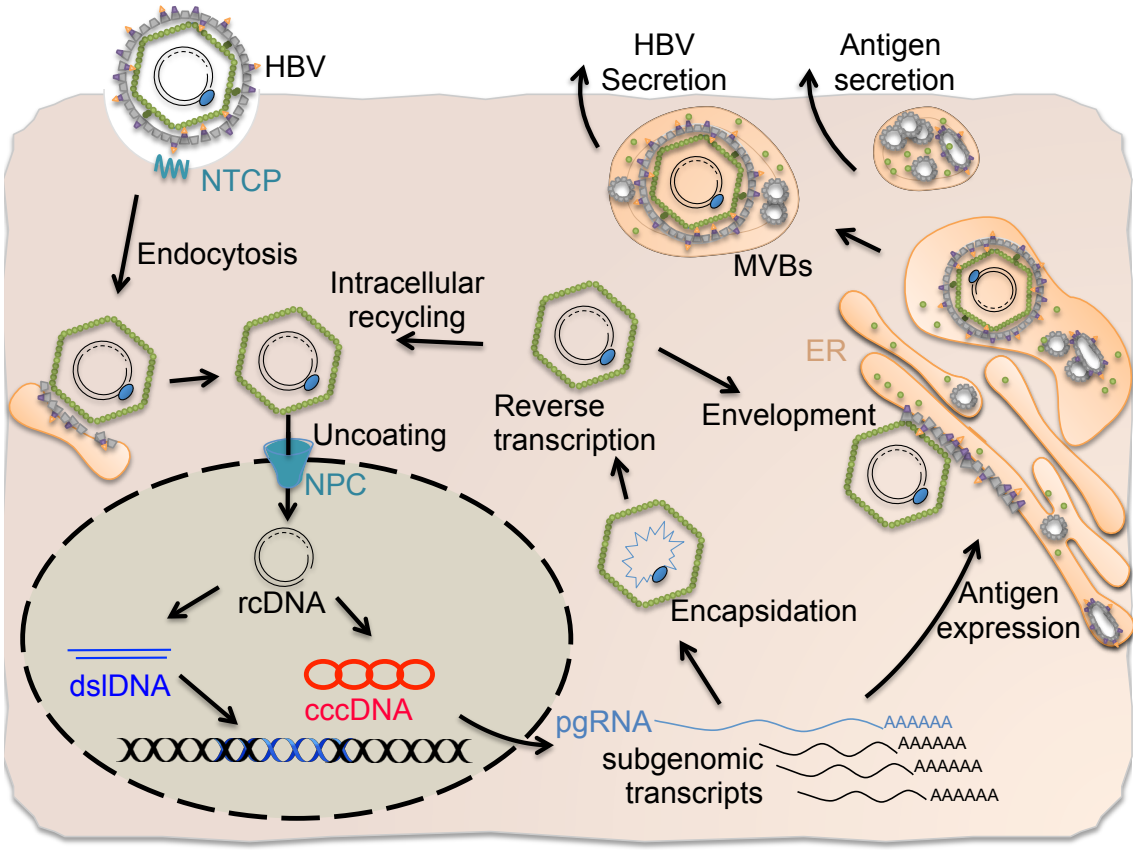

Figure 3. Schematic overview of HBV life cycle.

HBV enters the cell via the hepatocyte-specific NTCP receptor. The nucleocapsid is translocated to the nucleus and releases the HBV genome into the nucleoplasm in form of rcDNA. Host factors are involved in the formation of cccDNA that persists in the cell as minichromosome. *In situ* priming of the plus-strand can lead to the formation of double-stranded linear DNA (dslDNA) that can integrate into the host genome genome with low frequencies of 1 in ~10^5–10^6 infected cells [55; 56] and may contribute to the development of HCC and the continuous production of antigens [57]. Viral proteins are expressed in the cytoplasm and pregenomic (pg)RNA is encapsidated into the nucleocapsid, where reverse transcription of pgRNA to rcDNA occurs. Mature nucleocapsids can be reimported to replenish the pool of cccDNA or enveloped at the ER membrane and secreted. Illustration contains art from smart.servier.com

The pgRNA also serves as template for reverse transcription of the viral DNA. As the transcript is longer than its genome, it contains a redundant copy of its termini and comprises a second encapsidation ε and replication DR1 signal. The binding of the viral polymerase on ε at the 5´ end of the pgRNA triggers encapsidation of the ribonuleoprotein (RNP) complex by the core protein. Reverse transcription occurs in the nucleocapsid and is initiated by the TP domain of the viral polymerase. The minus strand is synthesized commencing from the DR1 region, followed by plus-strand synthesis from the DR2 region in a complex, discontinuous manner [58; 59].

The mature nucleocapsid particle containing the rcDNA can be re-imported into the nucleus to replenish the cccDNA pool or can be enveloped on the ER membrane and secreted, depending on the amount of intracellular surface protein [60]. In early stages of the infection, nucleocapsids are recycled for the intracellular amplification of cccDNA. In later stages of the infection, L-HBsAg in the ER membrane binds to the nucleocapsid and mediates envelopment [61]. The enveloped nucleocapsid is secreted via the endosomal sorting complex required for transport (ESCRT) pathway and multivesicular bodies (MVBs) [62]. In contrast, SVPs can be secreted by the secretory pathway via the ER-Golgi intermediate compartment (ERGIC) [63] and also via MVPs [64].

1.3. Hepatitis Delta Virus

Hepatitis delta virus (HDV) is the only member of the genus *Deltavirus* and not assigned to any family [65]. It is a virusoid and subviral satellite of HBV, as it needs the HBV surface antigens to form infectious particles [66]. Currently, roughly 5% of chronic HBV carriers are also chronically infected with HDV, representing about 15 to 20 million people worldwide [67]. Hepatitis D can manifest either via simultaneous coinfection of HBV and HDV or via HDV superinfection of a chronic HBV carrier. Whereas the coinfection is mostly self-limiting and progresses to chronic hepatitis D with the same rates as HBV monoinfection, i.e. less than 5% in adults, the superimposed HDV infection leads to chronic hepatitis D in about 80% of the cases [68]. Hepatitis D in combination with hepatitis B is the most severe form of viral hepatitis and leads to a greater probability of acute liver failure, a rapid progress to cirrhosis and HCC, and a high fatality rate [69]. Although vaccination against HBV is also effective against HDV, the current 240 million people already suffering from hepatitis B cannot be protected from an HDV superinfection.

1.3.1. HDV structural organization and life cycle

The hepatitis delta virion measures 35 to 37 nm in diameter and harbors a closed circular, single-stranded, negative-sense RNA genome of about 1672 to 1697 nt depending on genotype (Figure 4A). The genomic sequence has a high CG content and is mostly self-complementary (~74%) leading to a partially double-stranded RNA structure [70]. About 200 molecules of the small (S-) and large (L-) hepatitis delta antigen (HDAg), bind to the RNA genome and form the viral RNP complex. The RNP complex is

enveloped at the host cell membrane and subsequently harbors the small, medium and large HBV surface antigens in its outer coat. The HDV genome comprises a single ORF that leads to the synthesis of the 24 kDa S- and 27 kDa L-HDAg (Figure 4B). As the N-terminal sequence of both antigens is identical, small and large antigens only differ in a 19 aa C-terminal extension for the L-HDAg [71].

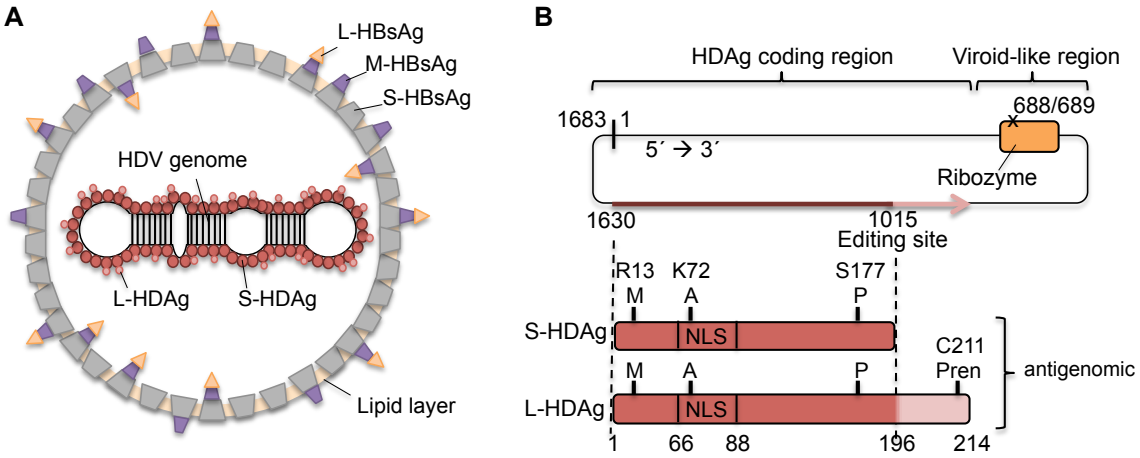

Figure 4. Schematic overview of HDV structure and genomic organization.

A) The HDV virion comprises a closed-circular, negative-sense RNA genome that binds hundreds of small and large HDAgs. The genome is highly self-complementary and enveloped by host-derived membrane containing the HBV surface proteins (S-, M-, L-HBsAgs). **B)** The ORF of HDAg is located on the complementary antigenome. During replication, the host cell enzyme ADAR1 edits the amber stop codon (UAG) of the S-HDAg at amino acid position 196 to a tryptophan codon (UGG), which enables the expression of L-HDAg [72; 73].

As HDV employs the same envelope proteins as HBV, both viruses share the same hepatotropic nature and similar entry mechanisms. An initial binding of the L-HBsAg to HSPGs on the hepatocyte surface mediates HDV attachment [74; 75]. Subsequently, HDV can enter the cell via binding of the myristoylated N-terminal binding site of the L-HBsAg preS1 domain to the NTCP receptor [15; 16]. Whether HDV enters via endocytosis or direct membrane fusion remains unclear. Nonetheless, the RNA complex is released into the cytosol and transported to the nucleus via the NLS signal in the HDAg [76; 77]. HDV replication and mRNA synthesis take place in the nucleus via the host cell RNA polymerase II [78] and RNA polymerase I [79]. Three forms of RNA are made comprising the circular genomic RNA, circular complementary antigenomic RNA and a linear polyadenylated, antigenomic RNA encoding the HDAg. Replication is catalyzed via a double rolling-circle mechanism of RNA synthesis of genomic and antigenomic RNA [80]. The generated RNA multimers are cleaved into monomers by the ribozyme activity

embedded in the genomic and antigenomic RNA sequence [81]. The monomers are subsequently ligated to form circular RNA.

The antigenomic RNA is exclusively located in the nucleus and encodes the HDAgs. In order to enable translation of the HDAgs, a 5´-capped and 3´-polyadenylated mRNA of about 0.8 kb is produced by RNA polymerase II and subsequently exported and translated in the cytoplasm [82; 83]. The S-HDAg is predominantly produced in early stages of infection and plays a supporting role in viral replication [84]. In contrast, the L-HDAg is produced in later stages of infection and acts as a direct inhibitor of viral replication and is required for assembly of viral particles [85-87]. In its C-terminal extension, the L-HDAg contains a nuclear export signal (NES) [88], a binding motif for the HBV surface antigens [89] and a prenylation site [90]. The host cell farnesyltransferase covalently links a farnesyl moiety to the prenylation site in the L-HDAg and thereby contributes to the inhibition of HDV RNA replication, the binding to the HBV surface antigens and the envelopment of the RNP complex [91; 92]. Finally, the HDV genome, but not the complementary antigenome, is assembled into HDV and released either via the classical secretory pathway or via multivesicular bodies.

The presence of the HBV surface antigens is required to form an infectious HDV particle, therefore assembly of HDV can only occur in HBV co-infected cells. However, defective HBV genomic integrates that still express the self-assembly-competent HBV surface proteins suffice to spread progeny HDV [93].

1.4. Antiviral therapy based on RNA interference

Current therapeutic options to treat chronic hepatitis B include immune modulators, such as conventional and PEGylated IFNα, as well as NUCs, such as tenofovir and entecavir, that inhibit the reverse transcriptase activity of the HBV polymerase. Although these medications control viremia and reduce liver inflammation in up to 75 or 80% of all patients [94], respectively, they barely affect cccDNA levels or viral antigen production and thus lead to a high relapse rate after discontinuation of even long-term treatment [95]. Available treatment for chronic hepatitis D is even more restricted, since HDV only encodes the delta antigen and otherwise relies strongly on host cellular factors, which provide only few therapeutic targets. Clinically approved HBV RT inhibitors do not interfere with HBsAg secretion and thus have no effect on HDV. Accordingly, current treatment options are limited to IFNα. Chronic hepatitis D can be treated in only 20 % of

all patients and reappears in about half of the successfully treated patients in long-term follow-up studies [96].

Several new medications against hepatitis B that are also effective against hepatitis D are under investigation in clinical trials, which directly target HBV infection at various steps of the life cycle including inhibition of viral entry (NTCP inhibitors like Myrcludex B), capsid assembly, HBsAg secretion [97; 98] and RNA interference (RNAi) mediated silencing of viral transcripts [99]. The latter approach seems to be especially attractive, since it enables the targeting of the pathogen directly without interfering with other cellular host factors.

1.4.1. The mechanism of RNA interference

RNA interference is a biological process that harnesses small RNA triggers to regulate gene expression post-transcriptionally. These small, roughly 20 to 30 nt non-coding RNAs bind to target mRNA by complementary base-pairing and initiate translational repression or degradation (Figure 5). Two major types of RNA molecules can be distinguished: microRNAs (miRNAs) that are of endogenous origin and small interfering RNAs (siRNA) that typically describe exogenous synthetic or viral inducers of RNAi [100].

MicroRNAs are genomically encoded either by non-protein coding transcripts or within introns of coding genes. Almost all eukaryotes possess miRNA and the associated processing pathways to regulate gene expression in a cell-type-specific manner. In humans, more than 1000 miRNAs are known that regulate at least 30 % of our genes [101]. MicroRNAs are transcribed as a primary miRNA (pri-miRNA) that is at least 1000 nt long and contains single or clustered hairpins as well as single-stranded 5´ and 3´ extensions [102]. These transcripts are further processed in the nucleus by the microprocessor complex consisting of Drosha, an RNase III enzyme, and DiGeorge syndrome critical region gene 8 (DGCR8), a protein that binds dsRNA [103]. The resulting pre-miRNAs are about 70 nt long, harbor a stem-loop structure and are exported by the RanGTP dependent dsRNA-binding protein Exportin-5 [104]. In the cytosol, Dicer processes the mature miRNA by trimming the RNA to a double-stranded, 21 to 25 nt long strand that consists of a guide strand that is complementary to the mRNA target sequence and a passenger strand. The mature miRNA is loaded into the RNA-induced silencing complex (RISC) that comprises at least Dicer, Argonaute (Ago) and TAR RNA binding protein (TRBP) [105].

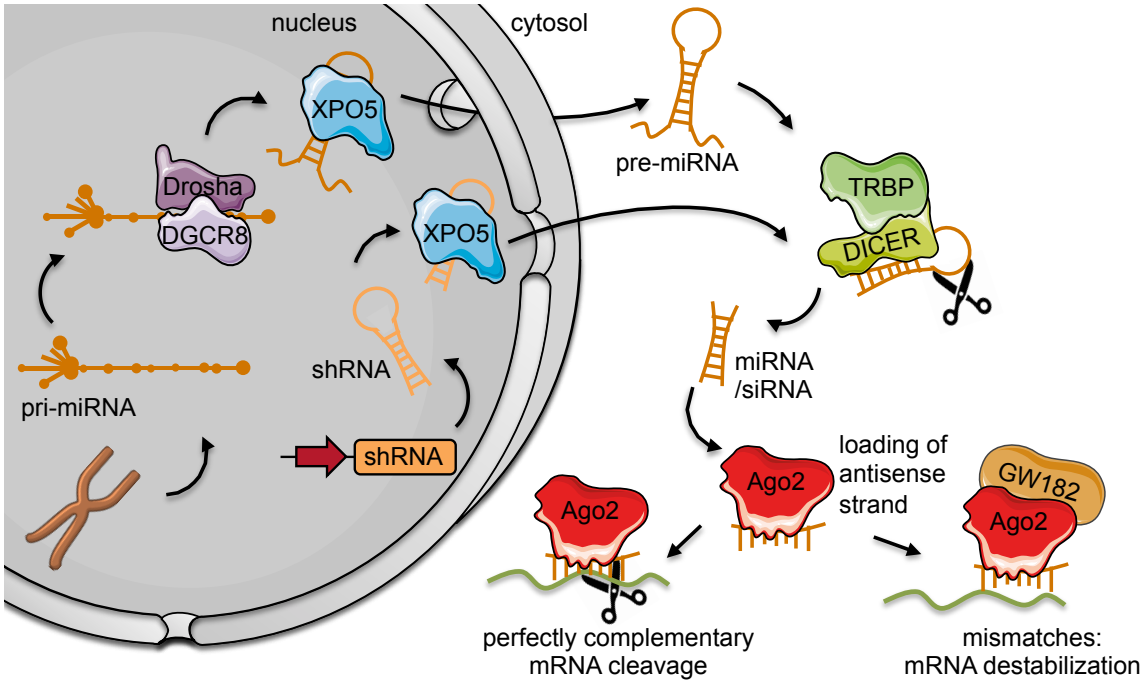

Figure 5. Schematic overview of the RNAi pathway.

MicroRNAs (miRNAs) are encoded in the genome and processed via Drosha and DGCR8, while short-hairpin RNAs (shRNAs) are expressed from a DNA template. Pre-miRNA and shRNAs are exported from the nucleus to the cytosol via Exportin-5 and further processed by TRBP and Dicer. Association with Ago2 forms the RNA-induced silencing complex (RISC) and induces loading of the antisense strand. Binding of siRNA/miRNA to the target mRNA via a perfect match leads to mRNA cleavage, whereas an imperfect targeting mediates mRNA destabilization. Illustration contains art from smart.servier.com

Within RISC, the passenger strand is removed and the guide strand remains bound to Ago and is directed to the complementary mRNA target. The seed region of the guide strand that comprises nucleotides 2-6 mediates binding to the target. If the sequence is perfectly complementary to the target, Ago2 (one of four human Ago proteins) can cleave the mRNA target [106]. In animals, the binding between miRNA and mRNA is mostly characterized by mismatches, which results in translational repression through inhibition of translation initiation and deadenylation and subsequent degradation of mRNA [107; 108].

The endogenous RNAi pathway can be easily harnessed for biotechnological and therapeutical applications by introducing a synthetic dsRNA of roughly 21 nt into the cell [109]. These RNAs are termed siRNAs and are designed to be perfectly complementary to the target mRNA sequence and thus initiate Ago2-mediated target cleavage. In contrast, short-hairpin (sh) RNAs are encoded on a DNA template and can be expressed by RNA polymerase III promoters, such as the U6, 7SK, H1 and tRNA promoters [110], as well as polymerase II promoters that permit cell-type specificity [111]. Upon transcription, the RNA

self-anneals via its complementary sequence and forms a hairpin structure. Akin to miRNAs, shRNAs are exported by Exportin 5 and processed by Dicer that eliminates the passenger (sense) strand. Subsequently, the guide (antisense) strand that is complementary to the designated mRNA target is loaded into RISC to mediate knock-down. As siRNAs or shRNAs can be easily adapted to any mRNA target by customizing their 21 nt sequence, high-throughput screens to probe gene functions on a whole genome scale [112; 113] and applications in the combat against gain-of-function autosomal dominant diseases, cancer and infectious diseases became feasible [114].

1.4.2. Therapeutic RNAi against HBV and HDV

Two approaches to combat HBV infections via RNAi were previously suggested, including i) the direct targeting of viral transcripts or ii) the inhibition of host cell factors that are important for viral entry, replication and release [115] or are involved in subsequent liver failure [116; 117]. Directly targeting HBV and/or HDV transcripts has the advantage that endogenous factors and pathways, besides the RNAi machinery itself, remain unaffected. In most studies that apply the RNAi machinery against HBV, the viral transcripts were directly targeted [118]. This seams reasonable, since viral transcripts serve as template for antigen production and replication intermediates. As the HBV genome has highly overlapping ORF and viral transcripts share the same 3´end and polyadenylation site, a single RNAi effector molecule could in principle inhibit the synthesis of all viral antigens and inhibit viral replication, simultaneously [99; 119].

Of particular interest is the previously suggested implication that RNAi therapeutics might be able to restore the anti-HBV immune response by inhibiting the excessive secretion of HBV antigens [120] that is known to skew an adequate immune reaction against the pathogen [121; 122]. Accordingly, although HBV is able to infect virtually the whole liver [123], studies from HBV transgenic mice suggested that efficient RNAi in a limited number of hepatocytes already suffice to clear the infection [120], as a restored host immune system might synergistically contribute to viral clearance [124-126].

In constrast to the abundance of studies that previously used RNAi to target HBV, only a single study employed this powerful technology to target plasmid-encoded HDV [127] and another bioinformatical paper suggested a potential design of siRNA to concurrently target various HDV genotypes [128]. However, as of yet studies are missing that investigate

therapeutic RNAi approaches against infectious HDV and, all the more, against HBV/HDV co-infections.

A drawback in targeting HBV and HDV directly via RNAi could be a high rate of viral escape, as viruses, in particular RNA viruses, have a high mutation rate and even develop quasispecies within an individual host. It is likely that an existing mutation within the virus rapidly becomes the dominant species within the host, when placed under selection pressure by the introduction of RNAi treatment. Indeed, several reports confirmed that many viruses could generate RNAi escape mutants, including HAV [129], HBV [130], HCV [131], HIV [132; 133], poliovirus [134] and possibly also HDV due to its high rate of mutation [135]. One strategy to efficiently counteract viral escape is a concept termed combinatorial RNAi (coRNAi) that describes the co-expression/ multiplexing of several RNAi effector molecules, against multiple viral and/or cellular targets [136; 137]. Targeting several conserved viral sequences simultaneously could minimize the chance of escape mutants. Indeed, it has been shown that the combination of two to six RNAi effector molecules provides an additive effect on single and multiple gene knockdowns in various hosts [138-143].

1.4.3. Towards safer RNAi therapeutics

Here, we raise a note of caution about possible cytotoxic effect and reported fatality in mice and many other species by high levels of shRNA expression [144-148]. These reports suggest that overexpression of shRNAs overwhelms the RNAi machinery and results in dysregulation of endogenous miRNAs. The reduction of shRNA expression, e.g. by weaker promoters or lower dosages, can limit toxic effects but might lead to a less efficient RNAi based therapy [149]. Further attempts to counteract cytotoxicity include the overexpression of rate-limiting cellular factors, such as Ago2 and Exportin 5 [150-152] or the integration of a specific RNAi effector into an endogenous miRNA locus in order to drive cell-type-specific expression at appropriate levels [153].

Further drawbacks of current RNAi technology include off-target effects that impact the expression of non-targeted genes. Off-targeting can occur and is difficult to prevent if the sequence of siRNAs/shRNAs resembles mRNA transcripts, due to the nature of the RNAi pathway to degrade or destabilize mRNA targets even when mismatches are present [154; 155]. Therefore, various software tools have been developed to evaluate the sequence specificity of the designed siRNA [156]. Unintended perturbation of gene

expression can also occur by the occasional loading of the sense strand, instead of the intended antisense strand, into RISC [157; 158]. Strand selectivity seems to be dependent on the 5´-thermodynamic stability of the antisense strand with a preference for lower internal stability [159], 5´-nucleotide identity, duplex structure of the seed region and competitive Ago2 binding on either strand [160]. Regardless of the actual mechanism of strand selectivity, co-delivered tough decoy (TuD) RNAs can reduce sense strand activity of vector-encoded shRNAs [161; 162]. TuD RNAs consist of two antisense strands connected by a loop sequence that act as sponges for the sense/passenger strand of the dedicated and co-delivered shRNA (Figure 6). The use of TuD RNAs in HBV-transgenic mice reduced side effects of the sense strand on unintended off-target genes and also increased the desired antiviral activity of an shRNA that was directed against the HBx region [163].

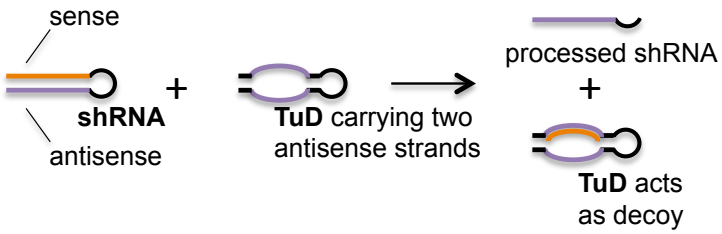

Figure 6. The principle of tough decoy (TuD) RNAs.

Sense strands of a designated shRNA are occasionally loaded into RISC and mediate off-targeting. TuD RNAs consist of two antisense strands that match the respective shRNA. Accordingly, TuD RNAs act as decoy to restrict the presence of free sense strands and limit their off-target acitivity.

Despite the recent advances in RNAi technology and the various approaches to enhance safety, RNAi remains ineffective against HBV cccDNA reservoirs and integrated derivatives as it acts on the RNA level. Thus, an alternative or additional tool for gene therapy is urgently needed to directly tackle the HBV genome.

1.5. Antiviral therapy based on CRISPR/Cas9

A new striking toolkit for precise genome engineering emerged with the discovery of the microbial adaptive immune system CRISPR (clustered regularly interspaced short palindromic repeats), which can be repurposed to edit virtually any genomic locus in a variety of model systems including mammalian cells. Compared to RNAi, the CRISPR

system solely depends on a single effector protein, the Cas (CRISPR-associated gene) 9, and a guide RNA sequence that can be likewise adapted to virtually any designated target locus. The major difference of the conventional CRISPR system and RNAi is the preference for DNA targets that results in the knock-out of the designated gene.

The CRISPR system is currently tested in clinical trials to fight several cancer types by knocking out PD-1 in T-cells *ex vivo* before re-administration to the patient [164]. Furthermore, its use *in vivo* is evaluated in a clinical trial that is applied by subretinal injection of an rAAV5 vector that expresses the CRISPR system, in order to correct a point mutation in the CEP290 gene that is responsible for an inheritable blindness called Leber congenital amaurosis (NCT03872479).

Adding to the long list of possible CRISPR applications, its use in antiviral therapies became a major research field and enabled scientists to target many incurable chronic viral infections in model systems [165]. Especially, HBV with its reservoirs of cccDNA and its genomic integrates that neither can be targeted with current therapeutic approaches nor with RNAi became susceptible with this new gene editing tool for the first time. Furthermore, as Cas9 and guide RNA are introduced into the cells exogenously, the CRISPR system remains independent of endogenous pathways that could cause cytotoxicity upon oversaturation. Considering these advantages, an abundance of studies utilized the CRISPR system to tackle HBV infection (summarized in Supplementary Table 1).

1.5.1. The CRISPR/Cas9 mechanism

The CRISPR system is a naturally occurring RNA-guided immune system found in bacteria and archaea that confers an adaptive, sequence-specific resistance to exogenous genetic material, such as viruses [166]. The CRISPR system can be divided in two classes according to different Cas effector proteins. While class 1 comprises multiple Cas proteins that form a complex in order to target and degrade foreign DNA, class 2 uses a single large protein for the same purpose [167]. Both classes use CRISPR RNAs (crRNAs) to mediate target recognition by complementary base pairing. Due to its modest requirements, class 2 is the best-studied CRISPR/Cas system and the most promising tool for genome engineering so far. Class 2 can be further divided into type II, V and VI comprising Cas9, Cpf1 and Cas13 effector proteins, respectively, which are characterized by a variety of different features. For reasons of simplicity, in the following

section, the mechanism and possible applications of the type II CRISPR/Cas9 system will be further discussed.

The Cas9 endonuclease is activated by the binding of two RNAs, the crRNA and trans-activating crRNA (tracrRNA). The first roughly 20 nt of the crRNA define the target specificity and the tracrRNA serves as a scaffold for Cas9 binding (Figure 7). The tracrRNA is highly complementary to itself and forms two to three stem loops (depending on the CRISPR ortholog). Furthermore, the tracrRNA and crRNA can to form an RNA duplex that is referred to as guide RNA [168]. The crRNA sequence is the only component of the system that needs to be adapted in order to direct Cas9 to a specific site of a double-stranded DNA substrate [169].

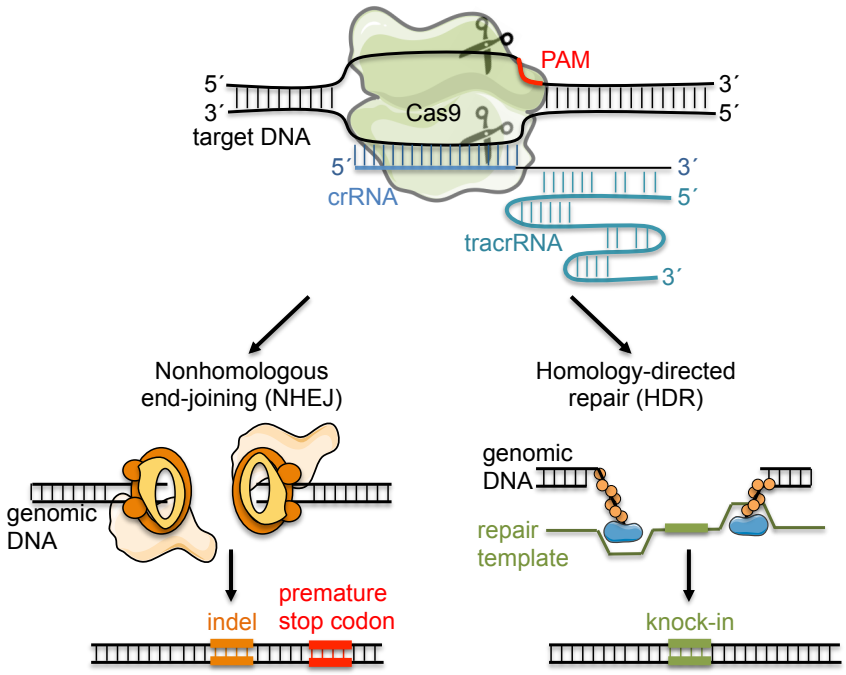

Figure 7. Schematic overview of the CRISPR/Cas9 mechanism.

Cas9 is directed to a designated target locus adjacent to a protospacer adjacent motif (PAM) by a target-complementary crRNA that is hybridized with the tracrRNA. Upon binding, Cas9 induces a double-strand break (DSB) at the target locus. The DSB is repaired by endogenous mechanisms, such as non-homologous end-joining and homology-directed repair, that in some instances induce mutations that lead to gene knock-out or insertions of DNA template sequences that lead to knock-in, respectively. Illustration contains art from smart.servier.com.

Furthermore, the crRNA:tracrRNA duplex can be fused to form a chimeric single guide RNA (sgRNA) by an artificial loop that mimicks the secondary structure in its hybridized state [169]. Once activated, Cas9 is directed to the designated target sequence and induces a DSB by two distinct active sites, the RuvC and HNH domain.

Mammalian cells employ genomic repair mechanisms to fix the induced DSB including homology-directed repair (HDR) and, in the absence of a homologous DNA template, non-homologous end joining (NHEJ) [170; 171]. According to the double Holliday junction model, the MRN complex (Mre11, Rad50, Nbs1) binds to damaged DNA on either side of the break and recruits further proteins that create 5´ and 3´ overhangs [172]. In the case of HDR, Rad 51 is recruited to the site of the DSB, recognizes DNA sequences that resemble the single-stranded 3´ overhang and invades the recipient DNA duplex [173]. The DNA polymerase uses the homologous DNA as repair template in a cross-shaped structure called Holliday junction. This process can be exploited for precise genome editing by providing the CRISPR/Cas9 system with a DNA repair template. In contrast, in the process of NHEJ, microhomologies within the single-stranded overhangs lead to the direct ligation of the DNA strands. This process is error-prone and can lead to the formation of insertions and deletions (indels), subsequent frame-shifts and the knock-out of a target gene [174].

Further advances in CRISPR/Cas9 technology fostered its development as the leading tool for genetic engineering. First of all, the co-expression of several sgRNAs in a single cell enables multiplexed genome editing that facilitates the deletion of large DNA fragments from the designated target gene or the concurrent knock-out of several genes [175]. Secondly, single point mutations in the RuvC and HNH domains inactivate their respective catalytic sites. Whereas a single mutation results in Cas9 nickases (nCas9) that induce only single-stranded DNA breaks, both mutations lead to catalytically dead Cas9 (dCas9) variants [175-177]. In both cases, the ability of Cas9 to bind the target locus is preserved. Lastly, these Cas9 variants can be utilized to remodel the epigenetic state of a specific locus by the fusion of various effector domains, e.g. transcriptional activator or repressor domains [176; 178], acetyltransferases, methylases or demethylases [179], or to create base editors that change single nucleotides adjacent to the target sequence [180]. Multiplexed genome editing and the use of orthologous CRISPR/Cas9 systems as well as their nCas9 and dCas9 variants gave rise to numerous options to rewire and control diverse cellular networks and to hit viral infections on multiple levels.

1.5.2. CRISPR/Cas9 orthologs

A wide variety of orthologous type II CRISPR/Cas9 systems are available that increase the flexibility of this powerful genome editing tool [181]. Popular variants are the systems from *Streptococcus pyogenes* (*Sp*), the first system that was characterized and applied

for gene editing purposes [168; 175; 182; 183], as well as *Staphylococcus aureus* (*Sa*) and *Neisseria meningitides* (*Nme1*) that are characterized by smaller Cas9 effector proteins (Figure 8). The smaller *Sa*Cas9 and *Nme1*Cas9 of about 1053 aa and 1082 aa, respectively, enable their packaging in viral vehicles for *in vivo* gene delivery. Although the Cas9 proteins share very little sequence similarity (only 17% for *Sp* and *Sa*Cas9), their crystal structures unveil several shared structural arrangements [184-187].

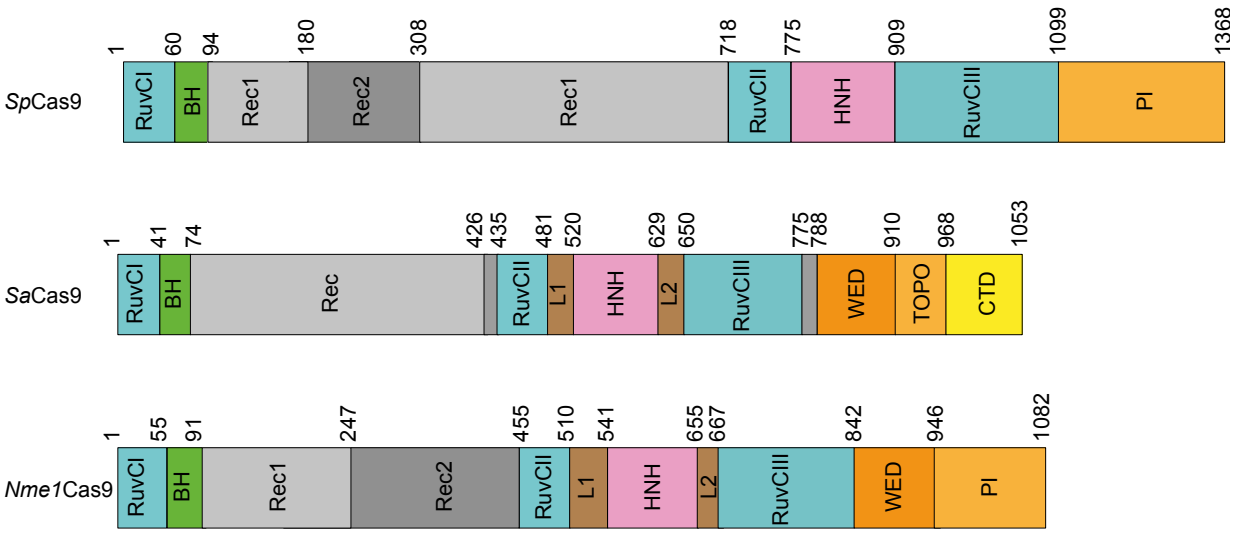

Figure 8. Domain organization of orthologous Cas9 endonucleases.

*Sp*Cas9, *Sa*Cas9 and *Nme1*Cas9 share similar domain organization. The domains can be divided into a recognition and nuclease lobe. Schematic representations are adapted from [184; 186; 187].

The nuclease (NUC) lobe consists of the three RuvC domains and an HNH domain that induce site-specific nicks on the DNA strand that is non-complementary or complementary to the guide RNA, respectively. Also part of the NUC lobe is the C-terminal PAM-interacting (PI) domain that mediates PAM recognition and DNA unwinding, and a wedge (WED) domain that recognizes the secondary structure of the guide RNA. The NUC lobe is separated into a small N-terminal and large C-terminal part by an intermediate recognition (REC) lobe comprising a bridge helix (BH) motif and several REC domains. Upon target binding, the REC lobe undergoes a major conformational rearrangement that positions the HNH domain to the DNA cleavage site and locks Cas9 in a DNA bound state [188]. Despite these similarities, the Cas9 orthologs vary in their tracrRNA sequence and the required PAM sequence. Whereas *Sp*Cas9 requires the 5´-NGG-3´ PAM sequence, *Sa*Cas9 utilizes 5´-NNGRRT-3´ [189] and *Nme1* Cas9 uses 5´-N_4GYTT-3´ [190], where “N” is any of the four nucleobases, and “R” and “Y” represents purine and pyrimidine bases, respectively.

1.5.3. Towards controllable gene editing by the use of anti-CRISPR proteins

A major limitation of the CRISPR/Cas9 system is the presence of off-target effects that hamper its transition to a successful therapeutic. Off-targeting is mediated by sequence similarities of the crRNA sequence and genomic targets. It has been reported that the seed region, consisting of approximately the eight to twelve bases proximal of the PAM sequence, are especially important to determine sequence specificity, as they interact with the BH domain within the REC lobe of Cas9 [184; 191]. Potential off-target cleavage could occur with even five base pair mismatches between crRNA and target [192; 193]; therefore it should be carefully evaluated in the crRNA *in silico* design whether the PAM-associated target site is unique within the genome, e.g. by the widely applied CCTop online platform [194]. Strategies to reduce off-targeting were extensively reviewed in the literature [195; 196]. Besides crRNA specificity, a strong and prolonged expression of the CRISPR/Cas9 components within cells is associated with an amplified rate of off-target events. Therefore, it would be highly preferable to control CRISPR/Cas9 mediated gene editing in a spatio-temporal manner and to be able to switch its activity on and off.

In the co-evolutionary battle between bacteria and phages, phages evolved mechanisms to directly bind and inactivate the bacterial CRISPR/Cas9 machinery, the so-called anti CRISPR (Acr) proteins. The first Acr proteins were discovered in prophages, which were able to infect and propagate in *Pseudomonas aeruginosa,* although this bacterial strain carries a functional multi-protein type I-F CRISPR system directed against the invader [197]. Bioinformatics approaches identified five distinct genomic regions encoding the AcrF1 through AcrF5 proteins that determine the anti-CRISPR phenotype. As none of these proteins disrupt the expression of the *cas9* genes nor influence the maturation of the required RNAs, it was assumed that these Acr proteins inhibit the CRISPR system by direct protein-protein binding [198]. Subsequently, the putative transcriptional regulators Aca (anti-CRISPR-associated) 1 and 2 were discovered that link the expression of Acr proteins to the infectious cycles of phages. Henceforth, the race to uncover further Acr proteins began and various CRISPR/Cas9 inhibitors were identified. In 2016, the first inhibitor against the single effector type II-C CRISPR/Cas9 system from *Neisseria meningitidis* was discovered comprising AcrIIC1, AcrIIC2 and AcrIIC3 [199]. A year later, studies confirmed the inhibition of the type II-A CRISPR/Cas9 system from *Listeria monocytogenes* by AcrIIA1 through AcrIIA4 [200]. Surprisingly, AcrIIA2 and AcrIIA4 efficiently counteract also the type II-A CRISPR/Cas9 system from *Streptococcus pyogenes*.

So far, about 21 distinct Acr families have been described that act against type I and II CRISPR systems [198]. Besides their small size of about 50 to 150 aa, the Acr proteins share no conserved sequences. Nevertheless, Acrs seem to act according to similar anti-CRISPR mechanisms by mostly inhibiting the DNA binding ability of CRISPR effector proteins. Whereas AcrF1 and AcrF2 prevent proteins from the multiple effector type I-F cascade complex to bind to target DNA, AcrIIA4 and AcrIIC3 directly act on the type II single effector Cas9 protein for the same purpose. By contrast, AcrIIC1 binds the catalytic HNH domain and locks *Nme*Cas9 in a DNA-bound, but catalytically inactive state [201].

Acr proteins can be applied to tightly regulate CRISPR/Cas9 mediated gene editing in a spatio-temporal manner by various strategies. The groups of Dominik Niopek and Roland Eils from the German Cancer Research Center (DKFZ) in Heidelberg have previously engineered an optogenetically controllable Acr variant, comprising a hybrid of AcrIIA4 and the LOV2 photosensor from *Avena sativa*, to regulate *Sp*Cas9 gene editing in a light-dependent manner [202]. Furthermore, in a collaborative effort, the Niopek lab and ours have developed a cell type-specific CRISPR-ON switch based on miRNA-regulated expression of Acr proteins [203]. To this end, binding sites for miRNA-122 or miRNA-1 that are expressed exclusively in hepatocytes and myocytes, respectively, were inserted in the 3´ UTR of the AcrIIA4, AcrIIC1 or AcrIIC3 transgenes (Figure 9).

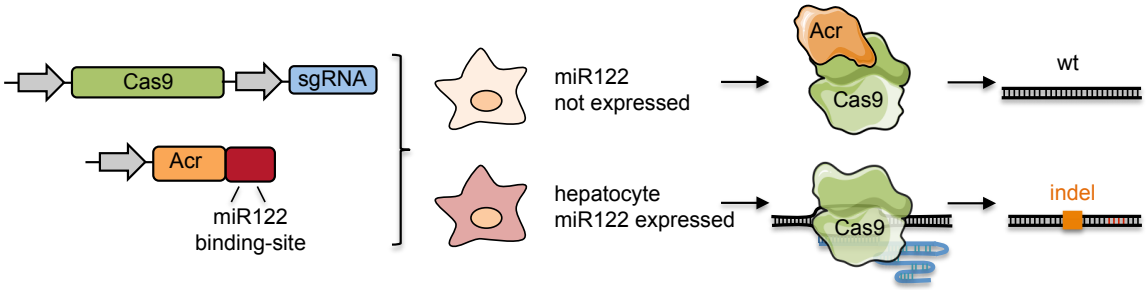

Figure 9. Principle of a miR-122-based CRISPR-ON switch.

The Acr variant harbors a binding site for the hepatocyte-specific miR-122 in the 3´ UTR of its transgene and is thus inhibited specifically in liver cells. Accordingly, Acr knock-down releases Cas9 from inhibition and enables gene editing in hepatocytes, while Cas9 is inhibited in off-target cells. Illustration contains art from smart.servier.com.

Co-expression of these Acr variants with the CRISPR components resulted in miRNA-mediated knock-down of Acr within the designated target cells and thus led to the release of its inhibitory effect on *Sp*Cas9 or *Nme*Cas9. Thus, different CRISPR/Cas9 orthologs can be switched on in specific miRNA-expressing target cells and remain inhibited in off-target cells.

1.6. Adeno-associated viral vectors: a delivery vehicle for gene therapy

A successful application of RNAi and CRISPR/Cas9 in postnatal animals and clinical applications strictly depends on the availability of vehicles that can deliver the required components to target cells. Recombinant Adeno-associated viruses (rAAVs) are attractive candidates for *in vivo* gene delivery due to many advantageous features including the long-term and probably even life-long expression of transgenes in a wide range of cell types *in vivo* [204]. In general, AAVs are considered very safe as compared to other viruses. First of all, wild-type (wt) AAVs are not associated with any disease and induce only a mild immune response that reduces the risk of immune-associated pathology [205; 206]. While wt AAVs can stably integrate into the host cell genome mainly at a specific site on chromosome 19, termed AAV safe harbor 1 (AAVS1) [207], rAAV vectors remain predominantly in a non-integrative, episomal state, thus reducing the risks of oncogenic mutations by random insertions [208].

Recent approvals of rAAV-based medications herald the emergence of a new class of therapies for genetic disorders, which had hitherto been considered as untreatable. The first rAAV gene therapy product, Glybera, was licensed in 2012 for the treatment of lipoprotein lipase deficiency. Since then, various clinical trials for the treatment of neurological [209], ocular [210] and other monogenetic diseases, such as hemophilia B [211] and alpha-1 antitrypsin deficiency [212], reported effective and encouraging therapeutic results. This led to the FDA approval of two additional rAAV-based therapeutics, namely Luxturna for the treatment of Leber´s congenital amaurosis, an inherited eye disease causing blindness, and Zolgensma for the treatment of spinal muscular atrophy that, if untreated, leads to the loss of motor neurons, progressing muscle atrophy and subsequent death in infants [213].

1.6.1. AAV structure and genome organization

AAV belongs to the family of *Parvoviridae* and harbors a 4.7 kb single-stranded, either positive- or negative-sensed, DNA genome. Its non-enveloped capsid of icosahedral symmetry is about 22 to 26 nm in diameter and is composed of 60 viral protein (VP) subunits [214-216]. The VPs are divided into VP1, VP2 and VP3 that are expressed in an estimated ratio of 1:1:10, respectively [217]. The genome of wt AAV encodes Rep proteins (Rep78, Rep68, Rep52 and Rep40) that are involved in virus replication and Cap or VP

proteins (VP1 to VP3) that compose the viral capsid. An alternative ORF for the assembly-activating protein (AAP) is located within the *cap* sequence and promotes assembly of viral capsids [218; 219]. Recently, an additional ORF within the *cap* sequence has been discovered that encodes the membrane-associated accessory protein (MAAP), which plays a role in the packaging of an AAV genome into its respective capsid, while excluding competitive AAV genomes that encode different capsid variants [220]. The coding sequence of the AAV genome is flanked by short, about 145 nucleotides long inverted terminal repeats (ITRs) that form T-shaped secondary structures and are required for genome packaging into the viral capsids.

AAVs are *Dependoparvoviruses*, since they depend on a helper virus to complete their replication cycle. Accordingly, AAV was first discovered as contamination in Adenovirus preparations and thus acquired its name [221]. Without co-infection of helper viruses, such as Ad, Herpes Simplex virus (HSV) or human papilloma virus (HPV) [222], AAV is replication-deficient.

To date, 13 naturally occurring AAV serotypes and hundreds of natural isolates have been reported that originated from a variety of different species including mammals, birds and reptiles [206]. Together, these AAV variants show a wide range of tropisms for different mammalian cell types *in vitro* and *in vivo.* Furthermore, individual AAV serotypes and variants show a varying degree of target specificity towards certain cell types and organs. For instance, while AAV8 especially targets the liver, AAV9 is considered as a ubiquitous transducer in mice [223; 224]. Most studies on the AAV life cycle and biology focus on wt AAV2, likely due to historical reasons (wt AAV2 was the first cloned serotype [225; 226]) and its wide tropism for laboratory cell lines that simplifies its research [227]. Differences in cell tropism profiles for the different AAV members are presumably determined by the molecular interactions between capsid and target cell surface receptors [228] and subsequent intracellular trafficking [214]. An initial attachment to the cell surface is achieved by the binding to mostly negative charged glycans or glycoconjugates, such as HSPG that has been identified as a glycan moiety for AAV2 [229]. AAV2 capsid mutants that forfeit the ability to bind to HSPG show reduced mouse liver transduction rates, but retain their tropism towards the heart, suggesting that AAV2 can use alternative entry modalities [230]. The initial attachment to the cell surface is followed by a specific binding to the universal AAV receptor (AAVR) [231; 232], that mediates AAV entry for all serotypes except AAV4 and its descendants [233].

1.6.2. The recombinant Adeno-associated virus

The rAAV vector is particularly attractive as delivery vehicle for genetic elements due to many favorable traits including, among others, i) the ease of virus production and purification, ii) the safe handling under biosafety level 1 conditions (depending on the nature of the cargo), and iii) the availability of various natural serotypes and numerous engineered variants [234]. For the packaging of rAAV genomes into viral capsids, the ITRs are the only elements in the viral genome that are required in *cis*, whereas all other elements can be provided in *trans* [235; 236] (Figure 10).

Accordingly, the entire coding sequence between the ITRs can be replaced by any desired transgene expression cassette that abides the packaging capacity of up to 5 kb. The rAAV genome is packaged into viral capsids by co-transfection of HEK293T cells together with plasmids that express the AAV proteins and Adenoviral components, which provide helper functions for rAAV vector production [237]. With the discovery of new AAV serotypes and the engineering of novel variants, the idea has emerged rapidly to vectorize the whole AAV diversity. To this end, a pseudotyping strategy has been developed that basically utilizes the ITRs from AAV2 for all recombinant genomes [238-240]. Dirk Grimm and co-workers in the lab of Mark Kay have previously extended this approach by the juxtaposition of ITRs of AAV2 and AAV4 on the same viral genome (patent US9150882B2), which successfully reduced the amount of recombination and associated loss of ITRs during cloning processes while maintaining efficient vector production. Moreover, they and others have previously reported that Rep proteins are mostly interchangeable across AAV serotypes [239; 241; 242], which is probably facilitated by the high sequence identity between ITRs of different serotypes (>95%), to which Rep proteins bind and cleave during genome replication. The only exception is AAV5, which harbors distinct ITRs and Rep proteins, and thus is unable to complement packaging of viral genomes flanked by ITRs from AAV2 and *vice versa* [243; 244]. Consequently, most rAAV vectors that are currently utilized in the field are pseudotyped with ITRs from AAV2 (or, in the case of the aforementioned hybrid genomes, a combination of ITRs from AAV2 and AAV4) and rely on the complementation with the AAV2 Rep proteins (encoded by *rep2*) for vector production. By contrast, the sequence of *cap* can be easily adapted according to the designated rAAV variant (*capX*).

For gene therapy purposes, the rAAV vector has been engineered on the capsid as well as the genome level in order to limit transgene expression to specific target cells [245; 246]. Especially when used as delivery vehicle for CRISPR/Cas9 and RNAi that currently

remain prone to off-targeting, specificity could be improved already on the level of cell selectivity [247].

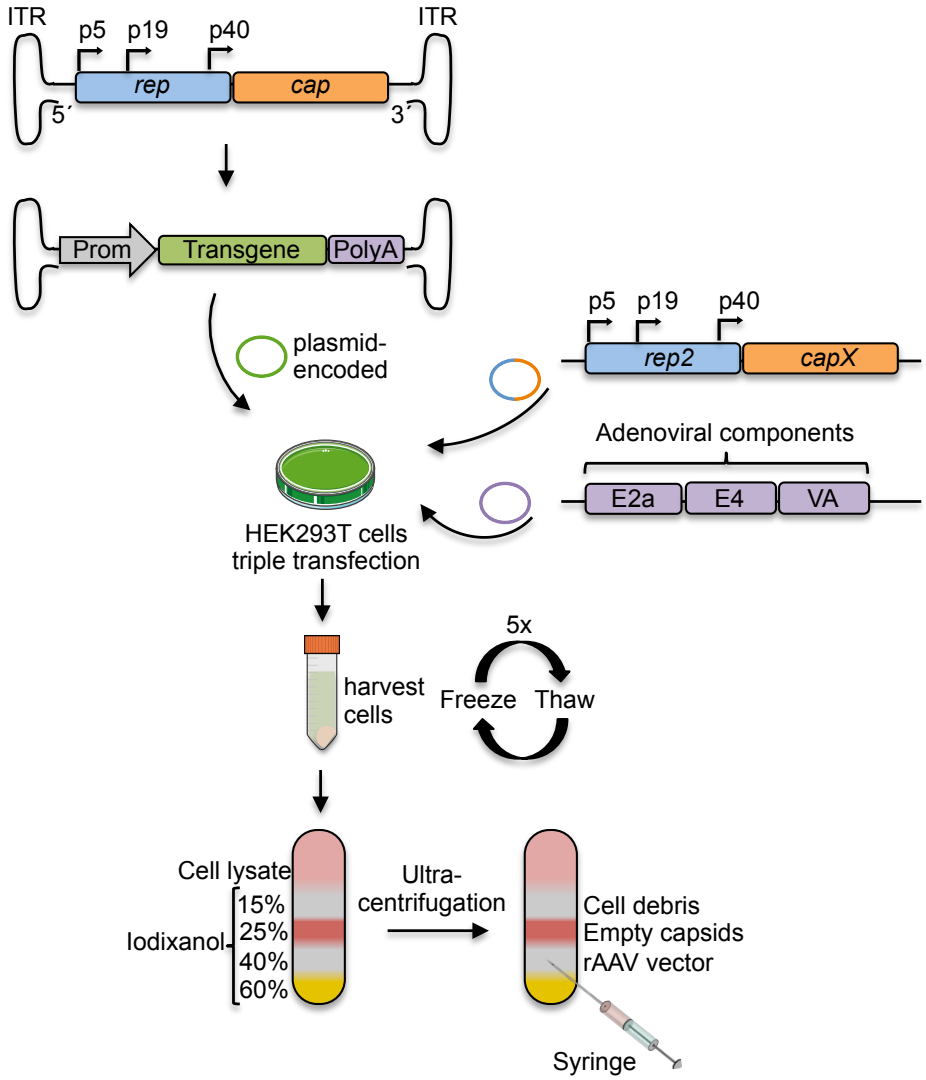

Figure 10. Production of rAAV vectors.

The coding sequence between the ITRs of wt AAV can be exchanged by any foreign DNA and *rep* and *cap* sequences, and Adenoviral genes can be supplied in *trans* for viral packaging in HEK293T cells. Three days post-transfection, cells are harvested and subjected to five freeze/thaw cycles in order to release the viral particles. Subsequently, the cell lysate is loaded on an iodixanol gradient and purified rAAV vectors can be extracted from the 40% iodixanol phase after ultracentrifugation. Illustration contains art from smart.servier.com

One popular strategy to increase rAAV specificity is the insertion of an oligonucleotide in the *cap* sequence encoding a short peptide that is then displayed on an exposed region on the viral capsid surface, hoping that this will mediate changes in receptor binding and virus uptake [227; 248]. Another strategy is termed “DNA family shuffling”, in which the DNA sequences of AAV capsid orthologs are fragmented and reassembled into chimeric

sequences based on homologies in a PCR-based approach [249; 250]. Both approaches typically result in capsid libraries that are screened in iterative rounds of selection under positive and/or negative selection pressure for higher specificity and/or efficiency towards designated cell types. In the past, both approaches have led to the identification of numerous novel capsid variants, such as AAV-DJ, a chimeric capsid composed of AAV2, AAV8 and AAV9 that exhibits high tropism towards mouse hepatocytes *in vivo* [249]. Furthermore, capsid modifications might also help to overcome a major drawback of naturally occurring AAV variants, namely, the presence of neutralizing anti-AAV antibodies in the general human population, which is a common exclusion criterion for participation in clinical trials [251; 252].

On the genome level, the rAAV vector has been engineered to overcome the barriers of transgene expression that are imposed by the single-stranded nature of the viral genome. The single-stranded rAAV (ssAAV) genome is converted to expression-competent, double-stranded DNA in a time-consuming and inefficient process that involves rate-limiting host factors [253-255]. Intriguingly, it has been reported that a mutation in the terminal resolution site in one of the ITRs prevents the cleavage of the dsDNA intermediate and arrests viral genome replication during vector production at a stage in which two inverted copies of the transgene are present [256; 257]. In transduced cells, these self-complementary AAV (scAAV) vectors, also referred to as double-stranded AAV (dsAAV) vectors, already represent the expression-competent state of the genome and thus have the advantage of an accelerated transgene expression compared to its ssAAV counterpart (Figure 11).

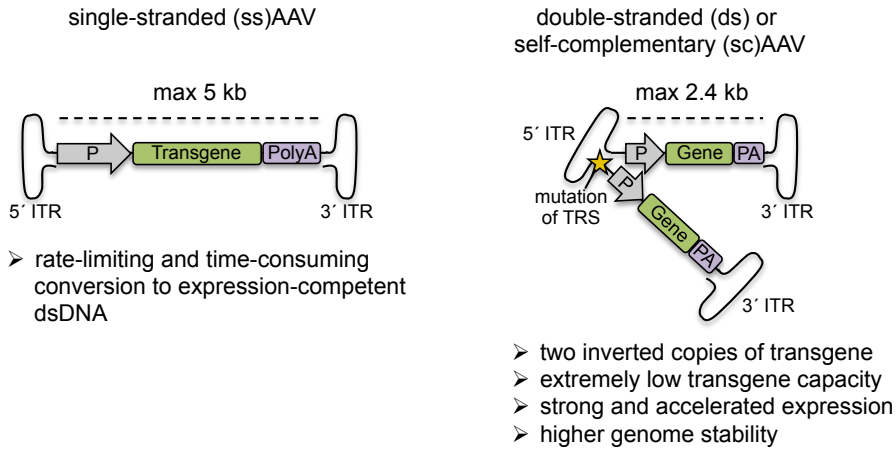

Figure 11. Single-stranded *versus* double-stranded AAVs.

A mutation in one of the ITRs leads to the formation of the dsAAV genome that expresses its transgenes more rapidly and more efficiently than conventional ssAAV vectors. Yet, this comes at the cost of a further reduction of the AAV packaging capacity to only 2.4 kb for dsAAVs.

On top, scAAVs show increased transgene expression rates of 5- to 140-fold depending on cell line [257] and higher *in vivo* genome stability, as they are more prone to circularization compared to the ssAAV vector [255]. However, transgenes exceeding packaging capacity of only 2.4 kb for dsAAV might be packaged with truncations at their 5´ end [258].

In general, transduction of both ssAAV and scAAV vectors in cell culture is a rather inefficient process, as about 10^3 to 10^5 viral particles per cell are required for an efficient transgene expression depending on rAAV variant and cell type. Whereas AAV internalization seems to be fast and efficient at least for AAV2 [214], processes involved in internal trafficking [259], capsid uncoating [260] and DNA replication [261] have been reported to be rate-limiting steps. Indeed, it has been shown that only a small fraction of virions enter the nucleus, while the majority accumulates in a perinuclear compartment and is subject to capsid ubiquitination and subsequent proteasomal degradation [214; 262; 263]. Thus, in order to improve rAAV transduction efficiencies, several chemical compounds are occasionally applied in cell culture experiments, including proteasome inhibitors [262; 264; 265], such as MG132 and Doxorubicin (Dox), and boosters of mTOR-dependent autophagy, such as rapamycin [266].

1.6.3. SplitCas9 systems circumvent packaging limitations by rAAV vectors

One of the major drawbacks of rAAV vectors is their limited cargo capacity of up to 5 kb and 2.4 kb for the packaging of designated transgene expression cassettes in ssAAV and dsAAV, respectively. Packaging *Sp*Cas9 (4.1 kb) and sgRNA (minimal cassette of 200 bp) into an all-in-one rAAV vector is barely feasible [267], but leaves little flexibility in the choice of regulatory elements, such as promoters and polyA signals. Thus, the smaller *Sa*Cas9 (3.16 kb) is considered as the preferred ortholog when it comes to rAAV vector delivery *in vivo*, but it still imposes major restrictions in the design of the expression cassette. Furthermore, any conventional CRISPR/Cas9 system exceeds the size restriction imposed by the dsAAV vector by far and thus forfeits its benefits in expression.

Over the past five years, researchers came up with a multitude of solutions to circumvent the size limitations of rAAV vectors and to improve expression of the CRISPR components. These strategies have in common that Cas9 (of various orthologous systems) is split in two parts and encoded on separate vehicles, including plasmids,

lentiviral and rAAV vectors, and after translation reunited in the target cell by various means. This comprises a variety of systems that enable an inducible and controllable Cas9 reconstitution and its gene editing activity, and thus contribute to safeguard CRISPR technology. Strategies to reconstitute the Cas9 holoenzyme can be divided into i) the use of the sgRNA as a scaffold, ii) rapamycin-controlled FKBP/FRB dimerization, iii) light-regulatable dimerization systems, and iv) inteins. Since we have reviewed these studies previously [268], this section focuses on the concept of intein-based splitCas9 systems [269-272].

Inteins (internal protein) are polypeptides that self-catalytically splice themselves out of a precursor protein after translation and connect their flanking amino acid residues, called exteins, via a newly synthesized peptide bond, resulting in a shorter, functional protein [273]. Inteins can also occur as split inteins that trigger *trans*-splicing of two independently expressed protein halves to reconstitute the holo-protein [274] (Figure 12).

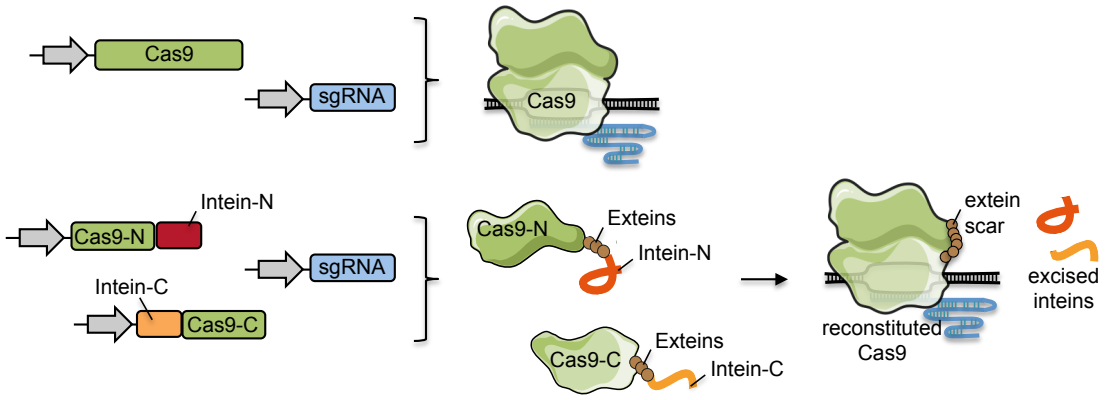

Figure 12. Intein-based splitCas9 system.

Split inteins can be used to segregate Cas9 in two halves and initiate reconstitution to the full-sized holo-enzyme after translation. To this end, N- and C- inteins are fused to the corresponding N-and C-terminal splitCas9 half. Furthermore, inteins are flanked by exteins that comprise the three amino acid residues that occur in their natural splicing context to allow an efficient splicing reaction. Exteins remain in the reconstituted Cas9 as extein scar, while inteins autocatalytically splice themselves out.

Examples of *trans*-splicing inteins that were shown to splice very efficiently are the DnaE intein of *Nostoc punctiforme* (*Npu*DnaE intein) [275; 276] and the gp41 DNA helicase intein (gp41-1 intein) [277]. It was demonstrated that *Npu*DnaE favors cysteine (C) and tryptophan (W) as first and second C-extein, respectively, and glycine (G) and lysine (K) as first and second N-extein, respectively, proximal to the splicing junction [278]. By contrast, gp41-1 was demonstrated to splice efficiently with an even wider range of

different exteins and seems to solely depend on serine (S) on the first position of the C-terminal splicing junction [276; 277; 279]. Additionally, several hundreds of different inteins were found in all three domains of life (bacteria, archaea and eukaryotes) occurring either as *cis*-splicing full-length intein or *trans*-splicing split intein and thus form a comprehensive toolbox for genetic engineering (http://www.inteins.com/ and http://2014.igem.org/Team:Heidelberg). Also, the inducible nature of the splicing reaction of some inteins by ligands [280; 281], temperature [282], light [283], pH [284] or reducing agents [285] already imply an abundance of possible approaches to regulate rAAV/CRISPR vectors.

Previously, in my M.Sc. work in the lab of Prof. Barbara Di Ventura and Prof. Roland Eils (also in collaboration with the Grimm lab), we have already harnessed the *Npu*DnaE and gp41-1 intein *trans*-splicing capability to split *Sa*Cas9 into two equal sized halves and to reconstitute the functional holo-enzyme [286]. Importantly, the split*Sa*Cas9 halves are, in principle, sufficiently small to allow packaging as dsAAV vectors.

1.7. The aim of this study

Over the last decade, the field of gene and cell therapy have emerged as a powerful platform for a new class of gene-based therapeutics to treat diseases, which had hitherto been considered as untreatable. This thesis validates the promise of combining very powerful tools for gene therapy—rAAV vectors, RNAi and CRISPR/Cas9—and implies its great potential to treat numerous diseases, such as hepatitis B and D.

In this study, we first harnessed a class of rAAV vectors that has previously been established in our lab and that enables the combination of CRISPR/Cas9 and RNAi technologies. As both technologies make use of guide RNA triggers, we first reassessed and compared several approaches to co-express small RNAs from rAAV vectors in the same target cell, including i) the separate production and subsequent mixing of each vector encoding a single small RNA, ii) their pooled production in the same dish, or iii) the multiplexing of several expression cassettes on a single AAV vector. The latter approach, named TRISPR, was further engineered to co-express sgRNAs and shRNAs to tackle HBV infections on the DNA and RNA level in selected cell culture systems, respectively. While many groups have previously applied either CRISPR/Cas9 or RNAi technology to target HBV, few have combined both approaches to achieve a synergistic effect in HBV elimination. Next, we employed the TRISPR strategy to direct the RNAi machinery against the HDV RNA genome and CRISPR/Cas9 against HBV cccDNA. To

our knowledge, this study provides the first evidence that CRISPR/Cas9 and RNAi can be combined to target HBV and HDV co-infections. Thus, this thesis paves the way for subsequent *in vivo* studies in HBV and HBV/HDV mouse models, with the aim to test the effect of a combinatorial knock-down and knock-out strategy on the host immune response.

We further increased the therapeutic index of the rAAV/CRISPR technology by contributing to solutions for major challenges in its application, namely, delivery, efficiency, specificity and safety. This thesis addressed these limitations by various means:

1) In collaboration with Michael Nassal's lab, we evaluated dimethyl sulfoxide (DMSO) as agent to boost rAAV transduction and expression rates in cell culture experiments, as similar effects have been reported for several other viral infections including HBV [17-20], HCV [287], HIV [288] and influenza A [289]. We further determined whether an improved DMSO-mediated rAAV/CRISPR delivery translates to higher targeted mutagenesis rates.

2) Next, we combined the inherent benefit of splitCas9 technologies with the assets of dsAAV vectors to drive accelerated and enhanced Cas9 expression. To this end, we followed up on our previous work from my M.Sc. thesis where we had segregated the smaller Cas9 ortholog from *Staphylococcus aureus* into two halves, each sufficiently small to allow packaging in dsAAV vectors, and had harnessed intein *trans*-splicing to reconstitute the Cas9 holo-enzyme. Here, we investigated whether the expression of split*Sa*Cas9 by dsAAV vectors can boost targeted mutagenesis rates beyond the ability of the inherently full-length *Sa*Cas9 that is limited to the expression by ssAAV. In view of accumulating evidence that Cas9 expression levels not only correlate with on- but also off-target cleavage rates [192; 193; 272; 290], we implemented a self-inactivating (SIN) approach developed by Julia Fakhiri in the lab that directs an sgRNA against the *Sa*Cas9 transgene and prevents its expression after cleavage of a designated on-target. To this end, we compared targeted mutagenesis rates and the ability to self-inactivate of the dsAAV/split*Sa*Cas9 system and conventional ssAAV/full-length Cas9 in cell culture and mouse experiments.

3) Lastly, we further increased the safety profile of the CRISPR/Cas9 system from *Staphylococcus aureus* by collaborating with the Niopek lab who has engineered its first designer anti-CRISPR protein. To this end, we contributed to their work using AcrIIC1, a broad-spectrum inhibitor targeting various type II-C Cas9 orthologs including those from *Neisseria meningitidis*, *Campylobacter jejuni* and *Geobacillus stearothermophilus*, whose

binding surfaces they have redesigned towards the HNH domain of *Sa*Cas9. We tested the novel AcrX inhibitor for its ability to inhibit *Sa*Cas9 on various genomic loci and also applied the miRNA-based CRISPR-ON switch strategy to restrict *Sa*Cas9 cleavage activity towards hepatocytes.

In summary, this doctoral thesis combined and further advanced major tools in the field of gene therapy by drawing on several principles of synthetic biology and bioengineering. Importantly, all project parts of the presented thesis are highly complementary and combinable to concurrently increase rAAV delivery and CRISPR/Cas9 mutagenesis rates, while improving the safety profile of rAAV/CRISPR technology. Beyond the presented technological advances, we also envisioned the combination of the rAAV vector, CRISPR/Cas9 and RNAi technologies to tackle so far uncurable diseases and demonstrated this potential using HBV infections and/or HBV/HDV co-infections as clinically relevant examples.

2. MATERIALS AND METHODS

2.1. Materials

Table 1. List of materials

Material	Company
Aluminium foil	Roth (Karlsruhe, Germany)
Amicon Ultra-15 centrifugal filter units (100,000 NMWL)	MERCK (Darmstadt, Germany)
BD microlance3	BD (Franklin Lakes, US)
BD plastipak (syringe)	BD (Franklin Lakes, US)
BZO Seal Film (qPCR)	Biozym Scientific GmbH
Cell culture flasks (75/ 175 cm2)	Greiner bio-one (Frickenhausen, Germany)
Cell culture plates (6/24/48/96 well)	Greiner bio-one (Frickenhausen, Germany)
Cell culture plates 140mm	Nunc, Thermo Fisher Scientific (Waltham, USA)
Cell lifter	Corning (New York, USA)
Centrifuge tube 500 ml	Corning (New York, USA)
Centrifuge tubes (16x76 mm and 25x89 mm)	Beranek Laborgeräte (Weinheim, Germany)
Coster 50ml reagent reservoir	Corning (New York, USA)
Countess^{IM} cell counting chamber slides	Thermo Fisher Scientific (Waltham, USA)
ddPCR plates, 96 well, semi-skirted	Bio-Rad (Hercules, USA)
DG8™ Cartridges for QX200™/QX100™ Droplet Generator	Bio-Rad (Hercules, USA)
DG8™ Gaskets for QX200™/QX100™ Droplet Generator	Bio-Rad (Hercules, USA)
DNA chip	Agilent Technologies (Waldbronn, Germany)
Erlenmeyer flasks	Thermo Fisher Scientific (Waltham, USA)
Filter tips	Sarstedt (Nümbrecht, Germany), Mettler-Toledo (Columbus, USA)
Flat top seal former	Beranek Laborgeräte (Weinheim, Germany)
Glass bottles	DURAN group (Wertheim, Germany)
Glass culture tubes	DURAN group (Wertheim, Germany)
Inoculation loops	Greiner bio-one (Frickenhausen, Germany)
Masterblock, 1 ml	Greiner bio-one (Frickenhausen, Germany)
Microlance canules 21G 0.8x40mm, 19G 1.1x40 mm	BD (Franklin Lakes, USA)
Microplates, 96 well, white	Greiner bio-one (Frickenhausen, Germany)

Mini-PROTEAN TGX Gels, 4-15%, 10 wells	Bio-Rad (Hercules, USA)
Mini-PROTEAN TGX Gels, 7.5%, 15 wells	Bio-Rad (Hercules, USA)
Nitrocellulose membrane	Whatman (Maidstone, UK), Ahlstrom (Helsinki, Finland)
Pasteur capillary pipettes (230 mm)	neoLab (Heidelberg, Germany)
PCR microplate, 96 well	Corning (New York, USA)
PCR plate 96-well (qPCR)	Biozym Scientific GmbH
PCR tubes 0.2 ml 8-Strip	STARLAB (Hamburg, Germany)
Petri dishes	Greiner bio-one (Frickenhausen, Germany)
Piercable Foil Heat Seal	Bio-Rad (Hercules, USA)
Pipette tips	Greiner bio-one (Frickenhausen, Germany), Kisker (Steinfurt, Germany)
Pipette tips, 10 µl, 200 µl	Mettler-Toledo (Columbus, USA)
Plates, 96 well, blavk and clear bottom	Corning (New York, USA)
QIAshredder tubes	QIAGEN (Hilden, Germany)
qPCR 0.1ml strip tubes and strip caps	QIAGEN (Hilden, Germany)
Reaction tubes (0.5, 1.5, 2ml)	SARSTEDT (Nümbrecht, Germany), Eppendorf (Hamburg, Germany)
Reaction tubes 15 ml, 50 ml	Greiner bio-one (Frickenhausen, Germany)
Reaction tubes 50 ml	Thermo Fisher Scientific (Waltham, USA)
Röhren/Tubes 75x13 mm	Sarstedt (Nümbrecht, Germany), Mettler-Toledo (Columbus, USA)
Scapell-blades	Heinz Herent (Hamburg, Germany)
Sealing foil (Adhäsive Verschlussfolie)	nerbe plus GmbH
Serological pipettes (2,5, 10, 25, 50 ml)	Greiner bio-one (Frickenhausen, Germany)
Stainless steel beads	QIAGEN (Hilden, Germany)
Sterile filter (0.22 µM pore size)	Greiner bio-one (Frickenhausen, Germany)
Steritop filter (0.22 µM)	MERCK (Darmstadt, Germany)
VacConnectors	QIAGEN (Hilden, Germany)
Whatman paper 3mm	Whatman (Maidstone, UK)

Table 2. Chemicals and reagents

Name	**Company**
Acetic acid	VWR chemicals (Fenenay-sous-Bais, France)
Agarose	Biozym Scientific GmbH (Hessisch Oldendorf, Germany)
Albumin fraction V (BSA)	Roth (Karlsruhe, Germany)

cOmpleteTM, EDTA-free Protease Inhibitor Cocktail	Roche (Penzberg, Germany)
ddPCR™ Droplet Generator Oil	Bio-Rad (Hercules, USA)
Diluent B	NEB (Ipswich, USA)
DirectPCR Lysis Reagent	Viagen Biotech Inc (Los Angeles, USA)
DMSO	Merck (Darmstadt, Germany)
Dodecylsulfate-Na-salt-pellets (SDS)	SERVA Electrophoresis GmbH (Heidelberg, Germany)
Doxorubicin	Santa Cruz Biotechnology (Dallas, USA)
Ethanol absolute	SIGMA-ALDRICH (St. Louis, USA)
Ethidium bromide	Roth (Karlsruhe, Germany)
Ethylendiamintetraacetate (EDTA)	GRÜSSING GmbH (Filsum, Germany)
GelredTM nucleic acid gel stain	Biotium Inc (Hayward, USA)
Glucose	MERCK (Darmstadt, Germany)
Glycerol	VWR chemicals (Fenenay-sous-Bais, France)
Hoechst 3000	Dianova (Hamburg, Germany)
Hydrochloric acid (HCl)	SIGMA-ALDRICH (St. Louis, USA)
Iodixanol (Optiprep^{IM})	Progen (Heidelberg, Germany)
Isopropanol	SIGMA-ALDRICH (St. Louis, USA)
Jetprime	Polyplus-transfection® SA
Lipofectamine 2000	Life Technologies GmbH (Paisley, UK)
Magnesium chloride (MgCl2)	Applichem (Darmstadt, Germany)
Methanol	SIGMA-ALDRICH (St. Louis, USA)
Milk powder	Roth (Karlsruhe, Germany)
MOPS	SERVA Electrophoresis GmbH (Heidelberg, Germany)
Myrcludex B (MyrB)	Bachem (Bubendorf, Switzerland).
Nuclease-free water	Ambion, Thermo Fisher Scientific (Waltham, USA)
Oligonucleotides (dNTPs)	NEB (Ipswich, USA)
Paraformaldehyde (PFA)	MERCK (Darmstadt, Germany)
PBS Dulbecco without Ca^{2+}	MERCK (Darmstadt, Germany)
PEG8000	Promega (Madison, USA)
Phenol red	MERCK (Darmstadt, Germany)
Polyethylenimine (PEI)	Polysciences Inc. (Eppelheim, Germany)
PonceauS	SIGMA-ALDRICH (St. Louis, USA)
Potassium acetate (KAc)	GRÜSSING GmbH (Filsum, Germany)
Potassium chloride (KCl)	GRÜSSING GmbH (Filsum, Germany)
Rapamycin	MERCK (Darmstadt, Germany)
Sodium chloride (NaCl)	GRÜSSING GmbH (Filsum, Germany)

Sodium deoxycholate (DOC)	MERCK (Darmstadt, Germany)
Sodium hydroxide (NaOH)	SIGMA-ALDRICH (St. Louis, USA)
TE buffer	Thermo Fisher Scientific (Waltham, USA)
TGS (Tris/Glycine/SDS buffer) 10x	Bio-Rad (Hercules, USA)
Tris-HCl/ Tris	Roth (Karlsruhe, Germany)
Triton X-100	MERCK (Darmstadt, Germany)
Trypan Blue	Thermo Fisher Scientific (Waltham, USA)
Tween20	Roth (Karlsruhe, Germany)
UltraPure™ TEMED	Thermo Fisher Scientific (Waltham, USA)
β-Mercaptoethanol	Roth (Karlsruhe, Germany)

Table 3. Cell culture medium and supplements

Name	**Company**
DMEM GlutaMAX +4.5 g/ L D-Glucose	Gibco by Thermo Fisher Scientific (Waltham, USA)
DPBS 1x	Gibco by Thermo Fisher Scientific (Waltham, USA)
Fetal Bovine Serum Gold (FBS)	Gibco by Thermo Fisher Scientific (Waltham, USA)
Penicillin-Streptomycin	Gibco by Thermo Fisher Scientific (Waltham, USA)
0.25% Trypsin/ EDTA	Gibco by Thermo Fisher Scientific (Waltham, USA)
Blasticidin	SIGMA-ALDRICH (St. Louis, USA)
Puromycin	SIGMA-ALDRICH (St. Louis, USA)
Recombinant human fibroblast growth factor-basic (bFGF)	PeproTech (Princeton Business Park, USA)
F-10 Nutrient mixture	Gibco by Thermo Fisher Scientific (Waltham, USA)
Cell culture media	500 ml DMEM GlutaMAX +4.5 g/ L D-Glucose 50 ml FBS 5 ml Penicillin-Streptomycin
Basic fibroblast growth factor (bFGF)	50 µg of /ml of bFGF (50 µg/ml) in 1 ml 5mM Tris (pH7.6) with 0.1% BSA stored at -80°C
Myoblast growth media (500ml) [291]	400 ml F-10 Nutrient mixture 100 ml filtered FBS 5 ml Pen/Strep add 10 ng/ml bFGF before use

Table 4. Bacterial medium and additives

Name	Company
Bacto™ Agar	BD (Franklin Lakes, USA)
Bacto™ Trypton	BD (Franklin Lakes, USA)
Bacto™ Yeast Extract	BD (Franklin Lakes, USA)
Ampicillin (50 mg/ ml, applied in 1:1000 dilution)	Roth (Karlsruhe, Germany)
Chloramphenicol (20 mg/ ml, applied in 1:1000 dilution)	SIGMA-ALDRICH (St. Louis, USA)

Table 5. List of kits

Name	Company
Agilent DNA 1000 Kit	Agilent Technologies (Waldbronn, Germany)
AllPrep DNA/RNA Mini Kit	QIAGEN (Hilden, Germany)
DNA clean & concentrator-5	zymo research (Irvine, USA)
DNeasy Blood & Tissue Kit	QIAGEN (Hilden, Germany)
Dual-Luciferase® Reporter Assay System	Promega (Madison, USA)
iTaq Universal SYBR Green Supermix	Bio-Rad (Hercules, USA)
Luciferase Assay System	Promega (Madison, USA)
NucleoBond® Xtra Midi / Maxi	Macherey-Nagel (Hœrdt, France)
Pierce BCA Protein Assay Kit	Thermo Fisher Scientific (Waltham, USA)
PureYield™ Plasmid Midiprep kit	Promega (Madison, USA)
Rnase-free Dnase Set	QIAGEN (Hilden, Germany)
SensiMix™II Probe Kit	Bioline (London, UK)
SensiMix™II SYBR Kit	Bioline (London, UK)
TetroTM Reverse Transcriptase Kit	Bioline (London, UK)
QIAprep Spin Miniprep Kit	QIAGEN (Hilden, Germany)
QIAquick Gel Extraction Kit	QIAGEN (Hilden, Germany)
QIAquick PCR Purification Kit	QIAGEN (Hilden, Germany)
Qubit dsDNA BR Assay Kit	Thermo Fisher Scientific (Waltham, USA)
Western Lightning® PLUS-ECL	PerkinElmer (Waltham, USA)

Table 6. List of standard markers

Name	Company
1 kb DNA ladder plus	Thermo Fisher Scientific (Waltham, USA)
Generuler ladder	Thermo Fisher Scientific (Waltham, USA)
PageRuler^{IM} Plus Prestained Protein Ladder	Fermentas (St. Leon-Rot, Germany)
Magic Marker	Thermo Fisher Scientific (Waltham, USA)

Table 7. List of enzymes

Name	Company
Antarctic Phosphatase	NEB (Ipswich, USA)
Benzonase	MERCK (Darmstadt, Germany)
ddPCR™ Supermix for Probes (No dUTP)	Bio-Rad (Hercules, USA)
DNase I	Thermo Fisher Scientific (Waltham, USA)
OneTaq® 2X Master Mix	NEB (Ipswich, USA)
Phusion Hot Start II DNA Polymerase	Thermo Fisher Scientific (Waltham, USA)
Proteinase K	Roche (Penzberg, Germany)
2x Q5 Polymerase Master Mix	NEB (Ipswich, USA)
RNaseA	QIAGEN (Hilden, Germany)
Restriction Enzymes	NEB (Ipswich, USA)
TypeII-S restriction enzymes (BsmBI, BbsI, BsaI)	Thermo Fisher Scientific (Waltham, USA)
T4 DNA Ligase	NEB (Ipswich, USA)
T7 endonuclease	NEB (Ipswich, USA)

Table 8. Compositions of buffers

Buffers	Composition
Benzonase buffer	50 mM Tris/HCl pH 8.5 150 mM NaCl 2 mM $MgCl_2$
Freezing medium	10% (v/v) DMSO 90% (v/v) FBS
15% Iodixanol phase	25% (v/v) Iodixanol, 75% (v/v) PBS-MK-NaCl
25% Iodixanol phase	41.66% (v/v) Iodixanol, 58.33% (v/v) PBS-MK, phenol red until it appears red
40% Iodixanol phase	66.67% (v/v) Iodixanol, 33.33% (v/v) PBS-MK

60% Iodixanol phase	100% Iodixanol (v/v), phenol red until it appears yellow
LB medium	1% (w/v) Bacto Tryptone 0.5% (w/v) Bacto Yeast Extract 1% (w/v) NaCl
LB Amp medium	LB medium supplemented with 1 ml 5% Ampicillin per liter
LB plates	LB medium plus 1.5% (w/v) Bacto Agar
LB Amp plates	LB plates supplemented with 1.5 ml 5% Ampicillin per liter
Miniprep P1 (pH 8.0)	50 mM Tris/HCl pH 8.0 100 µg/ml RNase A 10 mM EDTA
Miniprep P2	200 mM NaOH 1% SDS
Miniprep P3 (pH 5.1)	2.8 M KAc
PBS-MK	1 mM MgCl2 2.5 mM KCl in PBS
PBS-MK-NaCl	1 mM MgCl2 2.5 mM KCl 1M Nacl in PBS
Phenolred solution	0.5% (w/v) phenol red in H2O
6x Purple loading dye	NEB (Ipswich, USA)
Laemmli Sample Buffer 4x	Bio-Rad (Hercules, USA)
SOB medium (pH 7.0)	2% Bacto Tryptone 0.5% (w/v) Bacto Yeast Extract 10 mM NaCl 2.5 mM KCl 10 mM $MgSO_4$ (addition after autoclaving) 10 mM $MgCl_2$ (addition after autoclaving)
SOC medium	SOB medium plus 20mM glucose
RIPA buffer	50 mM Tris/HCl pH 8.0 150 mM NaCl 1 mM EDTA 1% Triton 0.1% SDS 0.5% DOC 1x Protease Inhibitor
50x TAE	1M Acetic acid 50mM EDTA 2M Tris

10x TBE	Applichem (Darmstadt, Germany)
10x TBS	250 mM Tris/HCl, pH 7.4 1.25 M NaCl
TBS-T	1x TBS 0.05% Tween20
TFBI buffer (pH 5.8)	16 mM $CaCl_2$ 13.2 % (v/v) glycerol 30.6 mM KAc 100 mM KCl 80 mM $MgCl_2$
TFBII buffer (pH 8.0)	76 mM $CaCl_2$ 13.2 % (v/v) glycerol 10 mM KCl 4.8 mM MOPS
10x TGS (Running buffer)	Bio-Rad (Hercules, USA)
Transferbuffer	1x TGS 20% Methanol in H_2O

Table 9. List of devices

Application	**Device**	**Company**
PCR	C1000 Touch Thermal Cycler	Bio-Rad (Hercules, USA)
	Corbett RG6000	QIAGEN (Hilden, Germany)
	QX200™ Droplet Generator	Bio-Rad (Hercules, USA)
	QX200™ Droplet Reader	Bio-Rad (Hercules, USA)
	StepOnePlus Real-Time PCR system	Applied Biosystems (Massachusetts, USA)
	Vapo Protect	Eppendorf (Hamburg, Germany)
Gel electro-phoresis	(MINI-)SUB CELL GT	Bio-Rad (Hercules, USA)
	CONSORT E835 power supply	Nexigen GmbH (Köln, Germany)
	Gel Doc Intas	Intas Science Imaging (Göttingen , Germany)
	Gel Doc XR	Bio-Rad (Hercules, USA)
	Mitsubishi P93D Printer	Mitsubishi Electric (Cypress, USA)
	UV-Transilluminator	Biostep GmbH (Jahnsdorf, Germany)
Bacterial inbubators	Heraus function line incubator	Thermo Fisher Scientific (Waltham, USA)
	Shaking Incubator Minitron & Multitron	INFORS HT (Basel, Switzerland)
Centrifu-gation	Avanti J-26 XP Centrifuge	Beckman Coulter (Brea, USA)
	Avanti J-25 Centrifuge	Beckman Coulter (Brea, USA)
	Benchtop Centrifuge 5415R	Eppendorf (Hamburg, Germany)

	Benchtop Centrifuge 5417R	Eppendorf (Hamburg, Germany)
	Beckman Tube Sealer	Beckman Coulter (Brea, USA)
	Centrifuge Bottles, 500 ml	Beckman Coulter (Brea, USA)
	Fixed angle type 70 Ti rotor	Beckman Coulter (Brea, USA)
	Fixed angle type 70.1 Ti rotor	Beckman Coulter (Brea, USA)
	Galaxy Minister	VWR (Fenenay-sous-Bais, France)
	JA-10 rotor	Beckman Coulter (Brea, USA)
	Optima™ L-90K Ultracentrifuge	Beckman Coulter (Brea, USA)
	Optima™ Ultracentrifuge tubes (26x77 mm)	Beckman Coulter (Brea, USA)
	Ultracentrifuge Tubes 16x76 mm	Seton Scientific (Petaluma, USA)
Cell culture	Countess	Thermo Fisher Scientific (Waltham, USA)
	HERA safe sterile work bench	Thermo Fisher Scientific (Waltham, USA)
	HERA cell 150 incubator	Thermo Fisher Scientific (Waltham, USA)
Microscopy	CKX 419F	Olympus cooperation (Tokyo, Japan)
	Olympus Biosystems IX81	Olympus cooperation (Tokyo, Japan)
	U-RPL-T	Olympus cooperation (Tokyo, Japan)
Flow cytometry	Cytomics FC500MPL analyzer	Beckman Coulter (Brea, USA)
Western Blot	ChemoCam (ECL Imager)	INTAS Science Imaging (Göttingen, Germany)
	Mini-PROTEAN Tetra cell chamber	Bio-Rad (Hercules, USA)
	PowerPac basic/ HV/ HC	Bio-Rad (Hercules, USA)
	Trans-Blot® SD Semi-Dry	Bio-Rad (Hercules, USA)
	TECAN Infinite M200	Tecan Group (Männedorf, Switzerland)
other applications	Agilent 2100	Agilent Technologies (Santa Clara, USA)
	GloMax 96 microplate luminometer	Promega (Madison, USA)
	Pipet boy accujet pro	BrandTech Scientific (Essex, UK)
	Lauda Aqualine AL5	DJB Labcare (Buckinghamshire, UK)
	Magnetic stirrer	Thermo Fisher Scientific (Waltham, USA)
	Microwave	Sharp Electronics (Hamburg, Germany)
	Mixing block MB-102	Biozym Scientific GmbH (Hessisch Oldendorf, Germany)
	Nanodrop 2000	Thermo Fisher Scientific (Waltham, USA)
	pH meter PB-11	Sartorius (Göttingen, Germany)
	Pipettes	Gilson (Middleton, Germany)
	Pipettes	Eppendorf (Hamburg, Germany)
	Qubit fluorometer	Thermo Fisher Scientific (Waltham, USA)
	Shaker DRS-12	neoLab (Heidelberg, Germany)

TissueLyser LT	QIAGEN (Hilden, Germany)
Tube roller TRM-V	neoLab (Heidelberg, Germany)
Vacuum pump	Promega (madison, USA)
Vortex Genie2	Scientific Industries (Bohemia, USA)
Water bath TW12	Julabo Labortechnik (Seelbach, Germany)
Weighing scale	KERN & SOHN GmbH (Balingen, Germany)

Table 10. List of softwares

Application	**Program**	**Company**
Automated Imaging	ScanR acquisition software	Olympus BioSystems GmbH
Bioanalyzer	2100 Expert	Agilent Technologies (Santa Clara, USA)
Crystal Structure visualization	PyMol	The PyMOL Molecular Graphics System, Version 2.0 Schrödinger, LLC.
ddPCR	QuantaSoft™ Software	Bio-Rad (Hercules, USA)
Figure design	MS office	Microsoft Corporation (Redmond, USA)
Flow cytometry	MXP software	Beckmann Coulter (Brea, USA)
Gel pictures	Quantity One	Bio-RAD (Hercules, USA)
Graphical analysis	GraphPad Prism	GraphPad Software, Inc. (La Jolla, USA)
Graphs and Statistical Analysis	GraphPad Prism v6	GraphPad Software, Inc.
Image processing	Matlab	MathWorks, Inc. (Massachusetts, USA)
Intas	ChemoStar v.0.2.26	INTAS Science Imaging (Göttingen, Germany)
Nanodrop	NanoDrop 2000	Thermo Fisher Scientific (Waltham, USA)
Picture anaylsis	ImageJ	Open source [292]
qRT-PCR (Titration)	Rotor Gene 6000 Series	QIAGEN (Hilden, Germany)
qRT-PCR	StepOne Software v2.3	Applied Biosystems (Massachusetts, USA)
Sequence and Cloning visualization	Geneious	Biomatters (Auckland, New Zealand)
Tecan Plate reader	Magellan™	Tecan Group (Männedorf, Switzerland)

2.2. Methods

2.2.1. Molecular Biology Methods

2.2.1.1. *In silico* cloning

Cloning strategies, design of plasmid maps and primers and verification of sequencing results were performed with Geneious version 7.1. The annealing temperature of primers was determined using NEB Tm calculator (https://tmcalculator.neb.com/). GuideRNAs were evaluated using the CCTop predictor (https://crispr.cos.uni-heidelberg.de) and Cas-OFFinder (www.rgenome.net/cas-offinder), shRNAs were designed using Biosettia shRNA Designer (https://biosettia.com/support/shrna-designer) and invivoGen siRNA Wizard (www.invivogen.com/sirnawizard/construct.php). Primer and probe sets were either designed manually or via Eurofins qPCR Primer&Probe design tool (www.eurofinsgenomics.eu/en/ecom/tools/qpcr-assay-design).

2.2.1.2. Polymerase chain reaction

For polymerase chain reaction (PCR) amplification of plasmid or genomic templates, the Phusion HS II DNA polymerase (Thermo Fisher Scientific) was used according to manufacturer´s protocol in total reaction volumes of 25 to 50 µl. In short, for a reaction volume of 50 µl, 10 µl 5x GC buffer, 1 µl dNTPs, 0.5 µl Polymerase, 20 ng (plasmid) to 200ng (genomic DNA) template, 2.5 µl of each forward and reverse primer (10 µM stock concentration) were used and adjusted to 50 µl with H_2O. For 25 µl reaction volumes, the listed reagents were adjusted correspondingly. PCR was performed in thermal cycler with 98°C for 2 min, followed by 35 to 38 cycles of denaturation at 98°C for 30 sec, annealing at 55 to 65°C for 30 sec and elongation at 72°C for 30 sec/ 1kb, a final elongation step of 72°C for 2 min was added.

Note that for PCRs concerning the AcrX inhibitor project, the Q5 High-fidelity DNA polymerase 2x Master Mix (NEB) was used for all cloning procedures and T7 endonuclease assays. In a reaction volume of 25 µl, 12.5 µl Master Mix, 1.25 µl of each forward and reverse primer (10 µM stock concentration)), 3 µl genomic template were used and adjusted to 25 µl with H_2O. Cycling conditions were performed with initial

denaturation of 98°C for 30 sec, 35 cycles of denaturation at 98°C for 30 sec, annealing at 60 to 70 °C, elongation at 72°C for 30 sec/kb, followed by a final elongation at 72°C for 2 min.

To test whether a cloning procedures was successful, a colony PCR was performed on bacterial colonies. Therefore, the Quick-Load Taq 2x Master Mix (NEB) was used according to manufacturer´s protocol in total reaction volumes of 10 µl, with 5 µl of Master Mix, 0.5 µl of each forward and reverse primer (10 µM stock concentration) and adjusted to 10 µl with H_2O. The bacterial colony was directly added to the reaction mix by means of a pipet tip and was directly streaked out on an agar plate bearing the appropriate antibiotic. The PCR reaction was performed by an initial denaturation step of 94°C, 35 cycles of denaturation at 94°C, annealing at 50 to 55°C and elongation at 68°C for 1min/kb, finalized by an additional elongation step at 68°C for 5 min was added. Since the Master Mix already contained loading dye, the reaction could be loaded directly on a 1% Agarose gel.

2.2.1.3. Agarose gel electrophoresis

DNA fragments were separated via agarose gel electrophoresis. The gels were prepared by dissolving 1-2% agarose in 1% TAE buffer or 1% TBE buffer for the AcrX project (to resolve smaller fragments). To visualize the DNA Ethidium bromide was added to the gels and DNA was mixed with 6x purple loading dye prior loading. For the AcrX project Gelred was directly applied to the loading dye in a final concentration of 1%. Electrophoresis was performed at 100 to 120V. The DNA was detected using UV light and the size of the DNA was determined by comparison with the 1 kb ladder plus (Thermo Scientific) or GeneRuler DNA ladder (Thermo Scientific).

2.2.1.4. Restriction digestion

For analytical restriction digests, 500 ng plasmid DNA, 0.5 µl of each required enzyme and 1 µl of appropriate buffer were used in a total volume of 10 µl. The samples were incubated for 2 h or over night at 37°C and visualized on an agarose gel. To verify the presence of ITRs in a ssAAV context, plasmids were digested with XmaI, whereas ITRs in a dsAAV context were digested with XmaI and KpnI.

For preparative restriction digests, 1 µg of plasmid DNA was mixed with 0.5 µl of each enzyme in a total volume of 20 µL and incubated for at least 2 h at 37°C.
If needed, a dephosphorylation step was performed by subsequently adding 2 µl buffer and 1 µl Antarctic Phosphatase (NEB) for 1 h at 37°C. The phosphatase was heat inactivated at 85°C for 2 min before subsequent usage of the DNA fragment.

2.2.1.5. DNA isolation

To purify DNA fragments from agarose gels and PCRs from reaction mixes, the QIAquick Gel Extraction Kit and PCR Purification Kit were used, respectively, according to manufacturer´s instructions. In order to isolate plasmids from bacteria in a small, medium or large scale, the QIAprep Spin Miniprep and Midiprep Kit and the NucleoBond® Xtra Maxi Kit were applied, respectively, according to manufacturer´s instructions. In general, 5ml, 80 ml or 300 ml of LB media containing the appropriate antibiotics for selection were inoculated for Mini, Midi or Maxipreps, respectively.

However, in most cases a house-made Miniprep protocol was applied to isolate plasmids on small-scale with self-made buffers P1, P2 and P3. The pellet of a 2 ml bacterial culture were resuspended in 300 µl P1 buffer and subsequently 300 µl P2 buffer were added, the tubes were gently inverted, followed by a 5 min incubation to lyse the cells. For neutralization 300 µl P3 buffer was added and after gentle inversion the samples were centrifuged at full speed for 10 min to dispose of cellular debris. The supernatant was mixed with 600 µl isopropanol to precipitate the DNA. DNA was pelleted by centrifugation at maximal speed for 10 min and subsequently washed with 500 µl of 70% ethanol by centrifugation at maximal speed for 5 min. Ethanol was carefully removed and DNA was solved in 50 µl H_2O.

2.2.1.6. Preparation of chemocompetent bacteria

For the preparation of chemocompetent cells, bacteria strains listed in Table 11 were streaked on an agar plate without antibiotics from glycerol stocks and incubated at 37°C over night. The next day, one colony was picked and inoculated in 6 mL LB medium over night. Around 16 h later, 250 mL SOC medium were inoculated with 1 mL of the over night culture and subsequently incubated at 37°C, 180 rpm. Cultures were then centrifuged at 4°C, 1,800.g for 15 min, once they reached an an OD_{600} of 0.5. The cell

pellet was resuspended in 40 mL TFB I buffer and incubated for 10 min on ice. Next, cells were pelleted again (4°C, 1,800.g for 15 min) and resuspended in 10 mL of TFB II. After an incubation period of 10 min on ice, cells were distributed with a stepper pipette into 50 µL aliquots and snap-frozen in liquid nitrogen. The aliquots were then stored at -80°C until thawn on ice for transformation experiments.

Table 11. List of bacterial strains.

Strain	Description	Source
E. coli MAX Efficiency DH5αTM	Chemocompetent	Thermo Fisher Scientific (Massachusetts, USA)
E. coli ccdB SurvivalTM T1R	Chemocompetent	Thermo Fisher Scientific (Massachusetts, USA)
E. coli Top10	Chemocompetent	Thermo Fisher Scientific (Massachusetts, USA)

2.2.1.7. Ligation and transformation

Ligation reactions were performed using a 1 : 3 molar ratio of backbone to insert DNA. Besides the DNA, 0.5 µl T4 ligase (NEB or Thermo Scientific), 1 µL T4 ligase buffer and ddH_2O were added to obtain a total volume of 10 µL. The samples were incubated for at least 30 min at room temperature or over night at 16 °C.

Five µl of the ligation reaction or 1 µl of previously purified plasmid DNA (retransformation) were added to 50 to 100 ul of chemically competent bacteria cells. For the transformation, bacteria incubated on ice for 10 min, followed by a heat shock at 42 °C for 30 sec and once again left on ice for 10 min. In case of ampicillin selection, bacteria were directly plated on agar plates containing ampicillin, whereas in case of chloramphenicol selected bacteria recovered in antibiotic-free LB medium for 1 h before plating 100 ul on agar plates containing chloramphenicol.

2.2.1.8. Bacterial culture conditions

Bacteria were cultured in LB medium carrying the respective antibiotic resistance. Ampicillin was added in a 1/1000 dilution from a 50 mg/ml stock solution (solved in H_2O) and chloramphenicol was added in a 1/1000 dilution from a 20 mg/ml stock solution (solved in ethanol). For cultivation on LB plates, 1.5% (w/v) agar was added to the medium and the antibiotic was added also in a 1/1000 dilution shortly before pouring of the plates. Plates incubated at 37°C overnight in a humidified incubator. Liquid cultures

incubated at 37°C and shaking at 180 rpm for at least 6 h and up to 16 h. For all successfully cloned constructs a glycerol stock was prepared by mixing 500 µl bacteria culture with 500 µl 70% glycerol and stored at -80°C.

2.2.1.9. Golden gate cloning

Golden gate assembly was performed as suggested in Engler *et al.* [293] and applied for the cloning of sgRNAs and shRNAs in plasmid backbones with BsmBI or BbsI. Therefore, sense and anti-sense oligos were annealed by mixing 2.5 µl of each oligo (100 µM stock concentration), 5 µl NEB buffer 2 and 40 µl H_2O. In a thermocycler the mixture of oligos were heated to 95 °C for 2 min and subsequently cooled by ramping (-0.1°C/sec) to 25 °C over a period of 25 min. For further usage, the annealed oligo mix was diluted 1:200 with H_2O.

Subseqently, the Golden Gate reaction was performed in a total reaction volume of 10 µl, including 0.5 µl of respective type II-S restriction enzyme, 0.5 µl T4 ligase (NEB or Thermo Scientific), and 1 µl T4 ligase buffer and an equimolar mixture of roughly 100ng backbone and insert (annealed and diluted oligo mix). The reaction incubated in a thermocycler using 16 cycles with alternating temperatures of 37 °C for 2 min and 16 °C for 3 min. Enzymes were heat inactivated by applying 85 °C for 10 min. Subsequently, 5 µl of the reaction mixture were transformed in chemocompetent bacteria.

2.2.1.10. Sequencing

Sanger sequencing was performed for each construct mentioned in this thesis, by the lightrun sequencing service offered by Eurofins Scientific. Therefore, about 400 to 800 ng plasmid DNA was mixed with 2.5 µl primer (10 µM) in a 10 µl reaction volume and send to sequencing in a 1.5 ml reaction tube.

2.2.1.11. Genomic DNA and RNA isolation

For simultaneous DNA and RNA extraction from cell culture and mouse tissue the QIAGEN AllPrep DNA/RNA mini kit was used according to manufacturer´s instructions with a few changes.

In case of samples from cell culture, the QIAshredder tubes were applied prior to DNA/RNA extraction. Therefore, the supernatant of the cells was removed and 300 µl RTL buffer (from the AllPrep kit) with 1% ß-Mercaptoethanol was added to the cells and incubated for 5 min. This caused the cells to lyse and the lysate was loaded directly on the QIAshredder column and centrifuged at 13000 g for 2 min. The flow-through was used for further processing.

In case of mouse tissue, a tiny piece of the frozen tissue was taken and added to 500 µl RTL buffer with 1% ß-Mercaptoethanol in 2 ml reaction tubes that also contained a metal beat. The tissue was homogenized with the Tissue Ruptor at 50 Hz for 45 sec. The lysate was centrifuged at 13000 g for 3 min and the supernatant was carefully removed and used for further processing.

To either the flow-through of the QIAshredder for samples from cell culture or the supernatant after tissue disruption of i*n vivo* samples, 10 µl Proteinase K (from the AllPrep kit) was added and incubated for 15 min at 55 °C. Subsequently, the samples were loaded on the AllPrep DNA spin column and centrifuged for 30 sec at 10000 g. The DNA columns containing the DNA were stored at 4 °C until they were further processed (on the same day), whereas the flow-through contained the RNA and was processed immediately. Therefore, 1 volume (300 µl for cell culture samples and 500 µl for mouse tissue samples) of 70% ethanol, or 50% ethanol in case of liver samples, were added to the flow-through containing the RNA and well mixed. 700 µl sample were transferred to the RNeasy spin column and centrifuged for 30 sec at 10000 g. The flow-through was discarded. Next, 350 µl of Buffer RW1 was added to the RNeasy spin column and centrifuged for 30 sec at 10000 g. An on-column DNAseI digest was performed by adding 80 µl of 1:8 diluted DNaseI in RDD buffer (10 µl DNaseI and 70 µl RDD buffer) directly on the column using the RNase-free DNase set from QIAGEN and incubated for 20 min at room temperature. Subsequently, another 350 µl of Buffer RW1 was added to the RNeasy spin column and centrifuged for 30 sec at 10000 g. Finally, the column was washed twice with 500 µl of Buffer RPE by centrifugation for 30 sec at 10000 g and a final dry centrifugation with no buffer at full speed for 1 min. The RNA was eluted in 30 µl H_2O, the concentration of the samples were determined by Nanodrop and the samples were stored at -80 °C.

Next, the DNA was further processed by adding 500 µl of Buffer AW1 to the AllPrep DNA spin column and centrifugation at 10000 g for 30 sec. The flow-through was discarded. Finally, another 500 µl of Buffer AW2 was added on the column and centrifuged at 10000r g for 30 sec, followed by a dry centrifugation with no buffer at full speed for 1 min.

The DNA was diluted in 30 µl H_2O, the concentration of the samples were determined by Nanodrop and the samples were stored at -80 °C.

2.2.2. Cloning procedures

2.2.2.1. Cloning of single small RNA expression vectors

Single small RNAs, as gRNAs or shRNAs, were expressed either under the U6, H1 or 7SK promoter. Therefore, sense and antisense oligonucleotides were annealed as described in section 2.2.1.9 and created a 5´CACC and 3´AAAC overhang or a 5´CACC and 3´AAAA overhang for gRNAs or shRNAs, respectively. Oligonucleotides for gRNAs and shRNAs are listed in Table 12. The acceptor plasmids harbored the corresponding Pol III promoter followed by a *ccdB* kill gene or stuffer sequence that was flanked with recognition sites for type IIS restriction enzymes. In case of gRNA expression vectors, the tracrRNA scaffold sequence compatible with SaCas9 adjoined the *ccdB* gene, whereas in case of shRNA an AAAAAA sequence terminated shRNA expression. The acceptor plasmids either harbored ITRs for packaging in AAVs as well as an RSV-GFP expression cassette and were amplified via Ampicillin selection (acceptor plasmids #1576, #1578, #1581, #1584), or were used as interim stage for multiplexed small RNA expression cassettes and in this case were amplified via Chloramphenicol selection (acceptor plasmids #1588, #1590, #1591, #1593, #1594, #1596). Golden Gate cloning as described in section 2.2.1.9 was performed using the type IIS restriction enzymes BsmBI or BbsI in order to exchange a *ccdB* kill gene or an empty stuffer sequence with the appropriate gRNA/ shRNA oligonucleotides. The acceptor plasmids as well as resulting plasmids are listed in Table 13. Note that in order to clone the TuD sequence via Golden Gate in its acceptor plasmid #1591, the complete TuD sequence was ordered as sense ans antisense oligonucleotides ans subsequently annealed as described for shRNA or sgRNA cloning. Accordingly, this cloning procedure deviated from the proposed TuD cloning strategy in [162].

Table 12. Oligonucleotide sequences used for gRNA and shRNA cloning

No	Name	Sequence 5´-3´
#1	gMecP2g8-fw	**CACC**GAGGCCAAAAAGAAAGCCGTGA
#2	gMecP2g8-rv	**AAAC**TCACGGCTTTCTTTTTGGCCTC
#3	gHBs-g1-fw	**CACC**GACCCCTTCTCGTGTTACAGG

#4	gHBs-g1-rv	**AAAC**CCTGTAACACGAGAAGGGGTC
#5	gHBs-g2-fw	**CACC**GGCGGGGTTTTTCTTGTTGAC
#6	gHBs-g2-rv	**AAAC**GTCAACAAGAAAAACCCCGCC
#7	gHBs-g3-fw	**CACC**GGTGGTCGGGAAAGAATCCCA
#8	gHBs-g3-rv	**AAAC**TGGGATTCTTTCCCGACCACC
#9	gHBs-g4-fw	**CACC**GGATTCTTTCCCGACCACCAG
#10	gHBs-g4-rv	**AAAC**CTGGTGGTCGGGAAAGAATCC
#11	gHBs-g5-fw	**CACC**GTCTAGACTCTGCGGTATTGT
#12	gHBs-g5-rv	**AAAC**ACAATACCGCAGAGTCTAGAC
#13	gHBs-g6-fw	**CACC**GAAAATTGAGAGAAGTCCACC
#14	gHBs-g6-rv	**AAAC**GGTGGACTTCTCTCAATTTTC
#15	gHBs-g7-fw	**CACC**GTGATGTTCTCCATGTTCAGCG
#16	gHBs-g7-rv	**AAAC**CGCTGAACATGGAGAACATCAC
#17	gHBs-g8-fw	**CACC**GGACCCCTTCTCGTGTTACAGG
#18	gHBs-g8-rv	**AAAC**CCTGTAACACGAGAAGGGGTCC
#19	gHBs-g9-fw	**CACC**GGGATTCTTTCCCGACCACCAG
#20	gHBs-g9-rv	**AAAC**CTGGTGGTCGGGAAAGAATCCC
#21	gHBs-g10-fw	**CACC**GACAAGAATCCTCACAATACCG
#22	gHBs-g10-rv	**AAAC**CGGTATTGTGAGGATTCTTGTC
#23	gHBxg11-fw	**CACC**GGCAGACGGAGAAGGGGACGA
#24	gHBxg11-rv	**AAAC**TCGTCCCCTTCTCCGTCTGCC
#25	gnontarget-fw	**CACC**GATCGTTTCCGCTTAACGGCG
#26	gnontarget-rv	**AAAC**CGCCGTTAAGCGGAAACGATC
#27	gmCherry-fw	**CACC**AGCCGTACATGAACTGAGGGGA
#28	gmCherry-rv	**AAAC**TCCCCTCAGTTCATGTACGGCT
#29	gLuc-fw	**CACC**GCACTGGCATGAAGAACTGCA
#30	gLuc-rv	**AAAC**TGCAGTTCTTCATGCCAGTGC
#31	gLuc_scr-fw	**CACC**GCAGTCAATTGCCGGGCGCTG
#32	gLuc_scr-rv	**AAAC**CAGCGCCCGGCAATTGACTGC
#33	gCas-fw	**CACC**GGTGATGCCGATGTCCAGGCC
#34	gCas-rv	**AAAC**GGCCTGGACATCGGCATCACC
#35	gCas_scr-fw	**CACC**GCAGTCAATTGCCGGGCGCTG
#36	gCas_scr-rv	**AAAC**CAGCGCCCGGCAATTGACTGC
#37	gEMX-fw	**CACC**GGCCTCCCCAAAGCCTGGCCA
#38	gEMX-rv	**AAAC**TGGCCAGGCTTTGGGGAGGCC
#39	gGrin2B-fw	**CACC**GAGAGTAGGCTGGTAGATGGAG
#40	gGRIN2B-rv	**AAAC**CTCCATCTACCAGCCTACTCTC
#41	gHBB-fw	**CACC**AGGGTTGCCCATAACAGCATC
#42	gHBB-rv	**AAAC**GATGCTGTTATGGGCAACCCT
#43	shHBV7-fw	**CACC**GCGCTGAATCCTGCGGACGACCTCAAGAGGGT CGTCCGCAGGATTCAGCGC
#44	shHBV7-rv	**AAAA**GCGCTGAATCCTGCGGACGACCCTCTTGAGGT CGTCCGCAGGATTCAGCGC
#45	shctrl-fw	**CACC**GGCCTTTCACTACTCCTACGATCAAGAGTCGTA GGAGTAGTGAAAGGCC
#46	sh-ctrl-rv	**AAAA**GGCCTTTCACTACTCCTACGACTCTTGATCGTA GGAGTAGTGAAAGGCC
#47	shHDV3-fw	**CACC**GGGATTTCCATAGGATATACTTCAAGAGAGTAT

		ATCCTATGGAAATCCC
#48	shHDV3-rv	**AAAA**GGGATTTCCATAGGATATACTCTCTTGAAGTAT ATCCTATGGAAATCCC
#49	shHDV4-fw	**CACC**GGGATTTCCATAGGATATATCAAGAGTATATCC TATGGAAATCCC
#50	shHDV4-rv	**AAAA**GGGATTTCCATAGGATATACTCTTGATATATCCT ATGGAAATCCC
#51	shHDV6-fw	**CACC**GCATCTCCTCCTATCGCTATGGTTCAAGAGACC ATAGCGATAGG AGGAGATGC
#52	shHDV6-rv	**AAAA**GCATCTCCTCCTATCGCTATGGTCTCTTGAACC ATAGCGATAGGAGGAGATGC
#53	shHDV7-fw	**CACC**GATTCCTCCCTCTGAGTGCTACTTCAAGAGAGT AGCACTCAGAG GGAGGAATC
#54	shHDV7-rv	**AAAA**GATTCCTCCCTCTGAGTGCTACTCTCTTGAAGT AGCACTCAGAGGGAGGAATC
#55	shHDV8-fw	**CACC**GCATCTCCTCCTATCGCTATGGTCTTCAAGAGA GACCATAGCGA TAGGAGGAGATGC
#56	shHDV8-rv	**AAAA**GCATCTCCTCCTATCGCTATGGTCTCTCTTGAA GACCATAGCGATAGGAGGAGATGC
#57	shHDV9-fw	**CACC**GTTCCAATGCTCTTTACCGTGACATTCAAGAGA TGTCACGGTAA AGAGCATTGGAAC
#58	shHDV9-rv	**AAAA**GTTCCAATGCTCTTTACCGTGACATCTCTTGAA TGTCACGGTAAAGAGCATTGGAAC
#59	shHDV3ed-fw	**CACC**GGGATTTCCATGGGATATACTTCAAGAGAGTAT ATCCCATGGAAATCCC
#60	shHDV3ed-rv	**AAAA**GGGATTTCCATGGGATATACTCTCTTGAAGTAT ATCCCATGGAAATCCC
#61	shHDV4ed-fw	**CACC**GGGATTTCCATGGGATATATCAAGAGTATATCC CATGGAAATCC C
#62	shHDV4ed-rv	**AAAA**GGGATTTCCATGGGATATACTCTTGATATATCC CATGGAAATCCC
#63	TuD_HBV7	**CACC**AGGTCGTCCGCAGGATTCAGCGCCAAGTATTC TGGTCACAGAATACAACGGTCGTCCGCAGGATTCAG CGCA
#64	TuD_HBV7	**AAAA**TGCGCTGAATCCTGCGGACGACCGTTGTATTCT GTGACCAGAATACTTGGCGCTGAATCCTGCGGACGA CCT
#65	TuD_scr	**CACC**AACCGTCGAGTGCTGCCGTAGCGCAAGTATTC TGGTCACAGAATACAACACCGTCGAGTGCTGCCGTA GCGA
#66	TuD_scr	**AAAA**TCGCTACGGCAGCACTCGACGGTGTTGTATTCT GTGACCAGAATACTTGCGCTACGGCAGCACTCGACG GTT

Table 13. Plasmids used for expression of single gRNAs and shRNAs

Internal No	Name	Description	Origin
#1576	dsAAV_U6-ccdB_shRNA	Acceptor plasmid for shRNA, ccdB is removed by GG with BsmBI, ITRs present	Florian Schmidt
#1578	dsAAV_U6-ccdB_Sa_Scaffold	Acceptor plasmid for gRNA for SaCas9, ccdB is removed by GG with BsmBI, ITRs present	Florian Schmidt
#1581	dsAAV_ H1-ccdB_Sa_Scaffold	Acceptor plasmid for gRNA for SaCas9, ccdB is removed by GG with BsmBI, ITRs present	Florian Schmidt
#1584	dsAAV_ 7SK-	Acceptor plasmid for gRNA for	Florian

	ccdB_Sa_Scaffold	SaCas9, ccdB is removed by GG with BsmBI, ITRs present	Schmidt
#1588	#48_GGC_1+2_pBSU6-ccdB_shRNA	Acceptor plasmid for shRNA, interim plasmid for TRISPR, ccdB is removed by GG with BsmBI	Florian Schmidt
#1590	#48_GGC_1+2_pBSU6-ccdB_Sa_Scaffold	Acceptor plasmid for gRNA compatible with SaCas9 , interim plasmid for TRISPR, ccdB is removed by GG with BsmBI	Florian Schmidt
#1591	#48_GGC_2+3_pBSH1_ccdB_shRNA	Acceptor plasmid for shRNA, interim plasmid for TRISPR, ccdB is removed by GG with BsmBI	Florian Schmidt
#1593	#48_GGC_2+3_pBSH1_ccdB_Sa_Scaffold	Acceptor plasmid for gRNA compatible with SaCas9 , interim plasmid for TRISPR, ccdB is removed by GG with BsmBI	Florian Schmidt
#1594	#48_GGC_3+4_pBS7SK_ccdB_shRNA	Acceptor plasmid for shRNA, interim plasmid for TRISPR, ccdB is removed by GG with BsmBI	Florian Schmidt
#1596	#48_GGC_3+4_pBS7SK_ccdB_Sa_Scaffold	Acceptor plasmid for gRNA compatible with SaCas9 , interim plasmid for TRISPR, ccdB is removed by GG with BsmBI	Florian Schmidt
#2637	dsAAV-U6-gMecP2-g8_RSV-GFP	GG of oligos in #1578, ITRs present, amp selection	Master Thesis
#2639	dsAAV-U6-EMXguide_RSV-GFP	GG of oligos in #1578, ITRs present, amp selection	Master Thesis
#2640	dsAAV-U6-mCherry-guide_RSV-GFP	GG of oligos in #1578, ITRs present, amp selection	Master Thesis
#2641	dsAAV-U6-gHBs-g1_RSV-GFP	GG of oligos in #1578, ITRs present, amp selection	This study
#2642	dsAAV-U6-gHBs-g2_RSV-GFP	GG of oligos in #1578, ITRs present, amp selection	This study
#2643	dsAAV-U6-gHBs-g3_RSV-GFP	GG of oligos in #1578, ITRs present, amp selection	This study
#2644	dsAAV-U6-gHBs-g4_RSV-GFP	GG of oligos in #1578, ITRs present, amp selection	This study
#2645	dsAAV-U6-gHBs-g5_RSV-GFP	GG of oligos in #1578, ITRs present, amp selection	This study
#2646	dsAAV-U6-gHBs-g6_RSV-GFP	GG of oligos in #1578, ITRs present, amp selection	This study
#2647	dsAAV-U6-gHBs-g7_RSV-GFP	GG of oligos in #1578, ITRs present, amp selection	This study
#2648	dsAAV-U6-gHBs-g8_RSV-GFP	GG of oligos in #1578, ITRs present, amp selection	This study
#2649	dsAAV-U6-gHBs-g9_RSV-GFP	GG of oligos in #1578, ITRs present, amp selection	This study
#2650	dsAAV-U6-gHBs-g10_RSV-GFP	GG of oligos in #1578, ITRs present, amp selection	This study
#2651	#48_GGC_1+2_U6-HBsg8_Cm	GG of oligos in #1590, interim plasmid for TRISPR, cam selection	This study
#2652	#48_GGC_2+3_H1-HBsg7_Cm	GG of oligos in #1590, interim plasmid for TRISPR, cam selection	This study
#2653	#48_GGC_3+4_7sk-HBsg6_Cm	GG of oligos in #1590, interim plasmid for TRISPR, cam selection	This study
#2655	#48_GGC_1+2_U6HBxg11_Cm	GG of oligos in #1590, interim plasmid for TRISPR, cam	This study

		selection	
#2656	#48_GGC_2+3_H1-HBsg6_Cm	GG of oligos in #1593, interim plasmid for TRISPR, cam selection	This study
#2657	#48_GGC_3+4_7sk-shHB_Cm	GG of oligos in #1594, interim plasmid for TRISPR, cam selection	This study
#2658	#48_GGC_1+2_U6-gctrl_Cm	GG of oligos in #1590, interim plasmid for TRISPR, cam selection	This study
#2659	#48_GGC_2+3_H1-gctrl_Cm	GG of oligos in #1593, interim plasmid for TRISPR, cam selection	This study
#2660	#48_GGC_3+4_7sk-shctrl_Cm	GG of oligos in #1594, interim plasmid for TRISPR, cam selection	This study
#2669	#48_GGC_1+2_U6-HBsg6_Cm	GG of oligos in #1590, interim plasmid for TRISPR, cam selection	This study
#2670	#48_GGC_2+3_H1-TuD_Cm	GG of oligos in #1594, interim plasmid for TRISPR, cam selection	This study
#2671	#48_GGC_2+3_H1-TuDctrlCm	GG of oligos in #1594, interim plasmid for TRISPR, cam selection	This study
#2684	#48_GGC_1+2_U6-sh3edHDV_Cm	GG of oligos in #1588, interim plasmid for TRISPR, cam selection	This study
#2685	#48_GGC_2+3_H1-shHBV7_Cm	GG of oligos in #1591, interim plasmid for TRISPR, cam selection	This study
#2686	#48_GGC_1+2_U6-shctrl_Cm	GG of oligos in #1588, interim plasmid for TRISPR, cam selection	This study
#2687	#48_GGC_2+3_H1-shctrl_Cm	GG of oligos in #1591, interim plasmid for TRISPR, cam selection	This study
#2688	#48_GGC_3+4_7sk-gctrlCm	GG of oligos in #1596, interim plasmid for TRISPR, cam selection	This study
#2689	#48_GGC_2+3_H1-HBsg3_Cm	GG of oligos in #1593, interim plasmid for TRISPR, cam selection	This study
#2706	dsAAV-U6-HDV_shRNA1_RSV-GFP	GG of oligos in #1576, ITRs present, amp selection	This study
#2707	dsAAV-U6-HDV_shRNA2_RSV-GFP	GG of oligos in #1576, ITRs present, amp selection	This study
#2708	dsAAV-U6-HDV_shRNA3_RSV-GFP	GG of oligos in #1576, ITRs present, amp selection	This study
#2709	dsAAV-U6-HDV_shRNA4_RSV-GFP	GG of oligos in #1576, ITRs present, amp selection	This study
#2710	dsAAV-U6-HDV_shRNA5_RSV-GFP	GG of oligos in #1576, ITRs present, amp selection	This study
#2711	dsAAV-U6-HDV_shRNA6_RSV-GFP	GG of oligos in #1576, ITRs present, amp selection	This study
#2712	dsAAV-U6-HDV_shRNA7_RSV-GFP	GG of oligos in #1576, ITRs present, amp selection	This study
#2713	dsAAV-U6-HDV_shRNA8_RSV-GFP	GG of oligos in #1576, ITRs present, amp selection	This study
#2714	dsAAV-U6-	GG of oligos in #1576, ITRs	This study

	HDV_shRNA9_RSV-GFP	present, amp selection	
#2715	dsAAV-U6-HDV_shRNA3ed_RSV-GFP	GG of oligos in #1576, ITRs present, amp selection	This study
#2716	dsAAV-U6-HDV_shRNA4ed_RSV-GFP	GG of oligos in #1576, ITRs present, amp selection	This study
#2741	dsAAV-H1-HBs-g7_RSV-GFP	GG of oligos in #1581, ITRs present, amp selection	This study
#2742	dsAAV-7sk-HBs-g6_RSV-GFP	GG of oligos in #1584, ITRs present, amp selection	This study
#2717	dsAAV-U6-gHBs-g8-Stuffer	gRNA for SaCas9 against HBsAg, stuffer ensures 2 kb size	This study
#2718	dsAAV-H1-HBs-g7-Stuffer	gRNA for SaCas9 against HBsAg, stuffer ensures 2 kb size	This study
#2719	dsAAV-7sk-HBs-g6-Stuffer	gRNA for SaCas9 against HBsAg, stuffer ensures 2 kb size	This study
#2743	dsAAV-H1-gCas9	gRNA for SaCas9 against itself	This study
#2744	dsAAV-H1-gscrCas9	scrambled gRNA for SaCas9 against itself	This study

Note that for the comparison of different multiplexing approaches, the RSV-GFP cassette of the constructs #2648, #2741and #2742 was partly exchanged with a LacZ stuffer sequence of various sizes (to ensure a final vector size of about 2 kb) via AgeI/NotI digestion resulting in constructs #2717, #2718 and #2719, respectively. Therefore, LacZ was PCR amplified using the forward primer #1 and the reverse primer #2, #3 or #4 (Table 14) for the final U6, H1 and 7SK construct, respectively.

Table 14. Oligos used for cloning

No	Name	Sequence 5´-3´
#1	LacZstufferNotI	ATATATGCGGCCGCAGGTTTGTTTGCCGGATCAAG
#2	LacZstuffer_630bp_AgeI	ATATATACCGGTAGAATCAGGGGATAACGCAGG
#3	LacZstuffer_950bp_AgeI	ATATATACCGGTGCTTTTGTTCCCTTTAGTGAGGG
#4	LacZstuffer_870bp_AgeI	ATATATACCGGTACAACATACGAGCCGGAAGC

2.2.2.2. Cloning of multiplexed small RNA expression vectors

Multiplexed small RNA expression vectors were cloned using the TRISPR strategy as illustrated in Figure 13. For this purpose, first three interim plasmids were cloned harboring single gRNA or shRNA expression cassettes (as described in section 2.2.2.1) under the U6 promoter flanked with overhang 1+2, under the H1 promoter flanked with overhang 2+3 and under the 7SK promoter flanked with overhang 3+4. In a second Golden Gate reaction using the restriction enzyme BbsI, the U6, H1 and 7SK expression cassettes were multiplexed on an assembly plasmid (#1600) that harbors overhang 1+4 and thus enables assembly in a final dsAAV vector.

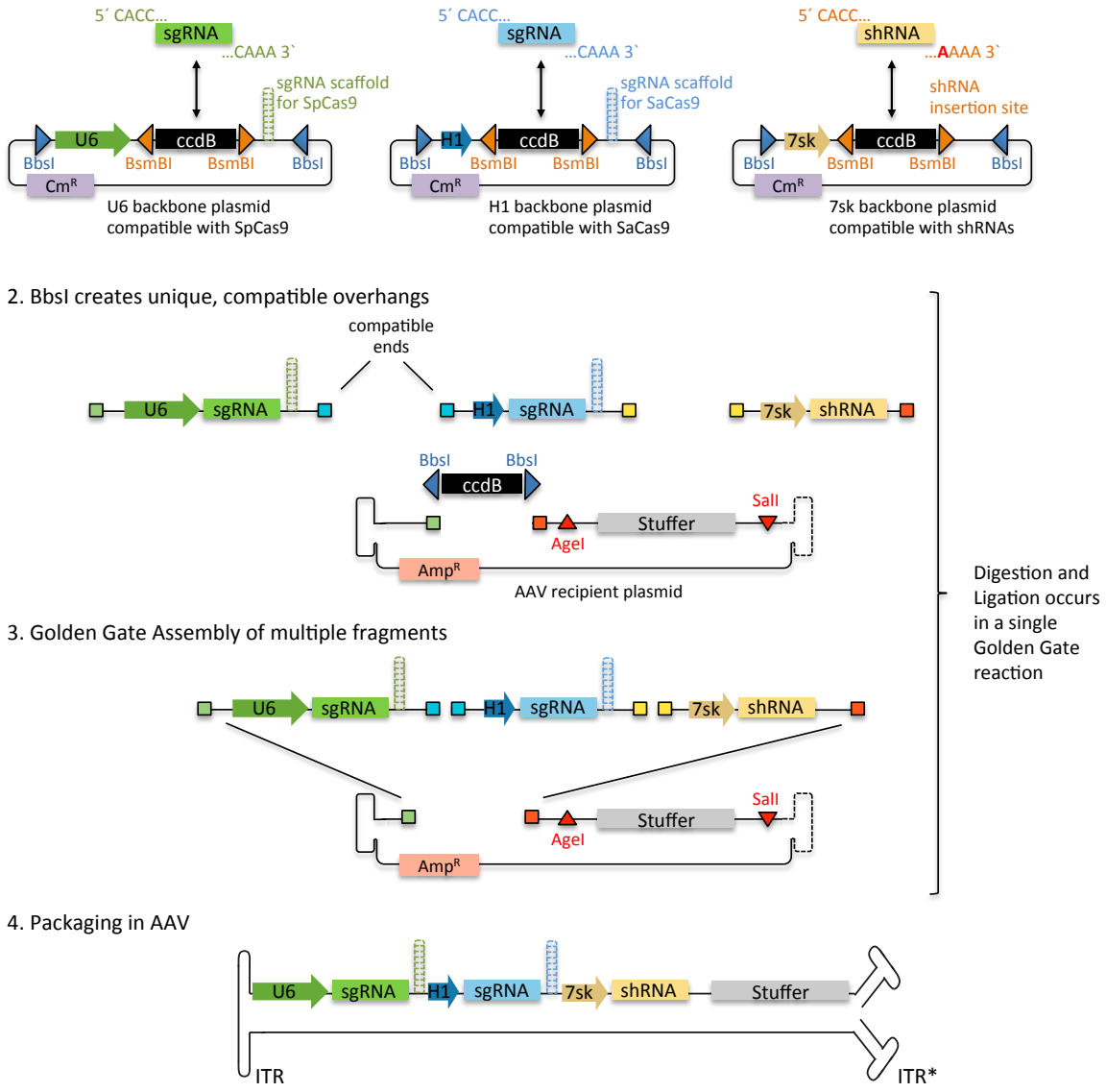

Figure 13. TRISPR cloning protocol.

TRISPR consists of several standardized plasmid backbones and a step by step protocol to multiplex three sgRNAs (compatible with *Sa* and *Sp*Cas9) and/or shRNAs on a single dsAAV vector and was invented by Florian Schmidt. The first cloning step comprises the substitution of the ccdB gene, a toxin for non-resistant bacteria, by either an shRNAs or the portion of the sgRNA that mediates target recognition (crRNA portion of the sgRNA), using highly efficient Golden Gate cloning. This first cloning step results in three different single RNA expression vectors that contain the three Pol III promoters U6, H1 or 7sk, respectively. The second cloning step results in the final TRISPR vector and comprises the assembly of each RNA expression cassette and an AAV recipient plasmid. The type IIS restriction enzyme BbsI creates unique overhangs for each RNA expression cassette and enables the assembly in a specified sequence, commencing with the U6, H1 and 7sk cassettes. The triple RNA expression cassettes are flanked by ITRs leading to the dsAAV vector.

The final dsAAV vector is termed TRISPR and harbors ITRs in order to allow vector packaging as well as a stuffer sequence to ensure a 2 kb viral genome size. A list of all TRISPR vectors is provided in Table 15.

Table 15. Plasmids used for multiplexed small RNA expression via TRISPR

Internal No	Name	Description	Origin
#1600	AAV TRISPR 2.0 ccdB GGC 1+4_	Acceptor vector with ITRs	Florian Schmidt
#2654	dsAAV_U6-HBsg8_H1-HBsg7_7SK-HBsg6	GG of #1600 &#2648+#2647+#2646	This study
#2661	dsAAV_U6-HBxg11_H1-HBsg6_7sk-shHB7	GG of #1600 &#2655+#2656+#2657	This study
#2662	dsAAV_U6-ctrlg_H1-HBsg6_7sk-ctrlsh	GG of #1600 &#2658+#2656+#2660	This study
#2663	dsAAV_U6-HBxg11_H1-HBsg6_7sk-shctrl	GG of #1600 &#2655+#2656+#2660	This study
#2664	dsAAV_U6-ctrlg_H1-HBsg6_7sk-shHB7	GG of #1600 &#2658+#2656+#2657	This study
#2665	dsAAV_U6-HBxg11_H1-gctrl_7sk-shctrl	GG of #1600 &#2655+#2659+#2660	This study
#2666	dsAAV_U6-ctrlg_H1-ctrlg_7sk-shHB7	GG of #1600 &#2658+#2659+#2657	This study
#2667	dsAAV_U6-HBxg11_H1-ctrlg_7sk-shHB7	GG of #1600 &#2655+#2659+#2657	This study
#2668	dsAAV_U6-gctrl_H1-gctrl_7sk-shctrl	GG of #1600 &#2658+#2659+#2660	This study
#2672	dsAAV_U6-HBxg11_H1-TuDHB7_7sk-shHB7	GG of #1600 &#2655+#2670+#2657	This study
#2673	dsAAV_U6-HBsg6_H1-TuDHB7_7sk-shHB7	GG of #1600 &#2669+#2670+#2657	This study
#2674	dsAAV_U6-HBxg11_H1-TuDscr_7sk-shctrl	GG of #1600 &#2655+#2671+#2660	This study
#2675	dsAAV_U6-HBsg6_H1-TuDscr_7sk-shctrl	GG of #1600 &#2669+#2671+#2660	This study
#2676	dsAAV_U6-HBxg11_H1-TuDHB7_7sk-shctrl	GG of #1600 &#2655+#2670+#2660	This study
#2677	dsAAV_U6-HBsg6_H1-TuDHB7_7sk-shctrl	GG of #1600 &#2669+#2670+#2660	This study
#2678	dsAAV_U6-HBxg11_H1-TuDscr_7sk-shHB7	GG of #1600 &#2655+#2671+#2657	This study
#2679	dsAAV_U6-HBsg6_H1-TuDscr_7sk-shHB7	GG of #1600 & #2669+#2671+#2657	This study
#2680	dsAAV_U6-gctrl_H1-TuDscr_7sk-shHB7	GG of #1600 &#2658+#2671+#2657	This study
#2681	dsAAV_U6-gctrl_H1-TuDHB7_7sk-shctrl	GG of #1600 &#2658+#2670+#2660	This study
#2682	dsAAV_U6-gctrl_H1-TuDHB7_7sk-shHB7	GG of #1600 &#2658+#2670+#2657	This study
#2683	dsAAV_U6-gctrl_H1-Tuscr_7sk-shctrl	GG of #1600 &#2658+#2671+#2660	This study
#2690	dsAAV_U6-HD_sh3ed_H1-HB-g3-S_7SK-g6-S	GG of #1600 &#2684+#2689+#2653	This study
#2691	dsAAV_U6-HD_sh3ed_H1-ctrlg_7SK-ctrlg	GG of #1600	This study

		&#2684+#2659+#2688	
#2692	dsAAV_U6-HD_sh3ed_H1-HB-g3-S_7SK-ctrlg	GG of #1600 &#2684+#2689+#2688	This study
#2693	dsAAV_U6-HD_sh3ed_H1-ctrlg_7SK-g6-S	GG of #1600 &#2684+#2659+#2653	This study
#2694	dsAAV_U6-ctrlsh_H1-HB-g3-S_7SK-g6-S	GG of #1600 &#2686+#2689+#2653	This study
#2695	dsAAV_U6-ctrlsh_H1-ctrlg_7SK-ctrlg	GG of #1600 &#2686+#2659+#2688	This study
#2696	dsAAV_U6-ctrlsh_H1-HB-g3-S_7SK-ctrlg	GG of #1600 &#2686+#2689+#2688	This study
#2697	dsAAV_U6-ctrlsh_H1-ctrlg_7SK-g6-S	GG of #1600 &#2686+#2659+#2653	This study
#2698	dsAAV_U6-HD_sh3ed_H1-sh7_7SK-g6-S	GG of #1600 &#2684+#2685+#2653	This study
#2699	dsAAV_U6-HD_sh3ed_H1-ctrlsh_7SK-ctrlg	GG of #1600 &#2684+#2687+#2688	This study
#2700	dsAAV_U6-HD_sh3ed_H1-sh7_7SK-ctrlg	GG of #1600 &#2684+#2685+#2688	This study
#2701	dsAAV_U6-HD_sh3ed_H1-ctrlsh_7SK-g6-S	GG of #1600 &#2684+#2687+#2653	This study
#2702	dsAAV_U6-ctrlsh_H1-sh7_7SK-g6-S	GG of #1600 &#2686+#2685+#2653	This study
#2703	dsAAV_U6-ctrlsh_H1-ctrlsh_7SK-ctrlg	GG of #1600 &#2686+#2687+#2688	This study
#2704	dsAAV_U6-ctrlsh_H1-sh7_7SK-ctrlg	GG of #1600 &#2686+#2685+#2688	This study
#2705	dsAAV_U6-ctrlsh_H1-ctrlsh_7SK-g6-S	GG of #1600 &#2686+#2687+#2653	This study

2.2.2.3. Cloning of promoter library to drive *Sa*Cas9 expression *in vivo*

For expression of *Sa*Cas9 *in vivo*, the CMV promoter of #1829 was exchanged by the indicated promoter. Therefore, the promoters were first PCR amplified using the primers listed in Table 16 and subsequently digested with PacI and NheI and ligated in #1829, resulting in the construct listed in Table 17.

Table 16. Primers used to clone the promoter library for SaCas9 expression in vivo

No	Name	Sequence 5´-3´	Template
1	TTR fw	TCTAGATTAATTAAGGATCTGTCAATTCACGCG	#1693
2	TTR rv	GTGGCGCTAGCGACCGGTGCGGCCG	
3	TBG fw	TCTAGATTAATTAAACGTAGCCATGCTCTAGTACGC	#522
4	TBG rv	GTGGCGCTAGCATCTTTCCATTTTTATAGCATGTCC	
5	EFS fw	TCTAGATTAATTAAGGGCAGAGCGCACATC	#1543
6	EFS rv	GTGGCGCTAGCCTGTGTTCTGGCGGCAAAC	

Table 17. Plasmids and promoter sequences used for *in vivo Sa*Cas9 expression.

Internal No	Name	Promoter sequence	Origin
#1830	ssAAV-LP1-SaCas9	CCCTAAAATGGGCAAACATTGCAAGCAGCAAACAGCAA ACACACAGCCCTCCCTGCCTGCTGACCTTGGAGCTGG GGCAGAGGTCAGAGACCTCTCTGGGCCCATGCCACCT CCAACATCCACTCGACCCCTTGGAATTTCGGTGGAGAG GAGCAGAGGTTGTCCTGGCGTGGTTTAGGTAGTGTGA GAGGGGAATGACTCCTTTCGGTAAGTGCAGTGGAAGC TGTACACTGCCCAGGCAAAGCGTCCGGGCAGCGTAGG CGGGCGACTCAGATCCCAGCCAGTGGACTTAGCCCCT GTTTGCTCCTCCGATAACTGGGGTGACCTTGGTTAATA TTCACCAGCAGCCTCCCCCGTTGCCCCTCTGGATCCA CTGCTTAAATACGGACGAGGACAGGGCCCTGTCTCCT CAGCTTCAGGCACCACCACTGACCTGGGACAGTGAAT CCGGACTCTAAGGTAAATATAAAATTTTTAAGTGTATAA TGTGTTAAACTACTGATTCTAATTGTTTCTCTCTTTTAGA TTCCAACCTTTGGAACTGAATTCTAG	Plasmid Library
#2747	ssAAV-TTR-SaCas9	GGATCTGTCAATTCACGCGAGTTAATAATTACCAGCGC GGGCCAAATAAATAATCGCGAGGGGCAGGTGACGTTT GCCCAGCGCGCGCTGGTAATTATTAACCTCGCGAATAT TGATTCGAGGCCGCGATTGCCGCAATCGCGAGGGGCA GGTGACCTTTGCCCAGCGCGCGTTCGCCCCGCCCCG GACGGTATCGATGTCGAGGGGGATCCCACTGGGAGGA TGTTGAGTAAGATGGAAAACTACTGATGACCCTTGCAG AGACAGAGTATTAGGACATGTTTGAACAGGGGCCGGG CGATCAGCAGGTAGCTCTAGAGGTACCCCAGATCTAGT GTCTGTCTGCACATTTCGTAGAGCGAGTGTTCCGATAC TCTAATCTCCCTAGGCAAGGTTCATATTTGTGTAGGTTA CTTATTCTCCTTTTGTTGACTAAGTCAATAATCAGAATC AGCAGGTTTGGAGTCAGCTTGGCAGGGATCAGCAGCC TGGGTTGGAAGGAGGGGGTATAAAAGCCCCTTCACCA GGAGAAGCCCAGCTG	This study
#2748	ssAAV-TBG-SaCas9 (2x alpha mic/bik in front and chimeric intron behind TBG)	AGGTTAATTTTTAAAAAGCAGTCAAAAGTCCAAGTGGC CCTTGGCAGCATTTACTCTCTCTGTTTGCTCTGGTTAAT AATCTCAGGAGCACAAACATTCCAGATCCAGGTTAATT TTTAAAAAGCAGTCAAAAGTCCAAGTGGCCCTTGGCAG CATTTACTCTCTCTGTTTGCTCTGGTTAATAATCTCAGG AGCACAAACATTCCAGATCCGGCGCGCCAGGGCTGGA AGCTACCTTTGACATCATTTCCTCTGCGAATGCATGTAT AATTTCTACAGAACCTATTAGAAAGGATCACCCAGCCT CTGCTTTTGTACAACTTTCCCTTAAAAAACTGCCAATTC CACTGCTGTTTGGCCCAATAGTGAGAACTTTTTCCTGC TGCCTCTTGGTGCTTTTGCCTATGGCCCCTATTCTGCC TGCTGAAGACACTCTTGCCAGCATGGACTTAAACCCCT CCAGCTCTGACAATCCTCTTTCTCTTTTGTTTTACATGA AGGGTCTGGCAGCCAAAGCAATCACTCAAAGTTCAAAC CTTATCATTTTTTGCTTTGTTCCTCTTGGCCTTGGTTTT GTACATCAGCTTTGAAAATACCATCCCAGGGTTAATGC TGGGGTTAATTTATAACTAAGAGTGCTCTAGTTTTGCAA TACAGGACATGCTATAAAAATGGAAAGATAGATCTGCT TCAGCTGGAGGCACTGGGCAGGTAAGTATCAAGGTTA CAAGACAGGTTTAAGGAGACCAATAGAAACTGGGCTTG TCGAGACAGAGAAGACTCTTGCGTTTCTGATAGGCACC TATTGGTCTTACTGACATCCACTTTGCCTTTCTCTCCAC AGGTG	This study

#2310	ssAAV-mCMV-SaCas9	ACTCACGGGGATTTCCAAGTCTCCACCCCATTGACGTC AATGGGAGTTTGTTTTGGCACCAAAATCAACGGGACTT TCCAAAATGTCGTAATAACCCCGCCCCGTTGACGCAAA TGGGCGGTAGGCGTGTACGGTGGGAGGTCTATATAAG CAGAGCTCGTTTAGTGAACCGTCAGAATTCTCGAGTGA TCGAAAGAGCCTGCTAAAGCAAAAAAGAAGTCACC	Master Thesis
#2749	ssAAV-EFS-SaCas9	GGGCAGAGCGCACATCGCCCACAGTCCCCGAGAAGTT GGGGGGAGGGGTCGGCAATTGATCCGGTGCCTAGAG AAGGTGGCGCGGGGTAAACTGGGAAAGTGATGTCGTG TACTGGCTCCGCCTTTTTCCCGAGGGTGGGGGAGAAC CGTATATAAGTGCAGTAGTCGCCGTGAACGTTCTTTTT CGCAACGGGTTTGCCGCCAGAACACAGGC	This study

2.2.2.4. Cloning of splitCas9 vectors

The split Cas9 vectors originated from my Master Thesis that was conducted in the lab of Barbara Di Ventura and Roland Eils in collaboration with Dirk Grimm, in which three different split-sites of SaCas9 were selected and each joined to the split NpuDnaE or split gp41 inteins [286]. To this end, the plasmid #1166 was used as basis for all constructs that harbor an ITR-4 preceding and an ITR-2 following the coding sequence leading to the dsAAV vector. The inteins were ordered as gBlocks from IDT as listed in Table 18 and the *Sa*Cas9 halves were PCR amplified from plasmid #1513 that was kindly provided by the Weinberg lab. Using a GoldenGate based strategy SaCas9 halves and intein were assembled. Subsequently, the promoter was substituted via the minimalCMV promoter, TK and MecP2 promoter. In order to clone the full-length SaCas9 within the single-stranded AAV context, harboring an ITR-2 on each site of the coding sequence, the plasmid #1604 pSSV-TK-spCas9 was digested using NheI and NotI in order to exchange the SpCas9 fragment with SaCas9 harboring exactly the same genetic elements as the split Cas9 (Kozak sequence, NLS, Flag-tag, 48 bp-PolyA). Subsequently, the promoter was substituted via the minimalCMV promoter and MecP2 promoter. For more details, see Master Thesis. In this study, the split Cas9 system was furthermore expanded by a kill-switch approach, previously developed by Julia Fakhiri from our lab [294]. All plasmids used for the splitCas9 project are listed in Table 19. Note that AAV vectors harboring two sgRNAs were cloned by using the TRISPR protocol, but instead of the 7sk cassette, oligos (5´TGACGATCGATC 3´ and 5´AAGCGATCGATC 3´) were annealed and inserted as placeholder.

Table 18. Sequence of gBlocks to clone inteins.

gBlock	Sequence 5´to 3
BbsI-Gate-gp41-1(N)-SPA-BbsI	GATCCAGAAGACGAGCCACGATGAGAGACGCGTCTCATGCTTGGAC CTGAAAACCCAGGTGCAGACCCCCCAGGGCATGAAGGAAATCTCCA ACATCCAGGTGGGCGACCTGGTGCTGTCCAACACCGGCTACAACGA GGTGCTGAACGTGTTCCCCAAGTCCAAGAAGAAGTCCTACAAGATCA CCCTGGAGGACGGCAAGGAGATCATCTGCTCCGAGGAGCACCTGTT CCCCACCCAGACCGGCGAGATGAACATCTCCGGCGGCCTGAAGGA GGGCATGTGCCTGTACGTGAAGGAGTAATGATCGATAATAAAATCGT TGATTTTCATTGGAAGCGTGTGTTGGTTTTTTGTGTGCGGCCGCTCT GTTGTCTTCAGGTAC
BbsI-gp41-1(C)-Gate-SPA-BbsI	GATCCAGAAGACGAGCCACGATGATGCTGAAGAAGATCCTGAAGAT CGAGGAGCTGGACGAGCGCGAGCTGATCGACATCGAGGTGTCCGG CAACCACCTGTTCTACGCCAACGACATCCTGACCCACAACAGAGACG CGTCTCGTAATGATCGATAATAAAATCGTTGATTTTCATTGGAAGCGT GTGTTGGTTTTTTGTGTGCGGCCGCTCTGTTGTCTTCAGGTAC
BbsI-Gate-NpuDnaE(N)-SPA-BbsI	GATCCAGAAGACGAGCCACGATGAGAGACGCGTCTCATGCTTGTCC TACGAAACCGAGATCCTGACCGTGGAGTACGGCCTGCTGCCCATCG GCAAGATCGTGGAGAAGCGCATCGAGTGCACCGTGTACTCCGTGGA CAACAACGGCAACATCTACACCCAGCCCGTGGCCCAGTGGCACGAC CGCGGCGAGCAGGAGGTGTTCGAGTACTGCCTGGAGGACGGCTCC CTGATCCGCGCCACCAAGGACCACAAGTTCATGACCGTGGACGGCC AGATGCTGCCCATCGACGAAATCTTCGAGCGCGAGCTGGACCTGAT GCGCGTGGACAACCTGCCCAACTAATGATCGATAATAAAATCGTTGA TTTTCATTGGAAGCGTGTGTTGGTTTTTTGTGTGCGGCCGCTCTGTTG TCTTCAGGTAC
BbsI-NpuDnaE(C)-Gate-SPA-BbsI	GATCCAGAAGACGAGCCACGATGATGATCAAGATCGCCACCCGCAA GTACCTGGGCAAGCAGAACGTGTACGACATCGGCGTGGAGCGCGAC CACAACTTCGCCCTGAAGAACGGCTTCATCGCCTCCAACAGAGACG CGTCTCGTAATGATCGATAATAAAATCGTTGATTTTCATTGGAAGCGT GTGTTGGTTTTTTGTGTGCGGCCGCTCTGTTGTCTTCAGGTAC

Table 19. Plasmids used in split*Sa*Cas9 experiments.

No	Name	Description	Origin
#2310	ssAAV-mCMV-NLS-flag-SaCas9-flag-NLS	minCMV expressing SaCas9	Master Thesis
#2330	dsAAV-mCMV-NLS-flag-(N)-SaCas9-gp41-1(N)_split 3	minCMV-driven N-Cas9 split3-intein	Master Thesis
#2331	dsAAV-mCMV-gp41-1(C)-C-SaCas9-flag-NLS_split 3	minCMV-driven C-Cas9 split3-intein	Master Thesis
#2727	ssAAV-mMecP2-NLS-flag-SaCas9-flag-NLS	mMecP2-expressing SaCas9	Master Thesis
#2732	dsAAV-mMecP2-NLS-flag-(N)-SaCas9-gp41-1(N)_split 3	mMecP2-driven N-Cas9 split3-intein	Master Thesis
#2733	dsAAV-mMecP2-gp41-1(C)-C-SaCas9-flag-NLS_split 3	mMecP2-driven C-Cas9 split3-intein	Master Thesis
#2734	ssAAV-mTK-NLS-flag-SaCas9-flag-NLS	mTK-expressing SaCas9	Master Thesis
#2739	dsAAV-mTK-NLS-flag-(N)-SaCas9-gp41-1(N)_split 3	mTK-driven N-Cas9 split3-intein	Master Thesis
#2740	dsAAV-mTK-gp41-1(C)-C-SaCas9-flag-NLS_split 3	mTK-driven C-Cas9 split3-intein	Master Thesis
#2333	mCMV-gp41-1-SaCas9-C-flag-NLS_H1-gCas	C-SaCas9 and H1-gCas9	Julia Fakhiri
#2334	mCMV-gp41-1-SaCas9-C-flag-NLS_H1-gscr	C-SaCas9 and H1-gscrCas9	Julia Fakhiri
#2339	TTR-hLuc-U6-gLuc	TTR driving luciferase, U6 expressing gRNA against Luc	This study
#2340	TTR-hLuc-U6-gscrLuc	TTR driving luciferase, U6 expressing scrambled gRNA	This study
#2743	dsAAV-H1-gCas9	gRNA for SaCas9 against itself	This study
#2744	dsAAV-H1-gscrCas9	scrambled gRNA for SaCas9 against itself	This study
#2646	dsAAV-U6-gHBs-g6_RSV-GFP	GG of oligos in #1578, ITRs present, amp selection	This study
#2637	dsAAV-U6-gMecP2-g8_RSV-GFP	GG of oligos in #1578, ITRs present, amp selection	Master Thesis
#2745	dsAAV-U6-gMecP2g8_H1-gCas9	U6 driven gRNA against MecP2, H1 driven gRNA againstCas9	This study
#2720	dsAAV-U6-gMecP2g8_H1-scr	U6 driven gRNA against MecP2, H1	This study

		driven scrRNA	
#2725	dsAAV-U6-gHBsg6_H1-gCas9	U6 driven gRNA against HBsAg, H1 driven gRNA againstCas9	This study
#2726	dsAAV-U6-gHBsg6_H1-scr	U6 driven gRNA against HBsAg, H1 driven scrRNA	This study

2.2.2.5. Cloning of AcrIIC1 variants

AcrIIC1 wt, single, double and triple mutants were cloned by me and Sabine Aschenbrenner in Niopek´s lab and are listed in Table 20. Mutations were introduced by around-the-horn PCR using phosphorylated primers that covered a single mutation site per cloning round. Subsequently, the amplicon of the complete plasmid was ligated and therefore created a circularized plasmid. AcrX represents the triple mutant DN (internal reference numer in the lab of Dominik Niopek) #1282. The plasmid DN #231 (Addgene #61591, kind gift from Feng Zhang) was used for *Sa*Cas9 and corresponding sgRNA expression. Oligonucleotides were ordered with a 5´CACC and 3´AAAC overhang (see Table 12,oligo #37/#38, #39/#40, #41/#42) and inserted in DN #231 via Golden Gate cloning using the type IIS restriction enzyme BsaI resulting in DN #1265 (CMV-SaCas9_U6-gEMX), DN #1294 (CMV-SaCas9_U6-gGrin2B) and DN #1333 (CMV-SaCas9_U6-gHBB). For the miR122 experiments, plasmids DN #1024 and DN #1026 were used that harbor a CMV-driven AcrIIC1 wt inhibitor with either a microRNA scaffold or miR122 binding site as reported in [203]. For miR122- dependent expression of AcrX, #1282 was digested with NheI/XhoI and AcrIIC1 in DN #1024 and DN #1026 replaced with AcrX.

Table 20. Plasmids used in AcrX experiments.

No	Name	Description	Origin
DN#231	ssAAV-CMV-SaCas9 _U6-SaScaffold	CMV-driven SaCas9 & U6-driven gRNA scaffold	Addgene 61591
DN#1265	ssAAV-CMV-SaCas9-U6-gEMX	GG of oligos in DNDN#231, all-in-one vector	Niopek lab
DN#1294	ssAAV-CMV-SaCas9-U6-gGrin2B	GG of oligos in DNDN#231, all-in-one vector	Niopek lab
DN#1333	ssAAV-CMV-SaCas9-U6-gHBB	GG of oligos in DNDN#231, all-in-one vector	Niopek lab
DN#948	CMV-AcrIIC1	CMV driven AcrIIC1 wt inhibitor	Niopek lab
DN#1207	CMV-AcrIIC1_A47I	Acr with single point mutation	Niopek lab
DN#1209	CMV-AcrIIC1_D14Q	Acr with single point mutation	Niopek lab
DN#1211	CMV-AcrIIC1_D42F	Acr with single point mutation	Niopek lab
DN#1213	CMV-AcrIIC1_D44F	Acr with single point mutation	Niopek lab
DN#1215	CMV-AcrIIC1_D45E	Acr with single point mutation	Niopek lab

DN#1217	CMV-AcrIIC1_K46Q	Acr with single point mutation	Niopek lab
DN#1220	CMV-AcrIIC1_M76S	Acr with single point mutation	Niopek lab
DN#1221	CMV-AcrIIC1_N2F	Acr with single point mutation	Niopek lab
DN#1223	CMV-AcrIIC1_N2Y	Acr with single point mutation	Niopek lab
DN#1224	CMV-AcrIIC1_R35D	Acr with single point mutation	Niopek lab
DN#1241	CMV-AcrIIC1_N2F/A47I	Acr with double point mutation	Niopek lab
DN#1244	CMV-AcrIIC1_N2F/K46Q	Acr with double point mutation	Niopek lab
DN#1267	CMV-AcrIIC1_D14Q/A47I	Acr with double point mutation	Niopek lab
DN#1268	CMV-AcrIIC1_N2Y/A47I	Acr with double point mutation	Niopek lab
DN#1269	CMV-AcrIIC1_D14Q/K46Q	Acr with double point mutation	Niopek lab
DN#1270	CMV-AcrIIC1_N2F/D14Q	Acr with double point mutation	Niopek lab
DN#1271	CMV-AcrIIC1_N2Y/D14Q	Acr with double point mutation	Niopek lab
DN#1273	CMV-AcrIIC1_N2Y/K46Q	Acr with double point mutation	Niopek lab
DN#1274	CMV-AcrIIC1_K46Q/A47I	Acr with double point mutation	Niopek lab
DN#1282	CMV-AcrIIC1_N2F/D14Q/A47I	Acr with triple point mutation	Niopek lab
DN#1286	CMV-AcrIIC1_N2Y/D14Q/A47I	Acr with triple point mutation	Niopek lab
DN#1024	pAAV_U6-BbsI_CMV-AcrIIC1-scaffold-BsmBI-BGH	AcrIIC1 with scaffold instead of miR122 bs	Niopek lab
DN#1026	pAAV_U6-BbsI_CMV-AcrIIC1-2xmir122-BsmBI-BGH	AcrIIC1 with miR122 binding site	Niopek lab
DN#1839	pAAV_U6-BbsI_CMV-AcrX-2xmir122-BsmBI-BGH	AcrIIX with miR122 binding site	Niopek lab
DN#1841	pAAV_U6-BbsI_CMV-AcrX-scaffold-BsmBI-BGH	AcrIIX with scaffold instead of miR122 bs	Niopek lab

2.2.3. Cell Culture Methods

2.2.3.1. Cell Maintainance

HEK293T, HepG2, Huh7, Hepa1-6 and Neuro2A cells, were maintained in phenol-red Dulebecco´s Modified Eagle Medium (DMEM) with GlutaMAX™, supplemented with 10% fetal bovine calf serum (FBS) and 1% Penicillin-Streptomycin, in this study referred to as cell culture medium. Cell culture medium for HepG2-hNTCP and Huh7-hNTCP cells were further supplemented with Puromycin in a final concentration of 5 µg/ml, for HepG2-hNTCP-HB2.7 and Huh7-hNTCP-HB2.7 cells the medium was furthermore supplemented with Blasticidin in a final concentration of 10 µg/ml. Cells were cultured in T75 to T175 flasks in a humidified atmosphere at 37 °C and 5% CO_2. Cells were split 1:5 to 1:20 every 3-4 days using 2.5% Trypsin-EDTA solution for detachment. Cell lines used in this study are listed in Table 21. Primary myoblasts were cultured in Myoblasts growth medium (MGM) and supplemented with fresh media every day.

Table 21. List of cell lines.

Cell Line	Origin	Description
HEK293T	*H. sapiens*	Human embryonic kidney cells expressing the SV40 large T-antigen used for AAV production [295]
HepG2	*H. sapiens*	Human liver carcinoma-derived cell line isolated from young patient with HCC [296]
Huh7	*H. sapiens*	Human hepatoma cell line derived from patient suffering from HCC [297]
Hepa1-6	*M. musculus*	Mouse hepatoma cell line derived from C57/L mice [298]
Neuro2A	*M. musculus*	Mouse neuroblastoma cell line [299]
HepG2-hNTCP	*H. sapiens*	HepG2 stably expressing hNTCP (Puromycin selection) [16]
HepG2-hNTCP-HB2.7	*H. sapiens*	HepG2 stably expressing hNTCP and HBsAg (Puromycin & Blasticidin selection) [300]
Huh7-hNTCP	*H. sapiens*	Huh7 stably expressing hNTCP (Puromycin selection) [16]
Huh7-hNTCP-HB2.7	*H. sapiens*	Huh7 stably expressing hNTCP and HBsAg (Puromycin & Blasticidin selection) [300]
HEK293T-mCherry	*H. sapiens*	HEK293T cells stably expressing mCherry ontained from Stefan Kallenberger
Primary Myoblasts	*M. musculus*	Mouse primary myoblast obtained from Oliver Müller

2.2.3.2. Transfection

For transfection in 96-well plates, 8 x10^3 cells per well were seeded using 100 µl cell culture medium. One day after seeding, cells were transfected with 200 ng total DNA using the Lipofectamine 2000 reagent. Therefore, 25 µl DMEM without supplements and 0,4 µl Lipofectamine 2000 were thoroughly mixed and incubated for 5 min. The DNA was diluted in 25 µl DMEM without supplements likewise. Subsequently, both mixes were vortexed and incubated for 30 min until added drop wise to the cells.

For the AcrX experiments, HEK293T cells were plated with a density of 12,500 cells per well and transfected using the JetPrime reagent. Therefore, 0.3 µl of JetPrime reagent was mixed with 5 µl buffer and a total of 200 ng DNA was likewise mixed with 5 µl buffer. Subsequently, both mixes were combined and incubated for 15 min until added to the cells. According to the indicated Acr : Cas9 ratios, cells were transfected with 100 ng plasmid expressing the Acr variants and 100 ng plasmid comprising a dual expression cassette for Cas9 and gRNA (1:1 ratio), 133 ng Acr and 67 ng Cas9/gRNA (2:1 ratio), 150 ng Acr and 50 ng Cas9/gRNA (3:1 ratio) or 160 ng Acr and 40 ng Cas9/gRNA (4:1 ratio).

2.2.4. Virological Methods

2.2.4.1. AAV production and purification

For large-scale AAV production, HEK293T cells were expanded in T175 flasks in order to attain enough cell material. Two days later, cells were seeded in 140 mm dishes (Nunc) with a density of $4x10^6$ cells/dish in 22 ml cell culture medium. Two days later, cells were transfected with 44.1 µg total DNA per plate with a 1:1:1 ratio of i) Adenohelper plasmid providing helper function for AAV packaging, ii) a plasmid providing AAV rep and cap of the diverse AAV variants, and iii) the plasmids with the transgene flanked by ITRs. Plasmid DNA was mixed with 1.23 ml H_2O, 1.58 ml 300 mM NaCl and 0.35 ml PEI for one dish, respectively. Note that for each construct at least five, but up to 150 dishes were produced. Mixes were thoroughly vortexed and incubated for 10 min at room temperature and 3.2 ml were added dropwise to each dish. Three days later, cells were harvested by scraping the cells from the dish. The cell suspension was either collected in 50 ml Falcon tubes or in Corning® 500 ml centrifuge tubes and centrifuged at 800 g for 15 min. The supernatant was disposed and cells were resuspended in 5 ml or 20 ml Benzonase buffer, for small gradients of up to 20 dishes or large gradients of up to 75 dishes, respectively. Remaining plasmid DNA was digested by the addition of 1 µl or 4 µl highly concentrated Benzonase for small or large gradients, respectively and incubated for 1 h at 37 °C with inversions every 10 min. Subsequently, cells were lysed by subjecting them to five freeze (in liquid nitrogen) and thaw (in 37°C waterbath) cycles. Cells were pelleted by centrifugation at 4000 g at 4 °C for 15 min twice and AAVs were collected within the supernatant. The AAVs were purified using an iodixanol gradient as described in Börner et al. [152]. Therefore, in case of small gradients the supernatant was filled in a smaller ultracentrifugation tube (Seton Scientific) and underlaid with 1.5 ml 15%, 25%, 40% and 60% iodixanol phases or alternatively for large gradients with 7 ml 15%, 5 ml 25%, 4 ml 40% and 4 ml 60% iodixanol phases using a Pasteur pipet. The gradients were centrifuged at 50000 rpm at 4°C for 2h or 2.5 h for small and large gradients, respectively. Subsequently 1 or 3 ml of the interface between the 40% and 60% iodixanol phase containing the purified AAVs were collected using a syringe for small and large gradients, respectively. AAVs were aliquoted and stored at -80°C until further use. AAV vectors that were used in this study are listed in Table 22.

Table 22. AAV vectors that were used in this study.

Virus	Description	Source
dsAAV1-YFP	Recombinant adeno-associated virus type 1 expressing CMY-YFP	this study
dsAAV2-YFP	Recombinant adeno-associated virus type 2 expressing CMY-YFP	this study
dsAAV3-YFP	Recombinant adeno-associated virus type 3 expressing CMY-YFP	this study
dsAAV4-YFP	Recombinant adeno-associated virus type 4 expressing CMY-YFP	this study
dsAAV5-YFP	Recombinant adeno-associated virus type 5 expressing CMY-YFP	this study
dsAAV6-YFP	Recombinant adeno-associated virus type 6 expressing CMY-YFP	this study
dsAAV7-YFP	Recombinant adeno-associated virus type 7 expressing CMY-YFP	this study
dsAAV8-YFP	Recombinant adeno-associated virus type 8 expressing CMY-YFP	this study
dsAAV9-YFP	Recombinant adeno-associated virus type 9 expressing CMY-YFP	this study
dsAAVrh10-YFP	Recombinant adeno-associated virus type rhesus10 expressing CMY-YFP	this study
dsAAVpoc1-YFP	Recombinant adeno-associated virus type poc1 expressing CMY-YFP	this study
dsAAV12-YFP	Recombinant adeno-associated virus type 12 expressing CMY-YFP	this study
dsAAVDJ-YFP	Recombinant adeno-associated virus created by DNA familiy shuffling expressing CMY-YFP	this study
dsAAVLK03-YFP	Recombinant adeno-associated virus created by DNA familiy shuffling expressing CMY-YFP	this study
dsAAV5p2NIS-YFP	Recombinant adeno-associated virus type 5 peptide insertion P2 in new insertion site (NIS) expressing CMY-YFP	this study
dsAAV7p2-YFP	Recombinant adeno-associated virus type 7 peptide insertion P2 expressing CMY-YFP	this study
dsAAVpoc1p2NIS-YFP	Recombinant adeno-associated virus type poc1 peptide insertion P2 in new insertion site (NIS) expressing CMY-YFP	this study
dsAAV7A6-YFP	Recombinant adeno-associated virus type 7 peptide insertion A6 expressing CMY-YFP	this study
dsAAV2A1NIS-YFP	Recombinant adeno-associated virus type 2 peptide insertion A1 in new insertion site (NIS) expressing CMY-YFP	this study
dsAAV4A1NIS-YFP	Recombinant adeno-associated virus type 4 peptide insertion A1 in new insertion site (NIS) expressing CMY-YFP	this study
dsAAV7A2-YFP	Recombinant adeno-associated virus type 7 peptide insertion A2 expressing CMY-YFP	this study
dsAAV9A2-YFP	Recombinant adeno-associated virus type 9 peptide insertion A2 expressing CMY-YFP	this study
dsAAV1A1NIS-YFP	Recombinant adeno-associated virus type 1 peptide insertion A1 in new insertion site (NIS) expressing CMY-YFP	this study
dsAAV2HSPGmut-YFP	wtAAV2-Rep2-Cap2-R484/585E (HSPG-k.o.) expressing CMV-YFP [230]	this study
ssAAV9A2- SaCas9	rAAV9A2 expressing SaCas9 under CMV promoter	this study
dsAAV9A2-U6-gMecP2	rAAV 9A2 expressing sgRNA against mecp2 under U6 promoter	this study

ssAAV5- SaCas9	rAAV5 expressing SaCas9 under CMV promoter	this study
dsAAV5-U6-gMecP2	rAAV5 expressing sgRNA against mecp2 under U6 promoter	this study
dsAAV9A2-U6-gHBs1 (to 10)	rAAV9A2 expressing one sgRNA (1 to 10) against HBsAg under U6 promoter	this study
dsAAV9A2-U6-gHBs8-stuffer	rAAV9A2 expressing sgRNA8 against HBsAg under U6 promoter, stuffer of 630 bp	this study
dsAAV9A2-H1-gHBs7-stuffer	rAAV9A2 expressing sgRNA7 against HBsAg under H1 promoter, stuffer of 950 bp	this study
dsAAV9A2-7SK-gHBs6-stuffer	rAAV9A2 expressing sgRNA6 against HBsAg under 7SK promoter,stuffer of 870 bp	this study
dsAAV9A2- HBs-TRISPR	rAAV9A2 multiplexing sgRNA8, 7 and 6 against HBsAg	this study
ssAAVLK03- SaCas9	rAAVLK03 expressing SaCas9 under CMV promoter	this study
dsAAVLK03- HBV-TRISPR	rAAVLK03 multiplexing sgRNAX, sgRNAS and shRNA against HBV	this study
dsAAVLK03- HBV-TRISPR/TuD	rAAVLK03 multiplexing sgRNAX or S and shRNA and ist TuD against HBV	this study
dsAAVLK03- U6-shHDV1 (to 9)	rAAVLK03 expressing one shRNA (1 to 9) against HDV under U6 promoter	this study
dsAAVLK03- HBV/HDV-TRISPR	rAAVLK03 multiplexing sgRNAs against HBV and shRNA against HBV and/or HDV	this study
ssAAV9A2-mCMV-SaCas9	rAAV9A2 expressing SaCas9 under a minimal CMV promoter	this study
dsAAV9A2-mCMV-splitCas9	rAAV9A2 expressing either N- or C-terminal of SaCas9 under a minimal CMV promoter	this study
ssAAV2-CMV-SaCas9-U6-gEMX	rAAV2 expressing SaCas9 under CMV promoter and sgRNA against the emx locus	this study
dsAAV2-CMV-AcrIIC1-miR122bs/sc	rAAV2 CMV-driven AcrIIC1 with either a miR122binding site or scaffold	this study
dsAAV2-CMV-AcrX-miR122bs/sc	rAAV2 CMV-driven AcrX with either a miR122binding site or scaffold	this study

2.2.4.2. Titration of purified AAV vectors

Prior to AAV titration, AAVs were treated with an alkaline lysis protocol. Therefore, 10 µl of AAV sample was mixed with 10 µl TE buffer and subsequently lysed with 20 µl 2M NaOH in a 30 min 56°C incubation. The lysis was neutralized by adding 38 µl of 1M HCL and 922 µl H_2O was added to obtain a 1:100 dilution. Samples were further diluted 1:10 and directly used for the subsequent titration.

In order to quantify AAV vector yields, TaqMan RT-PCR was performed using the Rotor Gene 6000 and the SensimixII Probe kit (Bioline, London, UK). Each sample was pipetted in triplicates, containing 17.5 µl SensiMixII Probe Master Mix, 1.4 µl of each forward and reverse primer, 0.35 µl Probe and 9.35 µl H_2O and 5 µl of AAV sample was added, which resulted in a further 1:7 dilution. Primers and Probes are listed in Table 23. To estimate the viral titer in copies/µl, plasmid DNA with known amounts of template molecules was applied. Therefore, a plasmid stock was prepared with exactly $3.5x10^8$ molecules/µl and diluted 1:10 ranging from $3.5x10^8$ to $3.5x10^3$ molecules/µl. Of each

dilution 5 µl was added to the Master Mix resulting in $5x10^8$ to $5x10^3$ molecules in a 10 µl reaction volume (unicum).

The PCR cycling conditions were performed as followed: 10 min at 95°C, followed by 40 cycles of heating at 95°C for 10 s and elongation at 60°C for 20 s. The fluorescent signal was acquired after each elongation step at 510 nm. After the run, samples and standard curve were analyzed with the accompanying RotorGene 6000 Series Software 1.7. The molecules of each AAV sample was extrapolated by the standard curve and multiplied by the applied dilution of x100 x10 x7 and x100 to get a concentration per ml. Furthermore titers of ssAAVs were multiplied x2, since the probe is only able to detect either the positive or negative genomic strand.

Table 23. Primer and probes for AAV titration.

Name	**Sequence 5´-3´**
YFP forward	GAGCGCACCATCTTCTTCAAG
YFP reverse	TGTCGCCCTCGAACTTCAC
YFP probe	FAM-ACGACGGCAACTACA-BHQ1
mCMV forward	GCACCAAAATCAACGGGAC
mCMV reverse	AGCAGGCTCTTTCGATCAC
mCMV probe	FAM- TTCCAAAATGTCGTAATAACCCCGCCCCG -BHQ1
CMVenh forward	AACGCCAATAGGGACTTTCC
CMVenh reverse	GGGCGTACTTGGCATATGAT
CMVenh probe	FAM-CGGTAAACTGCCCACTTGGCAGT-BHQ1

2.2.4.3. AAV transduction

Cells were seeded one day prior to AAV transduction. For AAV transduction in general, AAV vectors were first added in the indicated multiplicity of infection (MOI) to an appropriate amount of cell culture medium and mixed thoroughly. Subsequently, the medium on the cells was exchanged with the medium containing the AAV vectors. For transductions in 96-well format, $5x10^3$ to $1x10^4$ cells per well were seeded in 100 ul cell culture medium. If not otherwise indicated, cells were processed for further analysis three days after transduction.

For the comparison of AAV transduction efficiency without and with DMSO, AAV vectors with an MOI of 10^5 were added to 100 ul of cell culture medium without DMSO or with 2.5% DMSO. For an MOI of 10^3, the previous AAV transduction mix was diluted 1:100 in cell culture medium without or with 2.5% DMSO. Subsequently, the medium on the cells

was exchanged with the medium containing the AAV vectors. Cells were fixated for automated imaging three days after transduction.
For the comparison of different methods to increase AAV transduction, AAV vectors with an MOI of 10^5 were added to 100 ul of only cell culture medium (no treatment) or cell culture medium supplemented with either 1% or 2.5% DMSO, 0.5 µM or 2 µM Doxorubicin (stock contained 1mM Doxorubicin and was diluted 1:2000 or 1:500, respectively), 250 nM or 10 µM Rapamycin (stock contained 5 mM Rapamycin and was diluted 1:2000 or 1:500, respectively). Cells that received Doxorubicin were washed twice with PBS 12 hours after transduction and received fresh cell culture medium. For the pre-treatment with Rapamycin, cell culture medium with 10 µM or 40 µM Rapamycin (stock contained 5 mM Rapamycin and was diluted 1:500 or 1:125, respectively) was added on the cells for 1 h prior to transduction and was removed with fresh cell culture medium containing the AAVs. Three days later, cells were fixated for automated imaging.
For the screen of different sgRNAs against the HBsAg and the comparison of different multiplexing approaches, HepG2-hNTCP-HB2.7 cells were transduced in a 48-well format. Therefore, $1x10^5$ cells per well were seeded in 250 ul cell culture medium (without Puromycin or Blasticidin) one day prior to transduction. For transduction, the cell culture medium was exchanged with medium containing the AAV vectors.

2.2.4.4. HBV and HDV infection

For the experiments with HBV infections, HepG2-hNTCP cells were seeded in 24-well plates with a density of $5x10^5$ cells per well in 500 ul cell culture medium (without Puromycin). On day later, cells were infected with HBV using an MOI of 200. Therefore, 250 ul cell culture medium was supplemented with HBV, 2.5% DMSO and 10% PEG, thoroughly mixed and exchanged with the medium on the cells. On the following day, cells were washed twice with PBS and received 500 ul fresh cell culture medium supplemented with 2.5% DMSO. Three days after HBV infection, cells were transduced with AAVs with an MOI of 10^5 (using the amount of seeded cells for calculations) by exchanging the medium on the cells with 500 ul fresh cell culture medium supplemented with the AAV vectors and 2.5% DMSO. Subsequently, the medium was replaced with fresh cell culture medium, supplemented with 2.5% DMSO, on day 4, 6, 8 and 10 after HBV infection. The supernatant of day 8 to 10 and day 10 to 12 was collected for HBs and HBe measurements and cells were harvested for further analysis at day 12.

For the experiments with HDV infections, HepG2-hNTCP-HB2.7 cells, stably expressing the HBsAg, were seeded in 48- well plates with a density of $2x10^5$ cells per well in 250 ul

cell culture medium (without Puromycin and Blasticidin). In the immunization setting, one day after seeding cells were transduced with AAV vectors with an MOI of 10^5 by exchanging the medium on the cells with 250 ul medium containing the AAV vectors and 2.5% DMSO. On the following day, cells were washed twice with PBS. Two days after transduction, cells were infected with HDV using an MOI of 100. Therefore, 125 ul cell culture medium was supplemented with HDV, 2.5% DMSO and 10% PEG, thoroughly mixed and exchanged with the medium on the cells. On the following day, cells were washed twice with PBS and received 250 ul fresh cell culture medium supplemented with 2.5% DMSO. Cell were further processed for WB analysis and IF staining six days after HDV infection. In the curation setting, HepG2-hNTCP-HB2.7 cells were first infected with HDV using an MOI of 100 in 125 ul cell culture medium supplemented with 2.5% DMSO and 10% PEG. On the following day, cells were washed twice with PBS and received 250 ul fresh cell culture medium supplemented with 2.5% DMSO. Three days after HDV infection, cells were transduced with AAVs by exchanging the medium on the cells with 250 ul fresh cell culture medium supplemented with the AAV vectors and 2.5% DMSO. Subsequently, the medium was replaced with fresh cell culture medium, supplemented with 2.5% DMSO, on day 4, 6, 8 and 11 after HDV infection. The supernatant of day 11 to 13 was collected for HBs measurements and the supernatant was used to reinfect Huh7-hNTCP cells with newly produced HDV particles. For reinfection, Huh7-hNTCP cells were seeded in 48-well plates in a density of 10^5 cells per well one day prior to reinfection. Cells were reinfected with 15 ul supernatant containing the newly produced HDV particles in 125 ul cell culture medium supplemented with 2.5% DMSO and 10% PEG. On the following day, cells were washed twice with PBS and received 250 ul fresh cell culture medium supplemented with 2.5% DMSO every second day, until cells were fixated for quantitative imaging six days after reinfection.

Details on the viral stock of HBV and HDV are listed in Table 24.

Table 24. Viral stocks of HBV and HDV.

Virus	Description	Source
HBV genotype D, serotype ayw	Cell-culture derived, produced in HepAD38 cells, purified via heparin affinity chromatography	AG Urban, Heidelberg
HDV genotype 1	Cell-culture derived, produced in HuH7 cells by co-transfection and purified via heparin affinity chromatography	AG Urban, Heidelberg

2.2.5. Animal experiments

2.2.5.1. PBS-rebuffering of rAAV vectors

The rAAV vectors for *in vivo* experiments were rebuffered in PBS using Amicon Ultra-15 centrifugal filter units (Merck) according to manufacturer's instructions. Briefly, the filter units were first calibrated two times by applying 15 ml PBS on top of the filter and centrifugation at 800 g for 2 min. Sunsequently, the rAAV vectors that were previously extracted from the 40% Iodixanol phase after ultracentrifugation (see section 2.2.4.1) were diluted in 15 ml PBS and applied on top of the filter unit. The centrifugation of the samples at 800 g for 1 min enabled the solution of PBS/ Iodixanol to pass the filter, whereby rAAV vectors got stuck on the apical side of the filter. After centrifugation, samples were inverted three times to release the rAAV particles from the filter. Centrifugation and inverting were repeated until the solution on apical side of the filter was reduced to 1 ml. The filter unit was again refilled with 15 ml PBS and centrifugation and inverting were repeated until the PBS solution containing the rAAV particles was reduced to 500 ul. These 500 ul represented the final rAAV vector stock and was used for titration (see section 2.2.4.2) and was stored at -80°C until further usage.

2.2.5.2. Experimental setup

Animal experiments were performed with six weeks old female NMRI mice. PBS-rebuffered rAAV vectors of serotype 8 were directly injected into the mouse tail vein using a total volume of 130 ul or 200 ul per mouse for the promoter library or splitSaCas9, respectively. In these pilot studies, two mice per group/condition were used. The combinations and doses of injected rAAV vectors for each condition for the experiments regarding the promoter library and split*Sa*Cas9 are listed in Table 25 and Table 26, respectively. Mice were sacrificed 15 days post-injection. The liver (as well as other organs, such as pancreas, kidney, heart and other muscles) was extracted, smashed, transferred to 2 ml reaction tubes and frozen in liquid nitrogen until the organs of all mice were harvested. Organs were stored at -80°C until they were further processed in order to extract DNA and RNA (see section 2.2.1.11) or to measure the luciferase signal (see section 2.2.6.12).

Table 25. Experimental groups for promoter library driving *Sa*Cas9 expression *in vivo*.

Group	1. rAAV8 (10^{12} viral particles/mouse)	2. rAAV8 ($2x10^{11}$ viral particles/mouse)
1	ssAAV-LP1-*Sa*Cas9	U6-gLuc_TTR-Luc
2	ssAAV-TTR-*Sa*Cas9	U6-gLuc_TTR-Luc
3	ssAAV-TBG-*Sa*Cas9	U6-gLuc_TTR-Luc
4	ssAAV-mCMV-*Sa*Cas9	U6-gLuc_TTR-Luc
5	ssAAV-EFS-*Sa*Cas9	U6-gLuc_TTR-Luc
6	ssAAV-CMV-mCherry	U6-gLuc_TTR-Luc

Table 26. Experimental groups for split*Sa*Cas9/SIN *in vivo*.

Group	1. rAAV8 ($8x10^{11}$vg/mouse)	2. rAAV8 ($8x10^{11}$vg/mouse)	3. rAAV8 ($8x10^{11}$vg/mouse)	4. rAAV8 ($1.5x10^{11}$vg/mouse)
1	ssAAV-mCMV-fl*Sa*Cas9	-	dsAAV-H1-gCas9	U6-gLuc_TTR-Luc
2	ssAAV-mCMV-fl*Sa*Cas9	-	dsAAV-H1-scr	U6-gLuc_TTR-Luc
3	dsAAV-mCMV-*Sa*Cas9(N)	dsAAV-mCMV-*Sa*Cas9(C)-H1-gCas9	-	U6-gLuc_TTR-Luc
4	dsAAV-mCMV-*Sa*Cas9(N)	dsAAV-mCMV-*Sa*Cas9(C)-H1-scr	-	U6-gLuc_TTR-Luc
5	dsAAV-mCMV-*Sa*Cas9(N)	dsAAV-mCMV-*Sa*Cas9(C)	dsAAV-H1-gCas9	U6-gLuc_TTR-Luc
6	dsAAV-mCMV-*Sa*Cas9(N)	dsAAV-mCMV-*Sa*Cas9(C)	dsAAV-H1-scr	U6-gLuc_TTR-Luc
7	dsAAV-CMV-mCherry	dsAAV-mCMV-*Sa*Cas9(C)-H1-gCas9	-	U6-gLuc_TTR-Luc

2.2.6. Analyses

2.2.6.1. T7 endonuclease assay

Mutations induced by the CRISPR system were measured via T7 endonuclease assay. Therefore, cells were harvested in 70 µl DirectPCR cell lysis reagent, 70 µl ddH_2O and 1.4 µl Proteinase K for experiments in 96-well format, or with 140 µl DirectPCR cell lysis reagent, 140 µl ddH_2O and 2.8 µl Proteinase K for experiments in 48-well format (e.g. screen of sgRNA against HBsAg and comparison of different multiplexing approaches). Cells were incubated for at least 4 h at 55 °C and subsequently Proteinase K was deactivated by increasing the temperature to 85 °C for 45 min. The cell lysates were directly used as template for PCR as described in section 2.2.1.2 with primers flanking the target region and resulting in an amplicon of approximately 1kb. Primers with corresponding annealing temperatures are listed in Table 27. Subsequently, the entire PCR reaction was heated at 95 °C for 5 minutes in order to denature the DNA and reannealed by decreasing the temperature by -2°C per sec frpm 95 to 85°C and by -0.1°C per second from 85 to 25 °C in a thermal cycler. Note that for the AcrX experiments, 5 µl PCR product was diluted 1:4 in 1x NEB2 buffer and used for reannealing. Subsequently, T7 endonuclease was applied that detects and cleaves DNA heteroduplexes that form upon annealing of mutated and wild type sequences. Therefore, 0.5 µl T7 endonuclease was added to the reannealed PCR sample and gently mixed. After 15 min of incubation at 37 °C the samples were substituted with DNA loading dye that contains EDTA and therefore stops the T7 endonuclease activity. PCR products were directly loaded on a 2% agarose gel. In order to quantify the percentage of insertions and deletions caused by the CRISPR system, the band intensities of wild type sequence and cutting products on the agarose gel were quantified using ImageJ. Using the rectangle tool, the area with wild type sequence and cutting products were confined. With the “plot lanes” function the signal intensity within the rectangles were integrated and lanes plotted. Subsequently, the peaks were defined manually and quantified using the wand tool. The resulting values were used to calculate indel percentage by dividing the sum of the cutting products by the sum of all bands.

$$Indel\ (\%) = (1 - \sqrt{(1} - \frac{sum(b + c)}{sum(a + b + c)})) * 100$$

Whereby “a” is the integrated intensity of uncut wild type sequence and “b” and “c” the integrated intensity of mutated and therefore cleaved products. The T7 cutting products for each locus is listed in Table 27.

Table 27. Primers, annealing temperatures and T7 bands in T7 assays.

Target	Orientation	Sequence 5´to 3´	Tm °C	T7 bands
MecP2-g8	fw	GCCGGCAGGTCCTCTGTT	70	703/ 371
	rv	TGCAGATGCTGCTGCTCAA		
HBsAg -g1	fw	GTAGGCCCACTCACAGTTAATG	62	791/ 411
	rv	GGGATGGGAATACAGGTGC		
HBsAg -g2		see above		810/ 392
HBsAg -g3 preS1		see above		288/ 914
HBsAg -g4 preS1		see above		307/ 895
HBsAg -g5		see above		824/ 378
HBsAg -g6		see above		849/ 353
HBsAg -g7		see above		738/ 464
HBsAg -g8		see above		791/ 411
HBsAg -g9 preS1		see above		307/ 895
HBsAg -g10		see above		829/ 373
EMX1	fw	GGAGCAGCTGGTCAGAGGGG	70	418/ 271
	rv	GGGAAGGGGGACACTGGGGA		
GRIN2B	fw	AGAATTTTGTAATTGGTTCTACCAAAG	61	190/ 570
	rv	ACAACAGTGGAAGAAAGCTAGGGC		
HBB	fw	ATGGTGCATCTGACTCCTG	65	288/ 248
	rv	ACTGTACCCTGTTACTTATCCCC		

Note that the forward primer for the HBsAg only binds in the cell line with integrated HBsAg, but not in the infectious HBV.

2.2.6.2. TIDE analyses

The PCR products that were used for T7 endonuclease assay were also send to Sanger sequencing in order to perform analysis based on Tracking of Indels by Decomposition (TIDE) using the webtool https://tide.deskgen.com [301]. TIDE quantifies the mutation rates in edited compared to non-edited sample by decomposing the sequence trace data from Sanger reactions. Therefore, PCR products were purified from 1% agarose gels as described in section 2.2.1.5 and a total amount of 75 ng purified DNA and 2.5 µl primer (10 µM) was send to sequencing in a reaction volume of 10 µl as described in section 2.2.1.10. The primer sequence (5´ GCTACCACATCTGCCCAGG ´3) was used to sequence the *mecp2* locus binding about 200 bp upstream of the target site, whereas for all other loci the corresponding forward primer of the PCR reaction was used for sequencing.

2.2.6.3. Droplet digital PCR to quantify vector copy numbers

Droplet digital PCR was used to quantify the vector copy number of either SaCas9 or Luciferase per diploid genome. Therefore, DNA extracted via the DNA/RNA AllPrep kit as described in section 2.2.1.11 was first diluted to 1 ng/ µl for liver samples and 0.4 ng/ µl for cell culture samples. The diluted DNA samples were stored at 4 °C until further processing. Next, the ddPCR Master Mix was prepared by using the ddPCR™ Supermix for Probes (no UTP) from BioRad and the ddPCR 20x housekeeper RPP30 for mouse from BioRad (consisting of primers and probe). For the detection of SaCas9 or Luciferase, a 20x primer/probe mix was prepared by diluting 18 µl of each primer with 7 µl H_2O and 4.75 µl probe with 42.75 µl H_2O for the corresponding target, respectively. For the 20x transgene primer/probe mix, 0.25 µl of each diluted forward and reverse primer and 0.5 µl of diluted probe were mixed for one reaction. Furthermore, a digestion enzyme mix was prepared by diluting HindIII 1:4 in Diluent B (final concentration of 5 u/ µl). The components were combined using the volumes indicated in Table 28, per reaction 5.5 µl previously diluted DNA template was added to 16.5 µl of the combined components. After combining template and Master Mix, the reaction incubated for 15 min at room temperature in order to allow HindIII to digest genomic DNA. Note that HindIII is not supposed to cut within either PCR product. A list of used primer and probe sets is listed in Table 29.

Table 28. Master Mix for ddPCR

Component	**µl for one reaction**
Transgene 20x mix	1.1
Housekeeper 20x mix	1.1
HindIII enzyme mix	1.1
Supermix for probes	11
diluted DNA sample	5.5
H_2O	2.2

Table 29. Primer and probes used in ddPCR to quantify vector copy numbers

Name	**Sequence 5´to 3´**
hluc fwd	CGCCCGCGACCCTATTTTCG
hluc rev	CAGGTAGCCCAGGGTGGTGAAC
hluc probe	FAM-AACCAGATCATCCCCGACACCGCTATTCTGAGCGT-BHQ1
SaCas9_fwd	CCGCCCGGAAAGAGATTATT
SaCas9_rev	CGGAGTTCAGATTGGTCAGTT
SaCas9_probe	FAM-AGCTGCTGGATCAGATTGCCAAGA- BHQ1

Next, the droplet generator was used to produce oil droplets that contain a DNA template as well as all reagents needed to perform the PCR. Previously the DNA was diluted to such an extent that some (about 70 %) of the droplets remain without any DNA template. In the cartridge 20 µl of sample and 70 µl of Droplet Generation Oil for Probes (no UTP) were loaded in the appropriate wells. All wells, that are eight samples at a time, needed to be filled completely. The cartridge was sealed with a casket and the droplet generator was started. Subsequently, 40 µl of generated droplets were transferred to a 96 well Eppendorf plate and after transferring all samples, the plate was sealed with a foil using a foil heater.

Next, the PCR was run in the Biorad PCR machine with the following conditions: initial denaturation at 94 °C at 10 min, 39 cycles of denaturation at 94 °C for 30 sec and elongation at 58 °C for 1 min, followed by an inactivating and stabilizing step of 98 °C for 10 min.

Finally, the droplets were analyzed via the Droplet reader using the Quantasoft software. Therefore, the Supermix for probes (no UTP) was selected, channel 1 was selected to measure the fluorescence signal by FAM, representing the transgene, and channel 2 was selected to measure the fluorescence signal by HEX, representing the RPP30 house keeper and the droplet reader was started. To calculate the vector copy number per diploid genome the numbers provided in the concentration column (droplets/ µl) were used and the following formula was applied:

$$Vector\ Copy\ Number = \frac{concentration\ of\ transgene}{concentration\ of\ RPP30/2}$$

2.2.6.4. Droplet digital PCR to quantify mutagenesis rate *in vivo*

Droplet digital PCR has been previously applied to quantify targeted mutagenesis rates as reported in Sedlak *et al.* (2016) [302]. To this end, one probe is directed against the targeted mutagenesis site and multiplexed with another probe against a reference sequence within the same PCR amplicon (Figure 14). Sequences of drop-off probe, reference probe and primers are listed in Table 30. DdPCR was performed as previously described, but did not include the 20 x house keeper mix, but only one 20x transgene mix with two probes.

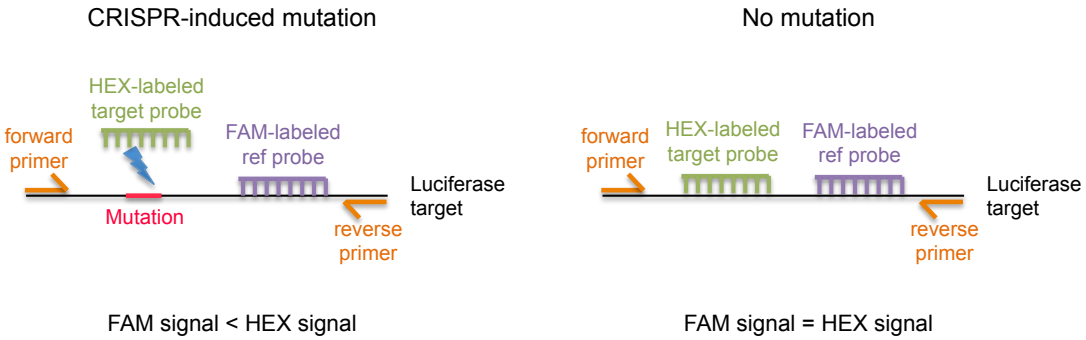

Figure 14. Principle of ddPCR to quantify targeted mutagenesis rates.

In the ddPCR one probe is directed against the site of mutation and multiplexed with a differently labeled reference probe that targets another unedited/reference probe within the same amplicon. If no mutation is present the signal of both probes match. In case of a mutation the target probe drops off and the signal is reduced.

Table 30. Primer and probes to quantify mutagenesis rate on luciferase target.

Name	**Sequence 5 to 3´**
hLuc_dropoff_ fw	CGAGATGTCTGTGCGCC
hLuc_dropoff_ rv	CGCGCTCGTTGTAAATG
hLuc_dropoff_ probe	HEX-TCTGCAGTTCTTCATGCC-BHQ_1
hLuc_reference_probe	FAM-AAGAGGTACGGCCTGAACA-BHQ_1

For the quantification of the mutation rate the concentration of positive droplets in each channel (FAM/HEX) as well as their overlap was applied. Positive droplets in both channels (FAM^+/HEX^+) indicated the absence of mutations and positive droplets in the FAM channel that were negative in the HEX channel (FAM^+/HEX^-) indicated the presence of mutations. Thus the mutation rate was calculated by the following formula:

$$Mutation\ rate\ (\%) = \frac{concentration\ of\ droplets\ (\mathrm{FAM}+/\mathrm{HEX}-)}{concentration\ of\ droplets\ (\mathrm{FAM}+/\mathrm{HEX}+)\ \mathrm{and}\ (\mathrm{FAM}+/\mathrm{HEX}-)}$$

2.2.6.5. Quantitative real-time PCR

Quantitative RT-PCR was performed using the Tetro™ Reverse Transcriptase Kit from Bioline for reverse transcription and the iTaq Universal SYBR Green Supermix from BioRad for quantitative PCR. Firstly, 500 ng extracted RNA via the DNA/RNA AllPrep kit as described in section 2.2.1.11 was applied for reverse transcription. The master mix for reverse transcription was composed as listed in Table 31 for one reaction in 20 µl total volume. Negative controls without reverse transcriptase were prepared to test for DNA contaminations.

Table 31. Composition of Tetro cDNA synthesis

Components	**for 1 reaction**
total RNA	500 ng
5x RT buffer	4 µl
Random Hexamer	1 µl
10 mM dNTP Mix	1 µl
RiboSafe RNase Inhibitor	1 µl
Tetro Reverse Transcriptase	1 µl
H_2O	fill to total 20 µl

Subsequently, the reverse transcription was performed in a thermal cycler with the following conditions: 10 min at 25 °C, 30 min at 45 °C and 5 min at 85 °C.

The quantitative PCR was performed using 5 µl iTaq Supermix, 0.5 µl of each forward and reverse primer (sequences listed in Table 32), 1 µl template that was previously diluted 1:10 and 3 µl H_2O in a total reaction volume of 20 µl in a 96-well plate from Biozym. For each sample, the expression of target and housekeeper (GAPDH expression) was measured in separate wells and samples were always pipetted in duplicates. The plate was sealed with BZO Seal Film (Biozym) and centrifuged at 3200 g for 1 min. The PCR was performed using the StepOnePlus qPCR from Applied Biosystems with the following conditions: Initial denaturation at 95 °C for 30 sec, 40 cycles of denaturation at 95 °C for 10 sec and annealing/elongation at 60 °C for 30 sec, a melting curve was performed by applying 95 °C for 15 sec, followed by a rising temperature from 65 to 95 °C with an increase of 2 °C per second (slope +0.5).

The data was analyzed by using the CT mean of the replicates. Subsequently, the ΔCT between target and house keeper (ΔCT=CT(Target)-CT(House Keeper)) was calculated and values were normalized to one positive control condition (ΔΔCT=ΔCT(condition1)-ΔCT(control)). Finally, the fold change in expression of one condition to the control condition was calculated by $2^{-\Delta\Delta CT}$.

Table 32. Primers used in RT-qPCR.

Name	Sequence 5´to 3´	Note
mGAPDH fw	TTGATGGCAACAATCTCCAC	used for mouse samples
mGAPDH rv	CGTCCCGTAGACAAAATGGT	used for mouse samples
SaCas9-N fw	CCGCCCGGAAAGAGATTATT	used for DMSO and in vivo
SaCas9-N rv	CGGAGTTCAGATTGGTCAGTT	experiments
SaCas9-N_v2 fw	TCGAGAACGTGTTCAAGC	v2 was used to quantify mCMV,
SaCas9-N_v2 rv	GCTGGTCACTCTGTAGCCC	mMecP2, mTK promoter strength
SaCas9-C_v2 fw	ACACCCTGTACTCCACCC	(comparison between N- and C-
SaCas9-C_v2 rv	TTTTTCAGCTTGTCATTGTCC	terminal Cas9)
MecP2 gRNA8 fw	GGCCAAAAAGAAAGCCG	N/A
MecP2 gRNA8 rv	AAAAAAATCTCGCCAACAAG	N/A

2.2.6.6. Bioanalyzer

In order to analyze DNA fragments on the Bioanalyzer, the Agilent DNA 1000 Kit was used according to manufacturer´s protocol. The PCR was performed as described in section 2.2.1.2. The PCR was performed in a 25 µl total reaction volume using 1 µl DNA template from cell lysates and 1.25 µl of each forward and reverse primer (5´CCACAACCTTCCACCAAAC3´ and 5´CGATAACCAGGACAAGTTGG3´, Tm=61 °C), respectively, which resulted in a 300 bp PCR product. The PCR product was loaded on a 1% agarose gel and purified as described in section 2.2.1.5.

To prepare the reaction on the Bioanalyzer, first the gel-dye mix was prepared by allowing the DNA dye concentrate and DNA gel matrix to equilibrate to room temperature for 30 min. 25 µl of the DNA dye concentrate was added to the DNA gel matrix vial. The solution was vortexed, spinned down and transferred to the spin filter. The gel-dye mix was centrifuged at 2000 g for 15 min and stored at 4 °C until further usage.

Next, the gel-dye mix was loaded on the DNA chip. Therefore, the gel-dye mix equilibrated at room temperature for 30 min before usage. The DNA chip was put on the chip priming station and 9 µl of gel-dye mix was added to the well marked with (G). The

chip primin station was closed and the plunger (previously set to 1 ml) pressed until it held by itself to distribute the gel-dye mix equally to all wells. Exactly after 60 sec the clip was released and after further 5 sec the plunger was pulled back at the 1 ml position. The clip priming station was opened and 9 µl of gel-dye mix was pipetted in the wells marked with G. Subsequently, 5 µl marker (reaction tube with green top) was pipetted in all sample and ladder wells. Finally, 1 µl of DNA ladder (reaction tube with yellow top) was loaded in the well marked with a small ladder and in each of the 12 sample wells 1 µl of sample (purified PCR product) or water (control) was added. The chip was vortexed at 2400 rpm and the chip run immediately on the Agilent 2100 Bioanalyzer using the 2100 Expert program. To analyze the data, the peaks of the PCR product were assigned manually and the concentration of each peak used for further analysis. The data was stored as a final PDF report. To quantify the fraction of excised PCR products, the sum of the concentrations of the smaller products were divided by the sum of the concentration of all PCR products.

2.2.6.7. Automated microscopy

The automated imaging procedure is described in detail in Börner et al. (2010) [303].
Prior to imaging the cells were fixated via PFA. Therefore, the supernatant of the cells was removed and 80 ul of 4% PFA (dissolved in PBS) per well was added on the cells, followed by 30 min to 1 h incubation at room temperature covered from light. Subsequently, Hoechst was used to stain the DNA, by adding 80 ul of a 1:1000 dilution of Hoechst in PBS per well in a final concentration of 1 ug/ml, followed by 30 min to 2 h incubation at room temperature covered from light. Finally, 120 ul PBS per well was added and the cells were imaged within one week.
For automated image acquisition, the Olympus Biosystems IX81 inverted microscope using the ScanR acquisition software was used. Images were acquired in 9 positions per well with a 10x objective and acquired in the Hoechst and GFP channel using the corresponding excitation and emission filters. For the imaging analysis, first the cell nuclei were segmented using the Hoechst channel, followed by segmentation using the GFP channel. As output the number of nuclei per image, the average signal intensity in the GFP channel per image, and the proportion of cells that were infected, were computed. A fully automated pipeline for image processing was implemented in Matlab and C++, in which the intensity of the GFP signal could be adjusted to discriminate between authentic GFP signal and background.

2.2.6.8. HBe/HBs measurements

Supernatant of HBV infected cells or cells that stably express the HBsAg was collected at the indicated days, centrifuged at 4000 rpm for 5 min to remove cellular debris and diluted 1:5 or 1:10 as indicated in PBS. HBs and HBeAg measurements were performed by the analytical center of the University Hospital Heidelberg via enzyme-linked immunosorbent assay ([ELISA], AxSYM; Abbott) or ADVIA Centaur XPTM automated chemiluminescence system (Siemens), respectively. Values are reported in international units per ml [IU/ml].

2.2.6.9. Immunofluorescence staining of HDAg

Immunoflourescence stainings of HDAg were performed by Florian Lempp as described in Lempp et al. [300]. Cells were fixed with 4% PFA for 30 min, followed by permeabilization in PBS/0.25% Triton X-100 for 30 min. Cells incubated with a patient serum containing anti-HDAg antibodies (VUDA, 1:3000 dilution) diluted in 5% milk powder in PBS overnight. After washing, the secondary antibody goat–anti-human-555 (Invitrogen) was added for 1 h, and the cells were imaged on an inverted epifluorescence microscope.

2.2.6.10. Western blot

The western blot for detection of HDAg was performed by Florian Lempp as described in Lempp et al. [300]. Therefore, the cell lysate was loaded on a 15% SDS gel. Proteins were transferred onto nitrocellulose membranes by semidry transfer and incubated with primary antibodies (HDAg: serum of a chronically infected patient [VUDA, 1:3000 dilution]; actin: mouse–anti-actin [Sigma, A1978, 1:5000 dilution]) diluted in 5% milk in TBS-T overnight at 4 °C. Membranes were washed with TBS-T and incubated with fluorescently labeled secondary antibodies (LI-COR Biosciences) for 1 h at RT, membranes were washed once more, and imaged on a LI-COR Odyssey imaging system.

To detect SaCas9 in the split Cas9 experiments either cells were seeded in 6 or 24 well plates with density of 3x 10^5 or 10^5 cells per well in 2 ml or 500 µl cell culture medium or mouse liver was used. Cells in 6- well plates were transfected with 1.5 µg total DNA and Lipofectamine 2000 reagent. Therefore, 4 µl Lipofectamine 2000 were mixed with 250 µl Optimem and DNA was mixed with another 250 µl Optimem. Subsequently, the DNA and Lipofectamine mix were combined and thoroughly mixed and incubated for 15 min at room temperature until it was applied drop-wise to the cells. Samples from cell culture were harvested in 100 µl RIPA buffer supplemented with protease inhibitors. After

incubation for 15 min on ice, samples were centrifuged for 15 min at 13000 rpm and the supernatant was resuspended in 4x Lämmli sample buffer supplemented with 10 % ß-Mercaptoethanol and cooked for 10 min at 95 °C. Samples from mouse liver were weighed and supplemented with 3 times the volume of RIPA buffer (100g liver = 3x 100 µl RIPA buffer) and Protease inhibitor. Samples were ruptured by using the Tissue Raptor and a metal beat at 50 Hz for 45 sec. The samples incubated for 15 min on ice and were centrifuged for 15 min at 13000 g. The supernatant was resuspended in 4x Lämmli sample buffer supplemented with 10 % ß-Mercaptoethanol and cooked for 10 min at 95 °C. Protein concentrations were measured using the BCA™ Protein Assay Kit from PerBio according to manufacturer's instructions. Finally, the samples from cell culture or mouse liver were loaded on precast mini-PROTEAN TGX gels with 7.5 % polyacrylamide and 15-well comb or 4-15% polyacrylamide and 10-well comb and 20 to 50 µg protein were loaded on the gels, respectively. As protein standard, 10 µl MagicMark and 10 µl PageRuler Plus pre-stained protein standard were used.

After SDS-PAGE electrophoresis, proteins were transferred onto a nitrocellulose membrane using semi-dry Western blot transfer. Therefore, Whatman paper and a nitrocellulose membrane were soaked in transfer buffer and a sandwich was assembled in a Trans-Blot® SD Semi-Dry Transfer Cell. Blotting was performed at 4°C, 150 mV for 1 h. Next, the blot was blocked in 5% milk in TBS-T for 1 h at room temperature. Primary antibodies were diluted in 5% milk in TBS-T and incubated with the membrane at 4°C over night. The next day, the membrane was washed three times with TBS-T. Subsequtnly, the appropriate horseradish peroxidase-conjugated secondary antibody was added for 1 h at RT. Primary and secondary antibodies are listed in Table 33. After washing 3 times with TBS-T, equal volumes of the two-component chemiluminescence substrate were mixed and applied on the membrane. The signal was recorded on the Intas camera.

Table 33. List of primary and secondary antibodies for Western Blot.

Name	**Description**	**Origin**
anti- FLAG Ab	monoclonal, produced in mouse	Sigma #F1804
anti ß-Actin Ab	monoclonal, produced in mouse	Santa Cruz #sc-47778
anti-SaCas9 Ab	monoclonal, against N-terminal, produced in mouse	Diagenode #C15200230
Secondary goat anti-mouse Ab	Peroxidase-conjugated Goat anti-Mouse IgG,	Jackson ImmunoResearch #115-035-068

2.2.6.11. Flow cytometry

For flow cytometry the Cytometrics FC 500 MPL flow cytometry (Beckman Coulter) equipped with a 561 nm laser and mCherry filter set was applied. Cells were measured in 96 well plate format and were detached at the indicated time points from the plates just before flow cytometry analysis. Therefore, the cell medium was removed from the cells, the cells were washed with PBS and 30 µl Trypsin was added per well. Cells incubated for 10 min at 37 °C and Trypsin was inactivated by adding 170 µl PBS with 1% BSA. For flow cytometry, 10.000 cells were recorded per data set and analyzed in using the Flowing software 2. For the analysis, the living cells were gated using the forward and side scatter.

2.2.6.12. Luciferase measurement

In order to test the TuD containing constructs, the plasmids #714, #1181 and #1182 from the Grimm internal plasmid library were used, that contain a Renilla and Firefly expression cassette and in case of plasmid #1181 and #1182 a binding site for the shRNA HBV7 sense and antisense strand in the 3´ UTR of Renilla luciferase, respectively. Besides, the multiplexing constructs, that were described in section 2.2.2.2, plasmids that drive shHBV7 expression from the H1 promoter (#1117), shHBV7 and TuD RNA expression both from an H1 promoter (#1118) or H1- driven shHBV7 expression and U6-driven TuD RNA expression (#1119) were used to test TuD RNA activity. Transfection were performed using lipofectamine as indicated in section 2.2.3.2 with 10 ng of plasmid containing luciferase and 100 ng of plasmids containing the shRNA and/or TuD RNA. Two days later, cells were processed for luciferase signal measurements. Luciferase assays were performed using the Dual-Luciferase® Reporter Assay System from Promega according to manufacturer´s protocol. Therefore, the 5x passive lysis buffer was diluted 1:5 with H_2O and 30 µl were added directly to the cells of each well of a 96 well plate. Cells incubated with the passive lysis buffer for 15 min at room temperature and 10 µl of the lysed cells were transferred to a white 96-well microplate (Greiner) and directly used for the Luciferase measurements.

For *in vivo* luciferase measurements, 40 to 150 mg of liver tissue was used and supplemented with three times the volume of 5x passive lysis buffer (100 mg = 300 µl). The tissue was homogenized using the Tissue Ruptor at 50 Hz for 45 sec. The lysate incubated for 15 min at room temperature and was centrifuged at 13000 g for 3 min. Subsequently, 10 µl of lysate was transferred to a white 96-well microplate (Greiner) and

directly used for Firefly Luciferase measurements using the Luciferase Assay Kit from Promega (only firefly luciferase).

The buffer for Firefly Luciferase measurements was prepared by adding 10 ml Luciferase Assay Reagent II to the one vial of lyophilized substrate. The buffer for Renilla Luciferase measurements was prepared adding 50x Stop& Glo Substrate to the required amount of Stop& Glo buffer. The buffers were subsequently inserted into the Glomax machine (Promega) with two independent injectors. The injectors were primed with 500 µl of each buffer. Subsequently, the firefly luciferase signal was measured in the previously prepared white 96-well microplate by adding 100 µl Firefly luciferase buffer with a speed of 200 µl/sec to the plate and the signal was integrated within 10 sec. After quantification of the firefly luminescence, this reaction was quenched by adding 100 µl Renilla luciferase buffer with a speed of 200 µl/sec to the plate. The Renilla luciferase signal was integrated within 10 sec. For the analysis of the luciferase data, the Renilla luciferase signal was normalized to the Firefly luciferase signal and are presented as relative light units.

To measure the luciferase signal from i*n vivo* samples, the same procedure was applied, but only Firefly luciferase buffer was used.

2.2.6.13. Statistical analysis

The statistical analysis was performed as indicated either with student´s t-test for the comparison of two groups or one-way ANOVA for the comparison between several groups. In general, a Gaussian distribution was assumed and the mean of each group was compared to the mean of (all) the other groups. To correct for multiple comparisons, Bonferroni´s post-hoc test was applied. Statistics were calculated using Prism 6.

3. RESULTS

3.1. Alternative strategies for small RNA multimerization in AAV

The RNAi and CRISPR/Cas9 machineries are guided by small RNAs to the designated RNA and DNA target, respectively. In order to combine both technologies, the small RNAs need to be co-expressed in the same target cell. To this end, our lab has previously envisioned three alternative strategies to multiplex small RNA triggers from rAAV vectors in the same target cell (Figure 15): i) Individual small RNAs can be packaged in separate rAAV vectors and "mixed" after production and rAAV titration, ii) the plasmids encoding the individual small RNAs can be "pooled" before transfection and the various rAAV vectors can be produced within the same dish, or. iii) in the approach named "TRISPR", multiple small RNA expression cassettes can be juxtaposed on one vector genome. The benefit of the first approach is that the individual rAAV vectors can be mixed in any desired ratios after vector titration and prior to transduction, which enables the adjustment of the proportion of each small RNA within the target cells. While the second approach is simpler in terms of handling as it requires only a single production and titration, the fine-tuning of each rAAV vector is impossible. The last approach convinces with an equal abundance of each small RNA expression cassette within the target cell. Also, as several expression cassettes are present within a single rAAV, less viral particles compared to the other approaches are required to deliver the same number of small RNAs to target cells. Importantly, the TRISPR cloning strategy and biological toolbox has previously been designed by Florian Schmidt, a former Bachelor student in our lab, who has also provided the first evidence of its superiority over the two alternative multiplexing strategies (i) and (ii) above. The toolbox contains all necessary plasmids to juxtapose three small RNA expression cassettes, in the predefined order of U6, H1, and 7SK promoter-driven cassette, on a single dsAAV vector and is compatible with the expression of shRNAs and/or sgRNAs for the CRISPR/Cas9 system of *Streptococcus pyogenes* and *Staphylococcus aureus* in any possible permutation (details on the cloning strategy are described in Florian's BSc thesis as well as in section 2.2.2.2 and Figure 13).

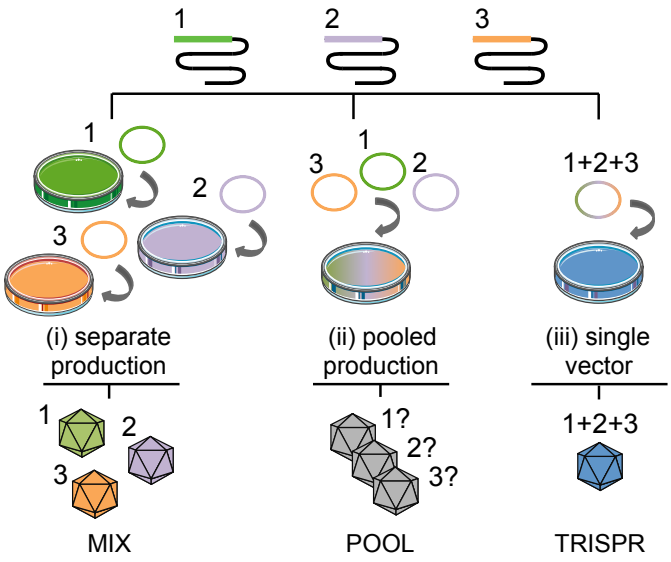

Figure 15. Alternative strategies to multimerize small RNAs.

i) Three small RNA expression cassettes (1 to 3) can be packaged separately in AAV capsids and subsequently mixed in any desired ratio prior to transduction (strategy "MIX"). ii) Alternatively, plasmids containing individual small RNA expression cassettes can be pooled before transfection and rAAV vectors can be produced in the same dish, resulting in a vector pool whose composition cannot be controlled experimentally (strategy "POOL").iii) Finally, the three small RNA expression cassettes can be multiplexed on a single vector genome, which ensures their equal abundance in the same target cells. Our lab has previously termed this strategy “TRISPR”. Figure adapted from Florian Schmidt's Bachelor thesis (manuscript in preparation).

3.1.1. Screening of different sgRNAs against HBsAg

We experimentally compared these different approaches in an HBV context, by applying three sgRNAs that induced the CRISPR/Cas9 system *Staphylococcus aureus* and served as stand-in for the multimerization of small RNAs in general. We first screened for sgRNAs that knock-out the surface antigen of HBV. To this end, HepG2-hNTCP-HB2.7 cells [300] that harbor the stable integrated hNTCP receptor and HBsAg were transduced with ten different rAAV vectors expressing sgRNAs against different positions of the surface antigen. The sgRNAs were packaged in the AAV capsid variant 9A2 [227], transduced with a multiplicity of infection (MOI) of 10^5 viral particles/cell and expressed by the strong U6 promoter. The *Sa*Cas9 was expressed by the CMV promoter and delivered in a separate rAAV vector of the same capsid variant and with the same MOI. The supernatant of the cells was collected at various time points that comprised the secreted HBsAg of day -3 to 0 prior to rAAV transduction, day 4 to 6 and day 6 to 8 post-transduction (Figure 16A). The levels of secreted HBsAg were measured via ELISA (see section 2.2.6.8 for methodological details). Furthermore, eight days post-transduction, cells were harvested for the quantification of targeted mutations in the HBsAg locus via T7 endonuclease assay (Figure 16B), in which the ratio of intensities of T7 fragments to input band is used as a measure for indel frequencies (see section 2.2.6.1 for methodological details).

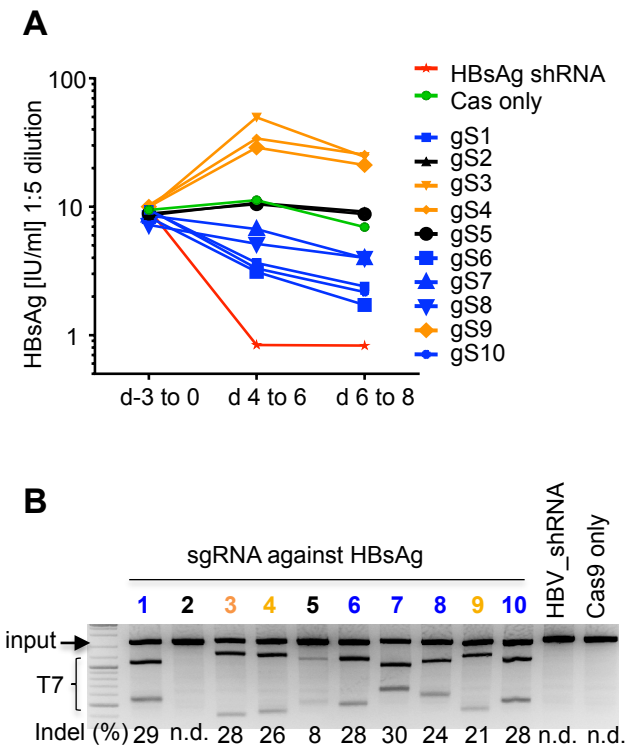

Figure 16. Screening of sgRNAs against the HBV surface antigen.

HepG2-hNTCP-HB2.7 cells were transduced with *Sa*Cas9 and 10 different sgRNAs that target the stably integrated HBsAg locus. **A)** Secreted HBsAg in the supernatant of cells between day -3 to 0 prior to AAV transduction, day 4 to 6 and day 6 to 8 after AAV transduction. The sgRNAs either reduce HBsAg levels (blue), maintain HBsAg levels (black) similar to controls (green, transduction of Cas9 only) or elevate HBsAg levels (orange). The shHBV7 was used as positive control (red) [163]. **B)** T7 endonuclease assay of transduced cells after eight days. Results are shown for a single experiment and were obtained in close collaboration with Florian Lempp from the lab of Stephan Urban (manuscript in preparation).

While all sgRNAs, except for sgRNA 2 and 5, showed efficient mutagenesis rates between 20 to 30 % in the T7 assay, only sgRNA 1, 6, 7, 8, and 10 reduced the levels of secreted antigens in the supernatant. Indeed, sgRNA 3, 4 and 9 even increased the amount of secreted antigens. Interestingly, these sgRNAs targeted the preS1 region that leads to the production of the large HBsAg, while all other sgRNAs target the small HBsAg. Note that the applied ELISA is not able to differentiate between the surface antigen variants, since a portion of the S-HBsAg, which is present in all variants, is used for quantification.

3.1.2. Quantitative comparison between multiplexing approaches

Subsequently, we used sgRNA 6, 7 and 8 to experimentally compare the alternative strategies to co-express these small RNAs from rAAV vectors. To this end, we created different dsAAV vectors that either carried individual U6, H1 or 7SK promoter driven sgRNA expression cassettes or that juxtaposed all three expression cassettes on a single viral genome (Figure 17A).

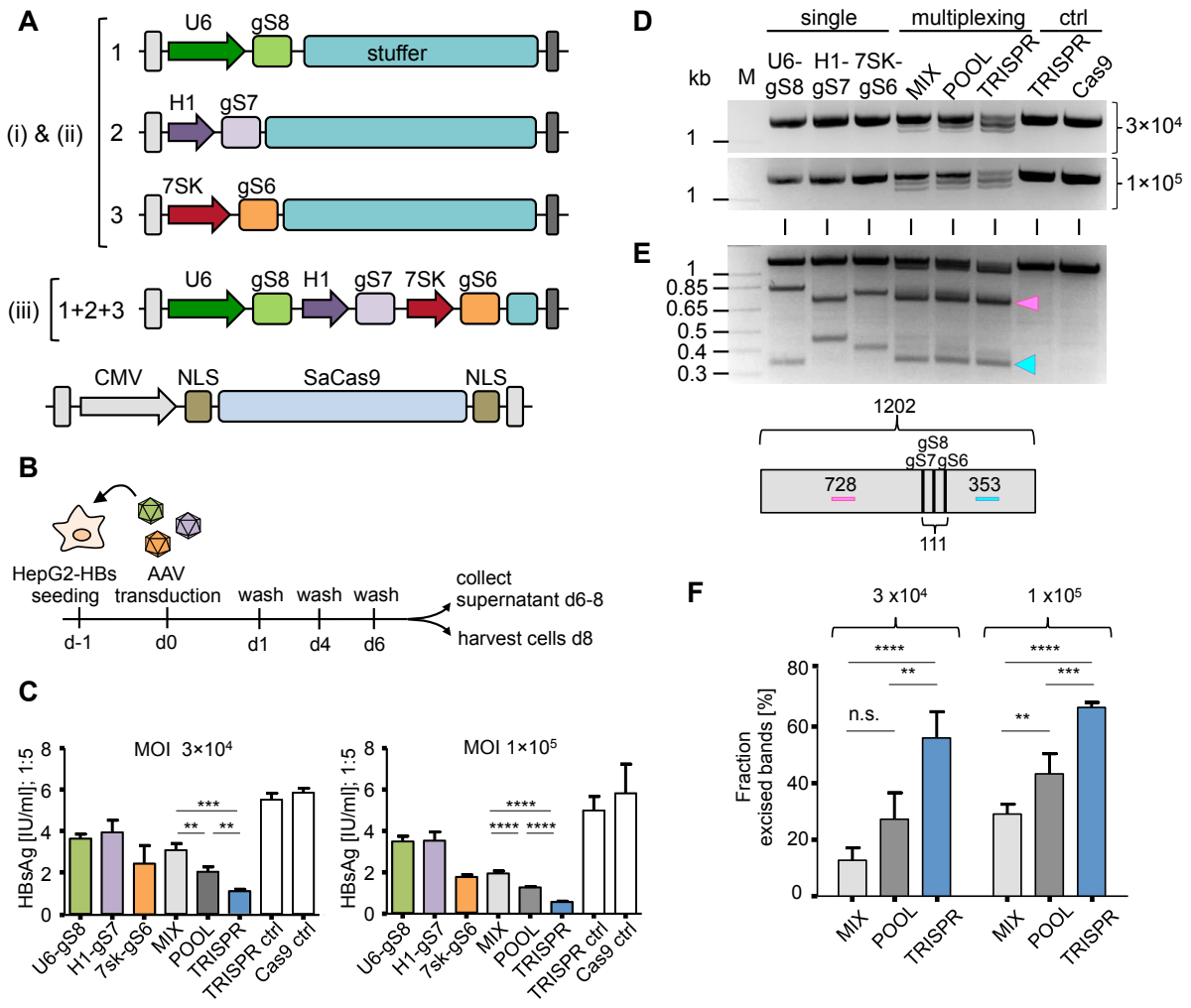

Figure 17. Experimental investigation of different multiplexing strategies.

A) To investigate multiplexing strategy i) and ii) as depicted in Figure 15, rAAV vectors were designed that express the sgRNA 8, 7 and 6 against HBsAg from the U6, H1 and 7SK promoter, respectively. Stuffer sequences were inserted to reach a vector size of 2 kb. To investigate strategy iii), the sgRNA expression cassettes were assembled on a single dsAAV vector by applying the TRISPR cloning strategy. *Sa*Cas9 was provided by an additional ssAAV. The light gray box represents the natural ITR that leads to packaging as a ssAAV genome, whereas the mutation of one ITR (dark gray box) leads to packaging as a dsAAV genome. **B)** Experimental layout. HepG2-hNTCP-HB2.7 cells were transduced with AAV9A2 vectors and the supernatant from day six to eigth post-transduction was collected and subsequently cells were harvested for genomic investogations. **C)** Secreted HBsAg in the supernatant was collected at six to eight days after transduction with an MOI of $3x10^4$ (left) and 10^5 (right). **D)** PCR and **E)** T7 assay of the HBsAg target locus showing gRNA-mediated fragmentation in samples treated with multiplexing strategies. **F)** PCR products were run on a Bioanalyzer 2100 and the fraction of excised bands in the histogram was divided by the fraction of all PCR products. Error bars represent standard deviations of three independent experiments. Differences between the conditions were determined using Bonferroni´s post-hoc test after one-way ANOVA (**p <0.01, ***p < 0.001, ****p < 0.0001) (manuscript in preparation).

After packaging of all necessary components in variant rAAV9A2 [227], HepG2-hNTCP-HB2.7 cells were transduced with the MOI of $3x10^4$ or 10^5 of each component either by

individual sgRNAs or by applying the MIX, POOL or TRISPR strategies (Figure 17B). Cells were regularly washed with PBS and supplied with fresh media. Secreted antigens were collected with the supernatant of day 6 to 8 and the cells were subsequently harvested for analysis on the DNA level. HBsAg measurements revealed a slight decrease in secreted antigens, when targeted by individual sgRNAs (Figure 17C). The multiplexing approaches conferred higher knock-out efficiencies in general, with the TRISPR strategy significantly outperforming all other strategies in the reduction of secreted HBsAg. This result was confirmed by the analysis on the DNA level, when the target locus was amplified via PCR (Figure 17D). TRISPR-treated samples showed a strong fragmentation of the target locus, as the simultaneous DSBs by CRISPR/Cas9 at two or more positions in close proximity leads to the complete excision of the fragments between the cut sites. For a more quantifiable result, the PCR products were run on a Bioanalyzer 2100. The chromatograms (Supplementary Figure 1) showed a single peak for the samples treated with individual sgRNAs and two smaller peaks for the different multiplexing approaches. While the largest peak corresponded to the complete size of the amplified target locus, which potentially harbored indels that are indistinguishable by this analysis, the smaller peaks represented the target locus after excision of the sequence between the sgRNA binding sites. The chromatograms were used to quantify the fraction of excised bands in the samples treated with the three multiplexing approaches, by dividing the areas under the curves of the smaller fragments by the area under the curves of all fragments (Figure 17F). The Bioanalyzer data confirmed the highest fragmentation of the target locus in TRISPR-treated samples, in which the sequences between the cut sites were excised in about 60% of all cells. Finally, the T7 endonuclease assay verified the correct cleavage pattern in all multiplexing approaches confirming that the three sgRNAs were indeed co-expressed (Figure 17E).

3.2. A combinatorial approach to knock-down HBV antigen expression and kock-out viral cccDNA

After we successfully validated the TRISPR strategy as superior multiplexing approach, we applied this approach to combine shRNA and sgRNA expression to tackle HBV on the RNA and DNA level. To this end, we designed a TRISPR vector with sgRNAs against the HBx and HBs antigens and an additional shRNA against the HBx antigen, driven by the U6, H1 and 7SK promoters, respectively (Figure 18A). For the knock-out of the HBsAg, we selected the most efficient sgRNA 6 from our previous screen (Figure

16). The sgRNA against the HBxAg was previously tested for its functionality and efficiency by Thomas Tu (lab of Stephan Urban, University Hospital Heidelberg). Furthermore, the shRNA targeting the HBx antigen (shHBV7) was previously published by our lab [163] and was shown to mediate very efficient HBV knock-down. We substituted the positions of each small RNA with control RNAs that do not match any HBV or genomic target. The substitution of each position with control RNAs in any possible sgRNA/ shRNA combination resulted in eight different TRISPR vectors.

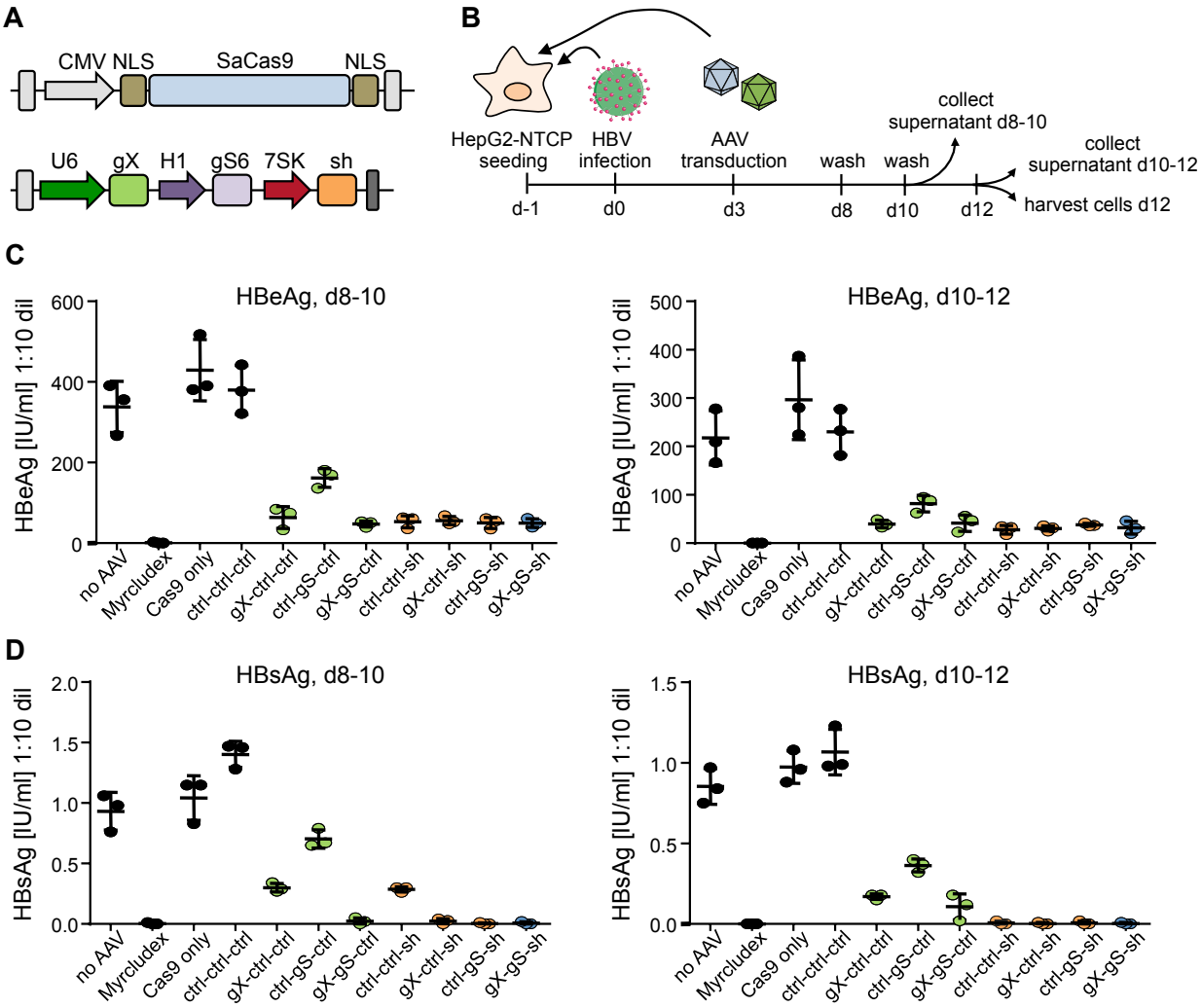

Figure 18. A combinatorial CRISPR/RNAi approach to tackle HBV infection.

A) TRISPR vector harboring two sgRNAs against the HBx and HBs antigens and an shRNA against the HBx antigen, driven by the U6, H1 and 7SK promoters, respectively. Note that each sgRNA and shRNA position was substituted with non-targeting sgRNA and shRNA controls, resulting in eight different TRISPR vectors. An additional ssAAV vector provided *Sa*Cas9. **B)** Experimental workflow: HepG2-hNTCP cells were infected with HBV using an MOI of 200 and three days later transduced with AAVLK03 expressing the indicating shRNAs/sgRNAs using an MOI of 10^5. Secreted HBeAg **(C)** and HBsAg **(D)** in the supernatant of day 8 to 10 (left) and day 10 to 12 (right) post-HBV infection was measured via ELISA. Each data point represents an independent experiment.

Subsequently, HepG2 cells with stably integrated hNTCP receptor were infected with HBV and three days later transduced with rAAVLK03 vectors [304] encoding either *Sa*Cas9 or the different TRISPR constrcucts (Figure 18B). The secreted antigens were collected with the supernatants from day 8 to 10 and day 10 to 12. Secreted HBeAg levels fluctuated around 400 and 250 IU/ml (1:10 dilution) for control samples (no rAAV vector, Cas9 only or TRISPR vector solely with control RNAs) in the supernatants of day 8 to 10 and day 10 to 12, respectively. By contrast, TRISPR vectors that expressed at least a single RNA trigger efficiently reduced the amount of secreted antigen (Figure 18C). Similar results were observed with HBsAg measurements of the same samples. Note that the magnitude of secreted surface antigen in HBV infection experiments were lower and reached about 1 IU/ml for control samples (Figure 18D). Similar values for secreted HBe and HBsAg in HBV infection experiments have been reported previously [305]. In general, the multiplexing of two sgRNAs led to an additive effect (green dots) and expression of the shRNA decreased antigen levels to the limit of detection thresholds (orange dots). Myrcludex B [306], an entry inhibitor of HBV, was able to fully block the infection.

3.2.1. A combinatorial approach with TuD RNAs

Next, we applied the TRISPR strategy to combine not only the CRISPR/Cas9 and RNAi technologies, but also TuD RNAs (see section 1.4.3 for details) in the same expression vector. To this end, we either expressed the sgRNA against the X or S antigen from the U6 promoter and shHBV7 and its corresponding TuD RNA from the 7SK and H1 promoter, respectively (Figure 19A). The substitution of each small RNA with control RNAs resulted in twelve different TRISPR vectors. We further used the same experimental approach as previously described (Figure 18B), *i.e.*, we infected HepG2-hNTCP cells with HBV and subsequently transduced them with the designated TRISPR vectors. First, we investigated the effect of the TRISPR vectors on secreted HBeAg and HBsAg levels in the supernatants of day 8 to 10 and day 10 to 12 after HBV infection (Figure 19B and C). We observed similar results as previously described, *i.e.*, TRISPR vectors with an individual sgRNA (green dots) reduced the amount of HBeAg efficiently and HBsAg levels to about 50%. Viral vectors with the shHBV7 (orange dots) reduce HBeAg and HBsAg to detection limits. The effect of shRNA on antigen levels remained unaffected by the presence of TuD RNAs. In contrast, previous experiments from our lab

reported an enhanced shRNA effect by the co-expression of corresponding TuD RNAs [162; 163].

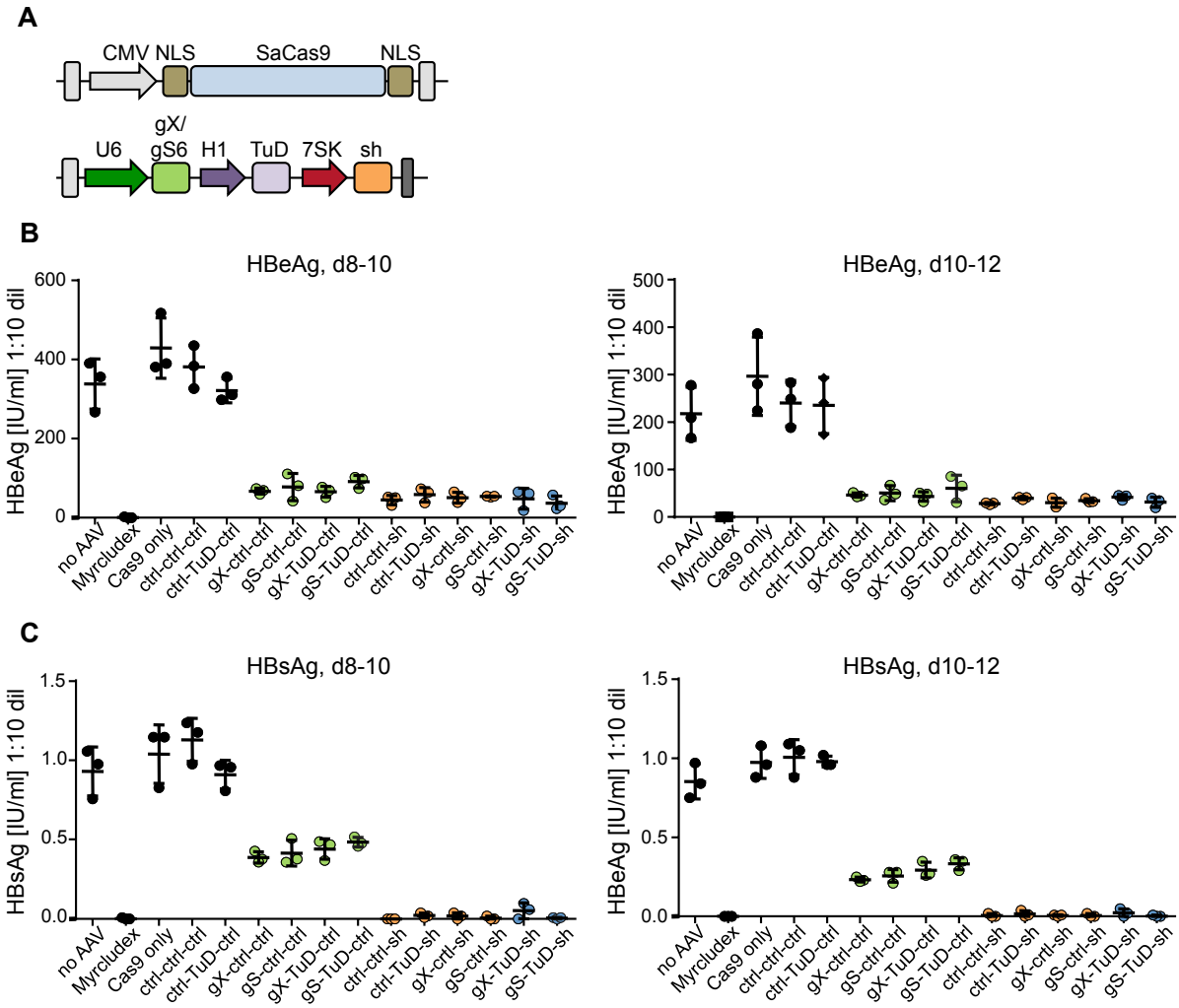

Figure 19. A combinatorial approach with TuD RNAs to tackle HBV infection.

A) Experiments follow the same workflow as previously, but differ in the applied TRISPR vectors. The U6 promoter drives either a sgRNA against HBx or HBsAg, while TuD RNA is expressed by the H1 promoter and shRNA against HBxAg remains under the 7SK promoter. Note that also constructs were designed in which each small RNA position was substituted with non-targeting sgRNA, TuD RNA or shRNA controls, resulting in twelve different TRISPR vectors. **C)** HBeAg measurements and **D)** HBsAg measurements after 8 to 10 days (left) and 10 to 12 days (right) post-HBV infection. Each data point represents an independent experiment.

Next, we investigated whether shHBV7 exhibits unintended sense strand activity and whether TuD RNAs can reduce this off-target effect. Therefore, we applied a reporter system consisting of *Renilla* and Firefly luciferase on the same plasmid (Figure 20A). The 3´ UTR of the *Renilla* luciferase harbored either a binding site (bs) for the antisense (as)-strand of the designated shRNA to investigate the desired on-target knock-down

efficiency, a binding site for the sense-strand to assess unintended off-target activity, or no binding site. The subset of TRISPR constructs that harbor the shRNA and either the TuD RNA or a scrambled TuD RNA version were co-transfected with the reporter system in HEK293T cells. Two days later, cells were lysed and *Renilla* and Firefly luciferase signals were measured. Transfection efficiencies between samples were corrected by the normalization of *Renilla* to Firefly luciferase signals and values are presented as relative light units (RLU) of *Renilla* luciferase (Figure 20B).

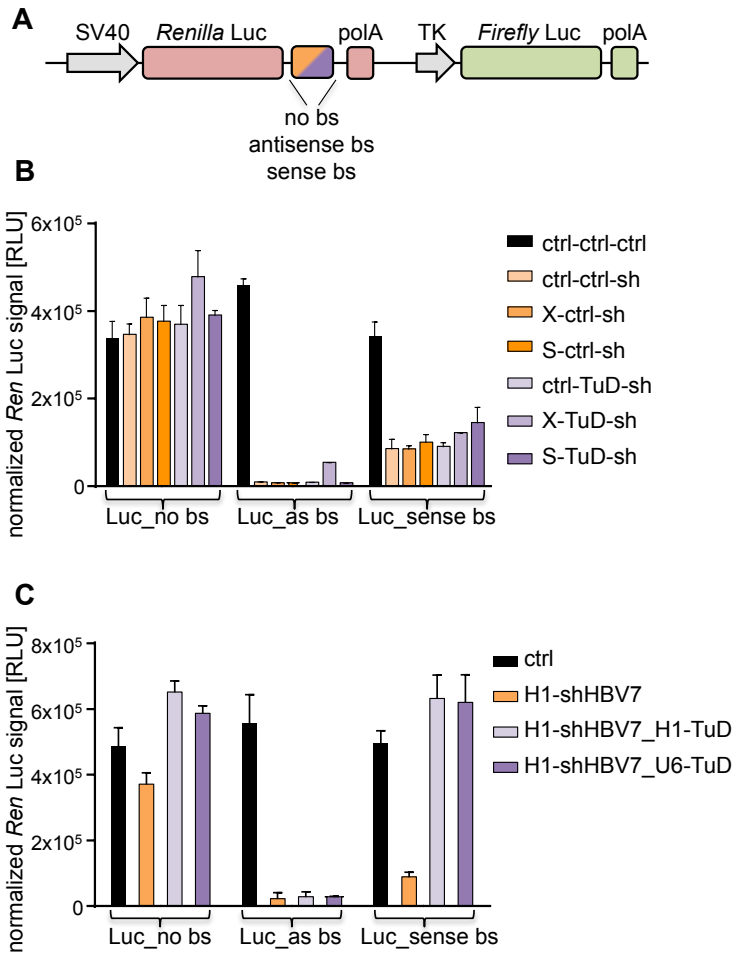

Figure 20. Evaluation of TuD RNAs in a luciferase reporter assay.

A)The reporter system comprised a *Renilla* and Firefly luciferase, in which either no binding site (Luc_no bs), an antisense-strand binding site (Luc_as bs) or a sense-strand binding site (Luc_sense bs) was inserted in the 3´ UTR of *Renilla* luciferase. **B)** HEK293T cells were transfected with 10 ng of reporter and 100 ng of the indicated TRISPR construct. Two days later cells were lysed and luciferase signals were measured. **C)** The shRNA was expressed by the weaker H1 promoter and TuD RNAs were either not expressed (orange), expressed by the H1 promoter (light violet) or by the strong U6 promoter (dark violet).

According to expectations, the luciferase signal remained unaffected when the TRISPR vectors were co-transfected with the reporter system that harbored no binding site and decreased when the reporter system contained the binding site for the antisense strand (on-target activity). Indeed, luciferase signals also decreased when the reporter system contained a sense-strand binding site, which reflects the extent of off-target activity by loading of the unintended passenger strand in RISC. However, TRISPR constructs that

contained a TuD RNA (violet bars) showed similar reductions in luciferase signals as constructs with scrambled TuD RNA controls (orange bars). Thus, in this experimental setting, the TuD RNAs were insufficient to restrict the activity of free sense strands and to avoid passenger strand-mediated off-target activity.

Therefore, we tested another experimental design, in which we expressed the shRNA from the weaker H1 promoter and the TuD RNA either from the H1 promoter or the strong U6 promoter (Figure 20C). In accordance with our previous experiment, the luciferase signal remained high for the reporter system without binding sites and decreased when the shRNA was able to bind its antisense counterpart (on-target activity). The shRNA also mediated down-regulation of the reporter with a sense-strand binding site (orange bar, right data set of the panel) reflecting its off-target activity, which was prevented and restored to control levels when TuD RNA was either expressed by the H1 (light violet bar) or U6 (dark violet bar) promoter.

3.2.2. Expression of rAAV/CRISPR in the mouse liver

The efficiency of CRISPR/Cas9 *in vivo* is strongly dependent on the delivery and expression of the CRISPR components in target cells. Thus, we evaluated the expression of *Sa*Cas9 by different promoters in the liver of mice. To this end, *Sa*Cas9 was packaged into ssAAV8 under either liver-specific promoters, including the LP1, TTR, TBG promoters, or minimal versions of the CMV and EF1α promoters, mCMV and EFS, respectively, which are about 220 bp (Figure 21A).

The rAAV/CRISPR vectors were co-injected with a kill-switch (KS) luciferase reporter that contains a Firefly luciferase expression cassette in addition to a U6-driven sgRNA against the luciferase transgene itself. This reporter was previously developed by Julia Fakhiri from our lab (patent application number WO2017182468A1) and efficiently measures the amount of present *Sa*Cas9 within the target cells by the degree of reduction in luciferase signals. Mice were co-injected with *Sa*Cas9 and luciferase vectors and sacrificed 15 days post-injection in order to extract the liver for further analysis. The strongest reduction in Luciferase signals were obtained by *Sa*Cas9 expression from the LP1 promoter, followed by the TTR and TBG promoters (Figure 21B). Whereas the mCMV promoter efficiently reduced luciferase signals about two-fold, the EFS promoter was unable to express sufficient amouts of *Sa*Cas9 to reduce the luciferase signal.

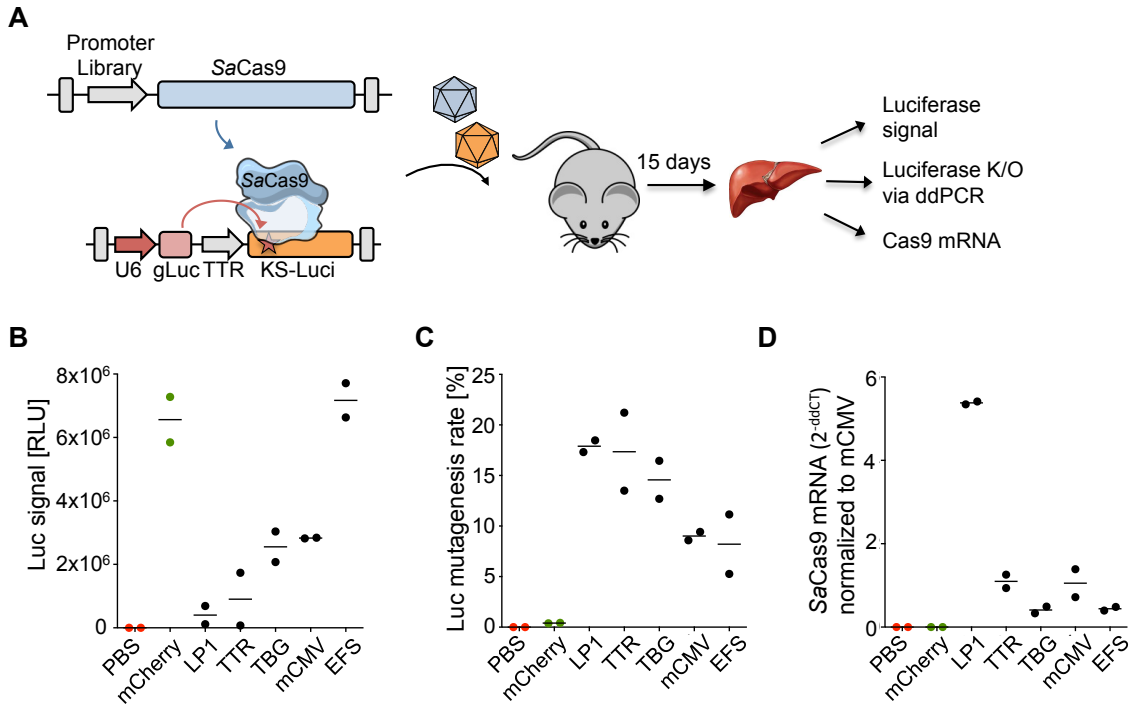

Figure 21. Evaluation of a promoter library driving *Sa*Cas9 expression in mouse liver.

A) Experimental layout. *Sa*Cas9 expressed by a small promoter library and KS-Luciferase were delivered in ssAAV8. The *Sa*Cas9 vector was injected at 10^{12} viral particles and the Luciferase vector at $2x10^{11}$ viral particles into the tail vein of female NMRI mice (6 weeks old). Mice were sacrificed after 15 days and the liver was extracted. **B)** Measurements of Firefly luciferase signal in relative light units (RLU) from liver pieces. The reduction in Luciferase signal indicates the amount of *Sa*Cas9 expression. **C)** DNA was extracted from liver pieces. The mutagenesis rates of the Luciferase target were quantified via ddPCR by multiplexing a primer/probe set against the target site and a reference site within the luciferase transgene. **D)** RNA was extracted from liver pieces and the amounts of *Sa*Cas9 mRNA were quantified via quantitative PCR including the reverse transcriptase step. CT values were normalized to the GAPDH house keeper. B) to D) Controls include mice injected with PBS instead of viral vectors (red) and ssAAV-mCherry instead of the *Sa*Cas9 vector (green). Each data point represents the measurements from an individual mouse. Results were acquired jointly with Julia Fakhiri and Nikolay Sergeev (practical student).

The reduction in luciferase signals strongly correlated with the amount of mutations at the luciferase target site as quantified via droplet digital (dd)PCR (Figure 21C). To quantify mutations on the DNA level via ddPCR, a HEX-labeled probe was directed against the target site and multiplexed with a FAM-labeled reference probe against an unedited site within the same PCR amplicon. If no mutations were induced at the luciferase target site, the FAM-labeled probe binds to its target sequence with the same efficiency as the HEX-labeled reference probe. In the case of CRISPR-induced mutations at the luciferase target site, the FAM-labeled probe is unable to bind and the FAM signal diminishes compared to the HEX signal. Finally, also *Sa*Cas9 mRNA levels

were quantified by qRT-PCR and revealed a high correlation of *Sa*Cas9 expression and luciferase knock-out (Figure 21D).

3.3. A combinatorial approach to knock-out/knock-down HBV/HDV co- or superinfections

We further translated our TRISPR-based knock-out and knock-down approach to tackle HBV and HDV co- or superinfections. To this end, we first screened for appropriate shRNAs against the HDV RNA genome. Prior to this work, Florian Schmidt (previous Bachelor student) and Florian Lempp (Urban lab, University Hospital Heidelberg) evaluated different shRNAs for their ability to inhibit delta antigen expression and HDV genome replication. In their experimental approach, nine shRNAs against HDV were packaged in rAAV vectors using a crude cell lysate protocol, in which rAAV particles are produced in a small-scale format (one well of a 6-well plate) but not purified from cell debris or other proteins over gradients. Subsequently, Huh7-hNTCP cells were first transduced with the crude lysates containing the shRNA expressing viral vectors and two days later infected with HDV (Supplementary Figure 2A). Western blot analysis and IF stainings revealed a strong decrease of delta protein expression in samples treated with shRNA 3 and 4, and a slight reduction when treated with shRNA 6 to 9, ten days after transduction (Supplementary Figure 2B and C). The inhibitory effect of these shRNAs was also observed for HDV genome levels after RT-PCR quantification (Supplementary Figure 2D). Note that shRNA 3 and 4 share the same sequence and differ only in their length of 21 nt and 19 nt, respectively. Interestingly, only shRNA 3 and 4 targeted the actual ORF of the delta protein, specifically around position 196, which represents the stop codon for the small delta antigen. Due to the high amount of secondary structures that leads to the rod-shaped HDV genome, only the area around the stop codon can be targeted via RNAi. All other shRNAs target HDV either before or after the delta antigen ORF.

3.3.1. Screening of different shRNAs against HDV

In this study, we first recapitulated the initial screen with selected shRNAs and purified rAAV vectors. Furthermore, we added an alternative version of shRNA 3 (named 3ed) and 4 (named 4ed) to the screen, which target the edited tryptophan (UGG) instead of

the stop codon (UAG) and thus should act on the large HDAg. As the small or large HDAgs are preferentially produced in early or late stages of the HDV infection cycle, respectively, we hypothesized that we might be able to differentiate the effect of shRNA 3/4 and 3ed/4ed in an immunization and curation setting.

In the immunization setting, HepG2-hNTCP-HB2.7 cells were first transduced with purified rAAV vectors containing the individual shRNAs and two days later infected with HDV (Figure 22A). Western blot analysis and IF staining six days post-transduction revealed a strong decrease of delta antigen in samples treated with shRNAs 3 and 4 and a slight decrease for samples treated with shRNA 6 to 9 (Figure 22B and C). Accordingly, these experiments recapitulated the results of the previous screen. By contrast, shRNAs 3ed and 4ed showed no effect on HDAg expression. This was expected, as the administration of shRNAs prior to HDV infection immunized the cells already against early stages of infection. Accordingly, shRNAs 3ed and 4ed are unable to act on early stages of infection, as the stop codon had not been edited to tryptophan at that time and thus HDV did not yet present a target for these shRNAs. The missing large HDAg in the Western blot (Figure 22B) throughout all samples including controls confirmed that HDV had not yet produced the large delta antigen within the indicated time frame.

In the curation setting, HepG2-hNTCP-HB2.7 cells were first infected with HDV and three days later transduced with the rAAV vectors containing the shRNAs (Figure 22D). In this setting, it remained difficult to observe any effect of the shRNAs on delta antigen expression levels in cells that were infected first, since large amounts of delta antigen were already expressed in the three days prior to shRNA transduction. This was apparent from the lack of a reduction in HDAg levels in Western blots of cells treated with the different shRNAs (Figure 22E). Thus, we included a reinfection step, in which the supernatant of day 7 to 10 was used to reinfect Huh7-hNTCP cells. The infected HepG2-hNTCP-HB2.7 cells harbored stably integrated hepatitis B surface antigens that are required by HDV to form infectious particles. If the transduced shRNAs would indeed reduce delta antigens or HDV genomes, fewer amounts of HDV RNP complexes could be formed and released in the supernatant as infectious progeny HDV. Indeed, the reinfection experiment was able to reveal the effect of shRNAs on the HDV RNA, when the quantity of HDAg positive-cells was counted after IF staining and automated microscopy (Figure 22F). Importantly, whereas most shRNAs reduced the amount of infectious HDV particles, shRNA 4 and especially shRNA 3 increased secreted HDV particles repeatedly in independent experiments. By contrast, shRNA 3ed and 4ed that

differ only in a single nucleotide to their shRNA 3 and 4 counterparts, efficiently reduce the amount of infectious HDV particles in the curation setting, as they act on the large delta antigen.

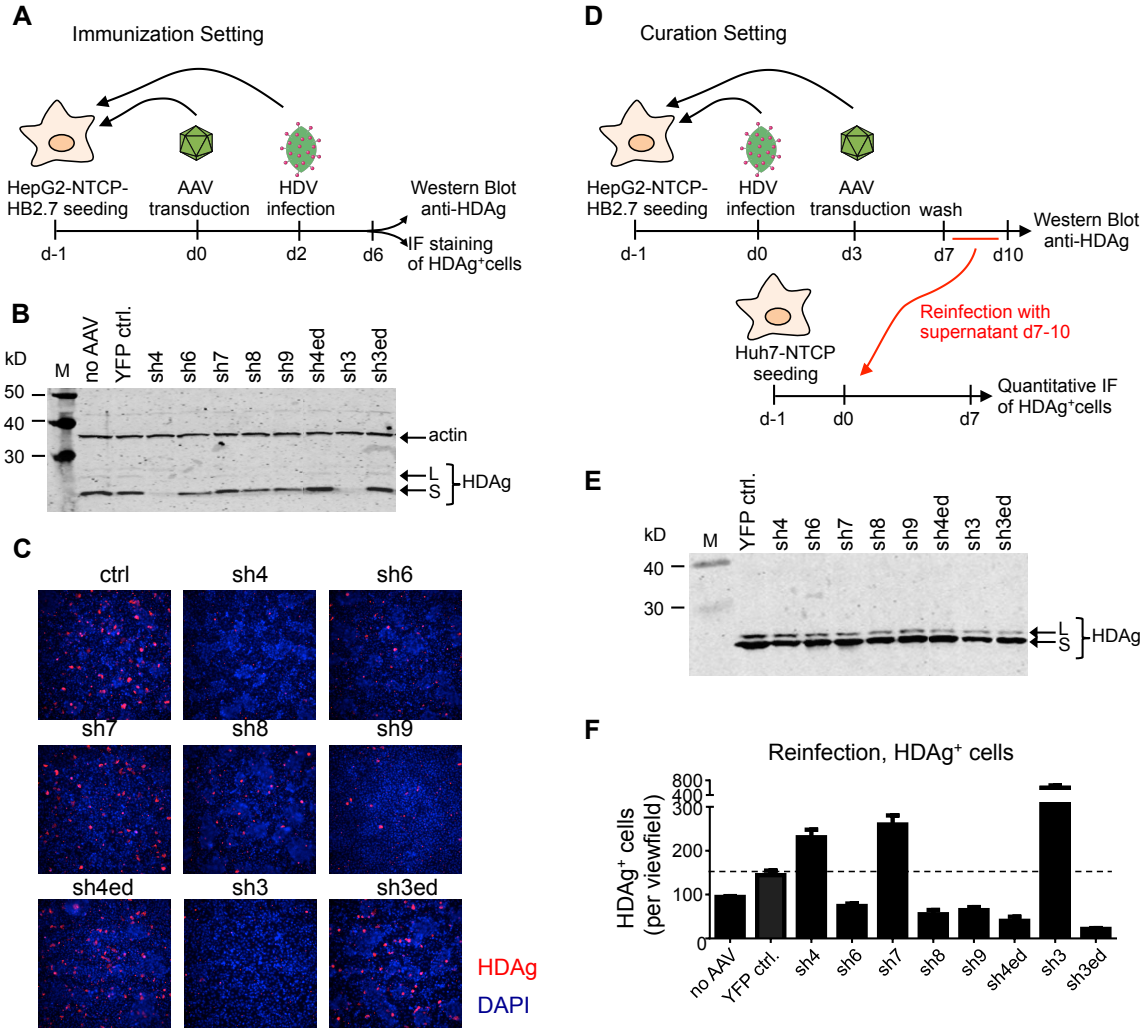

Figure 22. Screening of anti-HDV shRNAs in an immunization and curation setting.

A) Experimental workflow in the immunization setting: HepG2-hNTCP-HB2.7 cells were first transduced with AAVs of variant 9A2 expressing different U6 promoter-driven shRNAs against HDV using an MOI of 10^5 and two days later infected with HDV. Six days post-transduction, cells were analyzed via Western blotting **(B)** and IF staining **(C)** against HDAg. **D)** Experimental workflow for the curation setting: HepG2-hNTCP-HB2.7 cells were first infected with HDV and three days later transduced with AAV vectors expressing the different shRNAs against HDV. The supernatants from day 7 to 10 harboring newly produced HDV particles were used to reinfect Huh7-hNTCP cells. **E)** Western blot of primary infected HepG2-hNTCP-HB2.7 cells ten days after HDV infection **F)** Quantification of IF stainings via automated microscopy after reinfection of Huh7-hNTCP cells. Error bars represent standard deviation of three independent experiments. Results were obtained jointly with Florian Lempp (Urban lab).

3.3.2. The combination of RNAi and CRISPR against HBV/HDV infections

Next, we applied the shRNA 3ed in a combinatorial CRISPR/Cas9 and RNAi approach to tackle HBV and HDV co- or superinfections. To this end, we applied two shRNAs, one directed against HDV (shRNA 3ed) and the other directed against HBV (shHBV7), and expressed them by the U6 and H1 promoter, respectively (Figure 23A). Furthermore, we targeted the hepatitis B surface antigen using the sgRNA 6 from our previous screen (Figure 16) and expressed it under the 7SK promoter. To test the effect of the TRISPR vectors on HBV and HDV, a similar curation approach was applied as before (Figure 22D). HepG2-hNTCP-HB2.7 cells (with stably integrated HBsAg) were infected with HDV and three days later transduced with rAAVLK03 vectors that expressed the different TRISPR combinations. The supernatant of day 11 to 13 was collected to measure the amounts of secreted HBsAg and to reinfect Huh7-hNTCP cells.

As expected, HepG2-hNTCP-HB2.7 cells that were transduced with the sgRNA against the surface antigen (orange dots) and/or with the shRNA against HBx antigen (violet and blue dots) showed a reduction in secreted HBsAg (Figure 23B). The strong shHBV7 reduced secreted HBsAg levels to undetectable limits even by expression from the weak H1 promoter. Furthermore, all TRISPR vectors mediated a reduction in HDAg-positive cells compared to the control (black dots) in reinfection experiments (Figure 23C). Whereas the sgRNA against HBsAg and the shRNA against HDV alone or in combination (orange and green dots) pushed the amount of reinfected cells to 50% or 25%, respectively, the co-expression of shRNA against HBV decreased reinfected cells to undetectable levels (violet and blue dots).

Furthermore, we applied a strategy in which we multiplexed two sgRNAs against HBV and one shRNA against HDV (Figure 23D). In order to target the HBV surface antigen via CRISPR/Cas9, we selected sgRNA 6 and sgRNA 3 from our previous screen (Figure 16). There, sgRNA 6 had efficiently reduced HBsAg levels, whereas sgRNA 3 had elevated the amount of secreted HBsAg. Nevertheless, we hypothesized non-functional HBsAg had been secreted, as sgRNA 3 targeted the large HBsAg that is required for viral entry. HBsAg measurements in this experiment recapitulated previous findings, such that sgRNA 6 reduced HBsAg levels and sgRNA 3 increased amounts of secreted HBsAg (Figure 23E). Vectors that expressed both sgRNAs (ctrl-gS3-gS6 and shHD-gS3-gS6) showed a reduction in HBsAg levels, likely due to the excision of the sequence between both cut sites that resulted in the loss of small and large HBsAg. Reinfection experiments confirmed the hypothesis that sgRNA 3 led to non-functional HBV surface

antigens, as expression of sgRNA 3 alone (violet dots) resulted in the reduction of HDV-reinfected cells (Figure 23F).

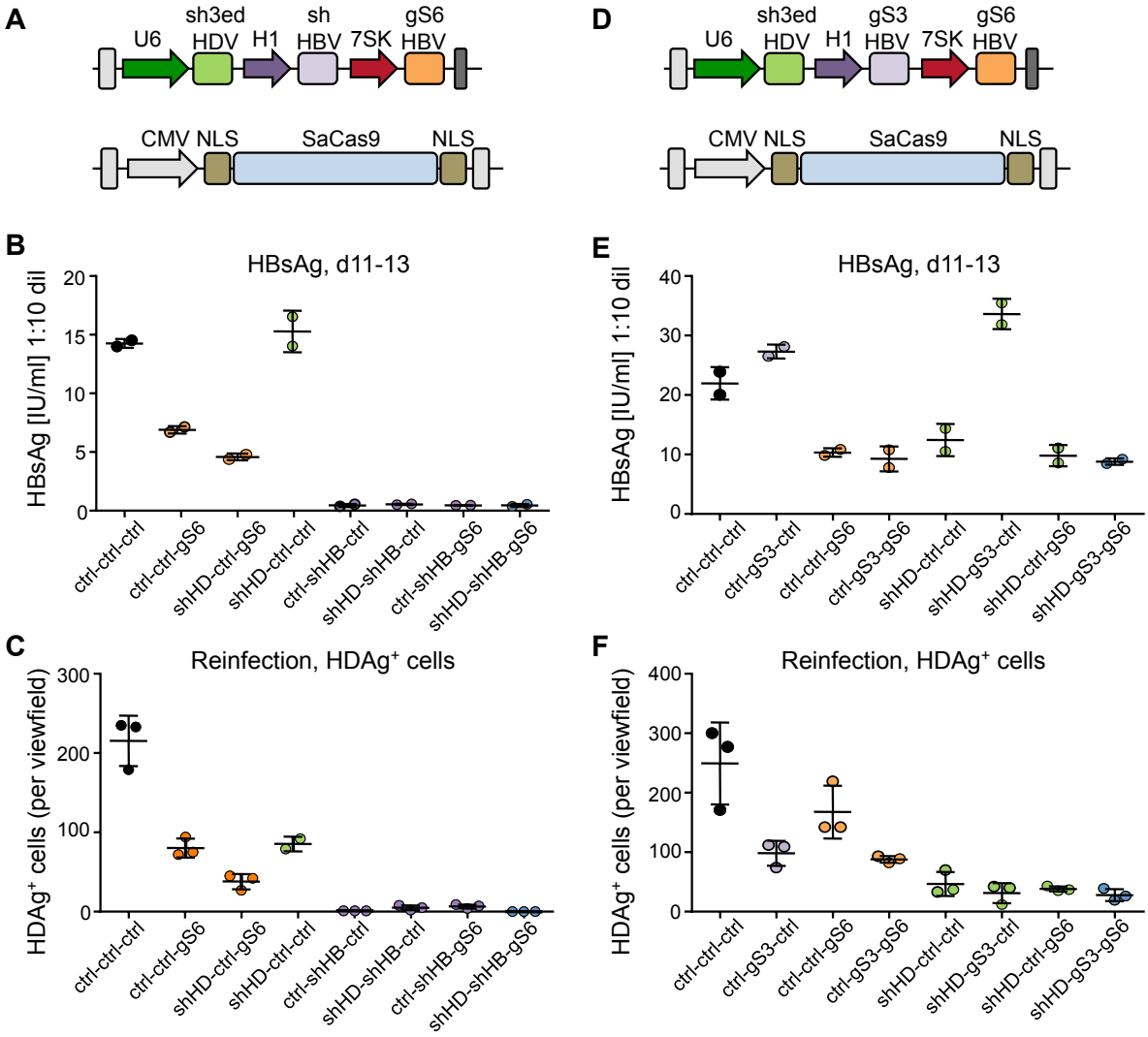

Figure 23. A combinatorial CRISPR/RNAi approach to tackle HBV/HDV co-infection.

A) Construct design of TRISPR vectors to tackle HBV/HDV infections in the curation setting. Note that sgRNA6 was directed against the integrated HBsAg locus in HepG2-hNTCP-HB2.7. Also constructs were designed that substitute each small RNA position with non-targeting sgRNA or shRNA controls resulting in eight different TRISPR vector. **B)** HBsAg levels were measured in the supernatants of day 11 to 13 of HDV-infected HepG2-hNTCP-HB2.7 cells. **C)** $HDAg^+$ cells were quantified after reinfection of Huh7-hNTCP cells with supernatants of day 11 to 13 by IF staining and automated microscopy. **D)** The same experimental workflow was applied to test TRISPR vectors that express the sgRNA 3 against HBsAg by the H1 promoter. **E)** HBsAg measurements of supernatant from HDV-infected HepG2-hNTCP-HB2.7 cells and **F)** $HDAg^+$ cells after reinfection of Huh7-hNTCP cells with supernatants of day 11 to 13 treated with the indicated rAAV vectors from D. Each data point represents an independent experiment. Results were obtained jointly with Florian Lempp (Urban lab).

Note that sgRNA 3 outperformed sgRNA 6 in reducing the amount of infectious HDV particles, even though sgRNA3 was expressed by the weak H1 promoter. The direct targeting of HDV by shRNA (green dots) and the combination of RNAi and CRISPR/Cas9 against HDV and HBV (blue dots), respectively, mediated the strongest reduction of HDV reinfected cells.

3.4. DMSO enhances rAAV vector transduction and expression efficiencies

During our highly collaborative work on HBV within the SFB TRR179, Professor Michael Nassal and his lab (University Hospital Freiburg) noticed a supportive effect of DMSO on rAAV transduction efficiencies. As described in detail in section 2.2.4.4, HBV and HDV infections are generally performed with an addition of 2.5% DMSO in the infection media to increase the infectivity and to restrain the cells from proliferating, in order to keep them in culture for the long experimental periods [17]. To our surprise, rAAV transductions after HBV or HDV infections resulted in much higher vector expression rates compared to transductions prior to infections. Eventually, we were able to attribute the high rAAV vector transduction rates to the presence of DMSO in the cell media after HBV or HDV infections. Thus, in the following, we systematically investigated DMSO as a method to enhance rAAV transduction efficiencies and boost the expression of transgenes, such as the components of the CRISPR/Cas9 technology.

3.4.1. DMSO enhances rAAV transduction in a high-throughput reporter assay

First, we evaluated the rAAV transduction efficiency of a CMV promoter-driven YFP reporter in the presence or absence of 2.5% DMSO (Figure 24A). To this end, we packaged the reporter in 23 rAAV variants, including 12 wt capsids and 11 peptide insertion variants that we previously described in Börner *et al*. [227], and transduced various cell lines at the MOI of 10^5 and 10^3 (1:100 dilution). Three days later, cells were analyzed by quantitative microscopy using an automated protocol.

In general, we observed that the promoting effect of DMSO strongly depended on the rAAV variant and cell line. The effect of DMSO on transduction in hepatoma cell lines was less pronounced compared to its influence on neuroblasts. A beneficial effect of DMSO ranged from a 3-fold (capsid variants LK03, DJ) to 10-fold (7A6, 7A2, 9A2)

increase in transduction rates in HepG2 cells (Figure 24B), and a 2-fold (2wt, 7A2, DJ) to 5-fold (1wt, LK03, 7P2, 9A2) increase in Hepa16 cells (Figure 24D). In contrast, transduction in Huh7 cells was barely affected by DMSO (Figure 24C).

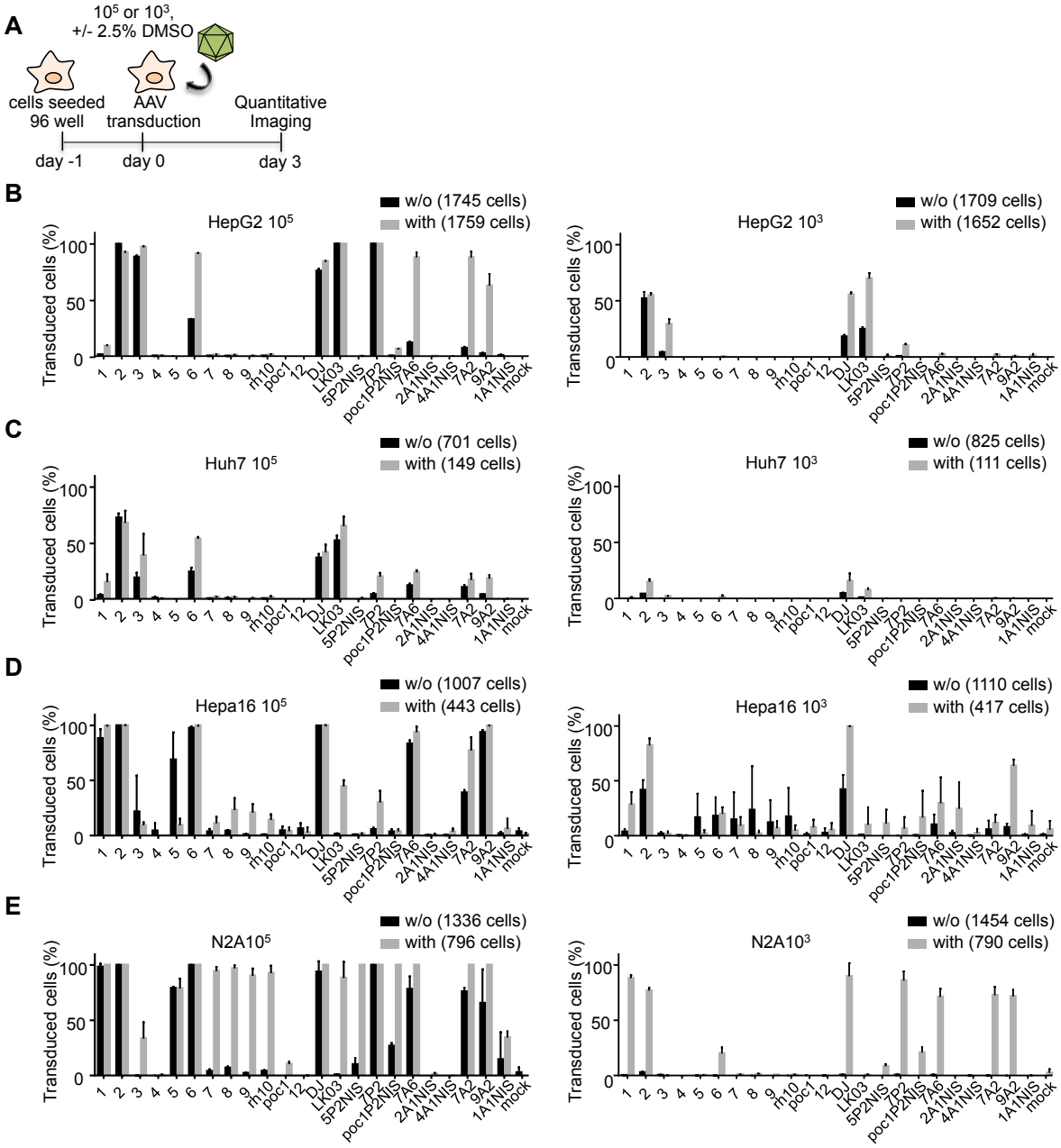

Figure 24. DMSO enhances transduction depending on rAAV variant and cell line.

A) Experimental approach: HepG2 **(B)**, Huh7 **(C)**, Hepa16 **(D)** and N2A **(E)** cells were seeded in 96-well plates and transduced on the following day with 23 different AAV variants harboring a CMV-YFP reporter at an MOI of 10^5 (left) or 10^3 (right) without (black) or with (gray) 2.5% DMSO in the transduction media. Three days later, cells were fixed and the percentage of transduced/YFP-positive cells was quantified via automated microscopy. Numbers in brackets represent the average amount of cells per microscopy picture that were analyzed. Error bars represent standard deviations of three independent experiments. In the mock conditions, no AAVs were transduced.

The most dramatic effects of DMSO were seen in N2A cells, in which transduction and expression rates of several rAAV variants that barely transduced these cells were boosted towards upper detection limits by the addition of DMSO (Figure 24E). In fact, all rAAV variants showed an increase in transduction and expression rates in at least one cell line, except for rAAV4, rAAV5, rAAVpo1, rAAV12, and rAAV1A1NIS that remained unaffected. Except for rAAV5 in Hepa16 cells, we did not observe a detrimental effect of DMSO on transduction efficiencies.

The experiments in Figure 24 were also analyzed for the extent of transgene expression, which was quantified by the YFP intensity of successfully transduced cells (Supplementary Figure 3). In most cases, higher transduction efficiencies also resulted in higher transgene expression levels. Figure 25 gives an impression of transduction and expression differences of selected rAAV variants with or without DMSO treatment in N2A cells.

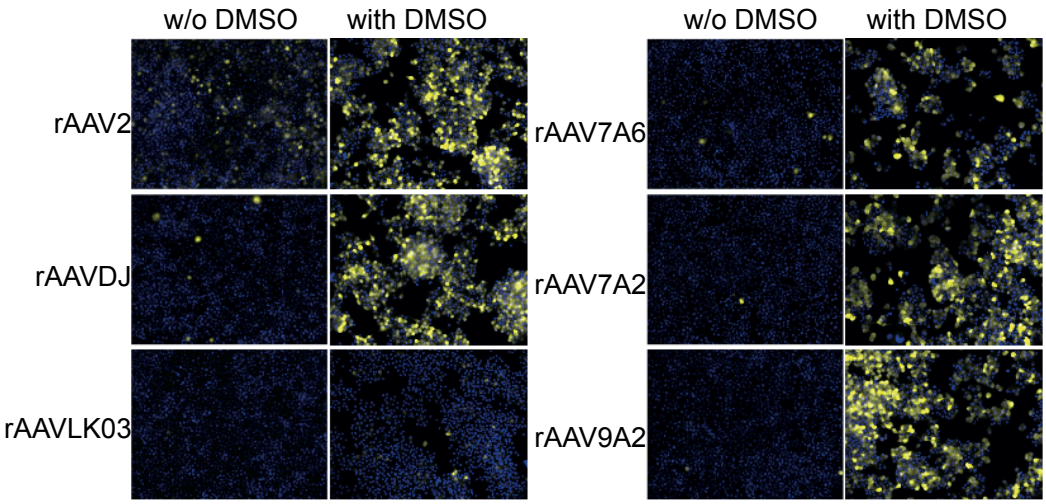

Figure 25. Images of transduced N2A cells with and without DMSO treatment.

Representative microscopy images of N2A cells transduced with six selected rAAV variants at the MOI of 10^3 with or without (w/o) DMSO that were used for the automated imaging pipeline in Figure 24. Cell nuclei were previously stained with Hoechst (blue) and subsequently YFP signals (yellow) were acquired.

We also observed an effect of DMSO on the rate of cell proliferation, which was halted or strongly reduced depending on the cell line as indicated by the cell numbers in brackets for each condition (Figure 24). Whereas cell numbers seemed unaffected for HepG2 cells, Hepa16 and N2A cells were slightly inhibited and Huh7 cells were strongly inhibited in cell proliferation. Cytotoxicity was not observed by the addition of DMSO to the cell media (data from Julia Miller from Nassal lab, not shown).

3.4.2. DMSO-mediated rAAV transduction remains receptor-dependent

The data above suggested that transduction efficiencies could be enhanced only if the rAAV variant transduced a respective cell line also in the absence of DMSO, even if only to minor extents. Thus, we hypothesized that the DMSO-mediated increase of rAAV vector uptake was receptor-mediated and, in the case of AAV2, dependent on HSPG receptor binding. To test this hypothesis, we studied an rAAV2 mutant (AAV2mut) variant carrying mutations on position R484E and R585E [230], which disturbed HSPG receptor binding. We packaged the CMV-YFP reporter either into AAV2mut or the conventional AAV2 capsid and transduced N2A and Huh7 cells in the absence or presence of 2.5% DMSO (Figure 26A and B).

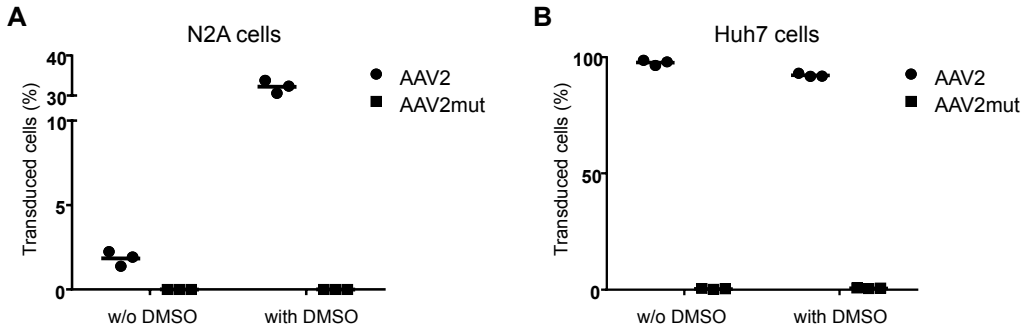

Figure 26. DMSO-mediated rAAV2 transduction is dependent on HSPG binding.

A) N2A and **B)** Huh7 cells were transduced with a CMV-YFP reporter using an MOI of 10^3 and 10^5, respectively, that was either packaged into the AAV2 capsid (circular dots) or AAV2mut (squared dots) without (w/o) or with 2.5% DMSO in the transduction media. Three days after transduction, the percentages of transduced cells were quantified via automated microscopy. Each data point represents an independent experiment.

While transduction rates increased for the rAAV2 vector in N2A cells by the addition of DMSO, transduction was completely inhibited for the rAAV2mut variant with or without DMSO (Figure 26A). Similar results were obtained for transductions in Huh7 cells, in which rAAV2 vectors maintained 100% transduction rates in the absence or presence of DMSO, whereas transduction of AAV2mut was completely abolished and not restored by the addition of DMSO (Figure 26B). Accordingly, we could confirm that an increase of viral uptake is an HSPG-receptor-mediated process.

3.4.3. Comparison of alternative methods to increase rAAV transduction

Next, we compared this new method to other chemical compounds, such as Doxorubicin [307], a topoisomerase and proteasome inhibitor, and Rapamycin, an inducer of autophagy [266], that have previously been used to enhance rAAV vector transduction rates (Figure 27).

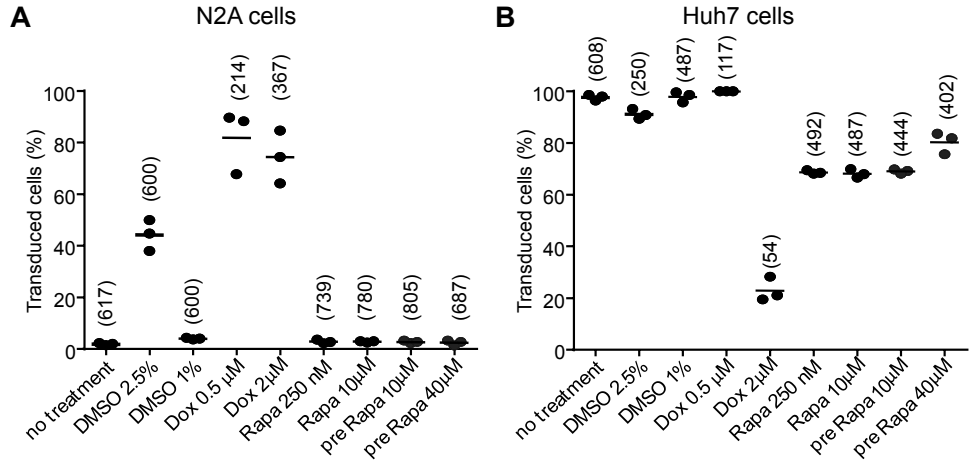

Figure 27. Comparison of different methods to increase rAAV transduction.

A) N2A and **B)** Huh7 cells were transduced with AAV2-CMV-YFP using an MOI of 10^3 and 10^5, respectively, and treated with either no additional chemical (no treatment), 2.5% or 1% DMSO, 0.5 µM or 2 µM Doxorubicin (Dox), 250 nM or 10 µM Rapamycin (Rapa) or pretreated (pre) for 1 h with 10 µM or 40 µM Rapamycin. Note that cells treated with Doxorubicin needed to be washed twice with PBS and supplemented with fresh media not later than 12 hours after addition of the chemical compound, due to strong cytotoxic effects of the compound. Three days later, percentages of transduced cells were quantified via automated microscopy. Numbers in brackets represent the average amount of cells per microscopy picture. Each data point represents an independent experiment.

Consistent with our previous results, transduction efficiencies were enhanced in N2A cells by 2.5% DMSO, whereas the addition of only 1% DMSO was insufficient to enhance transduction rates (Figure 27A). The application of either 0.5 or 2 µM Doxorubicin resulted in even higher transduction rates, but was associated with a high rate of cell death as indicated with the numbers in brackets that represent the average amount of cells within an image. In contrast to published results in Hosel *et al.* (2017) [266], any treatment with Rapamycin consistently failed to enhance transduction rates in our experiments. Similar results were obtained in Huh7 cells, although the experiments were oversaturated with rAAV2 vectors and therefore need to be repeated with lower MOIs (Figure 27B). Also consistent with our previous results, addition of DMSO did not affect transduction rates but strongly inhibited Huh7 cells from proliferating. By contrast, the

addition of Doxorubicin resulted in major cell death, to an extent that only 54 from 600 cells survived per microscopy picture on average. Moreover, the addition of Rapamycin resulted in decreasing numbers of transduced cells in repeated experiments.

3.4.4. DMSO enhances rAAV/CRISPR delivery and gene editing

Finally, we applied the DMSO method to increase transduction rates of rAAV vectors that expressed the CRISPR/Cas9 components. We hypothesized that an increased expression of CRISPR/Cas9 would lead to an enhanced targeted knock-out efficiency. To this end, we selected rAAV9A2 and rAAV5, which showed either increased transduction efficiencies or remained unaffected by DMSO in our previous reporter screen in N2A cells, respectively (Figure 24E). *Sa*Cas9 and an sgRNA targeting the *mecp2* locus were packaged in these rAAV vectors N2A cells were transduced in the presence (dark blue bars) or absence (light blue bars) of 2.5 % DMSO in the transduction media (Figure 28). The addition of DMSO resulted in a 4- and 20-fold increase in knock-out efficiencies by the CRISPR/Cas9 system packaged in rAAV9A2 in T7 endonuclease assay and TIDE analysis, respectively (Figure 28A and B). Note that TIDE analyses provide a more reliable and quantitative method for the estimation of mutation rates [308], while T7 endonuclease assays offer a visual guidance through respective bands on an agarose gel. Although transduction by rAAV5 remained unaffected by DMSO in N2A cells in our previous screen, we observed a slight DMSO-mediated increase in mutations rates via T7 assay and TIDE analysis.

Furthermore, we investigated whether the DMSO-mediated increase in knock-out efficiencies originated from elevated viral uptake, which would be reflected in elevated amounts of viral copy numbers per cells (per diploid genome), or from an increased expression from the viral vectors. To this end, we extracted DNA and RNA from N2A cells that were treated with the same experimental design as previously and quantified viral copy numbers per cell via ddPCR and expression rates via qRT-PCR. Whereas N2A cells that were transduced with rAAV9A2 vectors harbored about 100 viral genomes per cell in the absence of DMSO, the addition of DMSO increased the amount about 4.5-fold (Figure 28C). By contrast, rAAV5 generally showed a higher transduction rate, which was not affected by the presence or absence of DMSO. Surprisingly, the addition of DMSO induced an about 350-fold higher expression from the rAAV9A2 vector (Figure 28D. The strong differences in expression could not be attributed to the 4.5-fold increase in viral uptake alone, but needed to arise from an additional DMSO-mediated effect on

viral expression. Accordingly, although viral copy numbers are not elevated in case of rAAV5, expression levels increased 15-fold by the addition of DMSO. Note that expression levels of the housekeeper were not affected by DMSO.

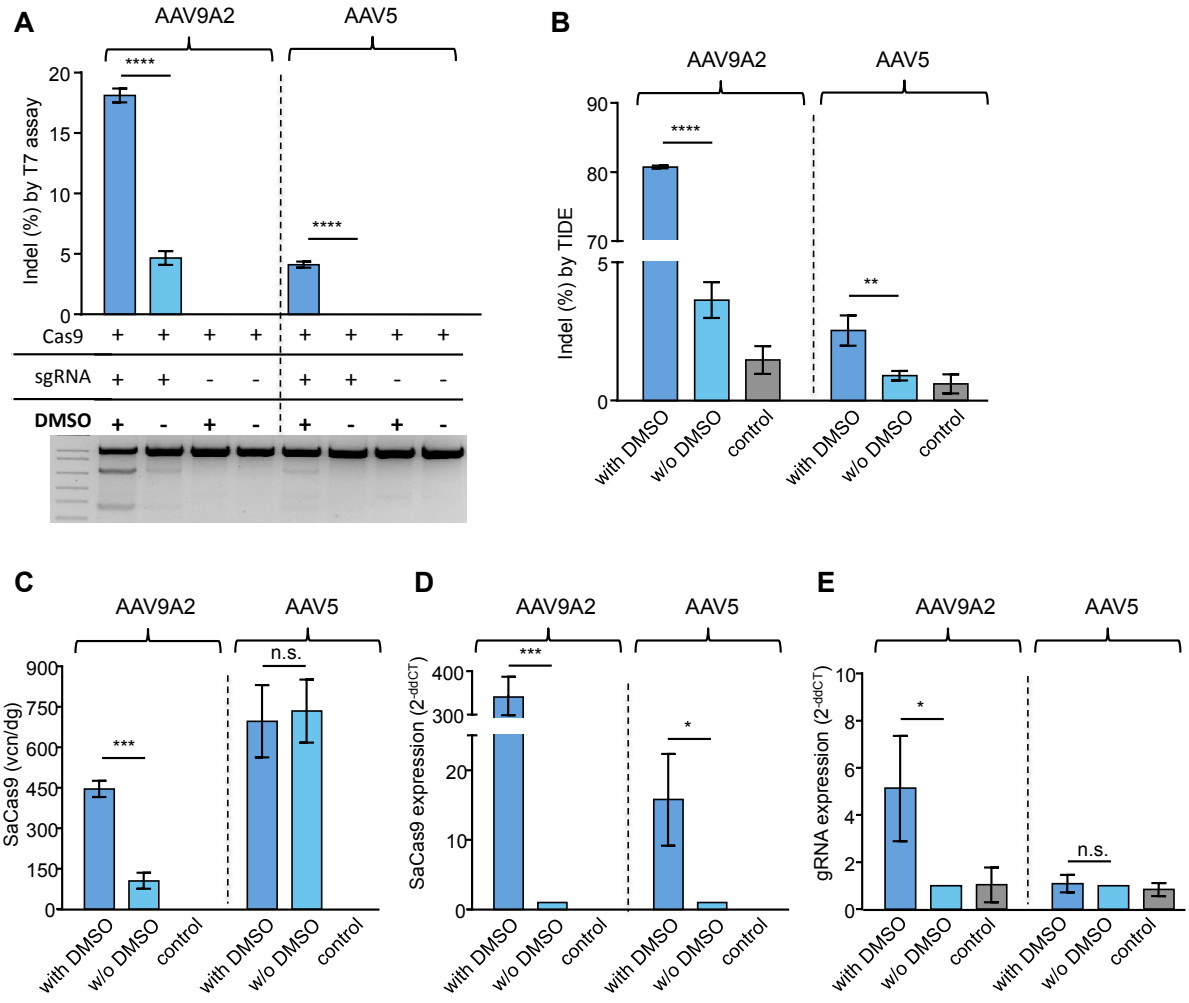

Figure 28. DMSO enhances rAAV/CRISPR transduction and gene editing rates.

N2A cells were transduced with either rAAV9A2 or rAAV5 that harbor *Sa*Cas9 and a sgRNA against the *mecP2* locus on two separate vectors using an MOI of 10^5. The transduction media contained either no (light blue, w/o) or 2.5% (dark blue) DMSO. Three days later, cells were harvested and indel frequencies were quantified via T7 endonuclease assay **(A)** or TIDE analysis **(B).** Controls in A) and B) were transduced with Cas9 but no sgRNA. **C)** DNA was extracted and vector copy numbers per diploid genome (vcn/dg) were quantified via ddPCR by applying a primer/probe set against the *Sa*Cas9 transgene and against the *Rpp30* house keeper **D)** *Sa*Cas9 and **E**) sgRNA expression were quantified via RT-PCR using using a primer/probe set against the cDNA of *Sa*Cas9 or a SYBR-based approach with a primer set against the small sgRNA cDNA, respectively. In both cases, GAPDH expression was measured as reference and expression levels were normalized to the corresponding without DMSO condition. Controls in C) to E) were transduced with a YFP reporter instead of Cas9 and sgRNA. Error bars represent standard deviations of three independent experiments, with and without DMSO. Samples were compared by unpaired t-tests. n.s.=not significant, *<.05, **<.01, ***<.001, ****<.0001

We also investigated the expression of sgRNA in presence or absence of DMSO (Figure 28E). However, due to strong secondary structures, it remained difficult to detect sgRNAs in a specific manner over background levels of controls. Thus, we were only able to detect high quantities of sgRNAs as in the case of rAAV9A2 expression in the presence of DMSO.

3.5. Self-complementary and self-inactivating rAAV-splitCas9 vectors

The use of chemical compounds to boost rAAV transduction is mainly restricted to cell culture, as their delivery *in vivo* in sufficient amounts is hardly possible without detrimental side effects. In order to increase transduction and expression efficiencies, we and many others use superior dsAAV vectors, which yield accelerated and enhanced transgene expression through an engineered double-stranded genome and are widely applied in *in vivo* experiments. In comparison with the ssAAV vector, the major disadvantage of dsAAV vector is its restricted transgenes packaging capacity of up to 2.4 kb. To this end, this work utilized a splitCas9 system, which was previously invented during my M.Sc. thesis in the lab of Prof. Barbara Di Ventura and Prof. Roland Eils, that took advantage of the reduced sizes of each split*Sa*Cas9 half and thus enabled the packaging as two independent dsAAV vectors.

Briefly, the previously M.Sc. work described the design and construction of a small split*Sa*Cas9 library consisting of three split sites in combination with the two *trans*-splicing inteins (*Npu*DnaE and gp41-1), which has been evaluated for its capability to induce targeted mutagenesis in plasmid transfection experiments. In the same work, it has been shown that each split*Sa*Cas9 half could be packaged as separate dsAAV vector and it has also been suggested that the expression by the superior dsAAV could improve *Sa*Cas9-mediated mutagenesis rates. However, a quantitative comparison between the dsAAV/split*Sa*Cas9 system to conventional ssAAV/wt*Sa*Cas9 with purified and titrated rAAV vectors has been missing. For the presented work in this doctoral thesis, we selected the gp41-1-bearing split*Sa*Cas9 version 3 and experimentally evaluated whether the enhanced expression of the split*Sa*Cas9 system by dsAAV vectors indeed translates into enhanced mutagenesis rates that exceed the efficiency of conventional ssAAV/wtSaCas9 vectors.

3.5.1. Expression rates determine the efficiency of the split*Sa*Cas9 system

During this doctoral work, we wondered why in my previous work, efficiencies of the split*Sa*Cas9 system compared to full-length *Sa*Cas9 had varied depending on the target cell line and promoter. We hypothesized that the efficiency of the split*Sa*Cas9 system is dependent on the amount of its expression, as a high abundance increases the chance of the split halves to meet in the cell and thus perform the splicing reaction. To test this hypothesis, we transfected the full-length (fl-) and split (spl-) *Sa*Cas9 system in N2A cells and expressed the systems from either the mCMV, mMecp2 or mTK promoter (Figure 29A). RT-PCR analysis of either the N- or the C-terminus of the full-length or split *Sa*Cas9 system by the mCMV, mMecp2 and mTK promoter revealed a strong, moderate and weak transcription, respectively (Figure 29B). Indeed, while knock-out efficiencies of fl-*Sa*Cas9 decreased slightly with weaker promoters, the split*Sa*Cas9 system was strongly reduced in its efficiency (Figure 29C).

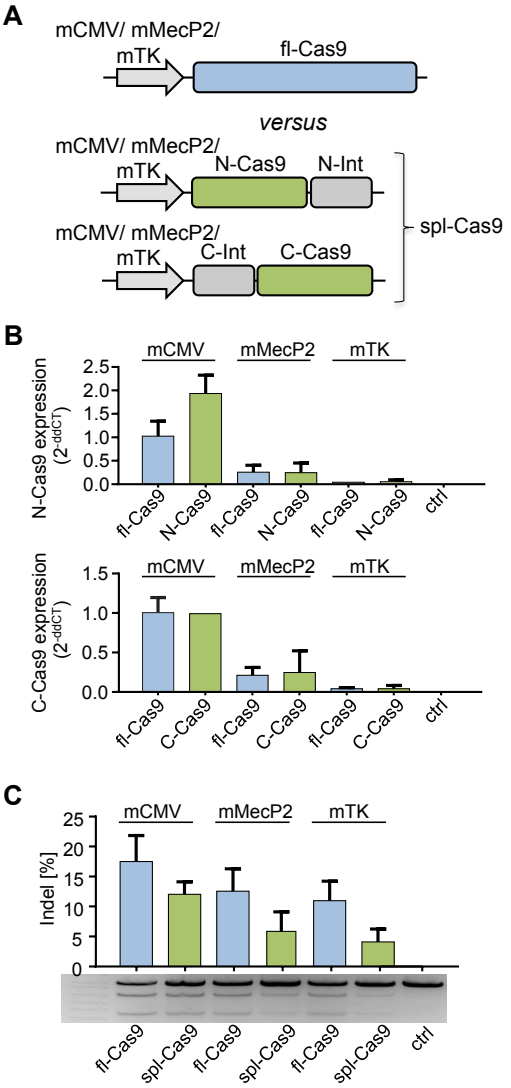

Figure 29. Split*Sa*Cas9 mutagenesis rates are determined by expression levels.

A) Full-length Cas9 (blue) and split*Sa*Cas9 (green, Gp41-1-split 3) are expressed by the three minimal promoters, mCMV, mMecP2 or mTK. **B)** and **C)** N2A cells were transfected with either 150 ng full-length *Sa*Cas9 or 75 ng of each split*Sa*Cas9 half (encoded on separate plasmids) and 50 ng plasmid-encoded sgRNA against the *mecp2* locus. Three days later cells were harvested to perform further analysis. **B)** Quantification of RNA expression levels of N-terminal (upper panel) and C-terminal (lower panel) *Sa*Cas9 expressed by either mCMV, mMecP2 or mTK promoter. Expression levels were normalized to the expression of GAPDH house keeper and mCMV promoter-driven fl-*Sa*Cas9. Three independent experiments were performed. **C)** Quantification of T7 assays from three independent experiments and representative agarose gel. ctrl = Transfection of mCMV-*Sa*Cas9 without sgRNA. Error bars represent standard deviations of the mean.

3.5.2. Split*Sa*Cas9 packaged in dsAAV outperforms the conventional system

Next, we evaluated knock-out efficiencies of the split*Sa*Cas9 system when packaged in dsAAV vectors (dsAAV-splitCas9) compared to the inherent full-length *Sa*Cas9 in ssAAV (ssAAV-flCas9). First, we (jointly with Daniel Heid in his B.Sc. thesis) investigated the different expression rates by ss *versus* dsAAV vectors using a CMV-mCherry reporter that we packaged in both vector types of capsid variant 9A2 (Supplementary Figure 4). Different cell lines were transduced with the reporters using MOIs ranging from 10^3 to 10^6 and transduction rates were analyzed either 1.5, 2.5 or 4 days after transduction via flow cytometry. While HEK293T cells showed no differences in expression by ss *versus* dsAAV, Huh7 and HepG2 showed a moderate increase of about 3-fold when the dsAAV vectors were applied, and N2A cells showed a strong increase in transduction of about 10-fold. Since N2A cells showed the highest differences in transduction between ss and dsAAV vectors, we used this cell line in our following experiments.

Next, we packaged full-length *Sa*Cas9 in ssAAV and split*Sa*Cas9 into two separate dsAAV vectors (Figure 30A). We provided an sgRNA targeting the *mecp2* locus by a separate dsAAV vector. N2A cells and primary myoblasts were transduced with different MOIs ranging from $5x10^4$ to 10^6 and $5x10^3$ to $5x10^4$, respectively, and were harvested either 2 or 5 days post-transduction for quantification of mutation rates at the *mecp2* locus by T7 endonuclease assay and TIDE analysis (Figure 30B and C). Indeed, we observed superior knock-out efficiencies for the dsAAV-split*Sa*Cas9 system (ds-spl, green bars) compared to ssAAV-full-length *Sa*Cas9 (ss-fl, blue bars) at all MOIs and time points in N2A cells and primary myoblasts. In N2A cells, knock-out rates above 10 % were only observed in the case of the dsAAV-split*Sa*Cas9 system even after an incubation of 5 days (Figure 30B). Only the dsAAV-split*Sa*Cas9 system applied at the highest MOI of 10^6 yielded a decent knock-out rate of 30%. These results matched our findings in the previous reporter experiment (Supplementary Figure 4), which confirmed that efficient transduction of N2A cells is only possible with dsAAV vectors and very high MOIs. Note that we also tested the splitCas9 system packaged in ssAAV (ss-spl) in N2A cells, which failed to induce any mutations at all MOIs and time points in the T7 assay (Figure 30B, left panel). Also primary myoblasts showed enhanced knock-out efficiencies when the dsAAV-split*Sa*Cas9 system was applied; however, with increasing MOIs and prolonged time points, differences between the systems became less pronounced (Figure 30C).

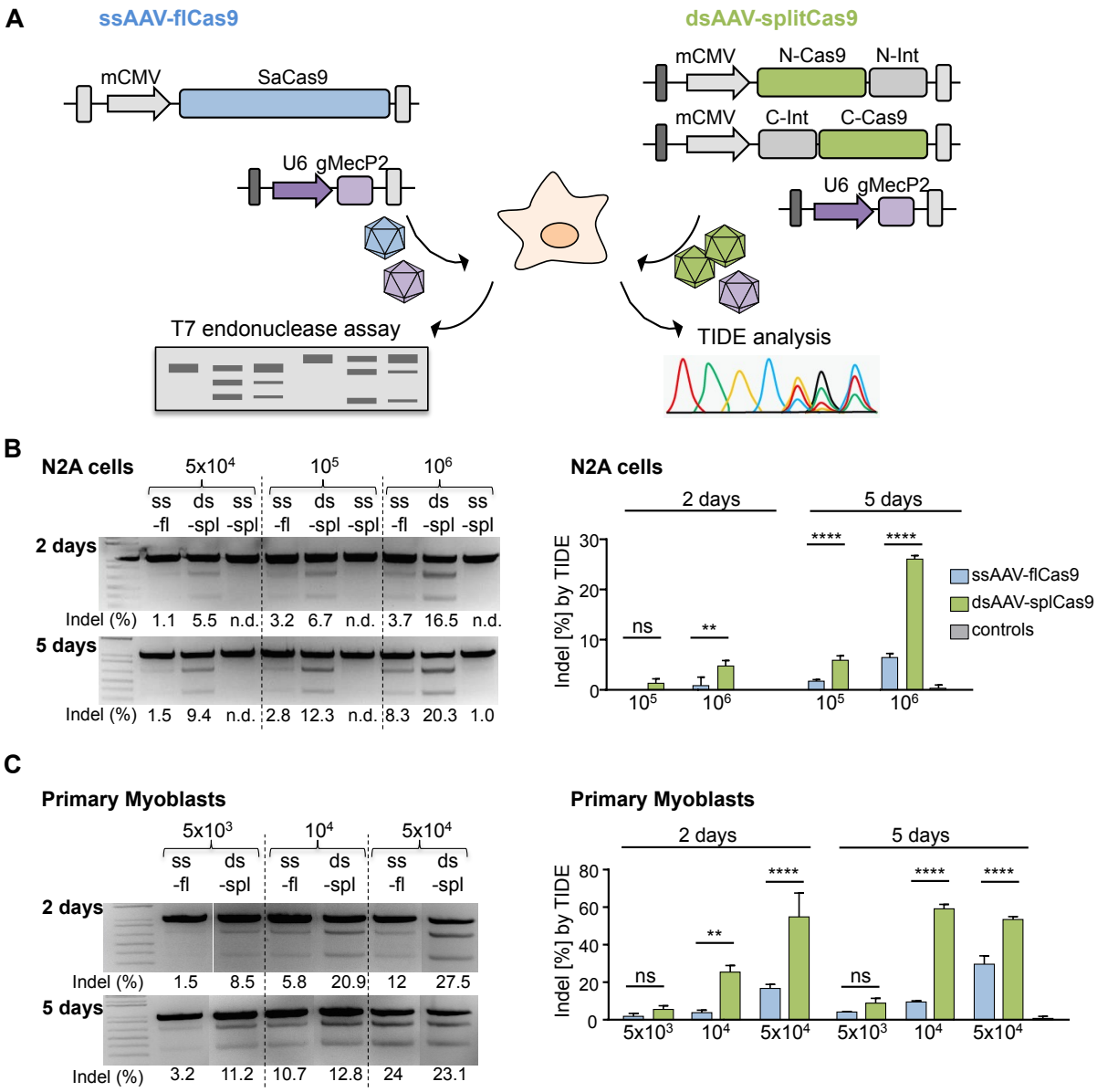

Figure 30. Enhanced gene editing rates by the dsAAV/split*Sa*Cas9 system.

A) Whereas the fl-*Sa*Cas9 (blue) is only compatible with ssAAV vectors (up to 5 kb), the reduced size of each split Cas9 half (green) allows its packaging in two individual dsAAV vectors (up to 2.2 kb). To investigate whether the accelerated and increased expression by dsAAVs can enhance knock-out efficiencies of the split Cas9 system even beyond the knock-out efficiencies of fl-*Sa*Cas9, the endogenous *mecp2* locus was targeted in N2A cells and in primary mice myoblasts**.** **(B)** N2A cells and **C)** myoblasts were transduced with the ssAAV-fl*Sa*Cas9 or dsAAV-splitCas9 using rAAV9A2 and a mosaic mixture of rAAV1 and rAAV2 and an MOI of 10^5 and 10^6 or $5x10^3$, 10^4, and $5x10^4$, respectively. Two and five days later cells were harvested for T7 endonuclease assay (left panel) and TIDE sequencing (right panel). Error bars indicate standard deviation of the mean of n=4 and n=3 experiments in N2A cells and primary myoblasts, respetively. Groups were compared by ANOVA and Bonferroni´s post-hoc test, n.s.=not significant, **<.01, ****<.0001

3.5.3. Split and self-inactivating rAAV-CRISPR systems

Furthermore, we combined the split*Sa*Cas9 system with a self-inactivating (SIN) approach, which was previously invented by Julia Fakhiri from our lab. In her PhD thesis [294], Julia screened various sgRNAs against the *Sa*Cas9 transgene itself and showed in various vector combinations that the CRISPR/Cas9 system is able to self-inactivate after knock-out of a luciferase reporter on-target. Here, we applied this approach to the dsAAV-split*Sa*Cas9 system in order to restrict its elevated *Sa*Cas9 expression after knock-out of an endogenous on-target and to prevent possible off-target effects by the lingering Cas9 endonuclease. To this end, the following systems were compared with one another using rAAV9A2 vectors (Figure 31A): 1.) The full-length *Sa*Cas9 was packaged as a ssAAV vector. The sgRNA that either targeted the endogenous *mecp2* locus or the integrated HBsAg locus (depending on target cell line) and an sgRNA against the N-terminal *Sa*Cas9 (SIN) were packaged in as additional dsAAV vector. The strong U6 and the weaker H1 promoter were used for the expression of the sgRNAs directed against the on-target locus and the *Sa*Cas9 transgene, respectively. Accordingly, the higher abundance of sgRNAs against the on-target was supposed to result in an initial fast process of targeted knock-out, whereas the less frequent sgRNA against *Sa*Cas9 was supposed to mediate a slower self-inactivation process. 2.) For the split*Sa*Cas9 system, each split half was produced as a separate dsAAV vector. The applied gp41-1-bearing split version 3 is asymmetrically divided into two parts, insofar that the smaller C-terminal *Sa*Cas9 construct leaves enough space for an additional H1-driven sgRNA cassette targeting the N-terminal *Sa*Cas9. A separate dsAAV vector provided the sgRNA targeting either the endogenous *mecp2* locus or an integrated HBsAg locus. 3.) Since the size of both split *Sa*Cas9 halves nearly reaches the limit of the dsAAV transgene capacity, the H1 promoter-driven sgRNA expression cassette could also be incorporated in the same dsAAV vector as the U6 promoter-driven sgRNA against the on-target. Note that the sgRNA against the endogeneous *mecp2* locus was used in transduction experiments with N2A cells and the sgRNA against the HBsAg was applied in transductions of Huh7-hNTCP-HB2.7 cells that harbored a stably integrated HBsAg. Furthermore, the sgRNA against the N-terminal *Sa*Cas9 transgene (gCas9 or gC) was also substituted with a scrambled sgRNA version (gscr) in order to investigate the levels of self-inactivation. N2A cells (Figure 31B) and Huh7-hNTCP-HB2.7 cells (Figure 31C) were transduced with the described conditions 1.) to 3.) and analyzed for targeted knock-out efficiency via T7 assay and ability to self-inactivate via Western blotting three days after transduction.

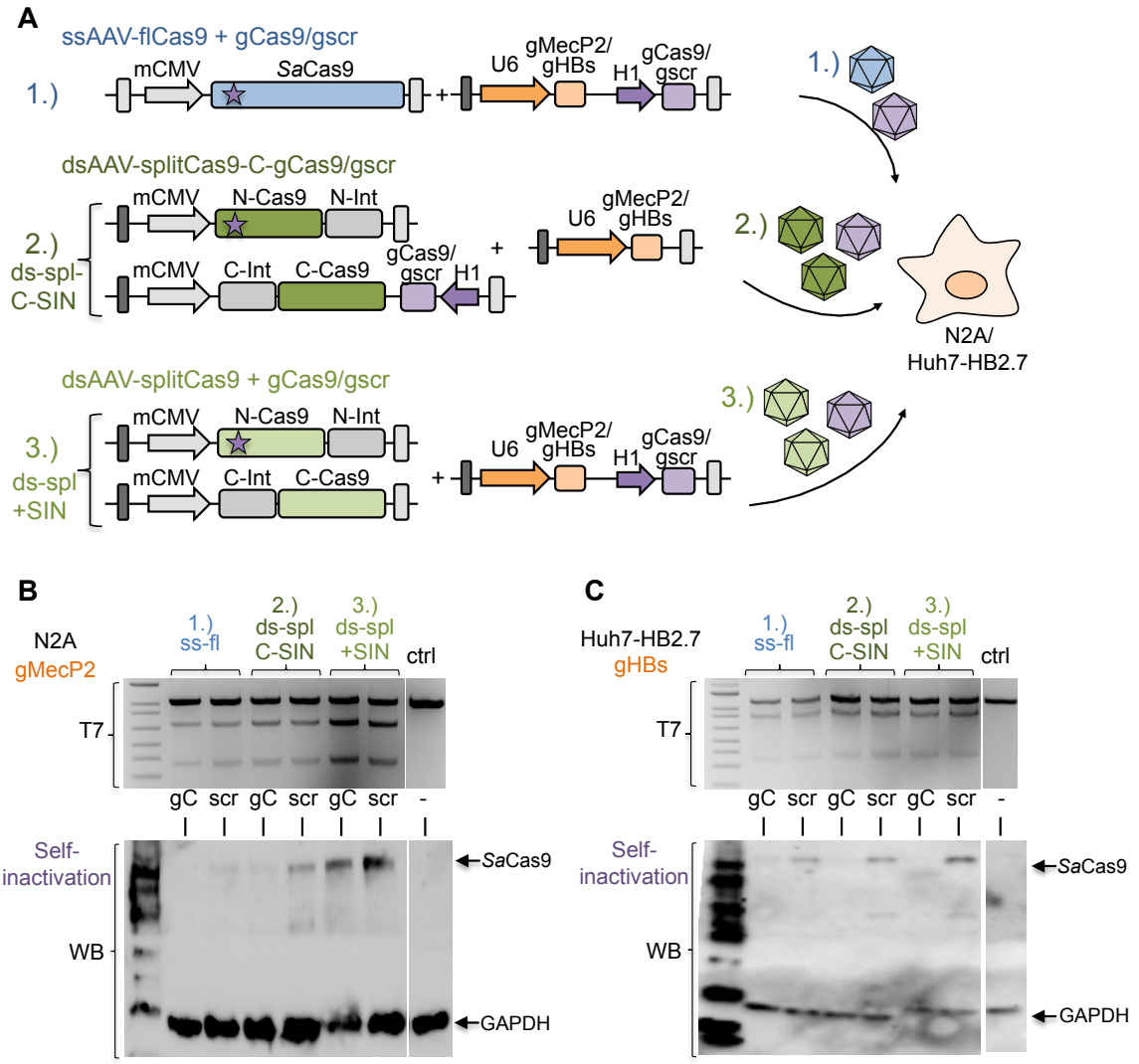

Figure 31. Split and self-inactivating rAAV/CRISPR vectors.

A) Two versions of the dsAAV/split*Sa*Cas9 & SIN system (conditions 2 and 3, one gray and one white ITR indicates dsAAV vectors) were compared to a conventional ssAAV/fl-*Sa*Cas9 & SIN system (condition 1, two white ITRs indicate ssAAV vectors). In order to evaluate the effect of the SIN approach, the sgRNA directed against the N-terminal *Sa*Cas9 (gC, violet star indicates the sgRNA target site) were also substituted with a scrambled version (gscr). **B)** N2A and **C)** Huh7-hNTCP-HB2.7 cells were transduced with the conditions 1.) to 3.) using an MOI of $5x10^5$ and 10^4 of each component, respectively, and analyzed for its on-target activity via T7 assay (upper panels) and for its self-inactivation via Western Blot (lower panels) three days post-transduction. Results were obtained jointly with Nikolay Sergeev (practical student).

In accordance with our previous experiments in N2A cells, the dsAAV-split*Sa*Cas9 system (without the additional H1 promoter-driven sgRNA cassette on the C-terminal part, condition 3.) mediated a higher on-target knock-out efficiency compared to the ssAAV-full length *Sa*Cas9 system (condition 1.) (Figure 31B, upper panel). However, when the H1 promoter-driven sgRNA cassette was provided with the C-terminal *Sa*Cas9 vector (condition 2.), targeted knock-out efficiencies on the *mecp2* locus decreased. In

the Western blot, expression of *Sa*Cas9 was detectable for both dsAAV-split*Sa*Cas9 systems in N2A cells, but barely for the ssAAV-full-length *Sa*Cas9 (Figure 31B, lower panel). Along these lines, the expression of *Sa*Cas9 correlated with the targeted knock-out efficiency of the *mecp2* locus, as the split system in condition 3.) showed the strongest *Sa*Cas9 expression and *mecp2* knock-out. Vectors that expressed the sgRNA against *Sa*Cas9 (gC) showed a reduced *Sa*Cas9 expression compared to rAAV vectors that expressed the scrambled variant (scr). In fact, *Sa*Cas9 expression by the dsAAV-split*Sa*Cas9 system in condition 2.) could be reduced to undetectable levels by the sgRNA against *Sa*Cas9. The use of either gC or scr variant showed no effect on the on-target knock-out rate in the T7 assay.

However, the results differ for experiments in Huh7-hNTCP-HB2.7 cells, where rAAV vectors in conditions 1.) to 3.) were applied to target the integrated HBsAg locus (Figure 31C). First of all, we did not observe a benefit of the dsAAV-split*Sa*Cas9 system in knock-out efficiencies of the HBsAg locus in Huh7-hNTCP-HB2.7 cells in repeated experiments (Figure 31C, upper panel). Accordingly, the dsAAV vectors did not mediate stronger expression of the split halves (Figure 31C, lower panel). Nevertheless, self-inactivation by the addition of the sgRNA against *Sa*Cas9 (gC) successfully reduced *Sa*Cas9 expression to undetectable levels in the Western blot, without affecting targeted knock-out efficiencies of the HBsAg.

3.5.4. Evaluation of split and self-inactivating dsAAV-CRISPR vector *in vivo*

We tested the dsAAV/split*Sa*Cas9 system in combination with the SIN approach also in a pilot *in vivo* study in order to evaluate the full potential of our system. To this end, full-length/SIN and split/SIN *Sa*Cas9 vectors were produced as ssAAV and dsAAV vectors, respectively, following a similar approach as in the previous cell culture experiments. Yet, this experimental layout slightly deviated as we directed the CRISPR system against the KS-Luciferase reporter that was already applied in our former *in vivo* experiments (Figure 21). Thus, instead of including the sgRNA against an endogeneous target, the KS-luciferase reporter carried its own sgRNA. Again, we tested three conditions including 1.) the full-length *Sa*Cas9 system in ssAAV with the SIN expression cassette on a separate dsAAV, 2.) the split*Sa*Cas9 system in two independent dsAAV and the SIN expression cassette as part of the C-terminal *Sa*Cas9 vector, and 3.) split*Sa*Cas9 and SIN expression cassette in a total of three independent dsAAV vectors (Figure 32A). All vectors were packaged in rAAV8 and each CRISPR vector and the KS-luciferase

vector were co-injected into mice. Mice were sacrificed 15 days post-injection and DNA, RNA and proteins were extracted from liver pieces for further quantifications.

The dsAAV/split*Sa*Cas9 systems (conditions 2. and 3.) outperformed the conventional ssAAV/fl*Sa*Cas9 (condition 1), as evidenced by the stronger reduction of luciferase signal (Figure 32B) and a higher mutation rate at the luciferase on-target site (Figure 32C). Importantly, the assays performed in Figure 32B and C only evaluated the performance of the CRISPR vectors on the luciferase on-target, but did not assess Cas9 self-inactivation. Accordingly, ideally, we expected no differences between groups harboring a sgRNA against Cas9 (gC) or a scrambled version (scr). The enhanced gene editing efficiencies of the dsAAV/split*Sa*Cas9 systems were accompanied by about 2-fold (condition 3) and 3-fold (condition 2) higher vector copy numbers per cell (Figure 32C), indicating improved *in vivo* dsAAV vector stability as reported in literature [255]. In addition, *Sa*Cas9 mRNA levels were strongly increased for the dsAAV/split*Sa*Cas9 system (Figure 32D). Interestingly, groups that harbored the sgRNA against the *Sa*Cas9 transgene (gC) showed decreased *Sa*Cas9 mRNA levels, when compared to their scrambled (scr) counterpart, indicating that *Sa*Cas9 was indeed self-inactivated. We were able to confirm an efficient reduction of *Sa*Cas9 protein via Western blot for the ssAAV/fl*Sa*Cas9 and dsAAV/split*Sa*Cas9 systems in conditions including the SIN approach (data from Julia Fakhiri, not shown).

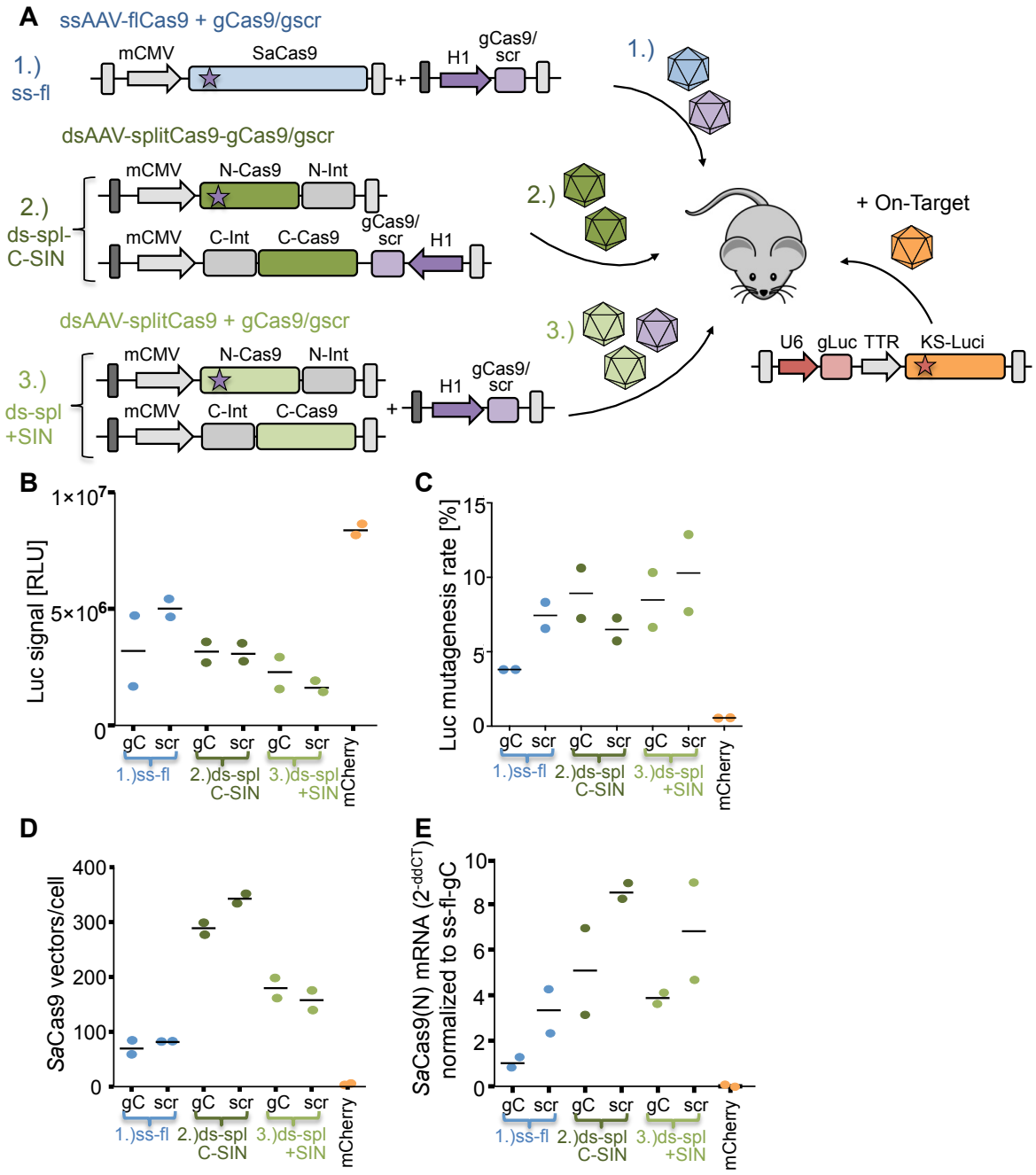

Figure 32. Evaluation of dsAAV/ split and SIN *Sa*Cas9 vector in mice liver.

A) The different *Sa*Cas9 systems were packaged into either ssAAV or dsAAV of serotype 8, as indicated in condition 1.) to 3.). and co-injected with $8x10^{11}$ viral particles of each CRISPR vector and 1.5 $x10^{11}$ viral particles of rAAV8-(KS) Luciferase into the tail vein of female NMRI mice (6 weeks old). **B)** Measurements of Firefly luciferase signal in relative light units (RLU) from liver pieces. **C)** DNA was extracted from the liver and mutagenesis rates of the Luciferase target site were quantified via ddPCR by multiplexing a primer/probe set against the target site and a reference site within the luciferase transgene. **D)** Vector copy numbers were quantified via ddPCR by multiplexing a primer/probe set against N-terminal *Sa*Cas9 and the Rpp30 house keeper gene. **E)** RNA was extracted from liver pieces and the amount of N-terminal *Sa*Cas9 cDNA was quantified via qRT-PCR and normalized to the GAPDH house keeper. B) to E) Control mice were injected with all vectors of condition 2.) but with dsAAV-mCherry instead of an N-terminal split*Sa*Cas9 half (orange). Each data point represents the measurements from an individual mouse. Results were acquired jointly with Julia Fakhiri and Nikolay Sergeev.

3.6. An engineered AcrX variant to inhibit the CRISPR/Cas9 system from *Staphylococcus aureus*

We wanted to go one step further towards safer applications of the CRISPR/Cas9 system from *Staphylococcus aureus* by the use of anti-CRISPR proteins. However, at that time no inhibitors were available that efficiently inhibited the *Sa*Cas9 ortholog. Our collaborator Dominik Niopek (University Hospital Heidelberg) speculated that AcrIIC1, a natural inhibitor of the *Nme*Cas9, might represent an ideal starting point to engineer an artificial *Sa*Cas9 inhibitor, as the structural arrangements of both HNH domains (the binding site of AcrIIC1 on *Nme*Cas9) shared high similarities, although the sequence identity reached only 33.7 %. Previous *in vitro* data suggested that AcrIIC1 fails to inhibit *Sa*Cas9 function [309]. Nevertheless, Dominik Niopek asked me to reproduce these findings in cell culture and indeed we encountered a very weak but reproducible *Sa*Cas9 inhibition in our own experiments (data not shown).

Thus, Dominik Niopek initiated a collaboration with the lab of Bruno Correia (Swiss Federal Institute of Technology Lausanne) to develop an engineered AcrIIC1 variant with improved interaction of the inhibitor on the *Sa*Cas9 HNH domain. Bruno Correia and his lab established a structural model that pointed to two regions in *Sa*Cas9 with suboptimal contacts to the corresponding AcrIIC1 residues. By performing *in silico* mutagenesis of these regions using Rosetta design [310], they provided the Niopek lab with different mutations in AcrIIC1 that could, based on their model, improve binding to *Sa*Cas9 HNH domain. Supported by Sabine Aschenbrenner (technician in the Niopek lab), we first cloned and evaluated these single point mutations for their functionality to inhibit *Sa*Cas9 activity and then iteratively combined the most promising variants in subsequent screening rounds. Note that the results presented here were published in Mathony, Harteveld & Schmelas *et al.* (2020) [311].

3.6.1. Iterative screening rounds towards an artificial *Sa*Cas9 inhibitor

We first evaluated the predicted single AcrIIC1 mutants for their potency to inhibit *Sa*Cas9 at the *emx* locus by co-transfecting HEK293T cells with a plasmid that harbored the *Sa*Cas9 and sgRNA and a separate plasmid containing the indicated inhibitor mutants (Figure 33A). After my first screening round of the mutants with single point mutations, Dominik Niopek had the impression that the substitution of specific amino

acid residues indeed improved *Sa*Cas9 inhibition (AcrIIC1 residues N2, D14, K46, A47, Figure 33B).

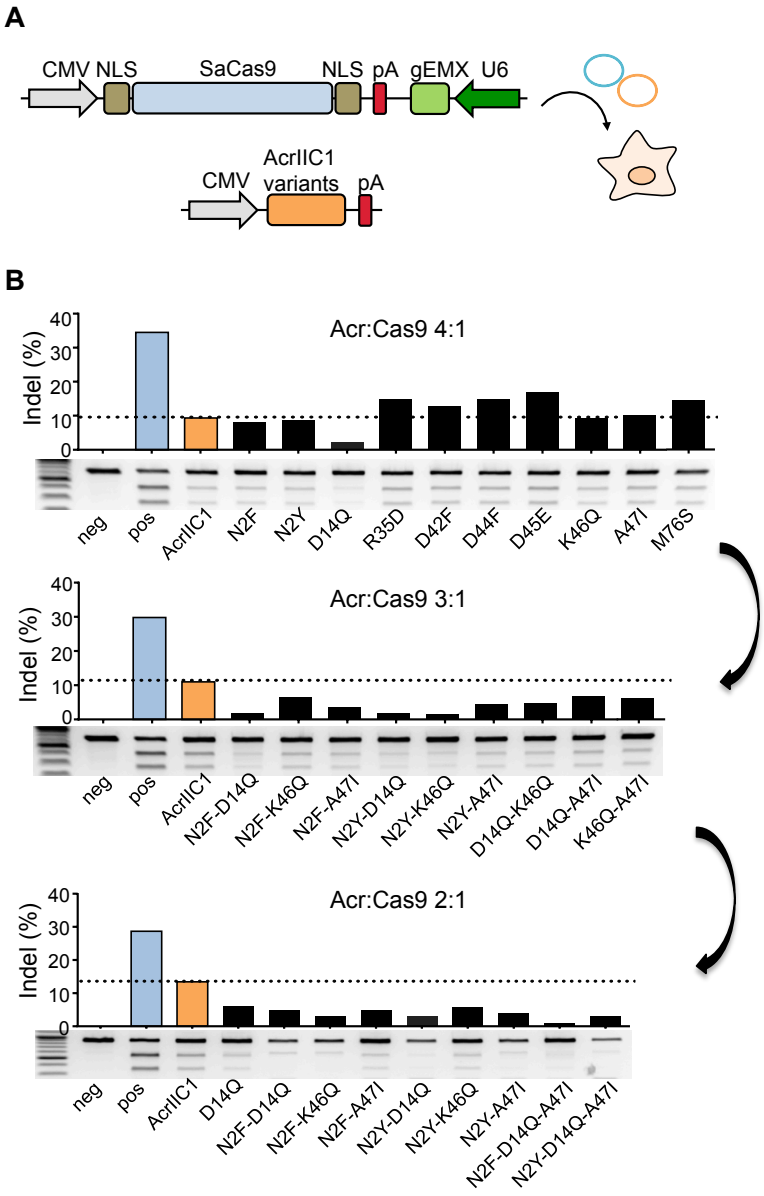

Figure 33. Iterative screening of computationally designed AcrIIC1 mutants.

A) HEK 293T cells were co-transfected in a 96-well plate format with *Sa*Cas9, a sgRNA targeting the EMX locus and either AcrIIC1 wild-type or the indicated AcrIIC1 mutant with a total amount of 200 ng and three days later harvested for analysis via T7 assay. **B***)* The Acr:*Sa*Cas9 vector ratio varied from 4:1 to 2:1 for each round of selection and increasing inhibition potency. In the first panel, computationally predicted single mutations were tested and in the second panel the pair-wise combination of single mutations that were as good as or better than the AcrIIC1 wild-type were validated. In the third panel, mutation A47I was added to the two best double mutants and compared to the lead candidates of previous selection rounds. The triple mutant N2F, D14Q, A47I was termed AcrX. Representative T7 gel images and corresponding quantifications of indel frequencies are shown. Dotted lines indicate the editing frequency in the presence of wild-type AcrIIC1. Neg, negative control (Cas9 only). Pos, positive control (Cas9 + sgRNA). Results were published in [311].

Thus, he asked me to further combine the best performing residue substitutions to double mutants and subsequent triple mutants and to perform the second and third screening round (clonings were performed jointly with Sabine Aschenbrenner). Indeed, the performance of the Acr mutants increased with the selection rounds (Figure 33B). We decreased the Acr:*Sa*Cas9 ratio with each screening round to better resolve the performance of improved candidates. The triple mutant N2F, D14Q, A47I that we referred to as AcrX achieved a near-complete inhibition of *Sa*Cas9. The addition of a fourth mutation did not further improve the mutant (data not shown).

3.6.2. AcrX efficiently inhibits *Sa*Cas9-mediated gene editing

Next, Dominik Niopek instructed me to evaluate the performance of the AcrX inhibitor on *Sa*Cas9 in detail at various genomic loci, including the *emx*, *grin2B* and *hbb* locus, via T7 endonuclease assay (Figure 34A) and TIDE analysis (Figure 34B). The AcrIIC1 wt inhibitor reduced *Sa*Cas9 knock-out activities to about 50% of the positive controls over all tested loci. By contrast, the engineered AcrX inhibitor efficiently suppressed *Sa*Cas9 genome editing to undetectable levels at all tested loci in T7 endonuclease assays and TIDE analyses, showing a highly improved inhibition as compared to its parental AcrIIC1.

Importantly, while data obtained by T7 endonuclease assays and TIDE analyses from the same samples revealed the same overall tendencies that confirmed the improved inhibition of AcrX, TIDE analyses showed an overall higher indel frequency for positive controls and less pronounced differences in *Sa*Cas9 inhibition of AcrIIC1 and AcrX.

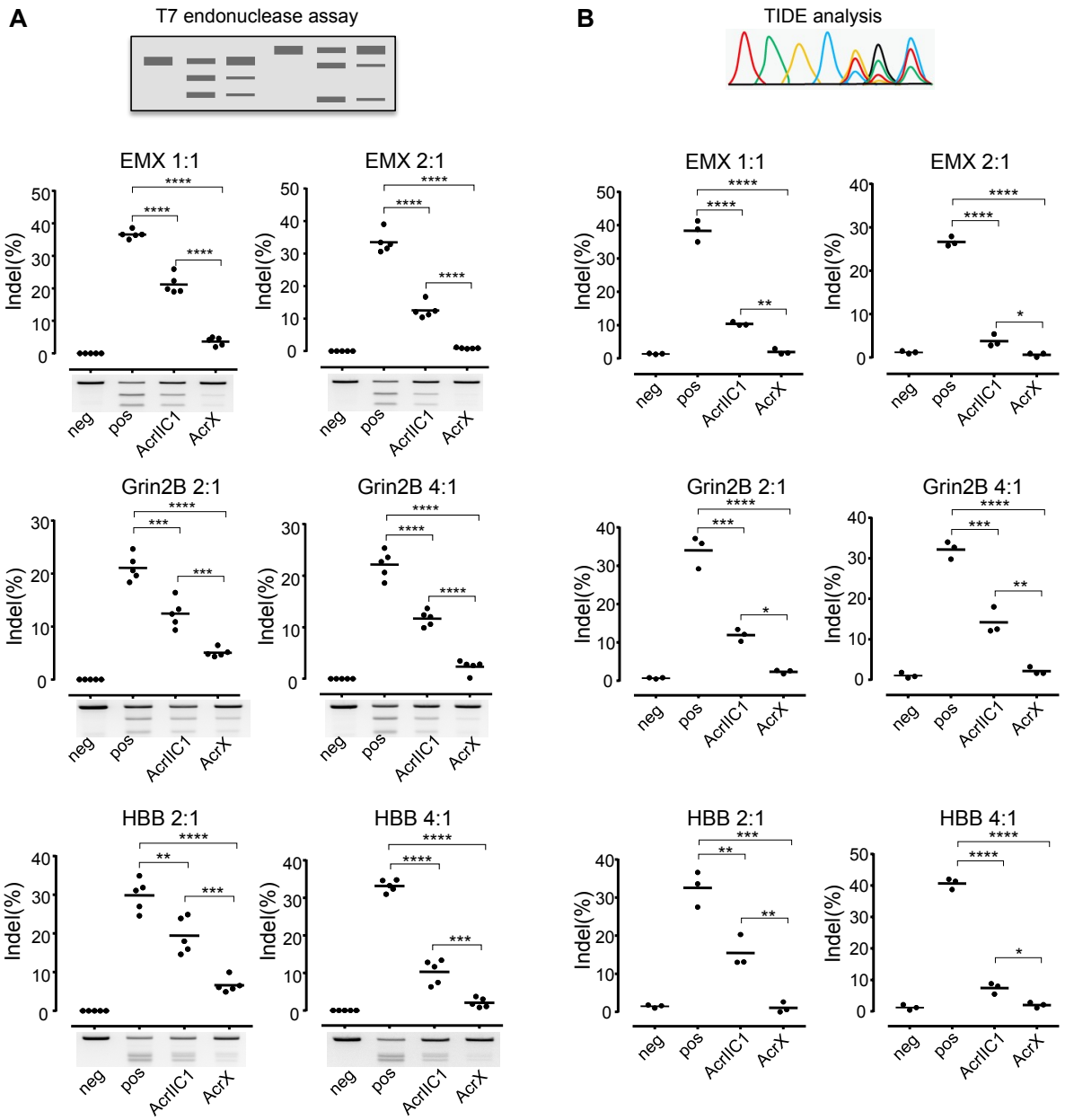

Figure 34. Validation of *Sa*Cas9 inhibition by AcrX.

HEK293T cells were co-transfected with *Sa*Cas9, an sgRNA targeting either the *emx, grin2B* or *hbb* locus and AcrIIC1 wild-type or AcrX using the indicated ratio of inhibitor:*Sa*Cas9 and total DNA of 200 ng in a 96-well plate scale. Positive controls (pos) were co-transfected with stuffer DNA instead of inhibitor and negative controls (neg) were only transfected with *Sa*Cas9. Three days later, cells were lysed and analyzed via T7 endonuclease assay **(A)** or TIDE sequencing **(B)**. Each data point represents an independent experiment. Samples were compared via ANOVA and Bonferroni´s multiple comparison test, *<.05, **<.01, ***<.001, ****<.0001. Results were published in [311].

3.6.3. The *Sa*Cas9-ON switch for hepatocyte-specific gene editing

Finally, to demonstrate the potential of AcrX to restrict *Sa*Cas9 activity to selected cell types, we made use of a miRNA-mediated Cas-ON switch and harnessed the hepatocyte-specific expression of miR-122 [203]. To this end, the lab of Dominik Niopek introduced miR-122 binding sites in the 3´ UTR of the AcrX transgene. Upon co-delivery of the miRNA-dependent AcrX and the CRISPR/Cas9 system, the expression of AcrX was supposed to be knocked down by the RNAi machinery specifically in hepatocytes, thereby permitting *Sa*Cas9 to be active. However, in off-target cells that do not express miR-122, the inhibitor was supposed to remain active and *Sa*Cas9 switched off.

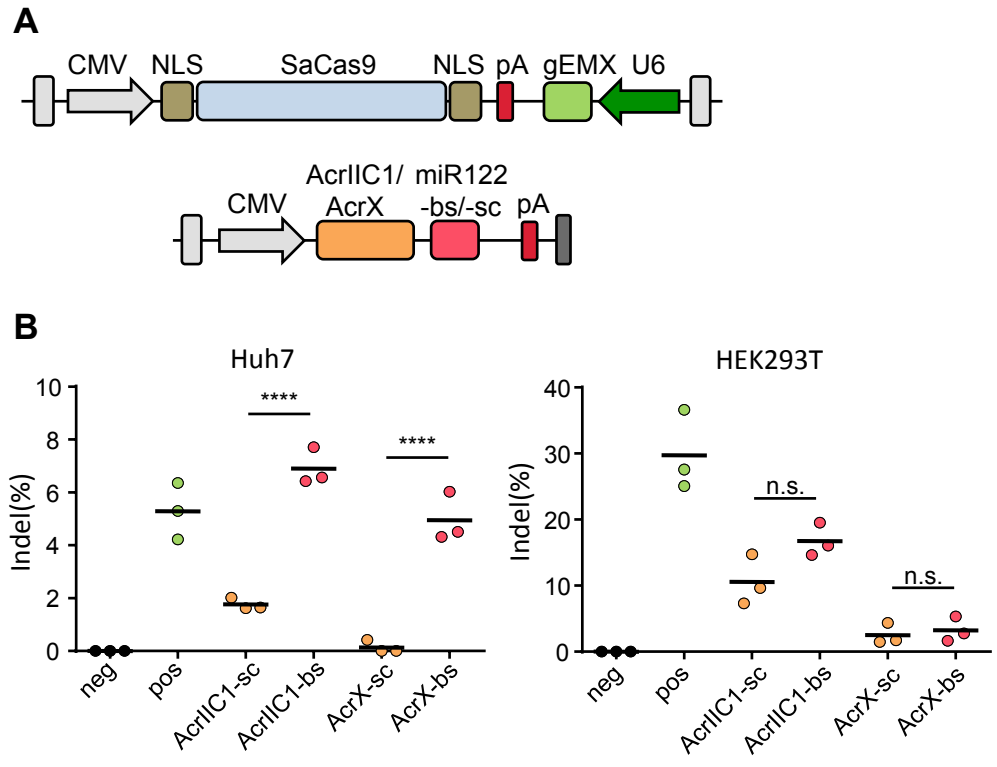

Figure 35. AcrX can be applied for cell-type-specific activation of *Sa*Cas9.

A) *Sa*Cas9 with sgRNA targeting the *emx* locus and AcrIIC1 or AcrX, both with miR122 binding site (bs) or scaffold (sc) in the 3´ UTR were packaged into AAV2. **B)** Huh7 cells (left, on-target) and HEK293T cells (right, off-target) were transduced with the indicated rAAV vectors using an MOI of $2.5x10^5$ for *Sa*Cas9 and 10^5 for the corresponding inhibitor. Three days later, cells were lysed and analyzed via T7 endonuclease assay. neg.= negative control of *Sa*Cas9 without sgRNA, pos.=positive control of *Sa*Cas9 with CMV-YFP instead of inhibitor. Each data point represents an independent experiment. Samples were compared via ANOVA and Bonferroni´s multiple comparison test. n.s.= not significant, ****<.0001.

Our lab produced the different components of the Cas-ON system, such as *Sa*Cas9 and an sgRNA targeting the *emx* locus, as well as AcrIIC1 or AcrX with either a miR-122 binding site (bs) or a miRNA-independent scaffold (sc), as rAAV2 vectors (Figure 35A). Subsequently, we transduced Huh7 cells that express miR-122 (on-target cell line) and HEK293T cells that do not express miR-122 (off-target cell line) with the rAAV vectors and harvested the cells for quantification of editing rates on the *emx* locus via T7 endonuclease assay (Figure 35B). In Huh7 cells, both inhibitors were successfully knocked down in a miR-122 binding site-dependent manner, as indicated by the presence of gene editing events. Inhibitors with scaffold instead of mir-122 binding site remained present within Huh7 cells and successfully repressed *Sa*Cas9 activity. CRISPR/Cas9-mediated editing was observed only in the presence of AcrIIC1 and AcrX with miR-122 binding site, whereas Acrs with scaffolds inhibited *Sa*Cas9 activity. Importantly, in HEK293T cells, inhibitors were not down-regulated by miR-122 binding and only the AcrX inhibitor, but not AcrIIC1, efficiently inhibited editing in the off-target cell line. These results demonstrate that AcrX, but not AcrIIC1 can be used to implement the Cas-ON switch for *Sa*Cas9 and restrict its activity to target cells.

4. DISCUSSION

The field of gene and cell therapy has been experiencing major breakthroughs in the development of novel treatments to cure hitherto untreatable diseases. On the one hand, over 120 clinical trials [312] illustrate the enormous safety and efficacy of rAAV vectors in human patients that culminated in the market authorization of Glybera, Luxturna and Zolgensma. On the other hand, equally encouraging developments have recently been made in the field of RNA interference- and CRISPR-based gene editing, two powerful and highly complementary technologies that can be applied to modulate gene expression and function in mammalian cell cultures and *in vivo*. RNAi-based treatments are under investigation in over 30 clinical trials [313], including three on chronic hepatitis B (NCT03672188, NCT03365947, NCT02631096). In addition, the FDA approved Onpattro in 2018 [314], the first siRNA-based medication against hereditary transthyretin-mediated amyloidosis, a rare disease that leads to fatal polyneuropathies. Even more striking are the rapid developments in the CRISPR/Cas9 field that led to several clinical trials within less than a decade and aim to treat blood cancers and other blood disorders in *ex vivo* therapies [164]. Furthermore, one *in vivo* clinical trial aims to treat LCA, an inherited disease causing blindness, by rAAV5-mediated delivery and expression of the CRISPR/Cas9 components (NCT03872479).

The combination of these powerful technologies provides a comprehensive tool kit that enables therapies to replace, silence and edit malfunctioning genes and whose scope can readily be expanded towards many diseases for which these technologies could provide therapeutical benefit. This, in turn, requires further technological advances to obtain more potent and safer modalities, which altogether initiated the study and fueled the research objectives presented here.

4.1. Current strategies to multiplex small RNAs

In this study, we aimed to validate and apply a new generation of rAAV vectors that has previously been established in the lab and that enables the combined application of RNAi and CRISPR/Cas9. So far, numerous studies have reported different strategies to co-express several shRNAs in the same cell, a concept termed combinatorial RNAi or "coRNAi", to either regulate several genes concurrently or to combat infectious diseases in a multi-hit attack [136]. A similar concept was applied for CRISPR/Cas9 that allows the co-expression, also referred to as “multiplexing”, of several sgRNAs and the concurrent targeting of multiple genes [175]. An abundance of studies highlight the benefit of targeting

infectious diseases with several RNAi or CRISPR triggers in order to increase efficiency and counteract viral escape [136; 137; 142; 143; 315; 316]. While Leonard and Schaffer (2005) predicted the need of four shRNAs or siRNAs to efficiently inhibit HIV without the occurance of escape mutants [317], the number of small RNAs remains undetermined that are needed to achieve this goal for other viral infections. For HBV, it was reported that the expression of a single sgRNA resulted in error-prone repair of the target site [318; 319], whereas a dual guided CRISPR system achieved a complete eradication of cccDNA [320].

In principle, small RNAs could be multiplexed or co-expressed in the same target cell by various strategies. One strategy aims to co-express several small RNAs by a single long transcript, which is further processed by enzymes to segregate the individual small RNA triggers. This approach was realized for the multiplexed expression of sgRNAs by a single promoter and the use of the Csy4 RNA endonuclease [321; 322], an enzyme that processes crRNA arrays in its natural context [323]. However, this strategy requires Csy4 co-delivery in addition to the large Cas9 endonuclease. Also the endogenous tRNA-processing machinery [324-326] or ribozymes [322; 326-328] were employed to trigger processing of the single long transcript into multiple sgRNAs, but involve further endogenous pathways that might overwhelm the cell machinery and could be associated with toxicity. An exiting recent discovery extending this strategy is Cas12a (also referred to as Cpf1), an orthologous CRISPR systems that harbors an inherent RNase activity and can thus process its own pre-crRNA array into multiple guide RNAs, which are sufficient to induce DSBs at designated DNA targets [329; 330].

Similarly, several approaches were invented to co-express multiple RNAi triggers on a single long transcript, including extended [331] and long [332; 333] shRNAs that are processed to give rise to two or more small RNAs and the use of miRNA polycistrons with embedded siRNA sequences that are further processed and released by Drosha as miRNA-based shRNAs [334-337]. The overall advantage of these approaches is the expression of several small RNAs by a single promoter that reduces the required sequence space and thus facilitates the packaging in rAAV vectors.

However, most studies in the field of gene and cell therapy apply another strategy and co-express either sgRNAs or shRNAs from individual promoters, as it represents a straightforward and more flexible strategy. Other advantages include the clear definition of the expression products that are free from any further processing signals that might interfere with their targeting capability, as well as the availability of several RNA polymerase III promoters, such as the U6, H1 or 7SK promoters that exhibit different expression strengths and thus allow for the modulation of RNA expression levels. In

spite of numerous studies that co-expressed several RNA triggers for RNAi or CRISPR, our lab has previously recognized two gaps that we have aimed to bridge. Firstly, the research field was missing a experimental comparison between different strategies to multiplex small RNAs and, secondly, a flexible cloning strategy was lacking that allows the co-expression of shRNAs and sgRNAs on a single rAAV vector. For this reason, our lab (Florian Schmidt, B.Sc. thesis) has designed and validated the TRISPR system that resolves these concerns and that has already been applied successfully in several collaborations from our lab, including for combinatorial expression of shRNAs against the cellular adaptor protein 1 [338], or of sgRNAs to induce exon skipping in a mutated dystrophin gene [339], or, most recently, to foster AAV vector self-linearization and enhanced gene repair in liver cells through co-expression of two sgRNAs [340].

4.1.1. Multiplexing of small RNAs in rAAV vectors

In this study, we harnessed the TRISPR system and thoroughly extended our previous comparison of this toolbox to commonly used approaches to co-express small RNAs from rAAV vectors to the context of HBV infections. To this end, we selected three sgRNAs that have previously been evaluated for their capability to knock out the HBsAg (Figure 16) and that served as representatives of small RNAs in general. In line with and expanding prior TRISPR validation work from our lab, we tested three alternative strategies to co-express these sgRNAs from rAAV vectors (Figure 15), including i) the separate production and subsequent “mixing” of each individual vector, ii) the “pooled” production of these vectors in the same dish, and iii) the juxtaposition of the three sgRNA expression cassettes on the same rAAV vector via TRISPR. Whereas approach i) and ii) might be associated with less preceding cloning effort (as they only require the insertion of appropriate oligonucleotides in separate rAAV vectors), they come with fundamental drawbacks. The premises for approach i) and ii) are a robust transduction of targeted cells and a homogenous expression of all vectors, to ensure that all target loci are hit within a single cell. In particular in hard-to-transfect/-transduce cells, a variable expression of sgRNAs may result in low reproducibility. Furthermore, as a consequence of co-packaging several genomes in a single pooled rAAV production (approach ii), there may be varying proportions of each vector in the final product. Although Doerfler *et al.* (2014) [341] reported that it was possible to retain the predicted AAV output ratios related to a pooled plasmid input that was used to produce these vectors by transfection, we are concerned that in other instances this coherency is not guaranteed. Indeed, recent data

suggests a detrimental influence of small RNA hairpins encoded on rAAV vectors on packaging efficiencies and particle integrity [342] that might perturb the proportions of sgRNAs and shRNAs expressing vectors in pooled productions. In our experiments, we observed that approach i) and ii) are clearly inferior strategies to multiplex small RNA expression cassettes (Figure 17), congruent with our initial notions (Florian Schmidt, BSc thesis) and probably because of the aforementioned reasons. Indeed, TRISPR is the most convenient and efficient strategy to multiplex RNA expression cassettes, as it requires the production of only a single rAAV vector and significantly outperforms the other strategies in knocking out HBsAg.

4.1.2. The TRISPR toolbox

Before the implementation of the TRISPR system by our lab, straightforward strategies to juxtapose either sgRNA or shRNA expression cassettes on a single construct were only realized through plasmid transfection [343-346] or in a lentiviral context [347]. Accordingly, prior to TRISPR, such a tool kit was missing for multiplexing approaches in the context of rAAV vectors that are currently among the most important *in vivo* delivery vehicles in the field of gene and cell therapy. TRISPR filled in this gap by providing all necessary DNA templates and step-by-step instructions to rapidly juxtapose three small RNA expression cassettes on a single rAAV vector (Figure 13). Moreover, in contrast to the other strategies, TRISPR is the first toolbox that facilitates the assembly of sgRNAs, compatible with the orthologous CRISPR systems of *S. pyogenes* and *S. aureus,* and shRNAs on the same vector in any possible permutation. Although the current version of the TRISPR toolbox permits the concatamerization of solely three small RNA expression cassettes in a predefined configuration (U6, H1 and 7SK promoter-driven expression cassette), it still leaves enough room for customization. Firstly, the expression of small RNAs by the three different promoters allows for the modulation of their expression levels, with the U6 promoter mediating the strongest expression [348], followed by the 7SK and H1promoter. Secondly, these expression cassettes could be exchanged or extended with any other desired promoters by the simple creation of additional donor plasmids for the assembly of the final rAAV recipient plasmid via Golden Gate cloning, as long as the final size remains within the dsAAV vector capacity of 2.4 kb. Encouraged by our findings that emphasized TRISPR as a powerful and flexible approach to co-express several small RNAs in the same cell, we set out to apply a combined knock-down and knock-out strategy to tackle HBV infections on mRNA and cccDNA.

4.2. A combinatorial knock-down/ knock-out approach to tackle HBV infections

Currently available medication to treat chronic hepatitis B control viremia and reduce liver inflammation, but barely affect cccDNA levels or antigen expression and thus fail to resolve viral persistence. Thus, this study has evaluated an approach that aims to directly combat viral antigen expression and cccDNA persistence by a combinatorial knock-down and knock-out strategy. Our lab has previously reported that HBV replication could be efficiently inhibited *in vitro* and i*n vivo* by HBV-targeting shRNAs in relevant cell culture systems and in HBV-transgenic mice [163]. The most potent shRNA (shHBV7) was targeting the X antigen region that is part of the 3´ UTR of every viral transcript and thus efficiently reduces the expression of all viral antigens. Here, we extended this approach by the addition of the CRISPR/Cas9 system that is able to not only inhibit antigen expression but can also directly attack the HBV cccDNA. An advantage of both technologies is their compatibility with rAAV vectors that enables an efficient and specific delivery of the required components in the liver of mice. Importantly, the rAAV vector specificity towards the liver can be further improved by molecular engineering and directed evolution of the rAAV capsid [249]. Furthermore, it has been reported that HBV serves as a helpervirus and facilitates nuclear transport and gene expression of rAAV vectors, thus providing a selectivity advantage towards HBV-infected hepatocytes [349]. Hence, a combination of RNAi, CRISPR/Cas9 and rAAV vectors would be highly favorable in the combat against HBV infection.

4.2.1. Knock-out of large surface antigen increases HBsAg secretion and releases ER stress

In this doctoral work, we first set out to target the HBV surface antigen via CRISPR/Cas9 (Figure 16) and noticed a complex interplay of small and large antigens. While targeting of the small HBsAg resulted in the expected decrease of secreted antigens, sgRNAs directed against the large HBsAg elevated antigen levels in the supernatant. Nonetheless, the higher amounts of surface antigens translated to lower quantities of infectious progeny HDV (Figure 23), implying that the L-HBsAg, which is essential for HBV and HDV infectivity, was indeed lacking. While a number of studies reported the correlation between L-HBsAg overexpression and reduced antigen secretion [22; 350; 351], to our knowledge, we are the first to observe that CRISPR-mediated knock-out of the large antigen in turn elevates antigen secretion.

In the course of chronic hepatitis B, some patients develop HBV mutants that contain deletions in the surface antigens and circulate in the serum as predominant species [352-355]. One class of such mutants develops in-frame deletions in the preS1 region that is unique to the large surface protein and overlaps with the S promoter of the middle and small variants. These mutants give rise to increased amounts of preS1 transcripts and thus L-proteins and decreased amounts of S transcripts and consecutive M- and S-proteins. While the small surface antigen can self-assemble into nucleocapsid-free subviral particles that are secreted from the cell, the L- and M- variants are not secreted when expressed alone [356]. As a consequence of increased L-HBsAg production, the surface antigen variants are trapped in insoluble particles or compartments in the cytosol [22; 350; 352]. Hepatocytes that are overexpressing the large surface antigen can turn into so-called ground glass cells [357], which die spontaneously and react very sensitively to gamma interferon, thus contributing to immunologically induced liver cirrhosis and hepatocellular carcinogenesis [22; 358; 359]. Although less SVPs are secreted in the serum, these mutants maintain their capability to release DNA-containing virions at a slightly higher rate than wt HBV [352]. Furthermore, these mutants might be able to evade the host immune system, which explains their appearance as the major viral species.

Accordingly, sgRNAs directed against the large surface antigen could help to reduce intracellular accumulation of HBsAgs and reduce the stress that is imposed on the ER and associated with cell death and HCC [360]. Thus, in our experiments on HBV/HDV infections (Figure 23), which are further discussed in section 4.3, we made use of the anti-L-HBsAg sgRNA 3 to greatly improve our combinatorial knock-out/ knock-down approach.

4.2.2. Targeting HBV via RNAi and CRISPR/Cas9

Whereas HBV is a well-established target for RNAi and CRISPR/Cas9 *in vitro* and *in vivo* (Supplementary Table 1)[361], only a single study has so far applied a combinatorial approach [362]. Wang et al. (2017) designed a single expression cassette with an anti-HBV pri-miRNA between two anti-HBV sgRNAs that resulted in the expression of an sgRNA-miRNA-sgRNA ternary transcript. This transcript was further processed by Drosha and DGCR8 in the RNAi pathway, which led to the separation of the three small RNAs resulting in a synergistic effect on HBV replication inhibition and cccDNA elimination. From a vector and gene therapy standpoint, this approach seems rather complex and difficult to adjust to further designated targets. In contrast, the conventional RNAi and

CRISPR approaches, which comprise the expression of each small RNA by their respective RNA polymerase III promoter, were tested frequently and in numerous model organisms.

Importantly, we issue a note of caution about possible toxic side effects by the overexpression of RNAi triggers that can arise from an oversaturation of the RNAi machinery and an associated dysregulation of endogenous pathways [144-148]. To counteract these effects, we deliberately scaled down our TRISPR approach to the use of only a single shRNA and relied on the combination with two additional sgRNAs to tackle HBV. In our first experiment, the two employed sgRNAs were directed against the X and surface antigens and juxtaposed with shHBV7, to target cccDNA and mRNA of infectious HBV in HepG2-hNTCP cells (Figure 18A and B). In order to investigate the influence of each small RNA trigger or their combinations, we also substituted each position with control RNAs in any possible permutation. Indeed, we measured a reduction of secreted HBs and HBeAg levels in all samples that were transduced with at least one targeting small RNA, indicating that all RNAs were independently expressed and functional (Figure 18C and D). As hoped for, we observed the anticipated additive effect on the inhibition of antigen expression by the co-expression of two sgRNAs or the combination with shHBV7. Vectors that expressed the shRNA overall outperformed all other constructs and mediated a reduction in antigen expression to detection limits. Thus, the synergistic effect of a combined RNAi and CRISPR approach was difficult to confirm in this assay. Nevertheless, we argue for a beneficial synergy of the RNAi and CRISPR/Cas9 approaches, as they tackle HBV on different levels and mediate either a transient effect on antigen expression or irreversible mutations and eradication of cccDNA, respectively. Long-term experiments that include the passaging of the HBV-infected cells and further experimental readouts on the cccDNA and pgRNA levels are required to unveil the differential effects of the two technologies on HBV.

4.2.3. TuD RNAs in multiplexing approaches enhance RNAi safety profiles

Another hurdle of the RNAi technology are off-target effects that impact the expression of unintended genes. In this study, we counteracted off-targeting from loading of the shRNA passenger strand in RISC by the use of “tough decoy” or “TuD” RNAs. TuD RNAs basically consist of two shRNA antisense strands and act as sponges to restrict the amount of free sense/passenger strands that might otherwise be employed by Ago2 and mediate off-targeting. In a collaborative effort, our lab previously validated TuD RNAs in

the context of RNAi-mediated targeting of HCV [162] and HBV [163] infections. In HBV-transgenic mice, the use of TuD RNAs neutralized the unintended off-target activity of the passenger strand and even increased the desired antiviral effect of the shHBV7. As the current version of the TRISPR toolbox allows for the concatamerization of exactly three small RNAs, we further extended the combined RNAi/CRISPR approach with TuD RNAs to counteract unwanted shRNA passenger strand activity and to avoid further side effects.

In our next experiment, we extended this combinatorial approach by replacing the second small RNA cassette with a H1 promoter-driven TuD RNA that corresponds to shHBV7 (Figure 19B). Consistent with our previous findings, the expression of either sgRNA or shRNA reduced the levels of secreted antigens and the RNAi approach generally outperformed CRISPR/Cas9 in this assay (Figure 19C and D). In contrast to the abovementioned literature, we did not observe any beneficial effect of TuD RNAs on the shRNA on-target performance. We further evaluated the TuD RNA ability to inhibit passenger strand-mediated off-targeting in a luciferase reporter assay (Figure 20A). Indeed, we observed a substantial amount of unintended luciferase knock-down through the passenger/sense strand when a sense-strand binding site was included in the 3´UTR of the luciferase transgene (Figure 20B). In contrast to our expectations, TRISPR constructs that expressed TuD RNAs showed similar reductions in luciferase signals as constructs with scrambled TuD RNA controls. Thus, in this experimental setting, the TuD RNAs were insufficient to restrict the abundance of free sense strands and to avoid off-target activity caused by the passenger strand. We therefore further evaluated whether functionality of TuD RNAs can be restored if they prevail in numbers compared to the shRNA within the cells. Thus, we expressed shHBV7 by the weak H1 promoter and the TuD RNA by either the H1 or U6 promoter (Figure 20C). Indeed, lowering the abundance of shHBV7 allowed the TuD RNAs to restrict off-targeting by the passenger strands, while maintaining an overall efficient on-target activity. In conclusion, we recommend a low and steady expression of RNAi triggers in general, which would help to decrease cytotoxicity, limit off-target effects and safeguard its applications *in vivo.*

Taken together, our study has used a clinically highly relevant target to exemplify the successful combination of very powerful tools for gene therapy, namely, rAAV vectors, RNAi and CRISPR/Cas9, and implies its great potential for treatment of numerous diseases that have a DNA and/or RNA component. Our results concurrently inform and encourage future *in vivo* studies in HBV animal models, to test the effect of our AAV-based combinatorial knock-down and knock-out strategy on the host immune response and the possible synergistic impact on viral clearance. Along these lines, a pioneering

study by the Protzer lab from Munich already indicated that mice that persistently replicate HBV showed reduced levels of HBV antigens, HBV replication and viremia after injection of anti-HBV shRNAs or siRNAs [363]. Importantly, in mice with high levels of HBV replication only the combination of HBV antigen knock-down with a therapeutic vaccination strategy increased the number of HBV-specific $CD8^+$- T-cell and yielded HBV elimination, indicating that the restoration of the host immune system contributed to viral clearance.

4.3. A combinatorial knock-out/ knock-down approach against HBV/ HDV co- and superinfections

The co- or superinfection of HDV with its helper virus HBV is associated with the most severe progression of viral hepatitis culminating in high rates of liver cirrhosis and hepatocellular carcinoma and a three-fold increased mortality rate compared to HBV monoinfections [10]. For chronic hepatitis D, treatment options are even more limited compared to HBV, due to its life cycle that depends entirely on cellular enzymes, except for its delta and HBV surface antigens. Thus, the preferred treatment of chronic hepatitis D is a functional control of HBV including HBsAg seroconversion that also limits the spread of progeny HDV. However, current anti-HBV or anti-HDV therapies rarely achieve a sustained antiviral response, thus emphasizing the urgent need for further antiviral interventions. As such, the HBV/HDV entry inhibitor Myrcludex B, a synthetic lipopeptide that comprises a part of the large HBV surface antigen that binds to the NTCP receptor, in combination with PEG-IFNα yielded encouraging results in a phase I/II clinical trial (NCT02637999) and enabled significant decreases in HBV DNA and HDV RNA levels [306]. Nevertheless, it would be highly favorable to have an alternative interventional approach that persistently suppresses or eradicates HBV and HDV with a single application and that directly targets the two viral genomes and/or their RNA transcripts instead of cellular host factors. From our perspective, HBV/HDV co- or superinfections represent the ideal target for a combinatorial RNAi and CRISPR intervention, as RNAi can target the HBV and HDV RNA component and CRISPR can eradicate persistent HBV cccDNA.

4.3.1. Targeting HDV via RNAi

To date, only a single study has applied RNAi to target HDV and investigated the susceptibility of the three HDV RNA species - the genome, antigenome and delta antigen mRNA - towards RNAi triggers [127]. In their study, Chang and Taylor (2003) co-transfected Huh7 cells with several HDV-targeting shRNAs and plasmid-encoded HDV mRNA that resulted in the expression of either the normal delta mRNA, or delta mRNAs with an additional sequence in their 3´ UTR that represented either portions of the genomic or antigenomic sequence. While shRNAs that targeted the HDV mRNA resulted in efficient suppression of RNA accumulation and thus delta antigen expression, genomic and antigenomic sequences were resistant to RNAi. The authors hence concluded that the HDV RNA genome and antigenome might be inaccessible for the RNAi machinery due to their nuclear localization.

The work presented here clearly differes from the previous report in several aspects. Firstly, we applied RNAi in the context of actual HDV infections instead of plasmid-encoded surrogates. Infection experiments in cell culture only became possible with the identification of NTCP as entry receptor of HBV and HDV [15; 16] and with its genomic integration and overexpression in hepatic cell lines that makes them receptive towards HBV and HDV infections [75]. Furthermore, the supply of HBV surface antigens, *e.g.* as stable genomic integrate, even allows continuous secretion of infectious progeny HDV following primary infection and enables reinfection experiments [300]. Secondly, we implemented two different experimental settings that enabled us to investigate the effects of RNAi in the context of anti-HDV immunization and curation. The specific targeting of small and large delta antigen in the two experimental settings further led to insights into their differential roles in the HDV life cycle, which are further discussed in the following section. Thirdly, we combined the highly complementary RNAi and CRISPR technologies to not only target HDV infections but also HBV surface antigens, which are required for viral propagation and thus enabled a multi-pronged strike against HBV/HDV infections. Notably, no published study hitherto attempted to combine RNAi and CRISPR technologies to concurrently target and inhibit HBV and HDV. Lastly, we made use of multiplexed, safe and hepatotropic rAAV vectors to deliver and express small RNAs in target cells, which facilitates an easy transfer to future *in vivo* studies in more relevant HBV/HDV animal models.

In this study, we directed the RNAi machinery against the HDV antigenome that encodes the delta antigen, by harnessing and expanding a respective shRNA set from our lab. The high GC content and the presence of extensive secondary structures render only a

single position in the delta mRNA vulnerable to RNAi, which spanned the stop codon of the small delta antigen at position 196. Whereas shRNA 3 and 4 (which share the same target sequence and only vary in length) target the stop codon of the small delta antigen, shRNA 3ed and 4ed target the edited tryptophan at the same position and thus the large delta antigen. All other shRNAs target sequences upstream or downstream of the delta antigen mRNA. We evaluated the capability of RNAi-mediated suppression of delta antigen expression and RNA accumulation in an immunization and curation setting (Figure 22 and Supplementary Figure 2).

The immunization setting might reflect the previous described study of Chang and Taylor (2003) [127] the most, since HDV was unable to complete its full life cycle before subjecting to RNAi. Indeed, we found similar results and observed that only shRNA 3 and 4 that target the delta mRNA exhibited efficient inhibitory potential, in contrast to shRNAs that bind outside of the mRNA sequence (Figure 22A to C and Supplementary Figure 2). Importantly, shRNA 3ed and 4ed did not reduce delta antigen levels in early stages of infection, as further discussed in the following section. Notably, shRNAs that were functional in previous reports (shTaylor 4 and 6) [127] failed to inhibit delta antigen expression in our experiments (Supplementary Figure 2), which might be explained by different secondary structures of plasmid- encoded and infectious HDV transcripts or the diverging experimental approach. At least in our preceding *in silico* design of functional anti-HDV shRNAs, the positions targeted by shTaylor 4 and 6 did not emerge as optimal RNAi targets.

The effects of shRNAs on late stages of HDV infection could be investigated in the curation setting that permits RNAi to attack at a stage in which the L-HDAg is already present and facilitates viral assembly and release. We found that several shRNAs (6, 8, 9, 4ed and 3ed) can decrease the formation and release of infectious HDV, which is only observable in reinfection experiments (Figure 22D to F). In contrast to the findings of Chang and Taylor (2003) [127], we were able to target the antigenomic HDV RNA in this experimental setting, since shRNA 6, 8 and 9 do not target the delta mRNA sequence, but nonetheless reduced the formation of progeny HDV. Yet, the most potent shRNAs 3ed and 4ed target the mRNA of the large delta antigen directly. Surprisingly, shRNA 3 and 4 that target the small delta antigen strongly elevated the amount of infectious HDV in the curation setting (Figure 22F). This unexpected outcome will be further discussed in the following section.

4.3.2. Increased secretion of progeny HDV by knock-down of small delta antigens in late infection stages

HDV encodes only a single ORF for the delta antigen that is expressed as small and large variant, as a consequence of RNA editing at the amber stop codon [72; 73]. The sequential appearance of the two forms of HDAg regulates the viral life cycle. Whereas the small delta antigen *trans*-activates RNA replication in early stages of infections [84], the large antigen is expressed later in the replication cycle and is essential for the envelopment of the RNP complex and the interaction with the HBV surface antigens [90; 91; 364] that directs the viral life cycle towards assembly and secretion of progeny virus [365; 366]. The large delta antigen also acts as dominant repressor of viral replication and a ratio of large to small delta antigen as low as 1:10 was shown to almost completely abolish HDV RNA replication [85; 367]. Thus, the appearance of the large delta antigen plays a key role in the switching of molecular events, in order to suppress HDV replication and drive the system towards secretion of progeny virus. In our experiments, we were able to further investigate the roles of the delta antigen variants in early and late stages of the HDV life cycle by the application of RNAi and the specific targeting of small and large antigen.

As previously indicated, we implemented two distinct experimental settings in which RNAi was either applied to immunize against HDV or to cure an existing HDV infection (Figure 22A and D). The immunization setting was characterized by the targeting of HDV in an early stage of infection, in which only the small delta antigen was expressed (Figure 22B). By contrast, the curation setting targeted HDV in later stages of its life cycle in which small and large antigen variants were present (Figure 22E). Furthermore, our shRNA design enabled us to differentiate between knock-down of small (shRNA 3 and 4) and large delta antigen (shRNA 3ed and 4ed) by targeting either the amber stop codon or the edited tryptophan codon, respectively. The differential targeting was demonstrated by the ability of shRNA 3 and 4 to reduce small delta antigen expression in the immunization setting, whereas shRNA 3ed and 4ed failed in this matter (Figure 22B & C). In turn, shRNA 3ed and 4ed successfully targeted the large delta antigen in the curation setting, as implied by the reduction of infectious progeny HDV, whereas shRNA 3 and 4 failed in this regard (Figure 22F). Surprisingly, the knock-down of the small delta antigen in later stages of the HDV life cycle even elevated the secretion of progeny HDV.

This finding was unexpected and we were unable to find any references about an elevated viral assembly or secretion by the inhibition of the small delta antigen in late stages of HDV infection. Yet, a reason may be that until now, it has been impossible to differentially inhibit small and large delta antigen expression in the context of a natural

infection. At least two assumptions are possible that might explain the observed phenomenon in the context of the known HDV biology. Firstly, the inhibition of the small antigen might shift the system towards an increased expression of large delta antigen. Indeed, it has been reported that high levels of small delta antigen inhibit RNA editing of amber stop to a tryptophan codon [368]. Thus, inhibition of small delta antigen could elevate RNA editing rates and result in higher large antigen expression. The elevated numbers of large delta antigens might direct the viral life cycle towards assembly and secretion of progeny virus. A second assumption could comprise a direct inhibitory feedback mechanism imposed by the small delta antigen to restrict progeny HDV secretion and to retain the viral genomes for their deposition and amplification in the nucleus. Although this assumption has so far not been confirmed by any experimental data and thus remains entirely theoretical, such inhibitory feedback mechanisms are regularly reported for viral infections.

4.3.3. Targeting HDV RNA and HBV cccDNA via RNAi and CRISPR/Cas9

We further applied the anti-HDV shRNA 3ed in a multiplexing approach spanning either the combination with anti-HBV shRNA and sgRNA (Figure 23A) or two anti-HBV sgRNAs (Figure 23D). Indeed, reduction of the HBV surface antigen in any form efficiently decreased formation and spread of HDV (Figure 23B and E), as previously described [369]. Furthermore, whereas shRNA 3ed alone reduced the amount of reinfected cells to only two- to three-fold, the combination with either shRNA and/ or sgRNAs against HBV yielded a synergistic inhibition of HDV infection and successfully decreased the amount of reinfected cells to lower detection thresholds. The anti-HBV sgRNA 3 that targets the integrated large HBV surface antigen increased the levels of secreted HBsAg in previous experiments (Figure 16 and Figure 23E), but resulted in the formation of non-functional HDV particles that were unable to reinfect cells (Figure 23F). The negative feedback mechanism that might be imposed by the large HBV surface antigen towards secretion of the other surface antigen variants has been discussed in section 4.2.1. Importantly, our presented combinatorial knock-out/knock-down strategies are fully compatible with conventional therapies and might contribute to highly efficient multi-level attacks on HBV and HDV.

Furthermore, it might represent a promising approach to gain further insights into the various feedback loops of both infections and their interplay. Similar to the study of Chang and Taylor (2003) [127], it would now be highly interesting to study the effect of

RNAi also on the genomic RNA sequence of infectious HDV. Such experiments could yield further insights into HDV biology and might unravel the mystery of HDV persistence in the nucleus and how it maintains resistant towards the endogenous RNAi machinery despite its highly self-complementary RNA structure that perfectly mimics RNAi substrates [370]. Notable are also recent additions to the CRISPR technology, such as Cas13 that targets ssRNA instead of DNA substrates [371] and that could be applied to extend the genetic tool kit to research and combat HDV (and HBV) infections.

4.4. DMSO enhances viral infectivity in cell culture

For many years, research on HBV and HDV has been hampered by the lack of knowledge about the molecular properties of viral entry into human liver cells. The identification of NTCP as entry receptor in 2012 [15; 16] provided new options and allowed the establishment of cell culture systems for the study of HBV and HDV infections. The overexpression of human NTCP confers susceptibility towards HBV and HDV infection in otherwise unreceptive cells [75]. Nevertheless, an efficient infection of these cell lines requires the addition of DMSO and PEG in the media during the process of HBV and HDV infections [16-20]. Also, DMSO is regularly used as a differentiation agent in hepatoma cell lines in order to restrict the cells from proliferating during the experimental period [372] by the reversible arrest of the cell cycle in its G1 stage [373].

However, so far no study has thoroughly dissected the mechanism by which DMSO exerts this effect on HBV infections. DMSO seems to have a broad impact on different biological processes and should thus be applied with caution [374]. It is commonly used as solvent for water-insoluble reagents or as control for drug therapies [266; 349], without fully understanding the multitude of effects that DMSO may impose on biological processes. DMSO might act directly on the DNA level, as it has been used for many years in PCR reactions to resolve DNA secondary structures and supercoiling [375; 376], and it has been shown to alter expression levels of DNA methylation enzymes and genome-wide DNA methylation profiles [377; 378]. Its effect on HBV infectivity has been linked to various processes including a reinforced viral attachment to HSPGs on the cell surface [44] and an enhanced expression of the NTCP receptor [379]. Additionally, it has been reported that DMSO exposure could lead to rearrangements of the cytoskeleton and an enhanced translocation of NTCP from intracellular pools to the cell surface [380-382]. Nevertheless, the enhanced susceptibility towards HBV cannot be solely attributed to the increased expression and presence of NTCP on the cell surface, since many viruses that make use

of other entry receptors also benefit from the addition of DMSO in the infection media, including HCV [287; 372], HIV [288] and influenza A [289].

4.4.1. DMSO increases rAAV transduction and expression rates

In this study, we followed up on the observation of our collaboration partner Michael Nassal that DMSO also enhances transduction rates of rAAV vectors and investigated this finding in more detail in a comprehensive reporter-based assay (Figure 24 and Supplementary Figure 3). This assay was adopted from a recent study from our lab, in which Börner, Kienle and colleagues screened 13 different AAV capsid variants in combination with 27 different peptide insertions that are displayed on their capsid surface for their capacity to transduce over 90 cell types [227]. The packaging of a CMV promoter-driven YFP reporter on a dsAAV vector genome into over 300 capsid variants allowed for an automated microscopy-based and high-throughput read-out to assess the percentage of transduced cells and the transgene expression rates in an experimental format of 96- or 384-well plates. Here, we used 12 AAV wt capsids and 11 selected peptide display variants that either did not efficiently transduce hepatoma cell lines of human (HepG2 and Huh7) or mouse (Hepa16) origin and mouse neuroblasts (N2A), or that exhibited high or medium transduction capabilities. The underlying idea was to try and further boost transduction efficiencies of under-performing AAV variants by the addition of 2.5% DMSO in the transduction media.

In general, we observed that the promoting effect of DMSO strongly depended on the rAAV variant and cell line (Figure 24 and Supplementary Figure 3). Indeed, all rAAV variants showed an increase in transduction and expression rates in at least one cell line, except for rAAV4, rAAV5, rAAVpoc1, rAAV12, and rAAV1A1NIS. These exceptions failed to be improved in any of the cell lines and will be further discussed in the following section. An extension of this reporter assay to investigate DMSO-mediated advantages in the transduction of primary cells and stem cells might be of interest and could be highly relevant for *ex vivo* therapies. However, we raise a note of caution about the wide and partly unknown impact of DMSO on different biological processes [374]. Instead of a therapeutic application, we would rather promote this method as an easy and straightforward option to boost rAAV-mediated transgene expression in cell culture experiments. For instance, DMSO could be used to test the functionality of rAAV vectors in relevant but otherwise non-permissive cell lines before applying the vector in *in vivo* experiments.

Accordingly, in a relevant cell culture experiment, we aimed to boost rAAV-mediated CRISPR/Cas9 expression by the addition of DMSO in order to enhance targeted mutagenesis rates to experimentally significant extents. In our experiments, we noticed that transduction of N2A cells was particularly difficult to accomplish with ssAAV vectors (Supplementary Figure 4). The Cas9 transgene exceeded the packaging capacity of dsAAV and thus allowed packaging only in the context of ssAAV genomes, which resulted in hardly any CRISPR-induced mutations at the targeted *mecp2* locus in N2A cells in all our experiments (Figure 28A, B and Figure 30B). Surprisingly, the addition of DMSO mediated an increase of up to 20-fold in mutagenesis rates for the rAAV9A2-delivered CRISPR system in TIDE sequencings (Figure 28B). While it has been implied before that DMSO facilitates DNA accessibility for the CRISPR/Cas9 system [383], this dramatic increase in knock-out efficiencies likely derived from an increased viral uptake (Figure 28C) and an additional increase in Cas9 and sgRNA expression (Figure 28D & E).

A slight improve in mutagenesis rates was also observed for the rAAV5-delivered CRISPR system (Figure 28A & B), which was not mediated by an increase of viral uptake (Figure 28C), but derived only from enhanced Cas9 expression (Figure 28D). Our previous reporter assay failed to reveal these subtle differences (Figure 24E). Indeed, a previous study pointed out that standard screening methods based on fluorescence reporters are not sensitive enough to track low rAAV transduction rates and that editing-dependent reporter systems are a more sensitive measure to investigate differences in rAAV tropism [384]. The diverging effects of DMSO on the transduction and expression rates of different rAAV variants are discussed in the following section.

4.4.2. Differences in AAV serotypes might lead to divergent DMSO-mediated effects

DMSO might differentially influence the different processes in the AAV life cycle of various serotypes, but more extensive experiments are required to clearly confirm this. Nonetheless, our experiments indicate that DMSO enhances viral uptake and transgene expression of rAAV9A2 and most other rAAV variants, while rAAV4 and rAAV5 remain almost unaffected (Figure 24 and Figure 28).

An increasing number of reports emphasize AAV4 and AAV5 as the most divergent serotypes among known AAV isolates with regard to their life cycle [385; 386]. Firstly, AAV4

and AAV5 strongly differ in their surface variable regions (I to IX) compared to other serotypes [387; 388] and make use of α2-3 O- and α2-3 N-linked sialic acids [389] instead of widely utilized HSPGs for their initial cell surface binding [229; 390]. Secondly, while nearly all AAV serotypes are internalized via interaction with the universal AAVR, which also plays a role in AAV trafficking through the Golgi network, AAV4 and its descendants enter cells through an alternate pathway [231; 233]. Lastly, many reports have suggested that the rate of intracellular trafficking to the nucleus, nuclear uptake and capsid uncoating are major barriers to efficient transduction [263; 391] and vary especially in the case of rAAV5 [386; 392-394]. In our experiments, although rAAV5 was able to enter N2A cells at remarkably high rates compared to rAAV9A2 (Figure 28C), it failed to induce efficient transgene expression (Figure 28D), probably due to inefficient internal processing.

In line with the observed effects of DMSO on HBV infection [44], it might be possible that DMSO also reinforces AAV attachment to HSPG on the cell surface. Indeed, we show that DMSO-mediated viral uptake remained dependent on HSPG binding (Figure 26). Alternatively, DMSO could also induce changes in the cytoskeleton and thus affect intracellular trafficking [382] or enhance expression or recycling of AAVR or other co-receptors (similar to DMSO-mediated effects on the NTCP receptor [379]) that differentially impact the AAV serotypes.

4.4.3. Alternative methods to increase rAAV tranduction

Many chemical compounds are in use to boost the rather inefficient process of rAAV transduction and most of them aim to inhibit the proteasome machinery [214]. It has been shown that the proteasome inhibitors MG132 and LLNL can enhance transduction rates by 10- to 100-fold for rAAV2 and rAAV5 in cell culture and also delay viral DNA decay [262; 265]. Furthermore, rAAV2 and rAAV5 capsids are ubiquitinated *in vivo* and *in vitro* [262; 264] and transduction can be increased, albeit only by about 3-fold, by treatment with an E3 ubiquitin ligase inhibitor [264]. This led to the hypothesis that a high amount of internalized rAAVs undergo ubiquitin conjugation of the capsid and become subjected to proteasome degradation. However, the mechanism of ubiquitination on rAAV transduction and the effect of proteasome inhibitors seem to be more complex and remain unexplained as-of-yet. It has also been suggested that the proteasome machinery is involved in internal trafficking and rAAV capsid processing [214; 395], as the dramatic increase in transduction rates induced by these inhibitors cannot be explained solely by the inhibition of proteasome-mediated virus degradation. Accordingly, proteasome inhibitors might

increase AAV trafficking to the nucleus by enigmatic mechanisms in a cell- and serotype-specific manner.

Likewise, it has been reported that Doxorubicin enhances transduction 10- to 100-fold for rAAV2 and rAAV5 [307; 395], and it also reinforced transduction rates in our own experiments (Figure 27A). Doxorubicin is known as a topoisomerase inhibitor [396] and also acts as a proteasome-modulating agent [397]. As such, it might contribute to rAAV accumulation in the nucleus and simultaneously increase second-strand genome conversion [395]. However, strong cytotoxic effects have been associated with the use of these proteasome inhibitors and modulators [396; 398-400] and were also evidenced in our experiments by high rates of cell death (Figure 27A).

Another study aimed to enhance rAAV transduction by increasing the levels of autophagy, which can be induced by the addition of rapamycin that acts as an inhibitor of the mammalian target of rapamycin (mTOR) pathway [266]. In their study [266], the authors argued that rAAV transduction induced autophagy (similar to other viral infections [401]) and that rAAV vectors require this cell response for efficient transduction, as inhibition of autophagy resulted in decreased levels of transgene expression [266]. In turn, the authors hypothesized that an increase of rapamycin-induced autophagic activity could also lead to enhanced rAAV transduction and, indeed, they observed an about 2- to 3-fold increase in transgene expression.

In our own experiments, we repeatedly failed to replicate this effect and even observed a decrease in transduction rates by the addition of rapamycin in various experimental approaches (Figure 27). It might be that we were not able to induce the described manipulation on autophagy upon rapamycin addition or that an increase in autophagic activity actually leads to decreased rAAV transduction. In line with the latter conclusion, others also reported reduced rAAV2 transduction efficiencies upon induction of autophagy [402]. In this scenario, autophagy is considered as the cell´s primary degradation mechanism in response to accumulated nano-sized particles and exerts antiviral properties [401]. Indeed, AAV might depend on autophagy to enter cells and thus inhibition of autophagy limits rAAV transduction, however, it was never highlighted as rate-limiting step in rAAV transduction.

Taken together, we propose DMSO as an alternative method to increase rAAV transduction rates in cell culture that is, however, dependent on the rAAV serotype and the cell line. Current transduction enhancers either failed to induce the predicted effect on rAAV transduction in our hands or relied on the modulation of proteasome-related mechanisms associated with substantial cytotoxic effects. In contrast, no toxic effects

were observed for the treatment with DMSO, yet in line with previous reports cell proliferation rates decreased [372; 373] depending on the cell line (Figure 24). Also noteworthy is the fact that DMSO is widely used for medical purposes in patients [403]. Still, it remains to be determined whether DMSO treatment can advance the therapeutic index of rAAV vectors *in vivo*.

4.5. Split and self-inactivating Cas9 are promising designs for rAAV-mediated delivery

Among all viral vectors that are currently used in the field of gene therapy, rAAV vectors emerged as the most promising candidate for *in vivo* applications. This success can be mostly attributed to the comparatively high safety profile of rAAV vectors that is characterized by low genotoxicity and mild immune reactions [404; 405]. Recombinant AAV vectors are widely applied for the delivery of the CRISPR/Cas9 components *in vivo* and permanent modifications of disease-relevant genes were realized in the liver [189; 267; 272; 406-408], brain [409-412], muscle [339; 413-415], eye [416-418], heart [272; 419; 420] and lung [409]. Nevertheless, some hurdles restrict the applicability of rAAV/CRISPR vectors that include i) the limited packaging capacity, ii) low transgene expression rates, and iii) the persistent transgene expression that might be beneficial in some cases, but raises major safety concerns for CRISPR applications. It would be highly favorable for the next generation of rAAV vectors to incorporate systems that help to overcome these barriers and contribute to safeguard the CRISPR technology. To this end, we built upon CRISPR systems that incorporate a splitCas9 (previously developed in my M.Sc. thesis) and self-inactivating approach (designed by Julia Fakhiri in the lab) that circumvents the size restriction imposed by the dsAAV vector and benefits from its enhanced and accelerated transgene expression. Next to enhanced on-target editing rates, the self-inactivating system contributes to an efficient reduction of lingering Cas9 protein and thereby reduces the risk of unintended off-target editing.

4.5.1. SplitCas9 systems circumvent the rAAV vector packaging limitations

One of the major drawbacks of rAAV/CRISPR vectors is their limited cargo capacity of about 5 kb for designated transgene expression cassettes. Vectors exceeding the upper size limit suffer from inefficient viral production and transgene truncations [421].

Considering the size of the most frequently used *Sp*Cas9 ortholog of 4.1 kb, or the smaller *Sa*Cas9 of 3.2 kb, this leaves little flexibility in the choice of regulatory elements, such as promoters and polyA signals, and an all-in-one vector that includes an sgRNA expression cassette is barely feasible [267]. Fortunately, work reported over the last five years produced an elegant solution in the form of various splitCas9 strategies [268], including Cas9 reconstitution via intein *trans* splicing [269-272].

Split inteins have been exploited in the past to circumvent ssAAV packaging limitations for various large proteins by the delivery of two independent rAAV vectors [422]. In 2015, the team of Oskar Ortiz was the first to apply this concept to split and reconstitute *Sp*Cas9 by the use of *Npu*DnaE inteins [269]. In their experiments, splitCas9 induced robust targeting of a fluorescence-based reporter and various endogenous genes at levels comparable to wt Cas9. Most notably, they also showed that the intein-splitCas9 could be packaged and delivered in two separate ssAAV vectors and induce gene editing after its reconstitution in different cell lines. However, as the wt/full-length Cas9 control was missing, it remained unclear whether there was a potential loss of CRISPR activity for the splitCas9 in context of rAAV vectors. On top the authors also developed a split system based on nCas9 mutants and demonstrated that the reduced sizes of the splitCas9 halves allow for the co-delivery of an HDR repair template on the same ssAAV vector.

Shortly after this study, the team of Gang Bao [270] reported a similar intein *trans*-splicing approach in which they used *Mxe GyrA* inteins (which are involved in the regulation of Gyrase A from *Mycobacterium xenopi* in its natural context) to split and reconstitute *Sp*Cas9. However, when tested in transient plasmid transfection, this splitCas9 version yielded only a fraction of the cleavage efficiency of wt Cas9 and failed to induce mutations in some of the tested target cell lines. The reasons for the lower potency of this splitCas9 system remained open, but could relate to the different intein systems. Indeed, it has been reported that *Npu*DnaE inteins are highly efficient protein *trans*-splicing agents and mediate a robust activity with an efficiency of >98%, which is superior to most other inteins [278; 423]. My own results previously obtained in my MSc work confirmed that splitCas9 based on *Npu*DnaE inteins yielded about 50% of wtCas9 activity in a fluorescence reporter assay. An alternative explanation for the reduced efficiency of their splitCas9 system is the fact that Fine *et al.* [270] transfected only half the amount of each plasmid containing the splitCas9 parts as compared to wt/full-length Cas9 in order to match the total amount of transfected DNA in all conditions. Accordingly, they might have encountered a stronger dose dependency of their splitCas9 system, suggesting that the kinetics of Cas9 reconstitution are rate-limiting. In our own

transfection experiments, we adopted the same approach as Fine *et al.* (2015) and used only half the amount of each splitCas9 part as compared to full-length Cas9 (Figure 29). Furthermore, by exchanging promoters of varying expression strength, we indeed confirm that the efficiency of the intein-splitCas9 system strongly depends on the expression and reconstitution of the splitCas9 halves (Figure 29).

Yet another study carried the intein-splitCas9 system to the next level by segregating *Sp*Cas9 in three instead of two parts [271]. This enabled the development of logic AND circuits and the coupling of sensory switches to different interchangeable dCas9 domains, which in turn enables differential regulation of various genes. The authors increased the complexity of this system by including C-terminal Cas9 domains with altered PAM specificity and by linking the activation of two different genes in response to cell-type specific microRNAs. Taken together, the remarkable flexibility of these splitCas9-based genetic circuits contribute to a comprehensive toolbox with minimized CRISPR components that are highly compatible with rAAV vectors.

Another impressive study from the team of George Church applied inteins from *Rhodothermus marinus* to split and reconstitute *Sp*Cas9 and demonstrated the feasibility of this approach in a comprehensive *in vivo* investigation [272]. In their approach, the two Cas9 halves were delivered by separate ssAAV vectors of various serotypes to multiple cell types and tissues in mice including the liver, heart, muscle, brain and gonads. SplitCas9 activity highly correlated with the vector copy numbers in each tissue, in so far that the highest rAAV vector copy number (of around 10^3 vector genomes per diploid cellular genome) resulted in the highest editing rate of 10.9% in the liver. In contrast, splitCas9 yielded very low editing rates in other organs (<3%). Nonetheless, these data provide the first evidence of the feasibility of *in vivo* gene editing by the rAAV/splitCas9 technology. Further results from this study show that expression of splitCas9 in muscles, either delivered in rAAV vectors or via electroporation of plasmid-encoded Cas9, induces a cellular and humoral anti-Cas9 immune response in mice. However, unlike other delivery methods, rAAV/splitCas9 did not induce extensive cellular damage and thus encourages the translation of the rAAV/splitCas9 platform towards clinical settings.

Finally, in my M.Sc. work in the lab of Prof. Barbara Di Ventura and Prof. Roland Eils, we also developed a splitCas9 system, which yet differed from other strategies by various properties. Firstly, in my previous work we compared *Npu*DnaE and gp41-1 inteins in their efficiency to reconstitute Cas9 to its full-sized version. We were able to confirm previous reports that demonstrated that the gp41-1 inteins are the most efficient inteins [277; 279] that also exhibit less stringent extein requirements compared to other inteins, as

they only depend on a C-terminal serine on the split junction in order to facilitate the *trans*-splicing reaction [276]. Secondly, we aimed to split the smaller Cas9 ortholog from *Staphylococcus aureus* that consequently resulted in even smaller split*Sa*Cas9 halves, thus further liberating the size restriction imposed by rAAV vectors. Altogether, my M.Sc. work evaluated a small split*Sa*Cas9 library consisting of three split sites in combination with two inteins in comprehensive plasmid transfection experiments and demonstrated efficient gene editing rates for all split variants (although gp41-1-bearing splitSaCas9 variants performed better). Lastly and most importantly, my M.Sc. work already suggested the compatibility of the smaller split*Sa*Cas9 system with dsAAV vectors, that might enable enhanced expression of the *Sa*Cas9 halves with improved kinetics and higher *in vivo* DNA stability of the vector [255; 257; 261].

4.5.2. Enhanced targeted mutagenesis by the dsAAV/split*Sa*Cas9 system

In this doctoral thesis, we built upon the split*Sa*Cas9 system that was previously developed in my M.Sc. work. While the previous work focused on the rational design and functional testing via plasmid transfection experiments of the split*Sa*Cas9 library, the presented work evaluated one selected split*Sa*Cas9 variant (gp41-1-split version 3) in the context of rAAV vectors.

Here, we were able to confirm our hypothesis that was already formulated during my previous M.Sc. thesis and indeed demonstrated an accelerated and highly enhanced knock-out efficiency for the dsAAV/split*Sa*Cas9 compared to ssAAV/wt*Sa*Cas9 (Figure 30). It has been reported that the expression benefit of dsAAV over ssAAV is strongly dependent on the cell type [255; 261] and, indeed, the efficiency of the dsAAV/split*Sa*Cas9 system also varied over our experiments. Our experiments demonstrated a strong advantage of the dsAAV/split*Sa*Cas9 system over ssAAV/wt*Sa*Cas9 in N2A cells and primary myoblasts (Figure 30 and Figure 31), while no advantages were observed in Huh7 cells (Figure 31).

This study also demonstrated that Cas9 expression is a rate-limiting factor for *in vivo* gene editing in the liver of mice. Firstly, this was evidenced by the comparison of different promoters that expressed *Sa*Cas9 with varying strength, which led to correlating gene editing rates of a luciferase reporter (Figure 21). Secondly, the delivery by dsAAV vectors resulted in stronger expression of the split*Sa*Cas9 system and higher vector

DNA stability in the liver (Figure 32D and E), and it was clearly associated with the degree of luciferase signal reduction and gene editing rates (Figure 32B and C).

The versatility of dsAAV vectors *in vivo* has been demonstrated by their ability to efficiently transduce many different cell types, including murine muscle, liver, central nervous system and many other organs [256; 424]. In addition to the enhanced vector expression rates, the dsAAV also seemed to mediate changes in *in vivo* vector distribution, as reported by a notable study that compared the expression of human factor 9 (hFIX) in mouse liver by a ssAAV vector of serotype 2 to the expression of hFIX by dsAAV [425]. The authors reported that delivery by ssAAV vectors led to the strong expression of hFIX in roughly 5% of all hepatocytes, while dsAAV-mediated expression resulted in a homogenous distribution of moderate hFIX levels over 80% of all hepatocytes, thus reflecting a more natural situation of hFIX expression throughout the liver.

Furthermore, in a clinical study, the application of high vector doses by administration of rAAV2 through hepatic artery injection and subsequent expression of hFIX in the liver of human patients has been associated with a transient elevation of liver transaminases and a decrease of hFIX levels [426]. In addition, although controversially discussed in the field, it has been observed that intravenous administration of a high dose of rAAV9 expressing human SMN (survival of motor neuron) protein resulted in severe hepatotoxicity in non-human primates and piglets [427]. In these cases, the dsAAV vector might offer a practical solution to the dose-dependent side effects on the host immune system, as it inherently mediates stronger and more homogenous transgene expression and thus can be applied at lower doses. Along these lines, the large-scale production of highly purified rAAV vectors that comply with good manufacturing practice is cost-intensive and currently a rate-limiting process. Thus, the use of lower dsAAV vector doses might help to overcome bottlenecks of production and facilitate a distribution of rAAV-based gene therapy to all patients in need [428].

However, the question lingers whether rAAV vectors represent the best possible solution to deliver the CRISPR technology *in vivo*. While the feature of rAAV vectors to express transgenes for life-long periods [204; 429] is beneficial for applications that require long-lasting expression, such as RNAi that only acts on the mRNA level and is reversible depending on the presence of its RNA trigger, it might be detrimental for CRISPR applications. Once CRISPR/Cas9 induced a mutation at a target locus, the effect is permanent and irreversible. Thus, although a strong CRISPR/Cas9 expression is desirable to achieve efficient on-target editing (as demonstrated in our experiments by

various means, *e.g.* addition of DMSO (Figure 28) and expression by dsAAV vectors (Figure 30)), no lasting expression is required. Indeed, the amount and duration of Cas9 expression has been associated with an increase in off-targeting [192; 193; 272; 430] and an aggravated host immune response against Cas9 [272]. To safeguard our technology, we included a self-inactivating (SIN) approach to our dsAAV/split*Sa*Cas9 system in order to restrict the presence of Cas9 after successful on-target cleavage, as described in the following section.

4.5.3. The dsAAV/split*Sa*Cas9 system efficiently self-inactivates after targeted knock-out

Intriguing alternative delivery systems for CRISPR applications *in vivo* with improved safety profiles are the delivery of Cas9 as mRNA, or as RNP complex of Cas9 protein and sgRNA via lipid nanoparticles (LNPs) instead of viral vectors [431-433]. The advantages of such alternative CRISPR delivery systems include the high immunotolerance and the transient Cas9 presence in cells, which was demonstrated to reduce off-target effects [434]. However, it remains to be evaluated whether LNP-based approaches are as efficient as rAAV-mediated delivery of the CRISPR components. Furthermore, while the capsids of rAAVs can be designed to increase specificity towards certain cell types and tissues, the majority of systemically injected LNPs accumulate in the liver. As long as the hurdles of efficiency and specificity for LNP-based approaches persist, the consensus prevails in the field that rAAV vectors represent the most attractive vehicles for CRISPR/Cas9 delivery *in vivo* [189; 267; 414].

Accordingly, the SIN CRISPR approach that has been implemented by Julia Fakhiri from our lab illustrates a great potential for a future generation of rAAV/CRISPR vectors with an increased safety profile [294]. The SIN approach utilizes the inherent DNA cleavage activity of Cas9 to destroy its own virally encoded transgene sequence by directing an additional sgRNA against itself. By the use of different RNA polymerase III promoters with varying kinetics to drive the two sgRNAs (against the on-target and the Cas9 transgene), the on-target knock-out can be realized before Cas9 self-inactivates (Figure 31). Here, we combined the dsAAV/split*Sa*Cas9 system with the SIN approach to circumvent its major limitation that at the same time represents its greatest asset, namely, the strong Cas9 expression that on the one hand leads to enhanced on-target mutagenesis rates and on the other hand also increases off-targeting [435]. Thus, the

presented and validated SIN rAAV vectors combine the efficient delivery of CRISPR/Cas9 by dsAAV vectors with restricted and thus safer Cas9 expression.

Notably, in parallel to our work, other research groups concurrently reported similar strategies to restrict Cas9 expression by supplying anti-Cas9 sgRNAs. These approaches include plasmid- [435], lentiviral- [430; 436; 437] and rAAV-based [438; 439] CRISPR delivery systems that mainly aim to self-restrict expression of Cas9 from *Streptococcus pyogenes* and in one study Cas9 from *Staphylococcus aureus* [439]. Most systems provide the anti-Cas9 sgRNA on an additional viral vehicle in order to prevent Cas9 cleavage during vector production. By contrast, in the lentiSLiCES system [430], a single lentiviral vector was designed to express the Cas9, the target sgRNA and the anti-Cas9 sgRNA simultaneously. Premature self-cleavage of Cas9 during vector preparations was inhibited by the regulation of Cas9 expression via tetracycline-responsive elements and the use of producer cell lines that stably expressed the Tet repressor.

In principle, Cas9 activity could also be inhibited on the protein level using phage-derived anti-CRISPR proteins that have been recently discovered [198]. Besides the tight control of Cas9 cleavage activity (that is further discussed in the following section), another interesting application of the Acr proteins might be the prevention of self-cleavage by SIN/CRISPR in all-in-one vectors during vector preparations.

4.6. Use of Acr proteins to safeguard the CRISPR technology

Despite its enormous potential, we raise a note of caution when using the CRISPR technology and recommend to carefully evaluate possible side effects. It has been reported that CRISPR is not only associated with possible off-target events, but could also lead to chromosomal translocations, inversions and large deletions by the concurrent presence of multiple DSBs that are either CRISPR-induced or occur naturally at breakpoint hotspots within the cell [290]. In this respect, HBV seems like a comparatively safe target, as it predominantly persists in the form of extrachromosomal cccDNA. However, HBV integrates have been reported that occur at low frequencies [55-57], and that should also be considered as possible CRISPR targets. Thus, a systematic analysis of desired and adverse effects, *e.g.* by next-generation sequencing [290], should be mandatory for *in vivo* evaluations of all CRISPR approaches that are destined for clinical translation.

One approach to safeguard the CRISPR technology is the use of anti-CRISPR proteins [198] that were previously engineered by the lab of Dominik Niopek to enhance the precision of gene editing in a spatio-temporal manner [202; 203]. The spectrum of Acr proteins is steadily increasing owing to the discovery of natural Acr orthologs by screening of phage libraries and interrogation of sequence databases [200; 440-443]. The lab of Dominik Niopek further extended the natural sequence space of Acr proteins by designing chimeric and, in a collaboration with us, engineered Acr variants.

One interesting inhibitor is AcrIIC1 [199], as it represents a broad-spectrum inhibitor that prevents cutting by multiple Cas9 orthologs including those from *Neisseria meningitidis*, *Campylobacter jejuni* and *Geobacillus stearothermophilus* [201]. AcrIIC1 binds to the Cas9 HNH domain and locks the endonuclease in a DNA-bound, but catalytically inactive state. This represents a unique mechanism, as other related inhibitors prevent Cas9 from either binding to its target DNA or from loading crRNAs [444] and it might also explain the weak inhibition of AcrIIC1 compared to AcrIIC3, AcrIIC4, or AcrIIC5 [445; 446].

The lab of Dominik Niopek was able to enhance inhibition of AcrIIC1 towards *Nme*Cas9 by inserting an exogenous domain in the surface-exposed loop 5 of the inhibitor [311]. Different AcrIIC1 chimeras were screened comprising an *Avena sativa* LOV2, mCherry or PDZ domain and indeed most (except for the AcrIIC1-PDZ chimera) efficiently inhibited *Nme*Cas9 cleavage to such an extent that they outperformed parental AcrIIC1 and also AcrIIC3, so far the most potent *Nme*Cas9 inhibitor [199]. Although the mechanism behind the effects of domain insertions remained unclear, they were able to assign the increased inhibition to higher AcrIIC1-chimera expression levels and more potent inhibition of *Nme*Cas9 activity. Similar to the parental AcrIIC1, the chimera did not interfere with *Nme*Cas9's binding ability as evidenced in electromobility shift assays. The chimeras demonstrate the versatility of AcrIIC1 and thus, in the second part of the same publication, Dominik Niopek initiated a collaboration with Bruno Correia (Institute of Bioengineering, Lausanne) and us to expand the AcrIIC1 specificity towards the type II-A CRISPR/Cas9 system from *Staphylococcus aureus.*

As indicated before, the *Sa*Cas9 is the preferred ortholog when it comes to *in vivo* gene editing, as its smaller size facilitates its packaging in rAAV vectors. The HNH domains of *Nme*Cas9 and *Sa*Cas9 resemble each other in terms of the overall structure (see section 1.5.2) [201], albeit they share only 33.7% identity on the sequence level [311]. Studies have reported either no detectable or very weak inhibition of AcrIIC1 on *Sa*Cas9 [309; 447]. Our own experiments confirmed a weak functional inhibition of AcrIIC1 on *Sa*Cas9 (Figure 33) and the lab of Bruno Correia verified an affinity of purified AcrIIC1 towards the HNH

domains of *Sa*Cas9 (K_D= 370 nM) in surface plasmon resonance affinity measurements, albeit to much weaker extent when compared to its actual *Nme*Cas9 target (K_D= 0.95 nM) [311]. Thus, Dominik Niopek figured that AcrIIC1 might be the ideal starting point to engineer its Cas9 binding surface and enhance affinity towards the *Sa*Cas9 HNH domain. A structural model that was developed by Bruno Correia and his team pointed to two regions in *Sa*Cas9 with suboptimal contacts to the corresponding AcrIIC1 residues. By performing *in silico* mutagenesis of these regions using Rosetta design [310], they provided Dominik Niopek with different mutations that could, based on their model, improve binding to *Sa*Cas9 HNH domain. In the presented work, Dominik Niopek initiated a collaboration with us to first evaluated these single point mutations and then iteratively combined the most promising variants in subsequent screening rounds (Figure 33). We yielded AcrX (also referred to as AcrIIC1X in the corresponding publication) that efficiently inhibited *Sa*Cas9 gene editing on several loci (Figure 34) [311]. Indeed, Bruno Correia and his team could verify that binding affinity towards *Sa*Cas9 HNH domain improved (K_D= 53 nM), compared to wt AcrIIC1 (K_D= 370 nM). Concomitantly, albeit the affinity of AcrX to *Nme*Cas9 HNH domain was reduced, it remained within low nanomolar range (K_D= 6.9 nM). While the insertion of an mCherry domain in loop 5 of AcrX did not improve inhibition of *Sa*Cas9, it again offered tight control over *Nme*Cas9.

Finally, we take note of the rapid developments in the anti-CRISPR field. In parallel to the work on AcrX, it has been reported that *Sa*Cas9 can be inhibited by AcrIIA5 [447-449] and AcrIIA13-15 (bioRxiv: https://doi.org/10.1101/799403). Still, the presented work is not to be seen as replacement to the search for natural Acrs, but instead as highly complementary approach to increase their inhibitory potential either by domain insertions or by structural guided designs.

In view of recent developments of CRISPR gene drives that enable the forced propagation of genetic elements over populations via CRISPR-directed biases in inheritance [450-453], anti-CRISPR interventions might be necessary safety measures to prevent the uncontrollable spread or exploitation of this powerful technology. Indeed, the spread of CRISPR gene drives into nature could even arise as a result of a laboratory accident and thereby could have the potential to genetically alter entire species [451; 454]. To prevent this, scientists have devised severeal strategies to safeguard this technology, *e.g.* i) synthetic target site gene drives that utilize target sites artificially introduced solely in a laboratory strains, thus preventing the spread to wild creatures that lack the synthetic target site, ii) split systems that segregate the CRISPR gene drive components in physically separate parts, namely an episomally encoded Cas9 gene and a gene drive

element encoding the sgRNA [451] and iii) anti-CRISPR proteins that enable an off-switch of the gene drive [455]. In principle, several of the developed strategies in the presented dissertation could be employed in future work to further safeguard the CRISPR technology, especially in the context of gene drives. First of all, the split*Sa*Cas9 system could enable a similar physical segregation of the CRISPR gene drive components as indicated in strategy ii) by encoding one split half as gene drive component, while the other half is provided episomally and thus enable a tighter control on the level of Cas9 effector protein. Furthermore, a SIN approach could be introduced that limits the presence of Cas9 and might be able to switch off the CRISPR gene drive. And lastly, the presented strategies of designer-Acrs could increase the inhibitory potency against CRISPR gene drives and enable inhibition of gene drives based on Cas9 orthologs, for which so far no natural Acr has been discovered.

5. REFERENCES

1. Stanaway, J.D., Flaxman, A.D., Naghavi, M., Fitzmaurice, C., Vos, T., Abubakar, I., Abu-Raddad, L.J., Assadi, R., Bhala, N., Cowie, B., et al. (2016). The global burden of viral hepatitis from 1990 to 2013: findings from the Global Burden of Disease Study 2013. Lancet 388, 1081-1088.
2. Cooke, G.S., Andrieux-Meyer, I., Applegate, T.L., Atun, R., Burry, J.R., Cheinquer, H., Dusheiko, G., Feld, J.J., Gore, C., Griswold, M.G., et al. (2019). Accelerating the elimination of viral hepatitis: a Lancet Gastroenterology & Hepatology Commission. Lancet Gastroenterol Hepatol 4, 135-184.
3. WHO. (2012). WHO position paper on hepatitis A vaccines - June 2012. Wkly Epidemiol Rec 87, 261-276.
4. Zhang, J., Zhang, X.F., Huang, S.J., Wu, T., Hu, Y.M., Wang, Z.Z., Wang, H., Jiang, H.M., Wang, Y.J., Yan, Q., et al. (2015). Long-term efficacy of a hepatitis E vaccine. N Engl J Med 372, 914-922.
5. WHO. (2017). Global Hepatitis Report 2017. In ISBN 978-92-4-156545-5 (
6. Vos, T.A., Christine; Arora, Megha; Barber, Ryan M.; Bhutta, Zulfiqar A.; Brown, Alexandria; Carter, Austin; Casey, Daniel C.; Charlson, Fiona J.; Chen, Alan Z.; Coggeshall, Megan; Cornaby, Leslie; Dandona, Lalit; Dicker, Daniel J.; Dilegge, Tina; Erskine, Holly E.; Ferrari, Alize J.; Fitzmaurice, Christina; Fleming, Tom; Forouzanfar, Mohammad H.; Fullman, Nancy; Gething, Peter W.; Goldberg, Ellen M.; Graetz, Nicholas; Haagsma, Juanita A.; Hay, Simon I.; Johnson, Catherine O.; Kassebaum, Nicholas J.; Kawashima, Toana. (2016). Global, regional, and national incidence, prevalence, and years lived with disability for 310 diseases and injuries, 1990-2015: a systematic analysis for the Global Burden of Disease Study 2015. Lancet 388, 1545-1602.
7. Hoofnagle, J.H. (1997). Hepatitis C: the clinical spectrum of disease. Hepatology 26, 15S-20S.
8. Webster, D.P., Klenerman, P., and Dusheiko, G.M. (2015). Hepatitis C. Lancet 385, 1124-1135.
9. McMahon, B.J. (2005). Epidemiology and natural history of hepatitis B. Semin Liver Dis 25 Suppl 1, 3-8.
10. Lempp, F.A., Ni, Y., and Urban, S. (2016). Hepatitis delta virus: insights into a peculiar pathogen and novel treatment options. Nat Rev Gastroenterol Hepatol 13, 580-589.
11. Tajiri, K., and Shimizu, Y. (2015). Unsolved problems and future perspectives of hepatitis B virus vaccination. World J Gastroenterol 21, 7074-7083.
12. Trepo, C., Chan, H.L., and Lok, A. (2014). Hepatitis B virus infection. Lancet 384, 2053-2063.
13. Alfaiate, D., Deny, P., and Durantel, D. (2015). Hepatitis delta virus: From biological and medical aspects to current and investigational therapeutic options. Antiviral Res 122, 112-129.
14. Honer Zu Siederdissen, C., Rinker, F., Maasoumy, B., Wiegand, S.B., Filmann, N., Falk, C.S., Deterding, K., Port, K., Mix, C., Manns, M.P., et al. (2016). Viral and Host Responses After Stopping Long-term Nucleos(t)ide Analogue Therapy in HBeAg-Negative Chronic Hepatitis B. J Infect Dis 214, 1492-1497.
15. Yan, H., Zhong, G., Xu, G., He, W., Jing, Z., Gao, Z., Huang, Y., Qi, Y., Peng, B., Wang, H., et al. (2012). Sodium taurocholate cotransporting polypeptide is a functional receptor for human hepatitis B and D virus. Elife 1, e00049.
16. Ni, Y., Lempp, F.A., Mehrle, S., Nkongolo, S., Kaufman, C., Falth, M., Stindt, J., Koniger, C., Nassal, M., Kubitz, R., et al. (2014). Hepatitis B and D viruses exploit sodium taurocholate co-transporting polypeptide for species-specific entry into hepatocytes. Gastroenterology 146, 1070-1083.
17. Gripon, P., Diot, C., Theze, N., Fourel, I., Loreal, O., Brechot, C., and Guguen-Guillouzo, C. (1988). Hepatitis B virus infection of adult human hepatocytes cultured in the presence of dimethyl sulfoxide. J Virol 62, 4136-4143.
18. Pugh, J.C., and Summers, J.W. (1989). Infection and uptake of duck hepatitis B virus by duck hepatocytes maintained in the presence of dimethyl sulfoxide. Virology 172, 564-572.
19. Paran, N., Geiger, B., and Shaul, Y. (2001). HBV infection of cell culture: evidence for multivalent and cooperative attachment. EMBO J 20, 4443-4453.
20. Gripon, P., Rumin, S., Urban, S., Le Seyec, J., Glaise, D., Cannie, I., Guyomard, C., Lucas, J., Trepo, C., and Guguen-Guillouzo, C. (2002). Infection of a human hepatoma cell line by hepatitis B virus. Proc Natl Acad Sci U S A 99, 15655-15660.

21. Babinet, C., Farza, H., Morello, D., Hadchouel, M., and Pourcel, C. (1985). Specific expression of hepatitis B surface antigen (HBsAg) in transgenic mice. Science 230, 1160-1163.
22. Chisari, F.V., Filippi, P., McLachlan, A., Milich, D.R., Riggs, M., Lee, S., Palmiter, R.D., Pinkert, C.A., and Brinster, R.L. (1986). Expression of hepatitis B virus large envelope polypeptide inhibits hepatitis B surface antigen secretion in transgenic mice. J Virol 60, 880-887.
23. Guidotti, L.G., Martinez, V., Loh, Y.T., Rogler, C.E., and Chisari, F.V. (1994). Hepatitis B virus nucleocapsid particles do not cross the hepatocyte nuclear membrane in transgenic mice. J Virol 68, 5469-5475.
24. Yang, P.L., Althage, A., Chung, J., and Chisari, F.V. (2002). Hydrodynamic injection of viral DNA: a mouse model of acute hepatitis B virus infection. Proc Natl Acad Sci U S A 99, 13825-13830.
25. Sprinzl, M.F., Oberwinkler, H., Schaller, H., and Protzer, U. (2001). Transfer of hepatitis B virus genome by adenovirus vectors into cultured cells and mice: crossing the species barrier. J Virol 75, 5108-5118.
26. Dion, S., Bourgine, M., Godon, O., Levillayer, F., and Michel, M.L. (2013). Adeno-associated virus-mediated gene transfer leads to persistent hepatitis B virus replication in mice expressing HLA-A2 and HLA-DR1 molecules. J Virol 87, 5554-5563.
27. Yang, D., Liu, L., Zhu, D., Peng, H., Su, L., Fu, Y.X., and Zhang, L. (2014). A mouse model for HBV immunotolerance and immunotherapy. Cell Mol Immunol 11, 71-78.
28. Wynne, S.A., Crowther, R.A., and Leslie, A.G. (1999). The crystal structure of the human hepatitis B virus capsid. Mol Cell 3, 771-780.
29. Kay, A., and Zoulim, F. (2007). Hepatitis B virus genetic variability and evolution. Virus Res 127, 164-176.
30. Gerlich, W.H., and Robinson, W.S. (1980). Hepatitis B virus contains protein attached to the 5' terminus of its complete DNA strand. Cell 21, 801-809.
31. Tong, S., and Revill, P. (2016). Overview of hepatitis B viral replication and genetic variability. J Hepatol 64, S4-S16.
32. Radziwill, G., Tucker, W., and Schaller, H. (1990). Mutational analysis of the hepatitis B virus P gene product: domain structure and RNase H activity. J Virol 64, 613-620.
33. Zhou, S., and Standring, D.N. (1992). Hepatitis B virus capsid particles are assembled from core-protein dimer precursors. Proc Natl Acad Sci U S A 89, 10046-10050.
34. Liaw, Y.F. (2009). HBeAg seroconversion as an important end point in the treatment of chronic hepatitis B. Hepatol Int 3, 425-433.
35. Okamoto, H., Tsuda, F., Akahane, Y., Sugai, Y., Yoshiba, M., Moriyama, K., Tanaka, T., Miyakawa, Y., and Mayumi, M. (1994). Hepatitis B virus with mutations in the core promoter for an e antigen-negative phenotype in carriers with antibody to e antigen. J Virol 68, 8102-8110.
36. Milich, D., and Liang, T.J. (2003). Exploring the biological basis of hepatitis B e antigen in hepatitis B virus infection. Hepatology 38, 1075-1086.
37. Peterson, D.L., Nath, N., and Gavilanes, F. (1982). Structure of hepatitis B surface antigen. Correlation of subtype with amino acid sequence and location of the carbohydrate moiety. J Biol Chem 257, 10414-10420.
38. Eble, B.E., Lingappa, V.R., and Ganem, D. (1990). The N-terminal (pre-S2) domain of a hepatitis B virus surface glycoprotein is translocated across membranes by downstream signal sequences. J Virol 64, 1414-1419.
39. Dane, D.S., Cameron, C.H., and Briggs, M. (1970). Virus-like particles in serum of patients with Australia-antigen-associated hepatitis. Lancet 1, 695-698.
40. Bruns, M., Miska, S., Chassot, S., and Will, H. (1998). Enhancement of hepatitis B virus infection by noninfectious subviral particles. J Virol 72, 1462-1468.
41. Lucifora, J., Arzberger, S., Durantel, D., Belloni, L., Strubin, M., Levrero, M., Zoulim, F., Hantz, O., and Protzer, U. (2011). Hepatitis B virus X protein is essential to initiate and maintain virus replication after infection. J Hepatol 55, 996-1003.
42. Tsuge, M., Hiraga, N., Akiyama, R., Tanaka, S., Matsushita, M., Mitsui, F., Abe, H., Kitamura, S., Hatakeyama, T., Kimura, T., et al. (2010). HBx protein is indispensable for development of viraemia in human hepatocyte chimeric mice. J Gen Virol 91, 1854-1864.
43. Kim, C.M., Koike, K., Saito, I., Miyamura, T., and Jay, G. (1991). HBx gene of hepatitis B virus induces liver cancer in transgenic mice. Nature 351, 317-320.

44. Schulze, A., Gripon, P., and Urban, S. (2007). Hepatitis B virus infection initiates with a large surface protein-dependent binding to heparan sulfate proteoglycans. Hepatology 46, 1759-1768.
45. Huang, H.C., Chen, C.C., Chang, W.C., Tao, M.H., and Huang, C. (2012). Entry of hepatitis B virus into immortalized human primary hepatocytes by clathrin-dependent endocytosis. J Virol 86, 9443-9453.
46. Macovei, A., Radulescu, C., Lazar, C., Petrescu, S., Durantel, D., Dwek, R.A., Zitzmann, N., and Nichita, N.B. (2010). Hepatitis B virus requires intact caveolin-1 function for productive infection in HepaRG cells. J Virol 84, 243-253.
47. Li, H.C., Huang, E.Y., Su, P.Y., Wu, S.Y., Yang, C.C., Lin, Y.S., Chang, W.C., and Shih, C. (2010). Nuclear export and import of human hepatitis B virus capsid protein and particles. PLoS Pathog 6, e1001162.
48. Schmitz, A., Schwarz, A., Foss, M., Zhou, L., Rabe, B., Hoellenriegel, J., Stoeber, M., Pante, N., and Kann, M. (2010). Nucleoporin 153 arrests the nuclear import of hepatitis B virus capsids in the nuclear basket. PLoS Pathog 6, e1000741.
49. Guo, H., Xu, C., Zhou, T., Block, T.M., and Guo, J.T. (2012). Characterization of the host factors required for hepadnavirus covalently closed circular (ccc) DNA formation. PLoS One 7, e43270.
50. Belloni, L., Pollicino, T., De Nicola, F., Guerrieri, F., Raffa, G., Fanciulli, M., Raimondo, G., and Levrero, M. (2009). Nuclear HBx binds the HBV minichromosome and modifies the epigenetic regulation of cccDNA function. Proc Natl Acad Sci U S A 106, 19975-19979.
51. Riviere, L., Gerossier, L., Ducroux, A., Dion, S., Deng, Q., Michel, M.L., Buendia, M.A., Hantz, O., and Neuveut, C. (2015). HBx relieves chromatin-mediated transcriptional repression of hepatitis B viral cccDNA involving SETDB1 histone methyltransferase. J Hepatol 63, 1093-1102.
52. Decorsiere, A., Mueller, H., van Breugel, P.C., Abdul, F., Gerossier, L., Beran, R.K., Livingston, C.M., Niu, C., Fletcher, S.P., Hantz, O., et al. (2016). Hepatitis B virus X protein identifies the Smc5/6 complex as a host restriction factor. Nature 531, 386-389.
53. Bar-Yishay, I., Shaul, Y., and Shlomai, A. (2011). Hepatocyte metabolic signalling pathways and regulation of hepatitis B virus expression. Liver Int 31, 282-290.
54. Tang, H., and McLachlan, A. (2001). Transcriptional regulation of hepatitis B virus by nuclear hormone receptors is a critical determinant of viral tropism. Proc Natl Acad Sci U S A 98, 1841-1846.
55. Yang, W., and Summers, J. (1999). Integration of hepadnavirus DNA in infected liver: evidence for a linear precursor. J Virol 73, 9710-9717.
56. Summers, J., and Mason, W.S. (2004). Residual integrated viral DNA after hepadnavirus clearance by nucleoside analog therapy. Proc Natl Acad Sci U S A 101, 638-640.
57. Tu, T., Budzinska, M.A., Shackel, N.A., and Urban, S. (2017). HBV DNA Integration: Molecular Mechanisms and Clinical Implications. Viruses 9.
58. Nassal, M., and Rieger, A. (1996). A bulged region of the hepatitis B virus RNA encapsidation signal contains the replication origin for discontinuous first-strand DNA synthesis. J Virol 70, 2764-2773.
59. Habig, J.W., and Loeb, D.D. (2003). Template switches during plus-strand DNA synthesis of duck hepatitis B virus are influenced by the base composition of the minus-strand terminal redundancy. J Virol 77, 12412-12420.
60. Lentz, T.B., and Loeb, D.D. (2011). Roles of the envelope proteins in the amplification of covalently closed circular DNA and completion of synthesis of the plus-strand DNA in hepatitis B virus. J Virol 85, 11916-11927.
61. Pastor, F., Herrscher, C., Patient, R., Eymieux, S., Moreau, A., Burlaud-Gaillard, J., Seigneuret, F., de Rocquigny, H., Roingeard, P., and Hourioux, C. (2019). Direct interaction between the hepatitis B virus core and envelope proteins analyzed in a cellular context. Sci Rep 9, 16178.
62. Watanabe, T., Sorensen, E.M., Naito, A., Schott, M., Kim, S., and Ahlquist, P. (2007). Involvement of host cellular multivesicular body functions in hepatitis B virus budding. Proc Natl Acad Sci U S A 104, 10205-10210.
63. Patient, R., Hourioux, C., Sizaret, P.Y., Trassard, S., Sureau, C., and Roingeard, P. (2007). Hepatitis B virus subviral envelope particle morphogenesis and intracellular trafficking. J Virol 81, 3842-3851.

64. Jiang, B., Himmelsbach, K., Ren, H., Boller, K., and Hildt, E. (2015). Subviral Hepatitis B Virus Filaments, like Infectious Viral Particles, Are Released via Multivesicular Bodies. J Virol 90, 3330-3341.
65. Magnius, L., Taylor, J., Mason, W.S., Sureau, C., Deny, P., Norder, H., and Ictv Report, C. (2018). ICTV Virus Taxonomy Profile: Deltavirus. J Gen Virol 99, 1565-1566.
66. Makino, S., Chang, M.F., Shieh, C.K., Kamahora, T., Vannier, D.M., Govindarajan, S., and Lai, M.M. (1987). Molecular cloning and sequencing of a human hepatitis delta (delta) virus RNA. Nature 329, 343-346.
67. Farci, P. (2003). Delta hepatitis: an update. J Hepatol 39 Suppl 1, S212-219.
68. Negro, F. (2014). Hepatitis D virus coinfection and superinfection. Cold Spring Harb Perspect Med 4, a021550.
69. Fattovich, G., Giustina, G., Christensen, E., Pantalena, M., Zagni, I., Realdi, G., and Schalm, S.W. (2000). Influence of hepatitis delta virus infection on morbidity and mortality in compensated cirrhosis type B. The European Concerted Action on Viral Hepatitis (Eurohep). Gut 46, 420-426.
70. Saldanha, J.A., Thomas, H.C., and Monjardino, J.P. (1990). Cloning and sequencing of RNA of hepatitis delta virus isolated from human serum. J Gen Virol 71 (Pt 7), 1603-1606.
71. Weiner, A.J., Choo, Q.L., Wang, K.S., Govindarajan, S., Redeker, A.G., Gerin, J.L., and Houghton, M. (1988). A single antigenomic open reading frame of the hepatitis delta virus encodes the epitope(s) of both hepatitis delta antigen polypeptides p24 delta and p27 delta. J Virol 62, 594-599.
72. Polson, A.G., Bass, B.L., and Casey, J.L. (1996). RNA editing of hepatitis delta virus antigenome by dsRNA-adenosine deaminase. Nature 380, 454-456.
73. Wong, S.K., and Lazinski, D.W. (2002). Replicating hepatitis delta virus RNA is edited in the nucleus by the small form of ADAR1. Proc Natl Acad Sci U S A 99, 15118-15123.
74. Lamas Longarela, O., Schmidt, T.T., Schoneweis, K., Romeo, R., Wedemeyer, H., Urban, S., and Schulze, A. (2013). Proteoglycans act as cellular hepatitis delta virus attachment receptors. PLoS One 8, e58340.
75. Verrier, E.R., Colpitts, C.C., Bach, C., Heydmann, L., Weiss, A., Renaud, M., Durand, S.C., Habersetzer, F., Durantel, D., Abou-Jaoude, G., et al. (2016). A targeted functional RNA interference screen uncovers glypican 5 as an entry factor for hepatitis B and D viruses. Hepatology 63, 35-48.
76. Chou, H.C., Hsieh, T.Y., Sheu, G.T., and Lai, M.M. (1998). Hepatitis delta antigen mediates the nuclear import of hepatitis delta virus RNA. J Virol 72, 3684-3690.
77. Tavanez, J.P., Cunha, C., Silva, M.C., David, E., Monjardino, J., and Carmo-Fonseca, M. (2002). Hepatitis delta virus ribonucleoproteins shuttle between the nucleus and the cytoplasm. RNA 8, 637-646.
78. Chang, J., Nie, X., Chang, H.E., Han, Z., and Taylor, J. (2008). Transcription of hepatitis delta virus RNA by RNA polymerase II. J Virol 82, 1118-1127.
79. Modahl, L.E., Macnaughton, T.B., Zhu, N., Johnson, D.L., and Lai, M.M. (2000). RNA-Dependent replication and transcription of hepatitis delta virus RNA involve distinct cellular RNA polymerases. Mol Cell Biol 20, 6030-6039.
80. Macnaughton, T.B., Shi, S.T., Modahl, L.E., and Lai, M.M. (2002). Rolling circle replication of hepatitis delta virus RNA is carried out by two different cellular RNA polymerases. J Virol 76, 3920-3927.
81. Kuo, M.Y., Sharmeen, L., Dinter-Gottlieb, G., and Taylor, J. (1988). Characterization of self-cleaving RNA sequences on the genome and antigenome of human hepatitis delta virus. J Virol 62, 4439-4444.
82. Hsieh, S.Y., Chao, M., Coates, L., and Taylor, J. (1990). Hepatitis delta virus genome replication: a polyadenylated mRNA for delta antigen. J Virol 64, 3192-3198.
83. Lo, K., Hwang, S.B., Duncan, R., Trousdale, M., and Lai, M.M. (1998). Characterization of mRNA for hepatitis delta antigen: exclusion of the full-length antigenomic RNA as an mRNA. Virology 250, 94-105.
84. Kuo, M.Y., Chao, M., and Taylor, J. (1989). Initiation of replication of the human hepatitis delta virus genome from cloned DNA: role of delta antigen. J Virol 63, 1945-1950.
85. Chao, M., Hsieh, S.Y., and Taylor, J. (1990). Role of two forms of hepatitis delta virus antigen: evidence for a mechanism of self-limiting genome replication. J Virol 64, 5066-5069.
86. Chang, M.F., Chen, C.J., and Chang, S.C. (1994). Mutational analysis of delta antigen: effect on assembly and replication of hepatitis delta virus. J Virol 68, 646-653.

87. Sato, S., Cornillez-Ty, C., and Lazinski, D.W. (2004). By inhibiting replication, the large hepatitis delta antigen can indirectly regulate amber/W editing and its own expression. J Virol 78, 8120-8134.
88. Lee, C.H., Chang, S.C., Wu, C.H., and Chang, M.F. (2001). A novel chromosome region maintenance 1-independent nuclear export signal of the large form of hepatitis delta antigen that is required for the viral assembly. J Biol Chem 276, 8142-8148.
89. O'Malley, B., and Lazinski, D.W. (2005). Roles of carboxyl-terminal and farnesylated residues in the functions of the large hepatitis delta antigen. J Virol 79, 1142-1153.
90. Glenn, J.S., Watson, J.A., Havel, C.M., and White, J.M. (1992). Identification of a prenylation site in delta virus large antigen. Science 256, 1331-1333.
91. Hwang, S.B., and Lai, M.M. (1993). Isoprenylation mediates direct protein-protein interactions between hepatitis large delta antigen and hepatitis B virus surface antigen. J Virol 67, 7659-7662.
92. Hwang, S.B., and Lai, M.M. (1994). Isoprenylation masks a conformational epitope and enhances trans-dominant inhibitory function of the large hepatitis delta antigen. J Virol 68, 2958-2964.
93. Freitas, N., Cunha, C., Menne, S., and Gudima, S.O. (2014). Envelope proteins derived from naturally integrated hepatitis B virus DNA support assembly and release of infectious hepatitis delta virus particles. J Virol 88, 5742-5754.
94. Zoulim, F., Lebosse, F., and Levrero, M. (2016). Current treatments for chronic hepatitis B virus infections. Curr Opin Virol 18, 109-116.
95. Liu, Y., Jia, M., Wu, S., Jiang, W., and Feng, Y. (2019). Predictors of relapse after cessation of nucleos(t)ide analog treatment in HBeAg-negative chronic hepatitis B patients: A meta-analysis. Int J Infect Dis 86, 201-207.
96. Heidrich, B., Yurdaydin, C., Kabacam, G., Ratsch, B.A., Zachou, K., Bremer, B., Dalekos, G.N., Erhardt, A., Tabak, F., Yalcin, K., et al. (2014). Late HDV RNA relapse after peginterferon alpha-based therapy of chronic hepatitis delta. Hepatology 60, 87-97.
97. Soriano, V., Barreiro, P., Benitez, L., Pena, J.M., and de Mendoza, C. (2017). New antivirals for the treatment of chronic hepatitis B. Expert Opin Investig Drugs 26, 843-851.
98. Gehring, A.J., and Protzer, U. (2019). Targeting Innate and Adaptive Immune Responses to Cure Chronic HBV Infection. Gastroenterology 156, 325-337.
99. Yuen, M.F., Schiefke, I., Yoon, J.H., Ahn, S.H., Heo, J., Kim, J.H., Chan, H.L.Y., Yoon, K.T., Klinker, H., Manns, M., et al. (2019). RNA Interference Therapy with ARC-520 Results in Prolonged HBsAg Response in Patients with Chronic Hepatitis B Infection. Hepatology.
100. Carthew, R.W., and Sontheimer, E.J. (2009). Origins and Mechanisms of miRNAs and siRNAs. Cell 136, 642-655.
101. Jinek, M., and Doudna, J.A. (2009). A three-dimensional view of the molecular machinery of RNA interference. Nature 457, 405-412.
102. Saini, H.K., Griffiths-Jones, S., and Enright, A.J. (2007). Genomic analysis of human microRNA transcripts. Proc Natl Acad Sci U S A 104, 17719-17724.
103. Gregory, R.I., Chendrimada, T.P., and Shiekhattar, R. (2006). MicroRNA biogenesis: isolation and characterization of the microprocessor complex. Methods Mol Biol 342, 33-47.
104. Bohnsack, M.T., Czaplinski, K., and Gorlich, D. (2004). Exportin 5 is a RanGTP-dependent dsRNA-binding protein that mediates nuclear export of pre-miRNAs. RNA 10, 185-191.
105. MacRae, I.J., Ma, E., Zhou, M., Robinson, C.V., and Doudna, J.A. (2008). In vitro reconstitution of the human RISC-loading complex. Proc Natl Acad Sci U S A 105, 512-517.
106. Liu, J., Carmell, M.A., Rivas, F.V., Marsden, C.G., Thomson, J.M., Song, J.J., Hammond, S.M., Joshua-Tor, L., and Hannon, G.J. (2004). Argonaute2 is the catalytic engine of mammalian RNAi. Science 305, 1437-1441.
107. Pillai, R.S., Bhattacharyya, S.N., Artus, C.G., Zoller, T., Cougot, N., Basyuk, E., Bertrand, E., and Filipowicz, W. (2005). Inhibition of translational initiation by Let-7 MicroRNA in human cells. Science 309, 1573-1576.
108. Humphreys, D.T., Westman, B.J., Martin, D.I., and Preiss, T. (2005). MicroRNAs control translation initiation by inhibiting eukaryotic initiation factor 4E/cap and poly(A) tail function. Proc Natl Acad Sci U S A 102, 16961-16966.
109. Elbashir, S.M., Harborth, J., Lendeckel, W., Yalcin, A., Weber, K., and Tuschl, T. (2001). Duplexes of 21-nucleotide RNAs mediate RNA interference in cultured mammalian cells. Nature 411, 494-498.

110. Gao, Z., Harwig, A., Berkhout, B., and Herrera-Carrillo, E. (2017). Mutation of nucleotides around the +1 position of type 3 polymerase III promoters: The effect on transcriptional activity and start site usage. Transcription 8, 275-287.
111. Giering, J.C., Grimm, D., Storm, T.A., and Kay, M.A. (2008). Expression of shRNA from a tissue-specific pol II promoter is an effective and safe RNAi therapeutic. Mol Ther 16, 1630-1636.
112. Kamath, R.S., Fraser, A.G., Dong, Y., Poulin, G., Durbin, R., Gotta, M., Kanapin, A., Le Bot, N., Moreno, S., Sohrmann, M., et al. (2003). Systematic functional analysis of the Caenorhabditis elegans genome using RNAi. Nature 421, 231-237.
113. Boutros, M., Kiger, A.A., Armknecht, S., Kerr, K., Hild, M., Koch, B., Haas, S.A., Paro, R., Perrimon, N., and Heidelberg Fly Array, C. (2004). Genome-wide RNAi analysis of growth and viability in Drosophila cells. Science 303, 832-835.
114. Tan, F.L., and Yin, J.Q. (2004). RNAi, a new therapeutic strategy against viral infection. Cell Res 14, 460-466.
115. Zhang, J., Yamada, O., Sakamoto, T., Yoshida, H., Iwai, T., Matsushita, Y., Shimamura, H., Araki, H., and Shimotohno, K. (2004). Down-regulation of viral replication by adenoviral-mediated expression of siRNA against cellular cofactors for hepatitis C virus. Virology 320, 135-143.
116. Song, E., Lee, S.K., Wang, J., Ince, N., Ouyang, N., Min, J., Chen, J., Shankar, P., and Lieberman, J. (2003). RNA interference targeting Fas protects mice from fulminant hepatitis. Nat Med 9, 347-351.
117. Zender, L., Hutker, S., Liedtke, C., Tillmann, H.L., Zender, S., Mundt, B., Waltemathe, M., Gosling, T., Flemming, P., Malek, N.P., et al. (2003). Caspase 8 small interfering RNA prevents acute liver failure in mice. Proc Natl Acad Sci U S A 100, 7797-7802.
118. Grimm, D., and Kay, M.A. (2006). Therapeutic short hairpin RNA expression in the liver: viral targets and vectors. Gene Ther 13, 563-575.
119. Ebert, G., Poeck, H., Lucifora, J., Baschuk, N., Esser, K., Esposito, I., Hartmann, G., and Protzer, U. (2011). 5' Triphosphorylated small interfering RNAs control replication of hepatitis B virus and induce an interferon response in human liver cells and mice. Gastroenterology 141, 696-706, 706 e691-693.
120. Uprichard, S.L., Boyd, B., Althage, A., and Chisari, F.V. (2005). Clearance of hepatitis B virus from the liver of transgenic mice by short hairpin RNAs. Proc Natl Acad Sci U S A 102, 773-778.
121. Milich, D.R., Chen, M.K., Hughes, J.L., and Jones, J.E. (1998). The secreted hepatitis B precore antigen can modulate the immune response to the nucleocapsid: a mechanism for persistence. J Immunol 160, 2013-2021.
122. Bertoletti, A., Tan, A.T., and Gehring, A.J. (2009). HBV-Specific Adaptive Immunity. Viruses 1, 91-103.
123. Guidotti, L.G., Rochford, R., Chung, J., Shapiro, M., Purcell, R., and Chisari, F.V. (1999). Viral clearance without destruction of infected cells during acute HBV infection. Science 284, 825-829.
124. McCaffrey, A.P., Nakai, H., Pandey, K., Huang, Z., Salazar, F.H., Xu, H., Wieland, S.F., Marion, P.L., and Kay, M.A. (2003). Inhibition of hepatitis B virus in mice by RNA interference. Nat Biotechnol 21, 639-644.
125. Hamasaki, K., Nakao, K., Matsumoto, K., Ichikawa, T., Ishikawa, H., and Eguchi, K. (2003). Short interfering RNA-directed inhibition of hepatitis B virus replication. FEBS Lett 543, 51-54.
126. Ying, C., De Clercq, E., and Neyts, J. (2003). Selective inhibition of hepatitis B virus replication by RNA interference. Biochem Biophys Res Commun 309, 482-484.
127. Chang, J., and Taylor, J.M. (2003). Susceptibility of human hepatitis delta virus RNAs to small interfering RNA action. J Virol 77, 9728-9731.
128. Singh, S., Gupta, S.K., Nischal, A., Khattri, S., Nath, R., Pant, K.K., and Seth, P.K. (2012). Design of potential siRNA molecules for hepatitis delta virus gene silencing. Bioinformation 8, 749-757.
129. Kusov, Y., Kanda, T., Palmenberg, A., Sgro, J.Y., and Gauss-Muller, V. (2006). Silencing of hepatitis A virus infection by small interfering RNAs. J Virol 80, 5599-5610.
130. Wu, H.L., Huang, L.R., Huang, C.C., Lai, H.L., Liu, C.J., Huang, Y.T., Hsu, Y.W., Lu, C.Y., Chen, D.S., and Chen, P.J. (2005). RNA interference-mediated control of hepatitis B virus and emergence of resistant mutant. Gastroenterology 128, 708-716.

131. Wilson, J.A., and Richardson, C.D. (2005). Hepatitis C virus replicons escape RNA interference induced by a short interfering RNA directed against the NS5b coding region. J Virol 79, 7050-7058.
132. Boden, D., Pusch, O., Lee, F., Tucker, L., and Ramratnam, B. (2003). Human immunodeficiency virus type 1 escape from RNA interference. J Virol 77, 11531-11535.
133. Das, A.T., Brummelkamp, T.R., Westerhout, E.M., Vink, M., Madiredjo, M., Bernards, R., and Berkhout, B. (2004). Human immunodeficiency virus type 1 escapes from RNA interference-mediated inhibition. J Virol 78, 2601-2605.
134. Gitlin, L., Karelsky, S., and Andino, R. (2002). Short interfering RNA confers intracellular antiviral immunity in human cells. Nature 418, 430-434.
135. Tabernero, D., Cortese, M.F., Buti, M., and Rodriguez-Frias, F. (2018). HDV evolution-will viral resistance be an issue in HDV infection? Curr Opin Virol 32, 100-107.
136. Grimm, D., and Kay, M.A. (2007). Combinatorial RNAi: a winning strategy for the race against evolving targets? Mol Ther 15, 878-888.
137. Bian, Z., Xiao, A., Cao, M., Liu, M., Liu, S., Jiao, Y., Yan, W., Qi, Z., and Zheng, Z. (2012). Anti-HBV efficacy of combined siRNAs targeting viral gene and heat shock cognate 70. Virol J 9, 275.
138. Anderson, J., and Akkina, R. (2005). HIV-1 resistance conferred by siRNA cosuppression of CXCR4 and CCR5 coreceptors by a bispecific lentiviral vector. AIDS Res Ther 2, 1.
139. Gonzalez, S., Castanotto, D., Li, H., Olivares, S., Jensen, M.C., Forman, S.J., Rossi, J.J., and Cooper, L.J. (2005). Amplification of RNAi--targeting HLA mRNAs. Mol Ther 11, 811-818.
140. Henry, S.D., van der Wegen, P., Metselaar, H.J., Tilanus, H.W., Scholte, B.J., and van der Laan, L.J. (2006). Simultaneous targeting of HCV replication and viral binding with a single lentiviral vector containing multiple RNA interference expression cassettes. Mol Ther 14, 485-493.
141. Song, J., Giang, A., Lu, Y., Pang, S., and Chiu, R. (2008). Multiple shRNA expressing vector enhances efficiency of gene silencing. BMB Rep 41, 358-362.
142. Gou, D., Weng, T., Wang, Y., Wang, Z., Zhang, H., Gao, L., Chen, Z., Wang, P., and Liu, L. (2007). A novel approach for the construction of multiple shRNA expression vectors. J Gene Med 9, 751-763.
143. Shih, Y.M., Sun, C.P., Chou, H.H., Wu, T.H., Chen, C.C., Wu, P.Y., Enya Chen, Y.C., Bissig, K.D., and Tao, M.H. (2015). Combinatorial RNA Interference Therapy Prevents Selection of Pre-existing HBV Variants in Human Liver Chimeric Mice. Sci Rep 5, 15259.
144. Grimm, D., Streetz, K.L., Jopling, C.L., Storm, T.A., Pandey, K., Davis, C.R., Marion, P., Salazar, F., and Kay, M.A. (2006). Fatality in mice due to oversaturation of cellular microRNA/short hairpin RNA pathways. Nature 441, 537-541.
145. Borel, F., van Logtenstein, R., Koornneef, A., Maczuga, P., Ritsema, T., Petry, H., van Deventer, S.J., Jansen, P.L., and Konstantinova, P. (2011). In vivo knock-down of multidrug resistance transporters ABCC1 and ABCC2 by AAV-delivered shRNAs and by artificial miRNAs. J RNAi Gene Silencing 7, 434-442.
146. Ahn, M., Witting, S.R., Ruiz, R., Saxena, R., and Morral, N. (2011). Constitutive expression of short hairpin RNA in vivo triggers buildup of mature hairpin molecules. Hum Gene Ther 22, 1483-1497.
147. McBride, J.L., Boudreau, R.L., Harper, S.Q., Staber, P.D., Monteys, A.M., Martins, I., Gilmore, B.L., Burstein, H., Peluso, R.W., Polisky, B., et al. (2008). Artificial miRNAs mitigate shRNA-mediated toxicity in the brain: implications for the therapeutic development of RNAi. Proc Natl Acad Sci U S A 105, 5868-5873.
148. Martin, J.N., Wolken, N., Brown, T., Dauer, W.T., Ehrlich, M.E., and Gonzalez-Alegre, P. (2011). Lethal toxicity caused by expression of shRNA in the mouse striatum: implications for therapeutic design. Gene Ther 18, 666-673.
149. Grimm, D. (2011). The dose can make the poison: lessons learned from adverse in vivo toxicities caused by RNAi overexpression. Silence 2, 8.
150. Grimm, D., Wang, L., Lee, J.S., Schurmann, N., Gu, S., Borner, K., Storm, T.A., and Kay, M.A. (2010). Argonaute proteins are key determinants of RNAi efficacy, toxicity, and persistence in the adult mouse liver. J Clin Invest 120, 3106-3119.
151. Diederichs, S., Jung, S., Rothenberg, S.M., Smolen, G.A., Mlody, B.G., and Haber, D.A. (2008). Coexpression of Argonaute-2 enhances RNA interference toward perfect match binding sites. Proc Natl Acad Sci U S A 105, 9284-9289.

152. Borner, K., Niopek, D., Cotugno, G., Kaldenbach, M., Pankert, T., Willemsen, J., Zhang, X., Schurmann, N., Mockenhaupt, S., Serva, A., et al. (2013). Robust RNAi enhancement via human Argonaute-2 overexpression from plasmids, viral vectors and cell lines. Nucleic Acids Res 41, e199.
153. Senis, E., Mockenhaupt, S., Rupp, D., Bauer, T., Paramasivam, N., Knapp, B., Gronych, J., Grosse, S., Windisch, M.P., Schmidt, F., et al. (2017). TALEN/CRISPR-mediated engineering of a promoterless anti-viral RNAi hairpin into an endogenous miRNA locus. Nucleic Acids Res 45, e3.
154. Qiu, S., Adema, C.M., and Lane, T. (2005). A computational study of off-target effects of RNA interference. Nucleic Acids Res 33, 1834-1847.
155. Gumienny, R., and Zavolan, M. (2015). Accurate transcriptome-wide prediction of microRNA targets and small interfering RNA off-targets with MIRZA-G. Nucleic Acids Res 43, 9095.
156. Naito, Y., Yoshimura, J., Morishita, S., and Ui-Tei, K. (2009). siDirect 2.0: updated software for designing functional siRNA with reduced seed-dependent off-target effect. BMC Bioinformatics 10, 392.
157. Gu, S., Jin, L., Zhang, F., Huang, Y., Grimm, D., Rossi, J.J., and Kay, M.A. (2011). Thermodynamic stability of small hairpin RNAs highly influences the loading process of different mammalian Argonautes. Proc Natl Acad Sci U S A 108, 9208-9213.
158. Kwak, P.B., and Tomari, Y. (2012). The N domain of Argonaute drives duplex unwinding during RISC assembly. Nat Struct Mol Biol 19, 145-151.
159. Khvorova, A., Reynolds, A., and Jayasena, S.D. (2003). Functional siRNAs and miRNAs exhibit strand bias. Cell 115, 209-216.
160. Noland, C.L., and Doudna, J.A. (2013). Multiple sensors ensure guide strand selection in human RNAi pathways. RNA 19, 639-648.
161. Haraguchi, T., Ozaki, Y., and Iba, H. (2009). Vectors expressing efficient RNA decoys achieve the long-term suppression of specific microRNA activity in mammalian cells. Nucleic Acids Res 37, e43.
162. Mockenhaupt, S., Grosse, S., Rupp, D., Bartenschlager, R., and Grimm, D. (2015). Alleviation of off-target effects from vector-encoded shRNAs via codelivered RNA decoys. Proc Natl Acad Sci U S A 112, E4007-4016.
163. Michler, T., Grosse, S., Mockenhaupt, S., Roder, N., Stuckler, F., Knapp, B., Ko, C., Heikenwalder, M., Protzer, U., and Grimm, D. (2016). Blocking sense-strand activity improves potency, safety and specificity of anti-hepatitis B virus short hairpin RNA. EMBO Mol Med 8, 1082-1098.
164. Zhan, T., Rindtorff, N., Betge, J., Ebert, M.P., and Boutros, M. (2019). CRISPR/Cas9 for cancer research and therapy. Semin Cancer Biol 55, 106-119.
165. Lee, C. (2019). CRISPR/Cas9-Based Antiviral Strategy: Current Status and the Potential Challenge. Molecules 24.
166. Mojica, F.J., Diez-Villasenor, C., Garcia-Martinez, J., and Soria, E. (2005). Intervening sequences of regularly spaced prokaryotic repeats derive from foreign genetic elements. J Mol Evol 60, 174-182.
167. Makarova, K.S., Wolf, Y.I., Alkhnbashi, O.S., Costa, F., Shah, S.A., Saunders, S.J., Barrangou, R., Brouns, S.J., Charpentier, E., Haft, D.H., et al. (2015). An updated evolutionary classification of CRISPR-Cas systems. Nat Rev Microbiol 13, 722-736.
168. Deltcheva, E., Chylinski, K., Sharma, C.M., Gonzales, K., Chao, Y., Pirzada, Z.A., Eckert, M.R., Vogel, J., and Charpentier, E. (2011). CRISPR RNA maturation by trans-encoded small RNA and host factor RNase III. Nature 471, 602-607.
169. Jinek, M., Chylinski, K., Fonfara, I., Hauer, M., Doudna, J.A., and Charpentier, E. (2012). A programmable dual-RNA-guided DNA endonuclease in adaptive bacterial immunity. Science 337, 816-821.
170. Rouet, P., Smih, F., and Jasin, M. (1994). Introduction of double-strand breaks into the genome of mouse cells by expression of a rare-cutting endonuclease. Mol Cell Biol 14, 8096-8106.
171. Lin, Y., Lukacsovich, T., and Waldman, A.S. (1999). Multiple pathways for repair of DNA double-strand breaks in mammalian chromosomes. Mol Cell Biol 19, 8353-8360.
172. Mimitou, E.P., and Symington, L.S. (2009). Nucleases and helicases take center stage in homologous recombination. Trends Biochem Sci 34, 264-272.
173. Sung, P., and Klein, H. (2006). Mechanism of homologous recombination: mediators and helicases take on regulatory functions. Nat Rev Mol Cell Biol 7, 739-750.

174. Moore, J.K., and Haber, J.E. (1996). Cell cycle and genetic requirements of two pathways of nonhomologous end-joining repair of double-strand breaks in Saccharomyces cerevisiae. Mol Cell Biol 16, 2164-2173.
175. Cong, L., Ran, F.A., Cox, D., Lin, S., Barretto, R., Habib, N., Hsu, P.D., Wu, X., Jiang, W., Marraffini, L.A., et al. (2013). Multiplex genome engineering using CRISPR/Cas systems. Science 339, 819-823.
176. Qi, L.S., Larson, M.H., Gilbert, L.A., Doudna, J.A., Weissman, J.S., Arkin, A.P., and Lim, W.A. (2013). Repurposing CRISPR as an RNA-guided platform for sequence-specific control of gene expression. Cell 152, 1173-1183.
177. Ran, F.A., Hsu, P.D., Lin, C.Y., Gootenberg, J.S., Konermann, S., Trevino, A.E., Scott, D.A., Inoue, A., Matoba, S., Zhang, Y., et al. (2013). Double nicking by RNA-guided CRISPR Cas9 for enhanced genome editing specificity. Cell 154, 1380-1389.
178. Gilbert, L.A., Larson, M.H., Morsut, L., Liu, Z., Brar, G.A., Torres, S.E., Stern-Ginossar, N., Brandman, O., Whitehead, E.H., Doudna, J.A., et al. (2013). CRISPR-mediated modular RNA-guided regulation of transcription in eukaryotes. Cell 154, 442-451.
179. Lo, A., and Qi, L. (2017). Genetic and epigenetic control of gene expression by CRISPR-Cas systems. F1000Res 6.
180. Eid, A., Alshareef, S., and Mahfouz, M.M. (2018). CRISPR base editors: genome editing without double-stranded breaks. Biochem J 475, 1955-1964.
181. Cebrian-Serrano, A., and Davies, B. (2017). CRISPR-Cas orthologues and variants: optimizing the repertoire, specificity and delivery of genome engineering tools. Mamm Genome 28, 247-261.
182. Cho, S.W., Kim, S., Kim, J.M., and Kim, J.S. (2013). Targeted genome engineering in human cells with the Cas9 RNA-guided endonuclease. Nat Biotechnol 31, 230-232.
183. Mali, P., Yang, L., Esvelt, K.M., Aach, J., Guell, M., DiCarlo, J.E., Norville, J.E., and Church, G.M. (2013). RNA-guided human genome engineering via Cas9. Science 339, 823-826.
184. Nishimasu, H., Ran, F.A., Hsu, P.D., Konermann, S., Shehata, S.I., Dohmae, N., Ishitani, R., Zhang, F., and Nureki, O. (2014). Crystal structure of Cas9 in complex with guide RNA and target DNA. Cell 156, 935-949.
185. Jinek, M., Jiang, F., Taylor, D.W., Sternberg, S.H., Kaya, E., Ma, E., Anders, C., Hauer, M., Zhou, K., Lin, S., et al. (2014). Structures of Cas9 endonucleases reveal RNA-mediated conformational activation. Science 343, 1247997.
186. Nishimasu, H., Cong, L., Yan, W.X., Ran, F.A., Zetsche, B., Li, Y., Kurabayashi, A., Ishitani, R., Zhang, F., and Nureki, O. (2015). Crystal Structure of Staphylococcus aureus Cas9. Cell 162, 1113-1126.
187. Sun, W., Yang, J., Cheng, Z., Amrani, N., Liu, C., Wang, K., Ibraheim, R., Edraki, A., Huang, X., Wang, M., et al. (2019). Structures of Neisseria meningitidis Cas9 Complexes in Catalytically Poised and Anti-CRISPR-Inhibited States. Mol Cell 76, 938-952 e935.
188. Palermo, G., Chen, J.S., Ricci, C.G., Rivalta, I., Jinek, M., Batista, V.S., Doudna, J.A., and McCammon, J.A. (2018). Key role of the REC lobe during CRISPR-Cas9 activation by 'sensing', 'regulating', and 'locking' the catalytic HNH domain. Q Rev Biophys 51.
189. Ran, F.A., Cong, L., Yan, W.X., Scott, D.A., Gootenberg, J.S., Kriz, A.J., Zetsche, B., Shalem, O., Wu, X., Makarova, K.S., et al. (2015). In vivo genome editing using Staphylococcus aureus Cas9. Nature 520, 186-191.
190. Lee, C.M., Cradick, T.J., and Bao, G. (2016). The Neisseria meningitidis CRISPR-Cas9 System Enables Specific Genome Editing in Mammalian Cells. Mol Ther 24, 645-654.
191. Pattanayak, V., Lin, S., Guilinger, J.P., Ma, E., Doudna, J.A., and Liu, D.R. (2013). High-throughput profiling of off-target DNA cleavage reveals RNA-programmed Cas9 nuclease specificity. Nat Biotechnol 31, 839-843.
192. Hsu, P.D., Scott, D.A., Weinstein, J.A., Ran, F.A., Konermann, S., Agarwala, V., Li, Y., Fine, E.J., Wu, X., Shalem, O., et al. (2013). DNA targeting specificity of RNA-guided Cas9 nucleases. Nat Biotechnol 31, 827-832.
193. Fu, Y., Foden, J.A., Khayter, C., Maeder, M.L., Reyon, D., Joung, J.K., and Sander, J.D. (2013). High-frequency off-target mutagenesis induced by CRISPR-Cas nucleases in human cells. Nat Biotechnol 31, 822-826.
194. Labuhn, M., Adams, F.F., Ng, M., Knoess, S., Schambach, A., Charpentier, E.M., Schwarzer, A., Mateo, J.L., Klusmann, J.H., and Heckl, D. (2018). Refined sgRNA efficacy prediction improves large- and small-scale CRISPR-Cas9 applications. Nucleic Acids Res 46, 1375-1385.

195. Zhang, X.H., Tee, L.Y., Wang, X.G., Huang, Q.S., and Yang, S.H. (2015). Off-target Effects in CRISPR/Cas9-mediated Genome Engineering. Mol Ther Nucleic Acids 4, e264.
196. Tsai, S.Q., and Joung, J.K. (2016). Defining and improving the genome-wide specificities of CRISPR-Cas9 nucleases. Nat Rev Genet 17, 300-312.
197. Bondy-Denomy, J., Pawluk, A., Maxwell, K.L., and Davidson, A.R. (2013). Bacteriophage genes that inactivate the CRISPR/Cas bacterial immune system. Nature 493, 429-432.
198. Pawluk, A., Davidson, A.R., and Maxwell, K.L. (2018). Anti-CRISPR: discovery, mechanism and function. Nat Rev Microbiol 16, 12-17.
199. Pawluk, A., Amrani, N., Zhang, Y., Garcia, B., Hidalgo-Reyes, Y., Lee, J., Edraki, A., Shah, M., Sontheimer, E.J., Maxwell, K.L., et al. (2016). Naturally Occurring Off-Switches for CRISPR-Cas9. Cell 167, 1829-1838 e1829.
200. Rauch, B.J., Silvis, M.R., Hultquist, J.F., Waters, C.S., McGregor, M.J., Krogan, N.J., and Bondy-Denomy, J. (2017). Inhibition of CRISPR-Cas9 with Bacteriophage Proteins. Cell 168, 150-158 e110.
201. Harrington, L.B., Doxzen, K.W., Ma, E., Liu, J.J., Knott, G.J., Edraki, A., Garcia, B., Amrani, N., Chen, J.S., Cofsky, J.C., et al. (2017). A Broad-Spectrum Inhibitor of CRISPR-Cas9. Cell 170, 1224-1233 e1215.
202. Bubeck, F., Hoffmann, M.D., Harteveld, Z., Aschenbrenner, S., Bietz, A., Waldhauer, M.C., Borner, K., Fakhiri, J., Schmelas, C., Dietz, L., et al. (2018). Engineered anti-CRISPR proteins for optogenetic control of CRISPR-Cas9. Nat Methods 15, 924-927.
203. Hoffmann, M.D., Aschenbrenner, S., Grosse, S., Rapti, K., Domenger, C., Fakhiri, J., Mastel, M., Borner, K., Eils, R., Grimm, D., et al. (2019). Cell-specific CRISPR-Cas9 activation by microRNA-dependent expression of anti-CRISPR proteins. Nucleic Acids Res 47, e75.
204. Nathwani, A.C., Reiss, U.M., Tuddenham, E.G., Rosales, C., Chowdary, P., McIntosh, J., Della Peruta, M., Lheriteau, E., Patel, N., Raj, D., et al. (2014). Long-term safety and efficacy of factor IX gene therapy in hemophilia B. N Engl J Med 371, 1994-2004.
205. Chirmule, N., Propert, K., Magosin, S., Qian, Y., Qian, R., and Wilson, J. (1999). Immune responses to adenovirus and adeno-associated virus in humans. Gene Ther 6, 1574-1583.
206. Flotte, T.R., and Berns, K.I. (2005). Adeno-associated virus: a ubiquitous commensal of mammals. Hum Gene Ther 16, 401-407.
207. Surosky, R.T., Urabe, M., Godwin, S.G., McQuiston, S.A., Kurtzman, G.J., Ozawa, K., and Natsoulis, G. (1997). Adeno-associated virus Rep proteins target DNA sequences to a unique locus in the human genome. J Virol 71, 7951-7959.
208. Nakai, H., Yant, S.R., Storm, T.A., Fuess, S., Meuse, L., and Kay, M.A. (2001). Extrachromosomal recombinant adeno-associated virus vector genomes are primarily responsible for stable liver transduction in vivo. J Virol 75, 6969-6976.
209. Mendell, J.R., Al-Zaidy, S., Shell, R., Arnold, W.D., Rodino-Klapac, L.R., Prior, T.W., Lowes, L., Alfano, L., Berry, K., Church, K., et al. (2017). Single-Dose Gene-Replacement Therapy for Spinal Muscular Atrophy. N Engl J Med 377, 1713-1722.
210. Bennett, J. (2017). Taking Stock of Retinal Gene Therapy: Looking Back and Moving Forward. Mol Ther 25, 1076-1094.
211. George, L.A., Sullivan, S.K., Giermasz, A., Rasko, J.E.J., Samelson-Jones, B.J., Ducore, J., Cuker, A., Sullivan, L.M., Majumdar, S., Teitel, J., et al. (2017). Hemophilia B Gene Therapy with a High-Specific-Activity Factor IX Variant. N Engl J Med 377, 2215-2227.
212. Mueller, C., Gernoux, G., Gruntman, A.M., Borel, F., Reeves, E.P., Calcedo, R., Rouhani, F.N., Yachnis, A., Humphries, M., Campbell-Thompson, M., et al. (2017). 5 Year Expression and Neutrophil Defect Repair after Gene Therapy in Alpha-1 Antitrypsin Deficiency. Mol Ther 25, 1387-1394.
213. Keeler, A.M., and Flotte, T.R. (2019). Recombinant Adeno-Associated Virus Gene Therapy in Light of Luxturna (and Zolgensma and Glybera): Where Are We, and How Did We Get Here? Annu Rev Virol 6, 601-621.
214. Nonnenmacher, M., and Weber, T. (2012). Intracellular transport of recombinant adeno-associated virus vectors. Gene Ther 19, 649-658.
215. Goncalves, M.A. (2005). Adeno-associated virus: from defective virus to effective vector. Virol J 2, 43.
216. Madigan, V.J., and Asokan, A. (2016). Engineering AAV receptor footprints for gene therapy. Curr Opin Virol 18, 89-96.
217. Johnson, F.B., Ozer, H.L., and Hoggan, M.D. (1971). Structural proteins of adenovirus-associated virus type 3. J Virol 8, 860-863.

218. Sonntag, F., Schmidt, K., and Kleinschmidt, J.A. (2010). A viral assembly factor promotes AAV2 capsid formation in the nucleolus. Proc Natl Acad Sci U S A 107, 10220-10225.
219. Herrmann, A.K., Grosse, S., Borner, K., Kramer, C., Wiedtke, E., Gunkel, M., and Grimm, D. (2019). Impact of the Assembly-Activating Protein on Molecular Evolution of Synthetic Adeno-Associated Virus Capsids. Hum Gene Ther 30, 21-35.
220. Ogden, P.J., Kelsic, E.D., Sinai, S., and Church, G.M. (2019). Comprehensive AAV capsid fitness landscape reveals a viral gene and enables machine-guided design. Science 366, 1139-1143.
221. Atchison, R.W., Casto, B.C., and Hammon, W.M. (1965). Adenovirus-Associated Defective Virus Particles. Science 149, 754-756.
222. Geoffroy, M.C., and Salvetti, A. (2005). Helper functions required for wild type and recombinant adeno-associated virus growth. Curr Gene Ther 5, 265-271.
223. Gao, G.P., Alvira, M.R., Wang, L., Calcedo, R., Johnston, J., and Wilson, J.M. (2002). Novel adeno-associated viruses from rhesus monkeys as vectors for human gene therapy. Proc Natl Acad Sci U S A 99, 11854-11859.
224. Zincarelli, C., Soltys, S., Rengo, G., and Rabinowitz, J.E. (2008). Analysis of AAV serotypes 1-9 mediated gene expression and tropism in mice after systemic injection. Mol Ther 16, 1073-1080.
225. Samulski, R.J., Berns, K.I., Tan, M., and Muzyczka, N. (1982). Cloning of adeno-associated virus into pBR322: rescue of intact virus from the recombinant plasmid in human cells. Proc Natl Acad Sci U S A 79, 2077-2081.
226. Tratschin, J.D., West, M.H., Sandbank, T., and Carter, B.J. (1984). A human parvovirus, adeno-associated virus, as a eucaryotic vector: transient expression and encapsidation of the procaryotic gene for chloramphenicol acetyltransferase. Mol Cell Biol 4, 2072-2081.
227. Borner, K., Kienle, E., Huang, L.Y., Weinmann, J., Sacher, A., Bayer, P., Stullein, C., Fakhiri, J., Zimmermann, L., Westhaus, A., et al. (2020). Pre-arrayed Pan-AAV Peptide Display Libraries for Rapid Single-Round Screening. Mol Ther.
228. Huang, L.Y., Halder, S., and Agbandje-McKenna, M. (2014). Parvovirus glycan interactions. Curr Opin Virol 7, 108-118.
229. Summerford, C., and Samulski, R.J. (1998). Membrane-associated heparan sulfate proteoglycan is a receptor for adeno-associated virus type 2 virions. J Virol 72, 1438-1445.
230. Kern, A., Schmidt, K., Leder, C., Muller, O.J., Wobus, C.E., Bettinger, K., Von der Lieth, C.W., King, J.A., and Kleinschmidt, J.A. (2003). Identification of a heparin-binding motif on adeno-associated virus type 2 capsids. J Virol 77, 11072-11081.
231. Pillay, S., Meyer, N.L., Puschnik, A.S., Davulcu, O., Diep, J., Ishikawa, Y., Jae, L.T., Wosen, J.E., Nagamine, C.M., Chapman, M.S., et al. (2016). An essential receptor for adeno-associated virus infection. Nature 530, 108-112.
232. Pillay, S., Zou, W., Cheng, F., Puschnik, A.S., Meyer, N.L., Ganaie, S.S., Deng, X., Wosen, J.E., Davulcu, O., Yan, Z., et al. (2017). Adeno-associated Virus (AAV) Serotypes Have Distinctive Interactions with Domains of the Cellular AAV Receptor. J Virol 91.
233. Dudek, A.M., Pillay, S., Puschnik, A.S., Nagamine, C.M., Cheng, F., Qiu, J., Carette, J.E., and Vandenberghe, L.H. (2018). An Alternate Route for Adeno-associated Virus (AAV) Entry Independent of AAV Receptor. J Virol 92.
234. Fakhiri, J., Nickl, M., and Grimm, D. (2019). Rapid and Simple Screening of CRISPR Guide RNAs (gRNAs) in Cultured Cells Using Adeno-Associated Viral (AAV) Vectors. Methods Mol Biol 1961, 111-126.
235. McLaughlin, S.K., Collis, P., Hermonat, P.L., and Muzyczka, N. (1988). Adeno-associated virus general transduction vectors: analysis of proviral structures. J Virol 62, 1963-1973.
236. Samulski, R.J., Chang, L.S., and Shenk, T. (1989). Helper-free stocks of recombinant adeno-associated viruses: normal integration does not require viral gene expression. J Virol 63, 3822-3828.
237. Grimm, D., Kern, A., Rittner, K., and Kleinschmidt, J.A. (1998). Novel tools for production and purification of recombinant adenoassociated virus vectors. Hum Gene Ther 9, 2745-2760.
238. Beck, S.E., Jones, L.A., Chesnut, K., Walsh, S.M., Reynolds, T.C., Carter, B.J., Askin, F.B., Flotte, T.R., and Guggino, W.B. (1999). Repeated delivery of adeno-associated virus vectors to the rabbit airway. J Virol 73, 9446-9455.
239. Rabinowitz, J.E., Rolling, F., Li, C., Conrath, H., Xiao, W., Xiao, X., and Samulski, R.J. (2002). Cross-packaging of a single adeno-associated virus (AAV) type 2 vector genome

into multiple AAV serotypes enables transduction with broad specificity. J Virol 76, 791-801.
240. Rutledge, E.A., Halbert, C.L., and Russell, D.W. (1998). Infectious clones and vectors derived from adeno-associated virus (AAV) serotypes other than AAV type 2. J Virol 72, 309-319.
241. Chiorini, J.A., Yang, L., Liu, Y., Safer, B., and Kotin, R.M. (1997). Cloning of adeno-associated virus type 4 (AAV4) and generation of recombinant AAV4 particles. J Virol 71, 6823-6833.
242. Grimm, D., Kay, M.A., and Kleinschmidt, J.A. (2003). Helper virus-free, optically controllable, and two-plasmid-based production of adeno-associated virus vectors of serotypes 1 to 6. Mol Ther 7, 839-850.
243. Chiorini, J.A., Afione, S., and Kotin, R.M. (1999). Adeno-associated virus (AAV) type 5 Rep protein cleaves a unique terminal resolution site compared with other AAV serotypes. J Virol 73, 4293-4298.
244. Chiorini, J.A., Kim, F., Yang, L., and Kotin, R.M. (1999). Cloning and characterization of adeno-associated virus type 5. J Virol 73, 1309-1319.
245. Waehler, R., Russell, S.J., and Curiel, D.T. (2007). Engineering targeted viral vectors for gene therapy. Nat Rev Genet 8, 573-587.
246. Kotterman, M.A., and Schaffer, D.V. (2014). Engineering adeno-associated viruses for clinical gene therapy. Nat Rev Genet 15, 445-451.
247. Schmidt, F., and Grimm, D. (2015). CRISPR genome engineering and viral gene delivery: a case of mutual attraction. Biotechnol J 10, 258-272.
248. Muller, O.J., Kaul, F., Weitzman, M.D., Pasqualini, R., Arap, W., Kleinschmidt, J.A., and Trepel, M. (2003). Random peptide libraries displayed on adeno-associated virus to select for targeted gene therapy vectors. Nat Biotechnol 21, 1040-1046.
249. Grimm, D., Lee, J.S., Wang, L., Desai, T., Akache, B., Storm, T.A., and Kay, M.A. (2008). In vitro and in vivo gene therapy vector evolution via multispecies interbreeding and retargeting of adeno-associated viruses. J Virol 82, 5887-5911.
250. Herrmann, A.K., Bender, C., Kienle, E., Grosse, S., El Andari, J., Botta, J., Schurmann, N., Wiedtke, E., Niopek, D., and Grimm, D. (2019). A Robust and All-Inclusive Pipeline for Shuffling of Adeno-Associated Viruses. ACS Synth Biol 8, 194-206.
251. Li, C., Narkbunnam, N., Samulski, R.J., Asokan, A., Hu, G., Jacobson, L.J., Manco-Johnson, M.J., Monahan, P.E., and Joint Outcome Study, I. (2012). Neutralizing antibodies against adeno-associated virus examined prospectively in pediatric patients with hemophilia. Gene Ther 19, 288-294.
252. Vandamme, C., Adjali, O., and Mingozzi, F. (2017). Unraveling the Complex Story of Immune Responses to AAV Vectors Trial After Trial. Hum Gene Ther 28, 1061-1074.
253. Ferrari, F.K., Samulski, T., Shenk, T., and Samulski, R.J. (1996). Second-strand synthesis is a rate-limiting step for efficient transduction by recombinant adeno-associated virus vectors. J Virol 70, 3227-3234.
254. Fisher, K.J., Gao, G.P., Weitzman, M.D., DeMatteo, R., Burda, J.F., and Wilson, J.M. (1996). Transduction with recombinant adeno-associated virus for gene therapy is limited by leading-strand synthesis. J Virol 70, 520-532.
255. Wang, Z., Ma, H.I., Li, J., Sun, L., Zhang, J., and Xiao, X. (2003). Rapid and highly efficient transduction by double-stranded adeno-associated virus vectors in vitro and in vivo. Gene Ther 10, 2105-2111.
256. McCarty, D.M., Fu, H., Monahan, P.E., Toulson, C.E., Naik, P., and Samulski, R.J. (2003). Adeno-associated virus terminal repeat (TR) mutant generates self-complementary vectors to overcome the rate-limiting step to transduction in vivo. Gene Ther 10, 2112-2118.
257. McCarty, D.M., Monahan, P.E., and Samulski, R.J. (2001). Self-complementary recombinant adeno-associated virus (scAAV) vectors promote efficient transduction independently of DNA synthesis. Gene Ther 8, 1248-1254.
258. Wu, Z., Yang, H., and Colosi, P. (2010). Effect of genome size on AAV vector packaging. Mol Ther 18, 80-86.
259. Bartlett, J.S., Wilcher, R., and Samulski, R.J. (2000). Infectious entry pathway of adeno-associated virus and adeno-associated virus vectors. J Virol 74, 2777-2785.
260. Rossi, A., Dupaty, L., Aillot, L., Zhang, L., Gallien, C., Hallek, M., Odenthal, M., Adriouch, S., Salvetti, A., and Buning, H. (2019). Vector uncoating limits adeno-associated viral vector-

mediated transduction of human dendritic cells and vector immunogenicity. Sci Rep 9, 3631.
261. McCarty, D.M. (2008). Self-complementary AAV vectors; advances and applications. Mol Ther 16, 1648-1656.
262. Yan, Z., Zak, R., Luxton, G.W., Ritchie, T.C., Bantel-Schaal, U., and Engelhardt, J.F. (2002). Ubiquitination of both adeno-associated virus type 2 and 5 capsid proteins affects the transduction efficiency of recombinant vectors. J Virol 76, 2043-2053.
263. Ding, W., Zhang, L., Yan, Z., and Engelhardt, J.F. (2005). Intracellular trafficking of adeno-associated viral vectors. Gene Ther 12, 873-880.
264. Duan, D., Yue, Y., Yan, Z., Yang, J., and Engelhardt, J.F. (2000). Endosomal processing limits gene transfer to polarized airway epithelia by adeno-associated virus. J Clin Invest 105, 1573-1587.
265. Douar, A.M., Poulard, K., Stockholm, D., and Danos, O. (2001). Intracellular trafficking of adeno-associated virus vectors: routing to the late endosomal compartment and proteasome degradation. J Virol 75, 1824-1833.
266. Hosel, M., Huber, A., Bohlen, S., Lucifora, J., Ronzitti, G., Puzzo, F., Boisgerault, F., Hacker, U.T., Kwanten, W.J., Kloting, N., et al. (2017). Autophagy determines efficiency of liver-directed gene therapy with adeno-associated viral vectors. Hepatology 66, 252-265.
267. Senis, E., Fatouros, C., Grosse, S., Wiedtke, E., Niopek, D., Mueller, A.K., Borner, K., and Grimm, D. (2014). CRISPR/Cas9-mediated genome engineering: an adeno-associated viral (AAV) vector toolbox. Biotechnol J 9, 1402-1412.
268. Schmelas, C., and Grimm, D. (2018). Split Cas9, Not Hairs - Advancing the Therapeutic Index of CRISPR Technology. Biotechnol J 13, e1700432.
269. Truong, D.J., Kuhner, K., Kuhn, R., Werfel, S., Engelhardt, S., Wurst, W., and Ortiz, O. (2015). Development of an intein-mediated split-Cas9 system for gene therapy. Nucleic Acids Res 43, 6450-6458.
270. Fine, E.J., Appleton, C.M., White, D.E., Brown, M.T., Deshmukh, H., Kemp, M.L., and Bao, G. (2015). Trans-spliced Cas9 allows cleavage of HBB and CCR5 genes in human cells using compact expression cassettes. Sci Rep 5, 10777.
271. Ma, D., Peng, S., and Xie, Z. (2016). Integration and exchange of split dCas9 domains for transcriptional controls in mammalian cells. Nat Commun 7, 13056.
272. Chew, W.L., Tabebordbar, M., Cheng, J.K., Mali, P., Wu, E.Y., Ng, A.H., Zhu, K., Wagers, A.J., and Church, G.M. (2016). A multifunctional AAV-CRISPR-Cas9 and its host response. Nat Methods 13, 868-874.
273. Perler, F.B., Davis, E.O., Dean, G.E., Gimble, F.S., Jack, W.E., Neff, N., Noren, C.J., Thorner, J., and Belfort, M. (1994). Protein splicing elements: inteins and exteins--a definition of terms and recommended nomenclature. Nucleic Acids Res 22, 1125-1127.
274. Martin, D.D., Xu, M.Q., and Evans, T.C., Jr. (2001). Characterization of a naturally occurring trans-splicing intein from Synechocystis sp. PCC6803. Biochemistry 40, 1393-1402.
275. Zettler, J., Schutz, V., and Mootz, H.D. (2009). The naturally split Npu DnaE intein exhibits an extraordinarily high rate in the protein trans-splicing reaction. FEBS Lett 583, 909-914.
276. Waldhauer, M.C., Schmitz, S.N., Ahlmann-Eltze, C., Gleixner, J.G., Schmelas, C.C., Huhn, A.G., Bunne, C., Buscher, M., Horn, M., Klughammer, N., et al. (2015). Backbone circularization of Bacillus subtilis family 11 xylanase increases its thermostability and its resistance against aggregation. Mol Biosyst 11, 3231-3243.
277. Carvajal-Vallejos, P., Pallisse, R., Mootz, H.D., and Schmidt, S.R. (2012). Unprecedented rates and efficiencies revealed for new natural split inteins from metagenomic sources. J Biol Chem 287, 28686-28696.
278. Cheriyan, M., Pedamallu, C.S., Tori, K., and Perler, F. (2013). Faster protein splicing with the Nostoc punctiforme DnaE intein using non-native extein residues. J Biol Chem 288, 6202-6211.
279. Bocker, J.K., Dorner, W., and Mootz, H.D. (2019). Light-control of the ultra-fast Gp41-1 split intein with preserved stability of a genetically encoded photo-caged amino acid in bacterial cells. Chem Commun (Camb) 55, 1287-1290.
280. Skretas, G., and Wood, D.W. (2005). Regulation of protein activity with small-molecule-controlled inteins. Protein Sci 14, 523-532.
281. Buskirk, A.R., Ong, Y.C., Gartner, Z.J., and Liu, D.R. (2004). Directed evolution of ligand dependence: small-molecule-activated protein splicing. Proc Natl Acad Sci U S A 101, 10505-10510.

282. Zeidler, M.P., Tan, C., Bellaiche, Y., Cherry, S., Hader, S., Gayko, U., and Perrimon, N. (2004). Temperature-sensitive control of protein activity by conditionally splicing inteins. Nat Biotechnol 22, 871-876.
283. Ren, W., Ji, A., and Ai, H.W. (2015). Light activation of protein splicing with a photocaged fast intein. J Am Chem Soc 137, 2155-2158.
284. Mathys, S., Evans, T.C., Chute, I.C., Wu, H., Chong, S., Benner, J., Liu, X.Q., and Xu, M.Q. (1999). Characterization of a self-splicing mini-intein and its conversion into autocatalytic N- and C-terminal cleavage elements: facile production of protein building blocks for protein ligation. Gene 231, 1-13.
285. Chong, S., Mersha, F.B., Comb, D.G., Scott, M.E., Landry, D., Vence, L.M., Perler, F.B., Benner, J., Kucera, R.B., Hirvonen, C.A., et al. (1997). Single-column purification of free recombinant proteins using a self-cleavable affinity tag derived from a protein splicing element. Gene 192, 271-281.
286. Schmelas, C. (2015). Intein-mediated reconstitution of split Staphylococcus aureus Cas9 as a strategy to deliver the CRISPR/Cas system using double-stranded adeno-associated viral vectors. Master Thesis.
287. Seipp, S., Mueller, H.M., Pfaff, E., Stremmel, W., Theilmann, L., and Goeser, T. (1997). Establishment of persistent hepatitis C virus infection and replication in vitro. J Gen Virol 78 (Pt 10), 2467-2476.
288. Seki, J., Ikeda, R., and Hoshino, H. (1996). Dimethyl sulfoxide and related polar compounds enhance infection of human T cells with HIV-1 in vitro. Biochem Biophys Res Commun 227, 724-729.
289. Scholtissek, C., and Muller, K. (1988). Effect of dimethylsulfoxide (DMSO) on virus replication and maturation. Arch Virol 100, 27-35.
290. Tsai, S.Q., Zheng, Z., Nguyen, N.T., Liebers, M., Topkar, V.V., Thapar, V., Wyvekens, N., Khayter, C., Iafrate, A.J., Le, L.P., et al. (2015). GUIDE-seq enables genome-wide profiling of off-target cleavage by CRISPR-Cas nucleases. Nat Biotechnol 33, 187-197.
291. Hindi, L., McMillan, J.D., Afroze, D., Hindi, S.M., and Kumar, A. (2017). Isolation, Culturing, and Differentiation of Primary Myoblasts from Skeletal Muscle of Adult Mice. Bio Protoc 7.
292. Schneider, C.A., Rasband, W.S., and Eliceiri, K.W. (2012). NIH Image to ImageJ: 25 years of image analysis. Nat Methods 9, 671-675.
293. Engler, C., Kandzia, R., and Marillonnet, S. (2008). A one pot, one step, precision cloning method with high throughput capability. PLoS One 3, e3647.
294. Fakhiri, J. (2019). With small viruses come giant responsibilities -

Next-generation parvoviral vectors for human gene therapy with extended packaging capacity and enhanced safety profile. Dissertation University Heidelberg.
295. Pear, W.S., Nolan, G.P., Scott, M.L., and Baltimore, D. (1993). Production of high-titer helper-free retroviruses by transient transfection. Proc Natl Acad Sci U S A 90, 8392-8396.
296. Aden, D.P., Fogel, A., Plotkin, S., Damjanov, I., and Knowles, B.B. (1979). Controlled synthesis of HBsAg in a differentiated human liver carcinoma-derived cell line. Nature 282, 615-616.
297. Nakabayashi, H., Taketa, K., Miyano, K., Yamane, T., and Sato, J. (1982). Growth of human hepatoma cells lines with differentiated functions in chemically defined medium. Cancer Res 42, 3858-3863.
298. Darlington, G.J., Bernhard, H.P., Miller, R.A., and Ruddle, F.H. (1980). Expression of liver phenotypes in cultured mouse hepatoma cells. J Natl Cancer Inst 64, 809-819.
299. Olmsted, J.B., Carlson, K., Klebe, R., Ruddle, F., and Rosenbaum, J. (1970). Isolation of microtubule protein from cultured mouse neuroblastoma cells. Proc Natl Acad Sci U S A 65, 129-136.
300. Lempp, F.A., Schlund, F., Rieble, L., Nussbaum, L., Link, C., Zhang, Z., Ni, Y., and Urban, S. (2019). Recapitulation of HDV infection in a fully permissive hepatoma cell line allows efficient drug evaluation. Nat Commun 10, 2265.
301. Brinkman, E.K., Chen, T., Amendola, M., and van Steensel, B. (2014). Easy quantitative assessment of genome editing by sequence trace decomposition. Nucleic Acids Res 42, e168.
302. Sedlak, R.H., Liang, S., Niyonzima, N., De Silva Feelixge, H.S., Roychoudhury, P., Greninger, A.L., Weber, N.D., Boissel, S., Scharenberg, A.M., Cheng, A., et al. (2016).

Digital detection of endonuclease mediated gene disruption in the HIV provirus. Sci Rep 6, 20064.
303. Borner, K., Hermle, J., Sommer, C., Brown, N.P., Knapp, B., Glass, B., Kunkel, J., Torralba, G., Reymann, J., Beil, N., et al. (2010). From experimental setup to bioinformatics: an RNAi screening platform to identify host factors involved in HIV-1 replication. Biotechnol J 5, 39-49.
304. Lisowski, L., Dane, A.P., Chu, K., Zhang, Y., Cunningham, S.C., Wilson, E.M., Nygaard, S., Grompe, M., Alexander, I.E., and Kay, M.A. (2014). Selection and evaluation of clinically relevant AAV variants in a xenograft liver model. Nature 506, 382-386.
305. Lempp, F.A., Qu, B., Wang, Y.X., and Urban, S. (2016). Hepatitis B Virus Infection of a Mouse Hepatic Cell Line Reconstituted with Human Sodium Taurocholate Cotransporting Polypeptide. J Virol 90, 4827-4831.
306. Bogomolov, P., Alexandrov, A., Voronkova, N., Macievich, M., Kokina, K., Petrachenkova, M., Lehr, T., Lempp, F.A., Wedemeyer, H., Haag, M., et al. (2016). Treatment of chronic hepatitis D with the entry inhibitor myrcludex B: First results of a phase Ib/IIa study. J Hepatol 65, 490-498.
307. Zhang, T., Hu, J., Ding, W., and Wang, X. (2009). Doxorubicin augments rAAV-2 transduction in rat neuronal cells. Neurochem Int 55, 521-528.
308. Sentmanat, M.F., Peters, S.T., Florian, C.P., Connelly, J.P., and Pruett-Miller, S.M. (2018). A Survey of Validation Strategies for CRISPR-Cas9 Editing. Sci Rep 8, 888.
309. Seamon, K.J., Light, Y.K., Saada, E.A., Schoeniger, J.S., and Harmon, B. (2018). Versatile High-Throughput Fluorescence Assay for Monitoring Cas9 Activity. Anal Chem 90, 6913-6921.
310. Leaver-Fay, A., Tyka, M., Lewis, S.M., Lange, O.F., Thompson, J., Jacak, R., Kaufman, K., Renfrew, P.D., Smith, C.A., Sheffler, W., et al. (2011). ROSETTA3: an object-oriented software suite for the simulation and design of macromolecules. Methods Enzymol 487, 545-574.
311. Mathony, J., Harteveld, Z., Schmelas, C., Upmeier zu Belzen, J., Aschenbrenner, S., Sun, W., Hoffmann, M., Stengl, C., Scheck, A., Georgeon, S., et al. (2020). Computational design of anti-CRISPR proteins with improved inhibition potency. Nature Chemical Biology accepted.
312. Wang, D., Tai, P.W.L., and Gao, G. (2019). Adeno-associated virus vector as a platform for gene therapy delivery. Nat Rev Drug Discov 18, 358-378.
313. Setten, R.L., Rossi, J.J., and Han, S.P. (2019). The current state and future directions of RNAi-based therapeutics. Nat Rev Drug Discov 18, 421-446.
314. Akinc, A., Maier, M.A., Manoharan, M., Fitzgerald, K., Jayaraman, M., Barros, S., Ansell, S., Du, X., Hope, M.J., Madden, T.D., et al. (2019). The Onpattro story and the clinical translation of nanomedicines containing nucleic acid-based drugs. Nat Nanotechnol 14, 1084-1087.
315. Sakuma, T., Masaki, K., Abe-Chayama, H., Mochida, K., Yamamoto, T., and Chayama, K. (2016). Highly multiplexed CRISPR-Cas9-nuclease and Cas9-nickase vectors for inactivation of hepatitis B virus. Genes Cells 21, 1253-1262.
316. Schiwon, M., Ehrke-Schulz, E., Oswald, A., Bergmann, T., Michler, T., Protzer, U., and Ehrhardt, A. (2018). One-Vector System for Multiplexed CRISPR/Cas9 against Hepatitis B Virus cccDNA Utilizing High-Capacity Adenoviral Vectors. Mol Ther Nucleic Acids 12, 242-253.
317. Leonard, J.N., and Schaffer, D.V. (2005). Computational design of antiviral RNA interference strategies that resist human immunodeficiency virus escape. J Virol 79, 1645-1654.
318. Lin, S.R., Yang, H.C., Kuo, Y.T., Liu, C.J., Yang, T.Y., Sung, K.C., Lin, Y.Y., Wang, H.Y., Wang, C.C., Shen, Y.C., et al. (2014). The CRISPR/Cas9 System Facilitates Clearance of the Intrahepatic HBV Templates In Vivo. Mol Ther Nucleic Acids 3, e186.
319. Seeger, C., and Sohn, J.A. (2014). Targeting Hepatitis B Virus With CRISPR/Cas9. Mol Ther Nucleic Acids 3, e216.
320. Wang, J., Xu, Z.W., Liu, S., Zhang, R.Y., Ding, S.L., Xie, X.M., Long, L., Chen, X.M., Zhuang, H., and Lu, F.M. (2015). Dual gRNAs guided CRISPR/Cas9 system inhibits hepatitis B virus replication. World J Gastroenterol 21, 9554-9565.
321. Kurata, M., Wolf, N.K., Lahr, W.S., Weg, M.T., Kluesner, M.G., Lee, S., Hui, K., Shiraiwa, M., Webber, B.R., and Moriarity, B.S. (2018). Highly multiplexed genome engineering using CRISPR/Cas9 gRNA arrays. PLoS One 13, e0198714.

322. Nissim, L., Perli, S.D., Fridkin, A., Perez-Pinera, P., and Lu, T.K. (2014). Multiplexed and programmable regulation of gene networks with an integrated RNA and CRISPR/Cas toolkit in human cells. Mol Cell 54, 698-710.
323. Haurwitz, R.E., Jinek, M., Wiedenheft, B., Zhou, K., and Doudna, J.A. (2010). Sequence- and structure-specific RNA processing by a CRISPR endonuclease. Science 329, 1355-1358.
324. Dong, F., Xie, K., Chen, Y., Yang, Y., and Mao, Y. (2017). Polycistronic tRNA and CRISPR guide-RNA enables highly efficient multiplexed genome engineering in human cells. Biochem Biophys Res Commun 482, 889-895.
325. Xie, K., Minkenberg, B., and Yang, Y. (2015). Boosting CRISPR/Cas9 multiplex editing capability with the endogenous tRNA-processing system. Proc Natl Acad Sci U S A 112, 3570-3575.
326. Xu, L., Zhao, L., Gao, Y., Xu, J., and Han, R. (2017). Empower multiplex cell and tissue-specific CRISPR-mediated gene manipulation with self-cleaving ribozymes and tRNA. Nucleic Acids Res 45, e28.
327. He, Y., Zhang, T., Yang, N., Xu, M., Yan, L., Wang, L., Wang, R., and Zhao, Y. (2017). Self-cleaving ribozymes enable the production of guide RNAs from unlimited choices of promoters for CRISPR/Cas9 mediated genome editing. J Genet Genomics 44, 469-472.
328. Walker, M.P., and Lindner, S.E. (2019). Ribozyme-mediated, multiplex CRISPR gene editing and CRISPR interference (CRISPRi) in rodent-infectious Plasmodium yoelii. J Biol Chem 294, 9555-9566.
329. Fonfara, I., Richter, H., Bratovic, M., Le Rhun, A., and Charpentier, E. (2016). The CRISPR-associated DNA-cleaving enzyme Cpf1 also processes precursor CRISPR RNA. Nature 532, 517-521.
330. Zetsche, B., Heidenreich, M., Mohanraju, P., Fedorova, I., Kneppers, J., DeGennaro, E.M., Winblad, N., Choudhury, S.R., Abudayyeh, O.O., Gootenberg, J.S., et al. (2017). Multiplex gene editing by CRISPR-Cpf1 using a single crRNA array. Nat Biotechnol 35, 31-34.
331. Liu, Y.P., Haasnoot, J., and Berkhout, B. (2007). Design of extended short hairpin RNAs for HIV-1 inhibition. Nucleic Acids Res 35, 5683-5693.
332. Konstantinova, P., de Vries, W., Haasnoot, J., ter Brake, O., de Haan, P., and Berkhout, B. (2006). Inhibition of human immunodeficiency virus type 1 by RNA interference using long-hairpin RNA. Gene Ther 13, 1403-1413.
333. Sano, M., Li, H., Nakanishi, M., and Rossi, J.J. (2008). Expression of long anti-HIV-1 hairpin RNAs for the generation of multiple siRNAs: advantages and limitations. Mol Ther 16, 170-177.
334. Liu, Y.P., Haasnoot, J., ter Brake, O., Berkhout, B., and Konstantinova, P. (2008). Inhibition of HIV-1 by multiple siRNAs expressed from a single microRNA polycistron. Nucleic Acids Res 36, 2811-2824.
335. Snyder, L.L., Ahmed, I., and Steel, L.F. (2009). RNA polymerase III can drive polycistronic expression of functional interfering RNAs designed to resemble microRNAs. Nucleic Acids Res 37, e127.
336. Steel, L.F., and Sanghvi, V.R. (2012). Polycistronic expression of interfering RNAs from RNA polymerase III promoters. Methods Mol Biol 815, 347-359.
337. Choi, J.G., Bharaj, P., Abraham, S., Ma, H., Yi, G., Ye, C., Dang, Y., Manjunath, N., Wu, H., and Shankar, P. (2015). Multiplexing seven miRNA-Based shRNAs to suppress HIV replication. Mol Ther 23, 310-320.
338. Pujol, F.M., Laketa, V., Schmidt, F., Mukenhirn, M., Muller, B., Boulant, S., Grimm, D., Keppler, O.T., and Fackler, O.T. (2016). HIV-1 Vpu Antagonizes CD317/Tetherin by Adaptor Protein-1-Mediated Exclusion from Virus Assembly Sites. J Virol 90, 6709-6723.
339. Amoasii, L., Long, C., Li, H., Mireault, A.A., Shelton, J.M., Sanchez-Ortiz, E., McAnally, J.R., Bhattacharyya, S., Schmidt, F., Grimm, D., et al. (2017). Single-cut genome editing restores dystrophin expression in a new mouse model of muscular dystrophy. Sci Transl Med 9.
340. Krooss, S.A., Dai, Z., Schmidt, F., Rovai, A., Fakhiri, J., Dhingra, A., Yuan, Q., Yang, T., Balakrishnan, A., Steinbruck, L., et al. (2020). Ex Vivo/In vivo Gene Editing in Hepatocytes Using "All-in-One" CRISPR-Adeno-Associated Virus Vectors with a Self-Linearizing Repair Template. iScience 23, 100764.

341. Doerfler, P.A., Byrne, B.J., and Clement, N. (2014). Copackaging of multiple adeno-associated viral vectors in a single production step. Hum Gene Ther Methods 25, 269-276.
342. Xie, J., Mao, Q., Tai, P.W.L., He, R., Ai, J., Su, Q., Zhu, Y., Ma, H., Li, J., Gong, S., et al. (2017). Short DNA Hairpins Compromise Recombinant Adeno-Associated Virus Genome Homogeneity. Mol Ther 25, 1363-1374.
343. Breunig, C.T., Durovic, T., Neuner, A.M., Baumann, V., Wiesbeck, M.F., Koferle, A., Gotz, M., Ninkovic, J., and Stricker, S.H. (2018). One step generation of customizable gRNA vectors for multiplex CRISPR approaches through string assembly gRNA cloning (STAgR). PLoS One 13, e0196015.
344. Sakuma, T., Nishikawa, A., Kume, S., Chayama, K., and Yamamoto, T. (2014). Multiplex genome engineering in human cells using all-in-one CRISPR/Cas9 vector system. Sci Rep 4, 5400.
345. Vidigal, J.A., and Ventura, A. (2015). Rapid and efficient one-step generation of paired gRNA CRISPR-Cas9 libraries. Nat Commun 6, 8083.
346. Zuckermann, M., Hlevnjak, M., Yazdanparast, H., Zapatka, M., Jones, D.T.W., Lichter, P., and Gronych, J. (2018). A novel cloning strategy for one-step assembly of multiplex CRISPR vectors. Sci Rep 8, 17499.
347. Kabadi, A.M., Ousterout, D.G., Hilton, I.B., and Gersbach, C.A. (2014). Multiplex CRISPR/Cas9-based genome engineering from a single lentiviral vector. Nucleic Acids Res 42, e147.
348. Makinen, P.I., Koponen, J.K., Karkkainen, A.M., Malm, T.M., Pulkkinen, K.H., Koistinaho, J., Turunen, M.P., and Yla-Herttuala, S. (2006). Stable RNA interference: comparison of U6 and H1 promoters in endothelial cells and in mouse brain. J Gene Med 8, 433-441.
349. Hosel, M., Lucifora, J., Michler, T., Holz, G., Gruffaz, M., Stahnke, S., Zoulim, F., Durantel, D., Heikenwalder, M., Nierhoff, D., et al. (2014). Hepatitis B virus infection enhances susceptibility toward adeno-associated viral vector transduction in vitro and in vivo. Hepatology 59, 2110-2120.
350. Xu, Z., Bruss, V., and Yen, T.S. (1997). Formation of intracellular particles by hepatitis B virus large surface protein. J Virol 71, 5487-5494.
351. Chua, P.K., Wang, R.Y., Lin, M.H., Masuda, T., Suk, F.M., and Shih, C. (2005). Reduced secretion of virions and hepatitis B virus (HBV) surface antigen of a naturally occurring HBV variant correlates with the accumulation of the small S envelope protein in the endoplasmic reticulum and Golgi apparatus. J Virol 79, 13483-13496.
352. Xu, Z., and Yen, T.S. (1996). Intracellular retention of surface protein by a hepatitis B virus mutant that releases virion particles. J Virol 70, 133-140.
353. Gerken, G., Kremsdorf, D., Capel, F., Petit, M.A., Dauguet, C., Manns, M.P., Meyer zum Buschenfelde, K.H., and Brechot, C. (1991). Hepatitis B defective virus with rearrangements in the preS gene during chronic HBV infection. Virology 183, 555-565.
354. Yamamoto, K., Horikita, M., Tsuda, F., Itoh, K., Akahane, Y., Yotsumoto, S., Okamoto, H., Miyakawa, Y., and Mayumi, M. (1994). Naturally occurring escape mutants of hepatitis B virus with various mutations in the S gene in carriers seropositive for antibody to hepatitis B surface antigen. J Virol 68, 2671-2676.
355. Nakajima, E., Minami, M., Ochiya, T., Kagawa, K., and Okanoue, T. (1994). PreS1 deleted variants of hepatitis B virus in patients with chronic hepatitis. J Hepatol 20, 329-335.
356. Heermann, K.H., Goldmann, U., Schwartz, W., Seyffarth, T., Baumgarten, H., and Gerlich, W.H. (1984). Large surface proteins of hepatitis B virus containing the pre-s sequence. J Virol 52, 396-402.
357. Su, I.J., Wang, H.C., Wu, H.C., and Huang, W.Y. (2008). Ground glass hepatocytes contain pre-S mutants and represent preneoplastic lesions in chronic hepatitis B virus infection. J Gastroenterol Hepatol 23, 1169-1174.
358. Gerber, M.A., and Thung, S.N. (1985). Molecular and cellular pathology of hepatitis B. Lab Invest 52, 572-590.
359. Gilles, P.N., Guerrette, D.L., Ulevitch, R.J., Schreiber, R.D., and Chisari, F.V. (1992). HBsAg retention sensitizes the hepatocyte to injury by physiological concentrations of interferon-gamma. Hepatology 16, 655-663.
360. Wang, H.C., Huang, W., Lai, M.D., and Su, I.J. (2006). Hepatitis B virus pre-S mutants, endoplasmic reticulum stress and hepatocarcinogenesis. Cancer Sci 97, 683-688.
361. Flisiak, R., Jaroszewicz, J., and Lucejko, M. (2018). siRNA drug development against hepatitis B virus infection. Expert Opin Biol Ther 18, 609-617.

362. Wang, J., Chen, R., Zhang, R., Ding, S., Zhang, T., Yuan, Q., Guan, G., Chen, X., Zhang, T., Zhuang, H., et al. (2017). The gRNA-miRNA-gRNA Ternary Cassette Combining CRISPR/Cas9 with RNAi Approach Strongly Inhibits Hepatitis B Virus Replication. Theranostics 7, 3090-3105.
363. Michler, T., Kosinska, A.D., Festag, J., Bunse, T., Su, J., Ringelhan, M., Imhof, H., Grimm, D., Steiger, K., Mogler, C., et al. (2020). Knockdown of Virus Antigen Expression Increases Therapeutic Vaccine Efficacy in High-Titer Hepatitis B Virus Carrier Mice. Gastroenterology.
364. Lee, C.Z., Chen, P.J., Lai, M.M., and Chen, D.S. (1994). Isoprenylation of large hepatitis delta antigen is necessary but not sufficient for hepatitis delta virus assembly. Virology 199, 169-175.
365. Chang, F.L., Chen, P.J., Tu, S.J., Wang, C.J., and Chen, D.S. (1991). The large form of hepatitis delta antigen is crucial for assembly of hepatitis delta virus. Proc Natl Acad Sci U S A 88, 8490-8494.
366. Ryu, W.S., Bayer, M., and Taylor, J. (1992). Assembly of hepatitis delta virus particles. J Virol 66, 2310-2315.
367. Glenn, J.S., and White, J.M. (1991). trans-dominant inhibition of human hepatitis delta virus genome replication. J Virol 65, 2357-2361.
368. Polson, A.G., Ley, H.L., 3rd, Bass, B.L., and Casey, J.L. (1998). Hepatitis delta virus RNA editing is highly specific for the amber/W site and is suppressed by hepatitis delta antigen. Mol Cell Biol 18, 1919-1926.
369. Vietheer, P.T., Netter, H.J., Sozzi, T., and Bartholomeusz, A. (2005). Failure of the lamivudine-resistant rtM204I hepatitis B virus mutants to efficiently support hepatitis delta virus secretion. J Virol 79, 6570-6573.
370. Chang, J., Provost, P., and Taylor, J.M. (2003). Resistance of human hepatitis delta virus RNAs to dicer activity. J Virol 77, 11910-11917.
371. Freije, C.A., Myhrvold, C., Boehm, C.K., Lin, A.E., Welch, N.L., Carter, A., Metsky, H.C., Luo, C.Y., Abudayyeh, O.O., Gootenberg, J.S., et al. (2019). Programmable Inhibition and Detection of RNA Viruses Using Cas13. Mol Cell 76, 826-837 e811.
372. Sainz, B., Jr., and Chisari, F.V. (2006). Production of infectious hepatitis C virus by well-differentiated, growth-arrested human hepatoma-derived cells. J Virol 80, 10253-10257.
373. Takase, K., Sawai, M., Yamamoto, K., Yata, J., Takasaki, Y., Teraoka, H., and Tsukada, K. (1992). Reversible G1 arrest induced by dimethyl sulfoxide in human lymphoid cell lines: kinetics of the arrest and expression of the cell cycle marker proliferating cell nuclear antigen in Raji cells. Cell Growth Differ 3, 515-521.
374. Santos, N.C., Figueira-Coelho, J., Martins-Silva, J., and Saldanha, C. (2003). Multidisciplinary utilization of dimethyl sulfoxide: pharmacological, cellular, and molecular aspects. Biochem Pharmacol 65, 1035-1041.
375. Montgomery, J.L., Rejali, N., and Wittwer, C.T. (2014). The influence of nucleotide sequence and temperature on the activity of thermostable DNA polymerases. J Mol Diagn 16, 305-313.
376. Chakrabarti, R., and Schutt, C.E. (2001). The enhancement of PCR amplification by low molecular-weight sulfones. Gene 274, 293-298.
377. Iwatani, M., Ikegami, K., Kremenska, Y., Hattori, N., Tanaka, S., Yagi, S., and Shiota, K. (2006). Dimethyl sulfoxide has an impact on epigenetic profile in mouse embryoid body. Stem Cells 24, 2549-2556.
378. Thaler, R., Spitzer, S., Karlic, H., Klaushofer, K., and Varga, F. (2012). DMSO is a strong inducer of DNA hydroxymethylation in pre-osteoblastic MC3T3-E1 cells. Epigenetics 7, 635-651.
379. Li, J., Zong, L., Sureau, C., Barker, L., Wands, J.R., and Tong, S. (2016). Unusual Features of Sodium Taurocholate Cotransporting Polypeptide as a Hepatitis B Virus Receptor. J Virol 90, 8302-8313.
380. Grune, S., Engelking, L.R., and Anwer, M.S. (1993). Role of intracellular calcium and protein kinases in the activation of hepatic Na+/taurocholate cotransport by cyclic AMP. J Biol Chem 268, 17734-17741.
381. Mukhopadhayay, S., Ananthanarayanan, M., Stieger, B., Meier, P.J., Suchy, F.J., and Anwer, M.S. (1997). cAMP increases liver Na+-taurocholate cotransport by translocating transporter to plasma membranes. Am J Physiol 273, G842-848.

382. Evripioti, A.A., Ortega-Prieto, A.M., Skelton, J.K., Bazot, Q., and Dorner, M. (2019). Phosphodiesterase-induced cAMP degradation restricts hepatitis B virus infection. Philos Trans R Soc Lond B Biol Sci 374, 20180292.
383. Stratigopoulos, G., De Rosa, M.C., LeDuc, C.A., Leibel, R.L., and Doege, C.A. (2018). DMSO increases efficiency of genome editing at two non-coding loci. PLoS One 13, e0198637.
384. Lang, J.F., Toulmin, S.A., Brida, K.L., Eisenlohr, L.C., and Davidson, B.L. (2019). Standard screening methods underreport AAV-mediated transduction and gene editing. Nat Commun 10, 3415.
385. Gao, G., Vandenberghe, L.H., Alvira, M.R., Lu, Y., Calcedo, R., Zhou, X., and Wilson, J.M. (2004). Clades of Adeno-associated viruses are widely disseminated in human tissues. J Virol 78, 6381-6388.
386. Agbandje-McKenna, M., and Kleinschmidt, J. (2011). AAV capsid structure and cell interactions. Methods Mol Biol 807, 47-92.
387. Govindasamy, L., Padron, E., McKenna, R., Muzyczka, N., Kaludov, N., Chiorini, J.A., and Agbandje-McKenna, M. (2006). Structurally mapping the diverse phenotype of adeno-associated virus serotype 4. J Virol 80, 11556-11570.
388. Govindasamy, L., DiMattia, M.A., Gurda, B.L., Halder, S., McKenna, R., Chiorini, J.A., Muzyczka, N., Zolotukhin, S., and Agbandje-McKenna, M. (2013). Structural insights into adeno-associated virus serotype 5. J Virol 87, 11187-11199.
389. Kaludov, N., Brown, K.E., Walters, R.W., Zabner, J., and Chiorini, J.A. (2001). Adeno-associated virus serotype 4 (AAV4) and AAV5 both require sialic acid binding for hemagglutination and efficient transduction but differ in sialic acid linkage specificity. J Virol 75, 6884-6893.
390. Wu, Z., Asokan, A., Grieger, J.C., Govindasamy, L., Agbandje-McKenna, M., and Samulski, R.J. (2006). Single amino acid changes can influence titer, heparin binding, and tissue tropism in different adeno-associated virus serotypes. J Virol 80, 11393-11397.
391. Johnson, J.S., and Samulski, R.J. (2009). Enhancement of adeno-associated virus infection by mobilizing capsids into and out of the nucleolus. J Virol 83, 2632-2644.
392. Keiser, N.W., Yan, Z., Zhang, Y., Lei-Butters, D.C., and Engelhardt, J.F. (2011). Unique characteristics of AAV1, 2, and 5 viral entry, intracellular trafficking, and nuclear import define transduction efficiency in HeLa cells. Hum Gene Ther 22, 1433-1444.
393. Bantel-Schaal, U., Braspenning-Wesch, I., and Kartenbeck, J. (2009). Adeno-associated virus type 5 exploits two different entry pathways in human embryo fibroblasts. J Gen Virol 90, 317-322.
394. Bantel-Schaal, U., Hub, B., and Kartenbeck, J. (2002). Endocytosis of adeno-associated virus type 5 leads to accumulation of virus particles in the Golgi compartment. J Virol 76, 2340-2349.
395. Yan, Z., Zak, R., Zhang, Y., Ding, W., Godwin, S., Munson, K., Peluso, R., and Engelhardt, J.F. (2004). Distinct classes of proteasome-modulating agents cooperatively augment recombinant adeno-associated virus type 2 and type 5-mediated transduction from the apical surfaces of human airway epithelia. J Virol 78, 2863-2874.
396. Tacar, O., Sriamornsak, P., and Dass, C.R. (2013). Doxorubicin: an update on anticancer molecular action, toxicity and novel drug delivery systems. J Pharm Pharmacol 65, 157-170.
397. Figueiredo-Pereira, M.E., Chen, W.E., Li, J., and Johdo, O. (1996). The antitumor drug aclacinomycin A, which inhibits the degradation of ubiquitinated proteins, shows selectivity for the chymotrypsin-like activity of the bovine pituitary 20 S proteasome. J Biol Chem 271, 16455-16459.
398. Ranek, M.J., and Wang, X. (2009). Activation of the ubiquitin-proteasome system in doxorubicin cardiomyopathy. Curr Hypertens Rep 11, 389-395.
399. Vlachostergios, P.J., Voutsadakis, I.A., and Papandreou, C.N. (2013). Mechanisms of proteasome inhibitor-induced cytotoxicity in malignant glioma. Cell Biol Toxicol 29, 199-211.
400. Stansborough, R.L., and Gibson, R.J. (2017). Proteasome inhibitor-induced gastrointestinal toxicity. Curr Opin Support Palliat Care 11, 133-137.
401. Chiramel, A.I., Brady, N.R., and Bartenschlager, R. (2013). Divergent roles of autophagy in virus infection. Cells 2, 83-104.

402. Popp, L., Gomez, E., Orji, W., Ho, M., Suh, J., and Segatori, L. (2017). TFEB-mediated activation of the lysosome-autophagy system affects the transduction efficiency of adeno-associated virus 2. Virology 510, 1-8.
403. Swanson, B.N. (1985). Medical use of dimethyl sulfoxide (DMSO). Rev Clin Basic Pharm 5, 1-33.
404. Li, H., Malani, N., Hamilton, S.R., Schlachterman, A., Bussadori, G., Edmonson, S.E., Shah, R., Arruda, V.R., Mingozzi, F., Wright, J.F., et al. (2011). Assessing the potential for AAV vector genotoxicity in a murine model. Blood 117, 3311-3319.
405. Vandendriessche, T., Thorrez, L., Acosta-Sanchez, A., Petrus, I., Wang, L., Ma, L., L, D.E.W., Iwasaki, Y., Gillijns, V., Wilson, J.M., et al. (2007). Efficacy and safety of adeno-associated viral vectors based on serotype 8 and 9 vs. lentiviral vectors for hemophilia B gene therapy. J Thromb Haemost 5, 16-24.
406. Yang, Y., Wang, L., Bell, P., McMenamin, D., He, Z., White, J., Yu, H., Xu, C., Morizono, H., Musunuru, K., et al. (2016). A dual AAV system enables the Cas9-mediated correction of a metabolic liver disease in newborn mice. Nat Biotechnol 34, 334-338.
407. Yin, H., Song, C.Q., Dorkin, J.R., Zhu, L.J., Li, Y., Wu, Q., Park, A., Yang, J., Suresh, S., Bizhanova, A., et al. (2016). Therapeutic genome editing by combined viral and non-viral delivery of CRISPR system components in vivo. Nat Biotechnol 34, 328-333.
408. Ohmori, T., Nagao, Y., Mizukami, H., Sakata, A., Muramatsu, S.I., Ozawa, K., Tominaga, S.I., Hanazono, Y., Nishimura, S., Nureki, O., et al. (2017). CRISPR/Cas9-mediated genome editing via postnatal administration of AAV vector cures haemophilia B mice. Sci Rep 7, 4159.
409. Platt, R.J., Chen, S., Zhou, Y., Yim, M.J., Swiech, L., Kempton, H.R., Dahlman, J.E., Parnas, O., Eisenhaure, T.M., Jovanovic, M., et al. (2014). CRISPR-Cas9 knockin mice for genome editing and cancer modeling. Cell 159, 440-455.
410. Swiech, L., Heidenreich, M., Banerjee, A., Habib, N., Li, Y., Trombetta, J., Sur, M., and Zhang, F. (2015). In vivo interrogation of gene function in the mammalian brain using CRISPR-Cas9. Nat Biotechnol 33, 102-106.
411. Chow, R.D., Guzman, C.D., Wang, G., Schmidt, F., Youngblood, M.W., Ye, L., Errami, Y., Dong, M.B., Martinez, M.A., Zhang, S., et al. (2017). AAV-mediated direct in vivo CRISPR screen identifies functional suppressors in glioblastoma. Nat Neurosci 20, 1329-1341.
412. Nishiyama, J., Mikuni, T., and Yasuda, R. (2017). Virus-Mediated Genome Editing via Homology-Directed Repair in Mitotic and Postmitotic Cells in Mammalian Brain. Neuron 96, 755-768 e755.
413. Tabebordbar, M., Zhu, K., Cheng, J.K.W., Chew, W.L., Widrick, J.J., Yan, W.X., Maesner, C., Wu, E.Y., Xiao, R., Ran, F.A., et al. (2016). In vivo gene editing in dystrophic mouse muscle and muscle stem cells. Science 351, 407-411.
414. Nelson, C.E., Hakim, C.H., Ousterout, D.G., Thakore, P.I., Moreb, E.A., Castellanos Rivera, R.M., Madhavan, S., Pan, X., Ran, F.A., Yan, W.X., et al. (2016). In vivo genome editing improves muscle function in a mouse model of Duchenne muscular dystrophy. Science 351, 403-407.
415. Long, C., Amoasii, L., Mireault, A.A., McAnally, J.R., Li, H., Sanchez-Ortiz, E., Bhattacharyya, S., Shelton, J.M., Bassel-Duby, R., and Olson, E.N. (2016). Postnatal genome editing partially restores dystrophin expression in a mouse model of muscular dystrophy. Science 351, 400-403.
416. Yu, W., Mookherjee, S., Chaitankar, V., Hiriyanna, S., Kim, J.W., Brooks, M., Ataeijannati, Y., Sun, X., Dong, L., Li, T., et al. (2017). Nrl knockdown by AAV-delivered CRISPR/Cas9 prevents retinal degeneration in mice. Nat Commun 8, 14716.
417. Huang, X., Zhou, G., Wu, W., Duan, Y., Ma, G., Song, J., Xiao, R., Vandenberghe, L., Zhang, F., D'Amore, P.A., et al. (2017). Genome editing abrogates angiogenesis in vivo. Nat Commun 8, 112.
418. Kim, E., Koo, T., Park, S.W., Kim, D., Kim, K., Cho, H.Y., Song, D.W., Lee, K.J., Jung, M.H., Kim, S., et al. (2017). In vivo genome editing with a small Cas9 orthologue derived from Campylobacter jejuni. Nat Commun 8, 14500.
419. Xie, C., Zhang, Y.P., Song, L., Luo, J., Qi, W., Hu, J., Lu, D., Yang, Z., Zhang, J., Xiao, J., et al. (2016). Genome editing with CRISPR/Cas9 in postnatal mice corrects PRKAG2 cardiac syndrome. Cell Res 26, 1099-1111.
420. Carroll, K.J., Makarewich, C.A., McAnally, J., Anderson, D.M., Zentilin, L., Liu, N., Giacca, M., Bassel-Duby, R., and Olson, E.N. (2016). A mouse model for adult cardiac-specific gene deletion with CRISPR/Cas9. Proc Natl Acad Sci U S A 113, 338-343.

421. Dong, B., Nakai, H., and Xiao, W. (2010). Characterization of genome integrity for oversized recombinant AAV vector. Mol Ther 18, 87-92.
422. Li, J., Sun, W., Wang, B., Xiao, X., and Liu, X.Q. (2008). Protein trans-splicing as a means for viral vector-mediated in vivo gene therapy. Hum Gene Ther 19, 958-964.
423. Iwai, H., Zuger, S., Jin, J., and Tam, P.H. (2006). Highly efficient protein trans-splicing by a naturally split DnaE intein from Nostoc punctiforme. FEBS Lett 580, 1853-1858.
424. Fu, H., Muenzer, J., Samulski, R.J., Breese, G., Sifford, J., Zeng, X., and McCarty, D.M. (2003). Self-complementary adeno-associated virus serotype 2 vector: global distribution and broad dispersion of AAV-mediated transgene expression in mouse brain. Mol Ther 8, 911-917.
425. Wu, Z., Sun, J., Zhang, T., Yin, C., Yin, F., Van Dyke, T., Samulski, R.J., and Monahan, P.E. (2008). Optimization of self-complementary AAV vectors for liver-directed expression results in sustained correction of hemophilia B at low vector dose. Mol Ther 16, 280-289.
426. Manno, C.S., Pierce, G.F., Arruda, V.R., Glader, B., Ragni, M., Rasko, J.J., Ozelo, M.C., Hoots, K., Blatt, P., Konkle, B., et al. (2006). Successful transduction of liver in hemophilia by AAV-Factor IX and limitations imposed by the host immune response. Nat Med 12, 342-347.
427. Hinderer, C., Katz, N., Buza, E.L., Dyer, C., Goode, T., Bell, P., Richman, L.K., and Wilson, J.M. (2018). Severe Toxicity in Nonhuman Primates and Piglets Following High-Dose Intravenous Administration of an Adeno-Associated Virus Vector Expressing Human SMN. Hum Gene Ther 29, 285-298.
428. Raj, D., Davidoff, A.M., and Nathwani, A.C. (2011). Self-complementary adeno-associated viral vectors for gene therapy of hemophilia B: progress and challenges. Expert Rev Hematol 4, 539-549.
429. Nathwani, A.C., Rosales, C., McIntosh, J., Rastegarlari, G., Nathwani, D., Raj, D., Nawathe, S., Waddington, S.N., Bronson, R., Jackson, S., et al. (2011). Long-term safety and efficacy following systemic administration of a self-complementary AAV vector encoding human FIX pseudotyped with serotype 5 and 8 capsid proteins. Mol Ther 19, 876-885.
430. Petris, G., Casini, A., Montagna, C., Lorenzin, F., Prandi, D., Romanel, A., Zasso, J., Conti, L., Demichelis, F., and Cereseto, A. (2017). Hit and go CAS9 delivered through a lentiviral based self-limiting circuit. Nat Commun 8, 15334.
431. Miller, J.B., Zhang, S., Kos, P., Xiong, H., Zhou, K., Perelman, S.S., Zhu, H., and Siegwart, D.J. (2017). Non-Viral CRISPR/Cas Gene Editing In Vitro and In Vivo Enabled by Synthetic Nanoparticle Co-Delivery of Cas9 mRNA and sgRNA. Angew Chem Int Ed Engl 56, 1059-1063.
432. Yin, H., Song, C.Q., Suresh, S., Wu, Q., Walsh, S., Rhym, L.H., Mintzer, E., Bolukbasi, M.F., Zhu, L.J., Kauffman, K., et al. (2017). Structure-guided chemical modification of guide RNA enables potent non-viral in vivo genome editing. Nat Biotechnol 35, 1179-1187.
433. Finn, J.D., Smith, A.R., Patel, M.C., Shaw, L., Youniss, M.R., van Heteren, J., Dirstine, T., Ciullo, C., Lescarbeau, R., Seitzer, J., et al. (2018). A Single Administration of CRISPR/Cas9 Lipid Nanoparticles Achieves Robust and Persistent In Vivo Genome Editing. Cell Rep 22, 2227-2235.
434. Givens, B.E., Naguib, Y.W., Geary, S.M., Devor, E.J., and Salem, A.K. (2018). Nanoparticle-Based Delivery of CRISPR/Cas9 Genome-Editing Therapeutics. AAPS J 20, 108.
435. Shen, C.C., Hsu, M.N., Chang, C.W., Lin, M.W., Hwu, J.R., Tu, Y., and Hu, Y.C. (2019). Synthetic switch to minimize CRISPR off-target effects by self-restricting Cas9 transcription and translation. Nucleic Acids Res 47, e13.
436. Chen, Y., Liu, X., Zhang, Y., Wang, H., Ying, H., Liu, M., Li, D., Lui, K.O., and Ding, Q. (2016). A Self-restricted CRISPR System to Reduce Off-target Effects. Mol Ther 24, 1508-1510.
437. Merienne, N., Vachey, G., de Longprez, L., Meunier, C., Zimmer, V., Perriard, G., Canales, M., Mathias, A., Herrgott, L., Beltraminelli, T., et al. (2017). The Self-Inactivating KamiCas9 System for the Editing of CNS Disease Genes. Cell Rep 20, 2980-2991.
438. Ruan, G.X., Barry, E., Yu, D., Lukason, M., Cheng, S.H., and Scaria, A. (2017). CRISPR/Cas9-Mediated Genome Editing as a Therapeutic Approach for Leber Congenital Amaurosis 10. Mol Ther 25, 331-341.
439. Li, A., Lee, C.M., Hurley, A.E., Jarrett, K.E., De Giorgi, M., Lu, W., Balderrama, K.S., Doerfler, A.M., Deshmukh, H., Ray, A., et al. (2019). A Self-Deleting AAV-CRISPR System for In Vivo Genome Editing. Mol Ther Methods Clin Dev 12, 111-122.

440. Bondy-Denomy, J., Garcia, B., Strum, S., Du, M., Rollins, M.F., Hidalgo-Reyes, Y., Wiedenheft, B., Maxwell, K.L., and Davidson, A.R. (2015). Multiple mechanisms for CRISPR-Cas inhibition by anti-CRISPR proteins. Nature 526, 136-139.
441. Marino, N.D., Zhang, J.Y., Borges, A.L., Sousa, A.A., Leon, L.M., Rauch, B.J., Walton, R.T., Berry, J.D., Joung, J.K., Kleinstiver, B.P., et al. (2018). Discovery of widespread type I and type V CRISPR-Cas inhibitors. Science 362, 240-242.
442. Hynes, A.P., Rousseau, G.M., Agudelo, D., Goulet, A., Amigues, B., Loehr, J., Romero, D.A., Fremaux, C., Horvath, P., Doyon, Y., et al. (2018). Widespread anti-CRISPR proteins in virulent bacteriophages inhibit a range of Cas9 proteins. Nat Commun 9, 2919.
443. Watters, K.E., Fellmann, C., Bai, H.B., Ren, S.M., and Doudna, J.A. (2018). Systematic discovery of natural CRISPR-Cas12a inhibitors. Science 362, 236-239.
444. Zhang, F., Song, G., and Tian, Y. (2019). Anti-CRISPRs: The natural inhibitors for CRISPR-Cas systems. Animal Model Exp Med 2, 69-75.
445. Lee, J., Mir, A., Edraki, A., Garcia, B., Amrani, N., Lou, H.E., Gainetdinov, I., Pawluk, A., Ibraheim, R., Gao, X.D., et al. (2018). Potent Cas9 Inhibition in Bacterial and Human Cells by AcrIIC4 and AcrIIC5 Anti-CRISPR Proteins. mBio 9.
446. Zhu, Y., Gao, A., Zhan, Q., Wang, Y., Feng, H., Liu, S., Gao, G., Serganov, A., and Gao, P. (2019). Diverse Mechanisms of CRISPR-Cas9 Inhibition by Type IIC Anti-CRISPR Proteins. Mol Cell 74, 296-309 e297.
447. Garcia, B., Lee, J., Edraki, A., Hidalgo-Reyes, Y., Erwood, S., Mir, A., Trost, C.N., Seroussi, U., Stanley, S.Y., Cohn, R.D., et al. (2019). Anti-CRISPR AcrIIA5 Potently Inhibits All Cas9 Homologs Used for Genome Editing. Cell Rep 29, 1739-1746 e1735.
448. Song, G., Zhang, F., Zhang, X., Gao, X., Zhu, X., Fan, D., and Tian, Y. (2019). AcrIIA5 Inhibits a Broad Range of Cas9 Orthologs by Preventing DNA Target Cleavage. Cell Rep 29, 2579-2589 e2574.
449. Agudelo, D., Carter, S., Velimirovic, M., Duringer, A., Rivest, J.F., Levesque, S., Loehr, J., Mouchiroud, M., Cyr, D., Waters, P.J., et al. (2020). Versatile and robust genome editing with Streptococcus thermophilus CRISPR1-Cas9. Genome Res 30, 107-117.
450. Esvelt, K.M., Smidler, A.L., Catteruccia, F., and Church, G.M. (2014). Concerning RNA-guided gene drives for the alteration of wild populations. Elife 3.
451. DiCarlo, J.E., Chavez, A., Dietz, S.L., Esvelt, K.M., and Church, G.M. (2015). Safeguarding CRISPR-Cas9 gene drives in yeast. Nat Biotechnol 33, 1250-1255.
452. Gantz, V.M., and Bier, E. (2015). Genome editing. The mutagenic chain reaction: a method for converting heterozygous to homozygous mutations. Science 348, 442-444.
453. Hammond, A., Galizi, R., Kyrou, K., Simoni, A., Siniscalchi, C., Katsanos, D., Gribble, M., Baker, D., Marois, E., Russell, S., et al. (2016). A CRISPR-Cas9 gene drive system targeting female reproduction in the malaria mosquito vector Anopheles gambiae. Nat Biotechnol 34, 78-83.
454. Sankar, P.L., and Cho, M.K. (2015). Engineering Values Into Genetic Engineering: A Proposed Analytic Framework for Scientific Social Responsibility. Am J Bioeth 15, 18-24.
455. Basgall, E.M., Goetting, S.C., Goeckel, M.E., Giersch, R.M., Roggenkamp, E., Schrock, M.N., Halloran, M., and Finnigan, G.C. (2018). Gene drive inhibition by the anti-CRISPR proteins AcrIIA2 and AcrIIA4 in Saccharomyces cerevisiae. Microbiology 164, 464-474.
456. Dong, C., Qu, L., Wang, H., Wei, L., Dong, Y., and Xiong, S. (2015). Targeting hepatitis B virus cccDNA by CRISPR/Cas9 nuclease efficiently inhibits viral replication. Antiviral Res 118, 110-117.
457. Karimova, M., Beschorner, N., Dammermann, W., Chemnitz, J., Indenbirken, D., Bockmann, J.H., Grundhoff, A., Luth, S., Buchholz, F., Schulze zur Wiesch, J., et al. (2015). CRISPR/Cas9 nickase-mediated disruption of hepatitis B virus open reading frame S and X. Sci Rep 5, 13734.
458. Kennedy, E.M., Bassit, L.C., Mueller, H., Kornepati, A.V.R., Bogerd, H.P., Nie, T., Chatterjee, P., Javanbakht, H., Schinazi, R.F., and Cullen, B.R. (2015). Suppression of hepatitis B virus DNA accumulation in chronically infected cells using a bacterial CRISPR/Cas RNA-guided DNA endonuclease. Virology 476, 196-205.
459. Liu, X., Hao, R., Chen, S., Guo, D., and Chen, Y. (2015). Inhibition of hepatitis B virus by the CRISPR/Cas9 system via targeting the conserved regions of the viral genome. J Gen Virol 96, 2252-2261.
460. Ramanan, V., Shlomai, A., Cox, D.B., Schwartz, R.E., Michailidis, E., Bhatta, A., Scott, D.A., Zhang, F., Rice, C.M., and Bhatia, S.N. (2015). CRISPR/Cas9 cleavage of viral DNA efficiently suppresses hepatitis B virus. Sci Rep 5, 10833.

461. Zhen, S., Hua, L., Liu, Y.H., Gao, L.C., Fu, J., Wan, D.Y., Dong, L.H., Song, H.F., and Gao, X. (2015). Harnessing the clustered regularly interspaced short palindromic repeat (CRISPR)/CRISPR-associated Cas9 system to disrupt the hepatitis B virus. Gene Ther 22, 404-412.
462. Seeger, C., and Sohn, J.A. (2016). Complete Spectrum of CRISPR/Cas9-induced Mutations on HBV cccDNA. Mol Ther 24, 1258-1266.
463. Zhu, W., Xie, K., Xu, Y., Wang, L., Chen, K., Zhang, L., and Fang, J. (2016). CRISPR/Cas9 produces anti-hepatitis B virus effect in hepatoma cells and transgenic mouse. Virus Res 217, 125-132.
464. Jiang, C., Mei, M., Li, B., Zhu, X., Zu, W., Tian, Y., Wang, Q., Guo, Y., Dong, Y., and Tan, X. (2017). A non-viral CRISPR/Cas9 delivery system for therapeutically targeting HBV DNA and pcsk9 in vivo. Cell Res 27, 440-443.
465. Li, H., Sheng, C., Wang, S., Yang, L., Liang, Y., Huang, Y., Liu, H., Li, P., Yang, C., Yang, X., et al. (2017). Removal of Integrated Hepatitis B Virus DNA Using CRISPR-Cas9. Front Cell Infect Microbiol 7, 91.
466. Scott, T., Moyo, B., Nicholson, S., Maepa, M.B., Watashi, K., Ely, A., Weinberg, M.S., and Arbuthnot, P. (2017). ssAAVs containing cassettes encoding SaCas9 and guides targeting hepatitis B virus inactivate replication of the virus in cultured cells. Sci Rep 7, 7401.
467. Liu, Y., Zhao, M., Gong, M., Xu, Y., Xie, C., Deng, H., Li, X., Wu, H., and Wang, Z. (2018). Inhibition of hepatitis B virus replication via HBV DNA cleavage by Cas9 from Staphylococcus aureus. Antiviral Res 152, 58-67.
468. Song, J., Zhang, X., Ge, Q., Yuan, C., Chu, L., Liang, H.F., Liao, Z., Liu, Q., Zhang, Z., and Zhang, B. (2018). CRISPR/Cas9-mediated knockout of HBsAg inhibits proliferation and tumorigenicity of HBV-positive hepatocellular carcinoma cells. J Cell Biochem 119, 8419-8431.
469. Kostyushev, D., Kostyusheva, A., Brezgin, S., Zarifyan, D., Utkina, A., Goptar, I., and Chulanov, V. (2019). Suppressing the NHEJ pathway by DNA-PKcs inhibitor NU7026 prevents degradation of HBV cccDNA cleaved by CRISPR/Cas9. Sci Rep 9, 1847.

6. SUPPLEMENTARY INFORMATION

Supplementary Table 1. Studies that applied CRISPR against HBV infections.

Targets	Cas9 Ortholog	CRISPR Delivery	HBV Model System	Multi-plexing	Ref
X, E, PCE, preS, S	*Sp*	Transfection, HDI	Huh7 cells transfected with HBV plasmid, mice transduced with AAV/HBV1.2	single	[318]
X,E	*Sp*	Lentivirus	HepAD38 with integrated HBV genome, HepG2-NTCP cells with HBV infection	single	[319]
X, C, P	*Sp*	Transfection, HDI	Huh7 cells transfected with pTHBV, HepG2.2.15 with integrated HBV, precccDNA hydrodynamically injected in BALB/c mice	single	[456]
X, S	*Sp* nickase	Transfection, Lentivirus	HeLa and HEK293 cells with transfected and integrated HBs and HBx reporter, HepG2.2.15 and HepG2-NTCP with HBV infection	dual as required for nickases	[457]
P, C, E	*Sp*	Transfection, Lentivirus	HEK293T with transfected Luc reporter, HepAD38 with integrated HBV, HepaRG with HBV infection	single	[458]
X, P, C, S	*Sp*	Transfection, Lentivirus, HDI	HepG2 cells with HBV infection,pHBV 1.3 hydrodynamically injected in BALB/c mice	single	[459]
X, P, C, S	*Sp*	Transfection, Lentivirus, HDI	HepG2 cells transfected pHBV 1.3, pHBV 1.3 hydrodynamically injected in NRG mice, HepG2.2.15 with integrated HBV, HepG2-NTCP with HBV infection	single	[460]
X, E, C, preS, S, En1	*Sp*	Transfection	Huh7-cells transfected with pBB4.5-HBV1.2,HepAD38 with integrated HBV genome	dual	[320]
X, C, S, P	*Sp*	Transfection, HDI	HepG2.2.15 with integrated HBV, HepG2 tramsfected with pHBV1.3, HDIof pHBV1.3 and HBV transgenic mice	dual	[461]
X, C, S	*Sp* & *Sp* nickase	Transfection	HepG2 and HEK293T cells transfected with pHBV1.4	up to 6 gRNAs, or 3 dual gRNAs	[315]
X, P	*Sp*	Lentivirus	HepG2-NTCP with HBV infection	single	[462]

X, S	*Sp*	Transfection, HDI	Huh7 and HepG2 transfected with pHBV1.3, M-TgHBV mice	single	[463]
X, C, S, P	*Sp*	Lipid-like nanoparticle	HDI of pHBV1.3	single	[464]
repeated C	*Sp*	Transfection	HepG2.A64 with integrated HBV	single	[465]
S, P	*Sa*	AAV2	HepG2.2.15 with integrated HBV, HepG2-NTCP with HBV infection	single	[466]
X, C, P, preS	*Sp*	Transfection, HDI	HepAD38 with integrated HBV genome, HepG2-NTCP-tet cells with HBV infection, hydrodynamically injected in C57BL/6 mice	dual, combined with RNAi	[362]
X/P, E, C/P, S	*Sa*	AAV8, HDI	Huh7cells transfected with pHBV1.3, HepG2.2.15 and HepAD38 cells with integrated HBV,HDI of pHBV1.2 in C57BL/6 mice and C3H	dual	[467]
X, P, P1	*Sp*	Transfection, Adenovirus	HEK293T and Huh7 cell transfected with pTHBV2, HepG2.2.15 with integrated HBV, HepG2-NTCP with HBV infection	triple	[316]
preS1, preS2, S	*Sp* nickase	Transfection	HepG2.2.15, PLC/PRF/5 and Hep3B with integrated HBV	single	[468]
X, C, En1	*Sp*	Transfection	HepG2-1.1 and-1.5mer integrated HBV	single	[469]

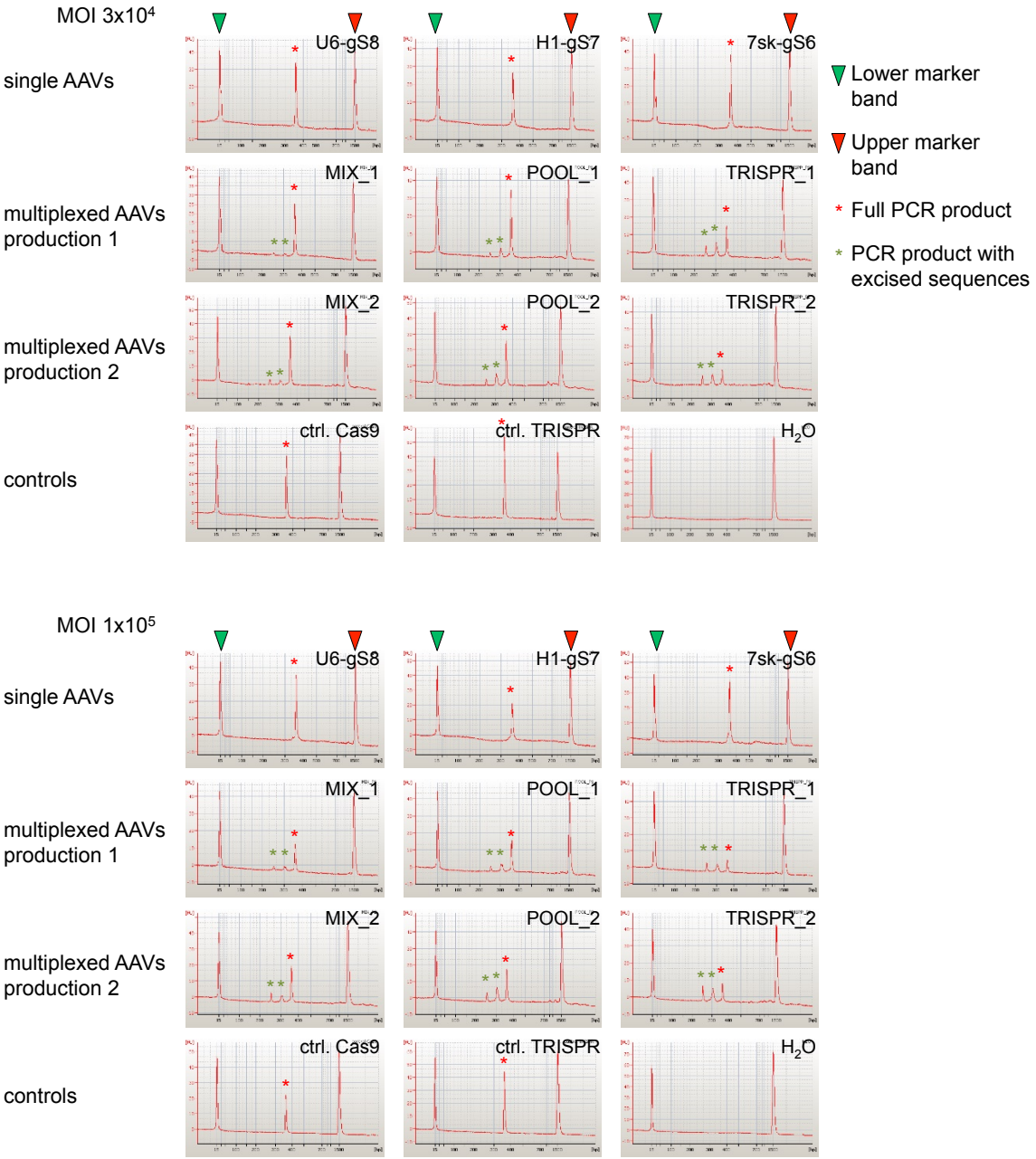

Supplementary Figure 1. Original Bioanalyzer chromatograms supporting Figure 17F.

HepG2-hNTCP-HB2.7 cells were transduced with sgRNA 6, 7 and 8 targeting the HBsAg locus using the different multiplexing approaches (MIX, POOL or TRISPR) and an MOI of 3 x10^4 (upper chromatograms) or 10^5 (lower chromatograms). Approaches with only single sgRNAs (U6-S8, H1-S7, 7sk- S6) resulted in a single 350 bp band (red star), whereas cells treated with the different multiplexing approaches revealed additional smaller PCR fragments (green stars).The smaller PCR fragments represent the excision of the sequence between the sgRNA binding sites. For quantifications, the area under the curves of the peaks with green stars were divided with the area under the curves of all peaks. Data shown for cells treated with two independent AAV productions using different multiplexing approaches. (Manuscript in preparation)

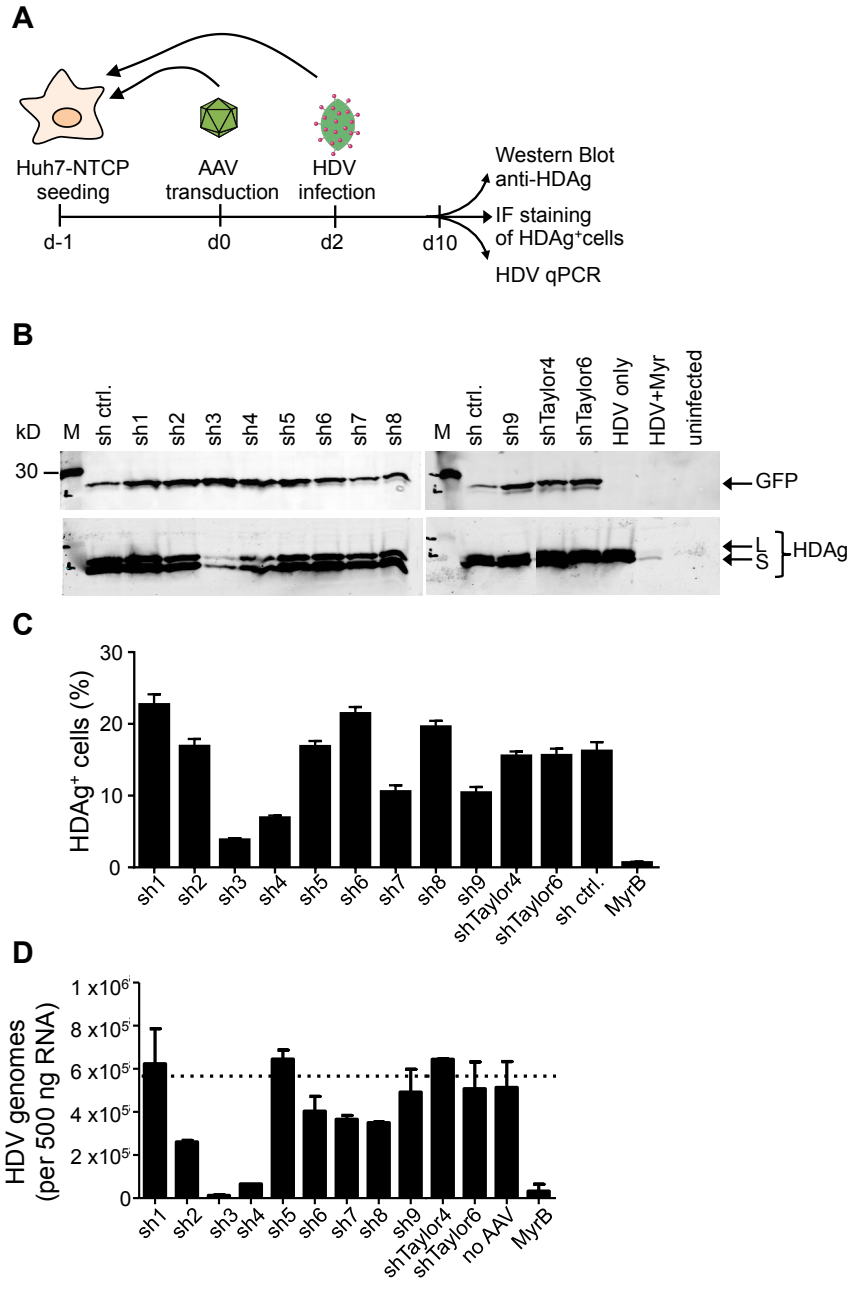

Supplementary Figure 2. Screening of shRNA 1 to 9 against HDV.

A) Experimental layout: Huh7-NTCP cells were first transduced with AAV crude lysates expressing nine different shRNAs against HDV under a U6 promoter and subsequently infected with HDV. Ten days after AAV transduction, cells were harvested for Western Blot analysis **(B)**, IF staining and automated microscopy **(C)** and qPCR against the HDV genome **(D)**. shTaylor 4 and 6 refer to the shRNAs used in [127]. sh ctrl. represent a non-targeting shRNA. Experiments were performed by Florian Lempp (AG Urban) and Florian Schmidt (former Bachelor student in our lab).

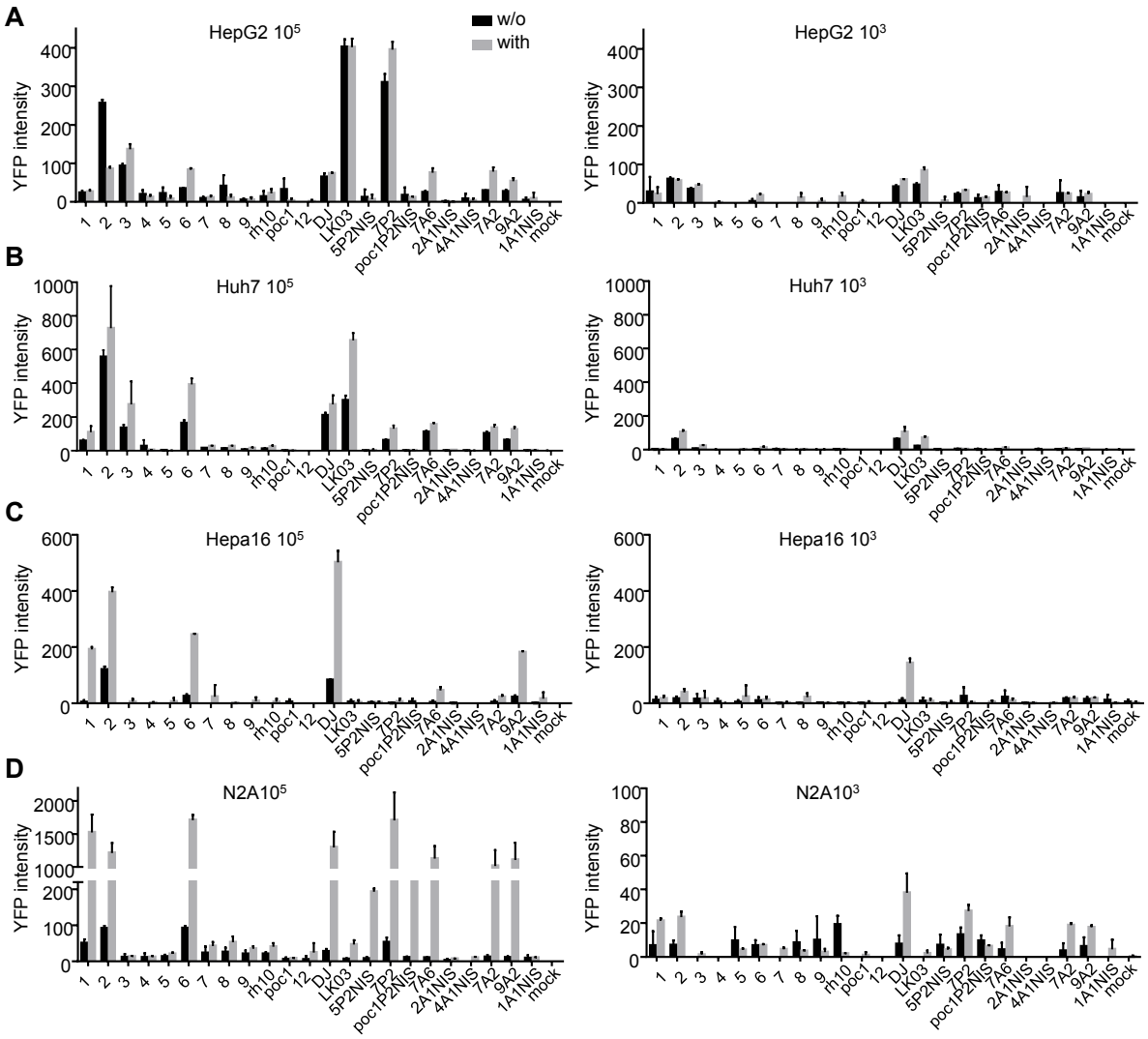

Supplementary Figure 3. DMSO can enhance AAV expression levels depending on AAV variant and cell line.

The experiments in Figure 24 were also analyzed for the intensity of the YFP signal via automated microscopy. HepG2 **(A)**, Huh7 **(B)**, Hepa16 **(C)** and N2A **(D)** cells were transduced with 23 different AAVs with an MOI of 10^5 (left) and 10^3 (right) without (black) or with 2.5% DMSO (gray) in the transduction media. Background intensity levels that were acquired in the mock condition (no AAV) were subtracted from all other conditions. Enhanced YFP expression rates correlate with DMSO-mediated enhanced transduction efficiencies. Error bars represent standard deviations of three independent experiments.

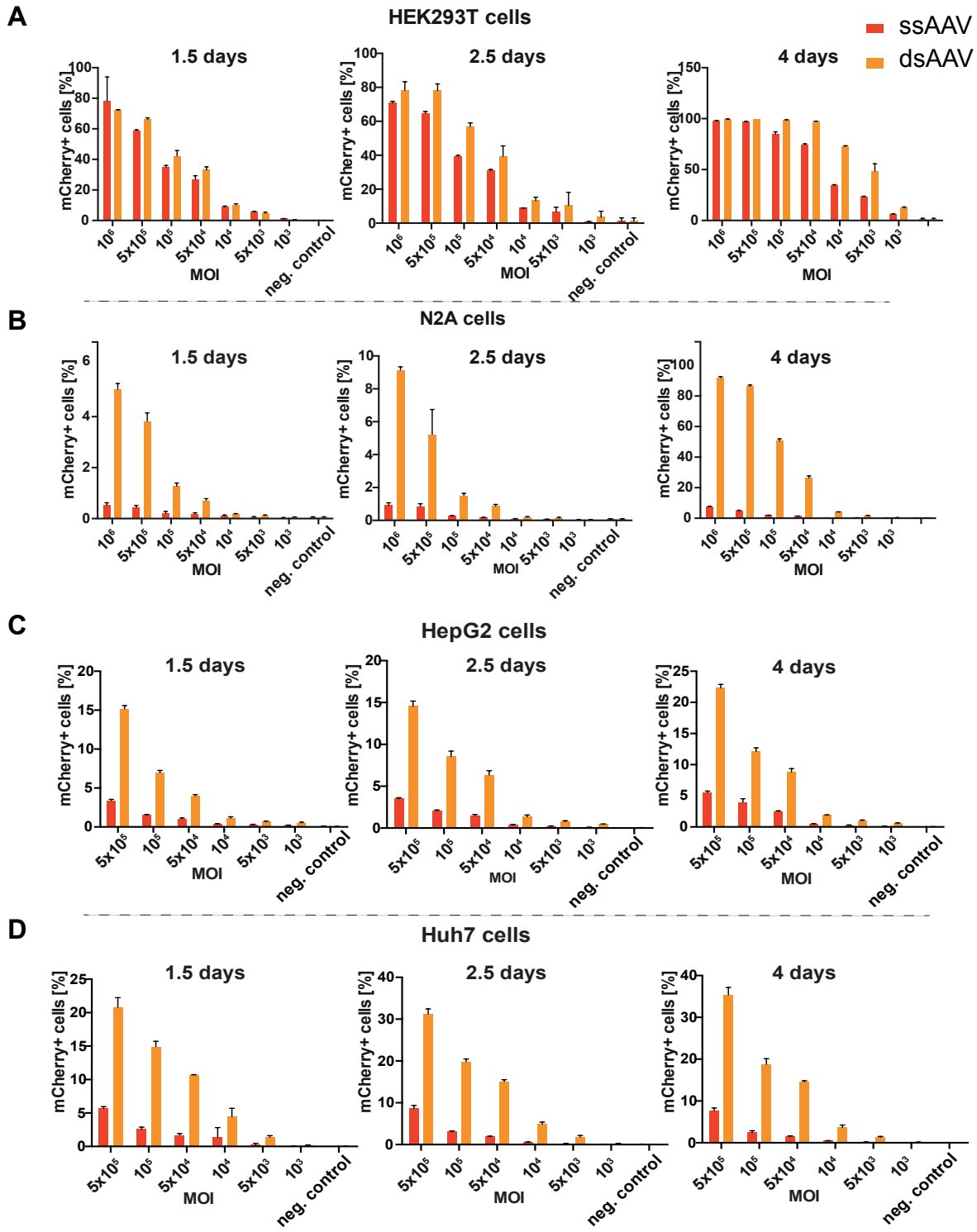

Supplementary Figure 4. Expression rates of ss versus dsAAV in different cell lines.

A) HEK293T, B) N2A, C) HepG2 and D) Huh7 cells were transduced with AAV9A2 expressing CMV-mCherry in the ssAAV (red) or scAAV (orange) context using the indicated MOIs (ranging from 10^6 to 10^3). Cells were analyzed via flow cytometry either 1.5, 2.5 or 4 days after transduction. Error bars indicate standard deviation of four independent experiments. Results obtained jointly with Daniel Heid in his Bachelor Thesis.

7. ACHIEVEMENTS

7.1. Publications

Mathony, J. **†**, Harteveld, Z**. †**, **Schmelas, C**. **†**, Upmeier zu Belzen, J., Aschenbrenner, S., Sun, W., Hoffmann, M. D., Stengl, C., Scheck, A., Georgeon, S., Rosset, S., Wang, Y., Grimm, D., Eils, R., Correia, B., Niopek, D. (2020). 'Computational design of anti-CRISPR proteins with improved inhibition potency'. *Nat. Chem. Biol. accepted*

† These authors contributed equally to this work.

Borner, K., Kienle, E., Huang, L. Y., Weinmann, J., Sacher, A., Bayer, P., Stullein, C., Fakhiri, J., Zimmermann, L., Westhaus, A., Beneke, J., Beil, N., Wiedtke, E., **Schmelas, C**., Miltner, D., Rau, A., Erfle, H., Krausslich, H.G., Muller, M., Agbandje-McKenna, M., and Grimm, D. 2020. 'Pre-arrayed Pan-AAV Peptide Display Libraries for Rapid Single-Round Screening', *Mol Ther.*

Upmeier zu Belzen, J., Bürgel, T., Holderbach, S., Bubeck, F., Adam, L., Gandor, C., Klein, M., Mathony, J., Pfuderer, P., Platz, L., Przybilla, M., Schwendemann, M., Heid, D., Hoffmann, M. D., Jendrusch, M., **Schmelas, C**., Waldhauer, M., Lehmann, I., Niopek, D., and Eils, R. 2019. 'Leveraging implicit knowledge in neural networks for functional dissection and engineering of proteins', *Nature Machine Intelligence*, 1: 225-35.

Schmelas, C., and D. Grimm. 2018. 'Split Cas9, Not Hairs - Advancing the Therapeutic Index of CRISPR Technology', *Biotechnol J*, 13: e1700432.

Bubeck, F., Hoffmann, M. D., Harteveld, Z., Aschenbrenner, S., Bietz, A., Waldhauer, M. C., Borner, K., Fakhiri, J., **Schmelas, C**., Dietz, L., Grimm, D., Correia, B. E., Eils, R., and Niopek, D. 2018. 'Engineered anti-CRISPR proteins for optogenetic control of CRISPR-Cas9', *Nat Methods*, 15: 924-27.

7.2. Conferences

Oral Presentation (only first author presentations are listed):

Schmelas, C., Gleixner J., Schmidt F., Eils, R., Di Ventura B., and Grimm, D. “Enhanced genome editing using split *Staphylococcus aureus* Cas9 delivered in double-stranded Adeno-associated viral vectors“. American Conference of Gene and Cell Therapy (ASGCT), 21st Annual Meeting, Chicago, USA, May 2018

Poster Presentation (only first author presentations are listed):

Schmelas, C., Gleixner J., Schmidt F., Eils, R., Di Ventura B., and Grimm, D. “Enhanced genome editing using split *Staphylococcus aureus* Cas9 delivered in self-complementary Adeno-associated viral vectors“. European Conference of Gene and Cell Therapy (ESGCT), 25th Anniversary Congress, Berlin, Germany, 17-20 October 2017

7.3. Awards

Meritorious Abstract Travel Award, American Conference of Gene and Cell Therapy (ASGCT), 21st Annual Meeting, Chicago, USA, May 2018

Travel Award awarded to the top 10 highest scored abstracts submitted by PhD students and first-docotral Congress delegates, European Conference of Gene and Cell Therapy (ESGCT), 25th Anniversary Congress, Berlin, Germany, 17-20 October 2017

Supervisor of Team Heidelberg in the iGEM (International Genetically Engineered Machine) competition 2017. Awarded as **2nd runner up** in the undergraduate section with 312 participating universities. **Price winners** of: best foundational advance, best integrated human practice, best software tool, best wiki, best presentation and best poster (http://2017.igem.org/Team:Heidelberg)

7.4. Patents

"Use of anti-CRISPR polypeptides for specific activation of Cas nucleases".
International Publication Number: WO 2019/034784 A1

8. ACKNOWLEDGMENTS

An erster Stelle danke ich meinem Betreuer Prof. Dr. Dirk Grimm für die Aufnahme als Doktorand in seinem Labor und die Möglichkeit viele spannende Themenfelder der Gentherapie kennenzulernen. Ohne seine wissenschaftlichen Ratschläge und seine außerordentliche Begeisterung für meine Forschungsschwerpunkte wäre meine Doktorarbeit in dieser Form nicht entstanden. Ich danke für die Vielzahl an erfolgreichen und spannenden Kooperationen, die durch ihn ermöglicht wurden und für seinen Einsatz in den Veröffentlichungen meiner Forschungsergebnissen. Ich danke herzlich für die Freiheit und sein entgegengebrachtes Vertrauen meine wissenschaftliche Arbeit maßgeblich selbst gestalten zu dürfen und mich damit als Wissenschaftler weiterzuentwickeln. Die Zeit in seinem Labor und die Arbeit in einem tollen Team haben meine persönliche Entwicklung geprägt und ich danke sehr dafür.

Mein Dank gilt auch Dr. Dominik Niopek für die intensive Zusammenarbeit in den letzten Jahren, die zahlreiche gemeinsame Veröffentlichungen ermöglichte. Ich danke für seinen wissenschaftlichen Enthusiasmus und seine packende Motivation, was in seinem ganzen Team zu spüren ist. Ich danke auch für die spannende und inspirierende Zeit während iGEM 2017.

Ein besonderer Dank gilt Prof. Dr. Ralf Bartenschlager und seinem Team für die Koordination des SFB TRR179. Für mich war die Zeit innerhalb des SFB geprägt durch zahlreiche Kooperationen, diverse spannenden Veranstaltungen und den freundschaftlichen Austausch mit anderen Doktoranden. Ich danke für die Möglichkeit ein Teil dieses Transregio-Projekts zu sein.

Ich danke Prof. Dr. Ralf Bartenschlager für die Bereitschaft Erstgutachter meiner Doktorarbeit zu sein, sowie Dr. Ilka Bischofs-Pfeifer und Dr. Petr Chlanda für ihr Engagement als Teil meiner Prüfungskommission. Danke für eure Mühe auch während dieser bedrückenden Zeiten der COVID-19-Pandemie.

Außerdem danke ich Prof. Dr. Ralf Bartenschlager, Prof. Michael Nassal und Prof. Dr. Dirk Grimm für ihre konstruktiven Beiträge und den ermutigenden und inspirierenden Austausch während meiner TAC- Meetings. Ich danke auch Martina Galvan und Rolf Lutz für ihr Engagement bei HBIGS, ihre Unterstützung und ihre schnellen Antworten.

Insbesondere danke ich zahlreichen Kooperationspartnern, die meine Doktorarbeit maßgeblich mitgestaltet haben. Ich danke Prof. Dr. Ulrike Protzer, Dr. Thomas Michler und Andreas Oswald für die Zusammenarbeit auf unserem HBV-Projekt. Besonderen Dank gilt Prof. Dr. Stephan Urban, Dr. Thomas Tu und Dr. Florian Lempp für die Unterstützung an den HBV-Experimenten vor Ort, sowie unsere tolle Zusammenarbeit am HBV/HDV-Projekt. Ich danke Prof. Michael Nassal, Julija Miller und Peter Zimmermann für die gemeinsame Arbeit am DMSO Projekt. Mein besonderer Dank gilt Dr. Dominik Niopek, Jan Mathony, Sabine Aschenbrenner, Mareike Hoffmann und Felix Bubeck, sowie Dr. Bruno Correia und Zander Harteveld, für die ergiebige Zusammenarbeit an diversen anti-CRISPR Projekten und die vielen daraus resultierenden Veröffentlichungen.

Ein ganz besonderer Dank gilt den ehemaligen und gegenwärtigen Mitarbeitern der AG Grimm! Ich danke für die offene, freundschaftliche und motivierende Arbeitsatmosphäre im Labor, welche ungeachtet der experimentellen Ergebnisse jeden Tag zu einem guten Tag gemacht hat! Ein großer Dank geht an Anne, Claire, Jonas, Janina, Julia, Jad, Kleopatra, Anna, Cindy, Ellen und Chiara für ihre Ermutigungen und Freundschaft. Außerdem danke ich Julia Fakhiri für das tolle Teamwork an dem splitCas9/SIN Projekt, welches mich sehr erfreut hat und woraus ich viel lernen konnte. Ich danke Anne Kleider für das Korrekturlesen meiner Doktorarbeit. Ich danke Florian Schmidt für seine Arbeit am TRISPR Design und die vielen Konstrukte, die er mir hinterließ und auf denen ich diese Arbeit teilweise aufbauen konnte.

Meinen größten Dank richte ich an Min. Danke, dass du in meinem Leben bist, mich tagtäglich unterstützt und mir so viel Freude und Liebe schenkst. Ohne dich wäre diese Arbeit nicht was sie ist, denn ich wäre nicht was ich bin.